

VILNIUS UNIVERSITY  
CENTRE OF PHYSICAL SCIENCES AND TECHNOLOGY

Aurelija  
SMALENSKAITĖ

# Layered Double Hydroxides: synthesis, characterization, modification and lanthanide ions substitution effects on luminescent properties

**DOCTORAL DISSERTATION**

Natural sciences  
Chemistry N 003

---

VILNIUS 2019

This dissertation was written between 2015 and 2019 at Vilnius University.

**Academic supervisors:**

**Prof. Habil. Dr. Aivaras Kareiva** (Vilnius University, Natural Sciences, Chemistry – N 003) (From 2015-10-01 to 2017-10-05).

**Prof. Dr. Aldona Beganskienė** (Vilnius University, Natural Sciences, Chemistry – N 003) (From 2017-10-05 to 2019-09-30).

This doctoral dissertation will be defended in a public meeting of the Dissertation Defence Panel:

**Chairman – Prof. Dr. Henrikas Cesiulis** (Vilnius University, Natural Sciences, Chemistry – N 003).

**Members:**

**Prof. dr. Rasa Pauliukaitė** (Centre of Physical Sciences and Technology, Natural Sciences, Chemistry – N 003);

**Prof. Dr. Sarah L. Stoll** (Georgetown University, Natural Sciences, Chemistry – N 003);

**Prof. Habil. Dr. Sigitas Tamulevičius** (Kaunas University of Technology, Technology Science, Material Engineering– T 008);

**Prof. Habil. Dr. Sigitas Tumkevičius** (Vilnius University, Natural Sciences, Chemistry – N 003).

The dissertation shall be defended at a public meeting of the Dissertation Defence Panel at 2 pm on January 17, 2020 in Inorganic Chemistry auditorium 141 of the Chemistry and Geoscience Faculty, Vilnius University.

Address: Naugarduko g. 24, LT-03225 Vilnius, Lithuania. Tel.: 2193108. Fax: 2330987.

The text of this dissertation can be accessed at the libraries of (name of the institutions granted the right to conduct doctoral studies in alphabetical order), as well as on the website of Vilnius University: [www.vu.lt/lt/naujienos/ivykiu-kalendorius](http://www.vu.lt/lt/naujienos/ivykiu-kalendorius)

VILNIAUS UNIVERSITETAS  
FIZINIŲ IR TECHNOLOGIJOS MOKSLŲ CENTRAS

Aurelija  
SMALENSKAITĖ

Sluoksniuotieji dvigubi hidroksidai:  
sintezė, apibūdinimas, modifikavimas ir  
lantanoidų jonų pakaitų įtaka  
liuminescencinėms savybėms

**DAKTARO DISERTACIJA**

Gamtos mokslai  
Chemija N 003

---

VILNIUS 2019

Disertacija rengta 2015–2019 metais Vilniaus universitete.

**Moksliniai vadovai:**

**prof. habil. dr. Aivaras Kareiva** (Vilniaus universitetas, gamtos mokslai, chemija – P 003). Nuo 2015-10-01 iki 2017-10-05;

**prof. dr. Aldona Beganskienė** (Vilniaus Universitetas, gamtos mokslai, chemija – P 003). Nuo 2017-10-05 iki 2019-09-30.

Gynimo taryba:

Pirmininkas: **prof. dr. Henrikas Cesiulis** (Vilniaus universitetas, gamtos mokslai, chemija – N 003).

Nariai:

**prof. dr. Rasa Pauliukaitė** (Fizinių ir technologijos mokslų centras, gamtos mokslai, chemija – N 003);

**prof. dr. Sarah L. Stoll** (Georgetown universitetas, gamtos mokslai, chemija – N 003);

**prof. habil. dr. Sigitas Tamulevičius** (Kauno technologijos universitetas, technologijos mokslai, medžiagų inžinerija – T 008);

**prof. habil. dr. Sigitas Tumkevičius** (Vilniaus universitetas, gamtos mokslai, chemija – N 003).3.

Disertacija bus ginama viešame Chemijos mokslo krypties gynimo tarybos posėdyje 2020 m. sausio 17 d. 14 val. Vilniaus universiteto Chemijos ir geomokslų fakulteto Neorganinės chemijos auditorijoje.

Adresas: Naugarduko g. 24, LT-03225 Vilnius, Lietuva. Tel.: 2193108. Faksas: 2330987.

Disertaciją galima peržiūrėti Vilniaus universiteto, Fizinių ir technologijos mokslų centro bibliotekose ir VU interneto svetainėje adresu: <https://www.vu.lt/naujienos/ivykiu-kalendorius>

## CONTENTS

LIST OF ABBREVIATIONS.....	7
INTRODUCTION.....	8
1. LITERATURE OVERVIEW .....	10
1.1. Structural features of layered double hydroxides (LDHs).....	10
1.2. Cations in LDHs .....	13
1.3. Anions in LDHs .....	13
1.4. Synthesis methods.....	14
1.5. Memory effect.....	17
1.6. Application of LDHs.....	17
2. EXPERIMENTAL.....	20
2.1. Materials.....	20
2.2. Synthesis of Mg-Al non-substituted and lanthanide-substituted LDHs by co-precipitation method .....	20
2.3. Synthesis of Mg-Al non-substituted and lanthanide-substituted LDHs by sol-gel method .....	21
2.4. Modification of Mg-Al non-substituted and lanthanide - substituted LDHs anions.....	21
2.5. Preparation of sol LDH suspension for dip-coating.....	22
2.6. Characterization techniques .....	22
3. RESULTS AND DISCUSSION.....	23
3.1. A comparative study of co-precipitation and sol-gel synthetic approaches to fabricate cerium-substituted Mg-Al layered double hydroxides .....	23
3.1.1. Synthesis and characterization by co-precipitation method.....	23
3.1.2. Synthesis and characterization by sol-gel method.....	28
3.1.3. Characterization of synthesized LDHs .....	31
3.1.4. Luminescent properties.....	36
3.2. Sol-gel synthesis and characterization of europium-substituted Mg-Al layered double hydroxides .....	38
3.2.1. Modification of LDH and characterization.....	38

3.2.2. Modification of $Mg_3Al_1$ and $Mg_3Al_{1-x}Eu_x$ LDH .....	40
3.2.3. Luminescent properties.....	49
3.3. Induced neodymium luminescence in the sol-gel derived Mg-Al layered double hydroxides.....	53
3.4. Sol-gel synthesis and characterization of terbium-substituted Mg-Al layered double hydroxides .....	56
3.4.1. Modification of LDH and characterization.....	56
3.4.2. Luminescent properties.....	60
3.5. Layered double hydroxides: Peculiarities of intercalation of organic anions.....	62
3.5.1. Modification of LDH with organic anions and characterization.....	63
3.5.2. Luminescent properties.....	73
3.6. Sol-gel synthesis and characterization of thin films of Mg-Al layered double hydroxides.....	75
3.6.1. Synthesis on Si and stainless-steel substrates and characterization.....	75
3.6.2. Modification of sol-gel processing.....	77
4. CONCLUSIONS .....	82
5. LIST OF PUBLICATIONS AND CONFERENCES PARTICIPATION.....	84
5.1. Publications included in the thesis .....	84
5.1.1. Articles in journals .....	84
5.1.2. Attended conferences .....	84
5.2. Publications not included in the thesis .....	86
5.2.1. Articles in journals .....	86
5.2.2. Attended conferences.....	86
6. ACKNOWLEDGEMENTS .....	87
7. REFERENCES.....	88
8. SUMMARY IN LITHUANIAN.....	99

## LIST OF ABBREVIATIONS

AFM	Atomic Force Microscopy
BPhAc	4-biphenylacetate
BTC	1,3,5-benzentricarboxylate
DMB	4-dimethylaminobenzoate
DTG	Derivative Thermogravimetry
FTIR	Fourier Transform Infrared Spectroscopy
LDH	Layered Double Hydroxide
MB	4-methylbenzoate
MMO	Mixed Metal Oxides
PEG	Polyethylene glycol
PVA	Polyvinyl alcohol
RE	Rare Earths
RMS	Root Mean Square
TAL	Terephthalate
TGA	Thermogravimetric Analysis
SEM	Scanning Electron Microscopy
XRD	X-ray diffraction

## INTRODUCTION

Layered double hydroxides (LDHs) are anionic clays with unique physical and chemical properties. The general term of LDH is hydrotalcite as Mg-Al hydroxycarbonate which was the first with exact formula of  $\text{Mg}_6\text{Al}_2(\text{OH})_{16}\text{CO}_3 \cdot 4\text{H}_2\text{O}$  discovered in Sweden and published in 1915 by Manasse [1]. Layered double hydroxides, hydrotalcite-type compounds are the commonly used to describe a class of layered materials based on the brucite ( $\text{Mg}(\text{OH})_2$ ) crystal structure and having a general chemical formula of  $[\text{M}^{2+}_{1-x}\text{M}^{3+}_x(\text{OH})_2]_{x+}(\text{A}^{m-})_{x/m} \cdot n\text{H}_2\text{O}$  [2]. A large number of LDHs can be synthesized by varying either the type of the cation or anion resulting in numerous new materials with multifunctional properties. Basic properties of LDHs are mainly determined by inter-layer cations,  $\text{M}^{2+}/\text{M}^{3+}$  ratio, compensation anions and activation parameters [3]. The LDH containing  $\text{Mg}^{2+}$  and  $\text{Al}^{3+}$  cations which is identical to the natural hydrotalcite was mostly used as a reference system.

LDHs can be fabricated by different synthesis methods. The most common preparation technique is co-precipitation method starting from soluble salts of the metals [4]. After calcination at temperatures from 200 to 600 °C, an LDH is converted to the mixed metal oxides (MMO) with high specific surface area and basic properties. An ability of MMO to recover the original layered structure is a property known as „memory effect” [5]. The most common second technique for the preparation of LDHs is anion-exchange [6]. Anions are intercalated between the layers in order to maintain electroneutrality of the compound. This flexibility of the LDHs host provide a large variety of multifunctional LDH materials with potential applications in catalysis [7], optics [8], anticorrosion inhibitors [9], separation science [10], photochemistry and electrochemistry [11].

Recently considerable attention has been focused on incorporating different metal ions into LDH host layers to develop new functional materials [12]. Many transition metal ions have been introduced into LDHs in the form of anionic complexes with organic ligands [13, 14]. Rare earth elements, especially those containing europium and terbium, have been the subject of extensive research because of their sharp and intense emission bands arising from f-f transitions [15, 16]. The rare-earth metal ions offer the possibility of obtaining blue, green and red colours, which are necessary for RGB devices [17, 18]. Today many investigations on luminescent materials based on aromatic carboxylates of lanthanides have been performed [19]. The study of luminescence of inorganic-organic LDH materials indicated that energy



transfer from the excited state of the intercalated anion guest molecules to lanthanide element centres influences the emission intensity [20-22].

The sol-gel synthesis route for the mixed metal oxides and related compounds have some benefits over other methods such as simplicity, synthesis at low temperatures, effectiveness, suitability for different systems and cost efficiency and also recently was developed for indirect preparation of LDHs [23-25].

The aim of this PhD study was to investigate luminescence properties of lanthanide-substituted Mg-Al LDHs. For the first time lanthanide-substituted LDHs were synthesized using indirect sol-gel synthesis processing. The novelty of this PhD thesis is the determined possibility to induce luminescence in some lanthanide-substituted LDHs by intercalation of different anions and to develop new thin films of Mg-Al LDHs.

To achieve this, doctoral dissertation's the tasks were formulated as follows:

1. To compare the co-precipitation and novel indirect sol-gel synthesis techniques for the preparation of  $\text{Ce}^{3+}$ -substituted Mg-Al LDHs and investigate luminescent properties.
2. To synthesize for the first time by sol-gel technique  $\text{Eu}^{3+}$ -substituted Mg-Al LDHs.
3. To investigate the possibility to induce  $\text{Nd}^{3+}$  luminescence in the sol-gel derived Mg-Al LDHs.
4. To synthesize for the first time by sol-gel technique  $\text{Tb}^{3+}$ -substituted Mg-Al LDHs.
5. To investigate the peculiarities of intercalation of organic anions to the LDHs structures.
6. To prepare the new thin films of Mg-Al LDHs by dip-coating technique.

# 1. LITERATURE OVERVIEW

## 1.1. Structural features of layered double hydroxides (LDHs)

Layered double hydroxides are compounds composed of positively charged brucite-like layers with an interlayer gallery containing charge compensating anions and water molecules. The metal cations occupy the centres of shared oxygen octahedra whose vertices contain hydroxide ions that connect to form infinite two-dimensional sheets [5]. A general chemical formula of an LDH can be expressed as  $[M^{2+}_{1-x}M^{3+}_x(OH)_2]_x(A^{m-})_{x/m} \cdot nH_2O$  where  $M^{2+}$  and  $M^{3+}$  are divalent and trivalent metal cations and  $A^{y-}$  is an intercalated anions. The metal cations are coordinated by six oxygen atoms forming  $M^{2+}/M^{3+}(OH)_6$  octahedra. These octahedra form two-dimensional sheets via edge sharing and may stack together by hydrogen bonding and other electrostatic interactions between the hydroxyl groups of contiguous sheets and interlayer anions (Fig.1.) [26].

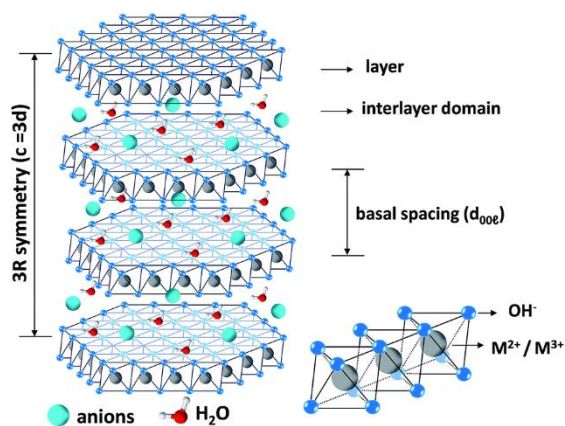


Fig.1. Schematic structure of layered double hydroxide<sup>26</sup>.

The brucite-like sheets can stack one on the other with two different symmetries, rhombohedral or hexagonal. The layers are three atoms thick and can be represented as ABC the three-fold axis of the -OH groups in the brucite-like layers, the stack may have the sequence BC-CA-AB-BC, thus having three sheets in the unit cell, or BC-CB-BC with two layers in the unit cell with hexagonal symmetry [27]. The hydroxyl ions in every alternate layer of octahedral sites are occupied by  $M^{2+}$  ions, which according [28, 29] are

forming the 1H polytype of brucite  $\text{Mg}(\text{OH})_2$  -like layer. The number “1” indicates the single-layer periodicity and “H” indicates the hexagonal symmetry. Periodic insertion of other layers, AB, CA, CB, etc., into the primary stacking sequence of 1H yields different polytypes, of which the most important are the two-layered polytypes of hexagonal symmetry ( $2\text{H}_1$ ,  $2\text{H}_2$ ,  $2\text{H}_3$ ) and triple-layered polytypes of rhombohedral symmetry ( $3\text{R}_1$ ,  $3\text{R}_2$ ). These polytypes differ from one to another in the nature of the interlayer sites that they generate. For instance, the  $3\text{R}_1$  and  $2\text{H}_1$  polytypes generate exclusively trigonal-prismatic interlayer sites, whereas  $3\text{R}_2$  and  $2\text{H}_2$  polytypes generate exclusively octahedral sites [30]. LDHs containing  $\text{CO}_3^{2-}$  crystallize in the structure of the  $3\text{R}_1$  or  $2\text{H}_1$  polytypes, having prismatic interlayer sites. These not only provide crystallographically well-defined sites for the C and O atoms of the  $\text{CO}_3^{2-}$  ions but also facilitate hydrogen bonding between the oxygen atoms of the carbonate ions and the hydroxyl ions of the layer. Therefore, the LDHs are characterized by the mineral hydrotalcite formula  $[\text{Mg}_6\text{Al}_2(\text{OH})_{16}]\text{CO}_3 \cdot 4\text{H}_2\text{O}$ , which is usually written as  $[\text{Mg}_{0.75}\text{Al}_{0.25}(\text{OH})_2](\text{CO}_3)_{0.125} \cdot 0.5\text{H}_2\text{O}$  in order to highlight its relationship to brucite. Many other minerals are known that have hydrotalcite (HT) structure but with different stoichiometries, with more than one anion and more than two cations, or with small amounts of cations in the interlayer and also with some ordering of the cation inside the brucite-like layers (Table 1) [31, 32].

Table1. Minerals with a HT structure.

Mineral	Symmetry	Chemical formula
Hydrotalcite	3R	$\text{Mg}_6\text{Al}_2(\text{OH})_{16}\text{CO}_3 \cdot 4\text{H}_2\text{O}$
Pyroaurite	3R	$\text{Mg}_6\text{Fe}_2(\text{OH})_{16}\text{CO}_3 \cdot 4\text{H}_2\text{O}$
Woodwardite	3R	$\text{Cu}_5\text{Al}_2(\text{OH})_{12}\text{SO}_4 \cdot 2 \cdot 4\text{H}_2\text{O}$
Sjogrenite	2H	$\text{Mg}_6\text{Fe}_2(\text{OH})_{16}\text{CO}_3 \cdot 4\text{H}_2\text{O}$
Stichtite	3R	$\text{Mg}_6\text{Cr}_2(\text{OH})_{16}\text{CO}_3 \cdot 4\text{H}_2\text{O}$
Meixnerite	3R	$\text{Mg}_6\text{Al}_2(\text{OH})_{16}(\text{OH})_2 \cdot 4\text{H}_2\text{O}$
Barbertonite	2H	$\text{Mg}_6\text{Cr}_2(\text{OH})_{16}(\text{OH})_2 \cdot 4\text{H}_2\text{O}$
Honessite	3R	$\text{Ni}_6\text{Fe}_2(\text{OH})_{16}\text{SO}_4 \cdot n\text{H}_2\text{O}$

Takovite	3R	$\text{Ni}_6\text{Al}_2(\text{OH})_{16}\text{CO}_3 \cdot 4\text{H}_2\text{O}$
Iowaite	3R	$\text{Mg}_5\text{Fe}(\text{OH})_{12}\text{Cl} \cdot 2\text{H}_2\text{O}$
Reevesite	3R	$\text{Ni}_6\text{Fe}_2(\text{OH})_{16}\text{CO}_3 \cdot 4\text{H}_2\text{O}$
Desautelsite	3R	$\text{Mg}_6\text{Mn}_2(\text{OH})_{16}\text{CO}_3 \cdot 4\text{H}_2\text{O}$
Chlormagaluminitite	2H	$\text{Mg}_4\text{Al}_2(\text{OH})_{12}\text{Cl}_2 \cdot 3\text{H}_2\text{O}$
Zaccagnaite	2H	$\text{Zn}_4\text{Al}_2(\text{OH})_{12}\text{CO}_3 \cdot 3\text{H}_2\text{O}$
Charmarite	2H	$\text{Mn}_4\text{Al}_2(\text{OH})_{12}\text{CO}_3 \cdot 3\text{H}_2\text{O}$
Quintinite	2H	$\text{Mg}_4\text{Al}_2(\text{OH})_{12}\text{CO}_3 \cdot 3\text{H}_2\text{O}$

LDHs have a well-defined layered structure within nanometre scale (0.3–3 nm) interlayer and contain important functional groups in both the metal hydroxide layers and interlayers [33]. The brucite-like sheets stack on each other with respect to rhombohedral 3R symmetry with the lattice parameter  $c$ , which corresponds to three times the spacing  $d$  between two consecutive layers. They are ascribed to diffraction by planes (003), (006), and (009) and the value can be calculated from Powder X-ray diffraction (XRD) patterns (Fig.2.) [34].

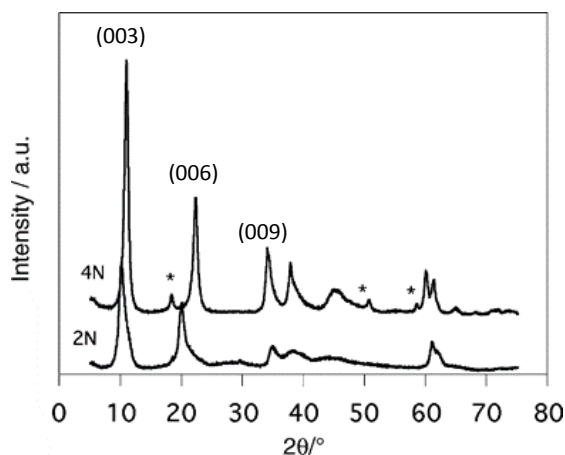


Fig. 2. Powder XRD patterns of Mg–Al LDHs with intercalated nitrate. Mg:Al ratios of 4 (pattern 4N) and 2 (pattern 2N). The phase of  $\text{Mg}(\text{OH})_2$  is marked with asterisks<sup>34</sup>.

Lattice parameter  $c$  can be calculated as three times the spacing of diffraction due to first plane (003), or averaging the positions of the signals  $c = d(003) + 2d(006) + 3d(009)$ , although the peak due to planes (009) is sometimes

overlapped because of disorder of the anions and the water molecules in the interlayer space [35].

### 1.2. Cations in LDHs

The number of natural and synthetic anionic clays containing different metallic divalent or trivalent cations studied is very large. In the composition of LDH materials the  $M^{2+}$  and  $M^{3+}$  cations can be substituted or partially replaced by other cations modifying their chemical and physical properties. The commonly found  $M^{2+}$  and  $M^{3+}$  cations like as:  $Mg^{2+}$ ,  $Zn^{2+}$ ,  $Co^{2+}$ ,  $Ni^{2+}$ ,  $Cu^{2+}$  or  $Mn^{2+}$  and  $Al^{3+}$ ,  $Cr^{3+}$ ,  $Co^{3+}$ ,  $Fe^{3+}$ ,  $V^{3+}$  or  $Y^{3+}$ , respectively [36, 37]. The most frequent divalent metals have the ionic radii from 0.65 Å (Mg) to 0.80 Å (Mn) whereas the radii of the trivalent metals are usually between 0.50 Å (Al) and 0.69 Å (Cr) [32].

Recently, it was found that lanthanide (Ln) cations such as  $Eu^{3+}$  [38],  $Tb^{3+}$  [39] or  $Nd^{3+}$  [40] can substitute  $M^{2+}$  and  $M^{3+}$  in LDHs to achieve green, red, or infrared luminescence. Layered lanthanide hydroxides of cationic rare earth elements such as  $Yb^{3+}$ ,  $Dy^{3+}$ ,  $Ho^{3+}$ ,  $Y^{3+}$  have been also prepared [41] and characterized. The use of LDHs as host materials for optically active lanthanides is still a relatively new topic.

### 1.3. Anions in LDHs

Intercalation of different anions in LDH is a challenging topic, the anion-exchange could be performed mostly, when the introduced anion has higher affinity with the LDH layer than the host anion. Usually, the anions with small size and high charge density are used for such investigations. Nevertheless, the low-charge large organic anions could also be introduced to the LDH structure [1]. The possibility to substitute of monovalent anions in the Mg-Al LDH could be expressed by following order  $OH^- > F^- > Cl^- > Br^- > NO_3^-$ . More selective are anions with higher charge  $CO_3^{2-} > SO_4^{2-}$  [42]. The anion-exchange selectivity is usually related to the guest orientation. Two orientations are observed for the organic anion within the gallery either vertical perpendicular to the layers or horizontal. Whether a vertical or horizontal orientation exists, depends upon the charge on the layers and the degree of hydration of the sample. Moreover, the water molecules stabilize the LDH structure via formation of a hydrogen bond [43–45]. The organic anions can create negative charge in the LDH particles, which can be associated to the micellization or formation of self-assembly of exchanged or

adsorbed organic anions on the LDH surface. Furthermore, interaction between LDHs carbonate and carboxylate-containing substances is an important aspect of the high affinity of these types of anions to the LDH surface. Multivalent anions exhibit also high affinity to the LDH surfaces neutralizing the charge of the surface or even making it reversal at higher concentrations. This feature is more pronounced for anions with higher negative charge and platelets of significant negative charge could be formed. These results allow one to design the LDH-based anion-exchange systems for different applications [46-49].

#### 1.4. Synthesis methods

There are many general methods for the preparation of LDHs such as co-precipitation [50], sol-gel [51], urea hydrolysis [52], hydrothermal synthesis [53], anion-exchange [54], combustion synthesis, electrochemical synthesis and synthesis using microwave irradiation [55, 56]. The most common method applied for the preparation of LDHs is the co-precipitation [57-59]. The co-precipitation method is performed at constant pH by the same time adding metal salts and base solutions. The aqueous solutions of  $M^{2+}$  or mixtures of  $M^{2+}$  and  $M^{3+}$  species containing the anion that is to be incorporated into the LDH are used as precursors. The precipitating agents such as NaOH or  $NaHCO_3$  are added to the solution containing  $Mg^{2+}$  and  $Al^{3+}$  ions until the pH of the reaction mixture reaches value (around 10 - 11) and a solution of NaOH is then used to maintain the pH value until the precipitation is complete [31]. The first containing the metal cations nitrate salts were prepared with molar ratios of 2:1, 3:1 and 4:1 by adding  $Mg(NO_3)_2 \cdot 6H_2O$  and  $Al(NO_3)_3 \cdot 9H_2O$  in de-ionized water. After complete dissolution, the above solution was added drop wise to a stirred  $Na_2CO_3$  solution in de-ionized water. The prepared 1 M NaOH solution was then added drop wise to the above solution to maintain constant pH (~ 11). The precipitate was separated from the solution by centrifugation, washed several times with de-ionized water and dried in vacuum. All these reactions were carried out in an inert atmosphere [60]. The co-precipitation method is the most preferred as it is simple to carry out and does not require any unstable solvents or other expensive chemicals or apparatus [61, 62]. The LDHs precipitates and form homogenous mixtures if solubility products of the metal hydroxides are very similar. Unfortunately, LDHs prepared by co-precipitation often suffer from poor crystallinity and the presence of impurities. Low supersaturation conditions usually give rise to more crystalline precipitates [57].

In contrast, the sol-gel synthesis route for mixed metal oxides and related compounds have some benefits over co-precipitation method such as simplicity, synthesis at low temperatures, effectiveness, suitability for different systems and cost efficiency [63, 64]. During the sol-gel processing, the preferable metal inorganic salts or metal organic compounds are hydrolyzed in water, aqueous solution or liquid-organic solvent in ambient temperature to produce a polymeric or particulate sol. An appropriate amount of acid or base can be added into the sol mixture during hydrolysis to facilitate peptization of the solution [65]. The heat treatment of the gels resulted in high crystalline mixed metal oxide (MMO) powders, which were hydroxylated in an aqueous media providing well-crystallized LDH phase [66]. The direct sol-gel method for the preparation of LDHs has some limitations, since amorphous materials could be obtained. Another feature that makes these sol-gel materials distinguishable from those prepared by other synthetic methods is their high specific surface area [55]. However, if metal alkoxides in the sol-gel processing are used as starting materials, the synthesis conditions should be more strictly controlled than in the co-precipitation method. Besides, the synthesis processing in that case is rather expensive.

The major drawback of the urea hydrolysis is that only the carbonate containing LDH could be prepared. The carbonate is continuously being generated due to the decomposition of the urea [67]. The effects of variation of the temperature, total metal cations concentration, the molar fraction of  $M^{2+}/Al$ -carbonate and molar fraction of urea/ $M^{2+}+Al$  in solution on the composition and the crystallinity of the samples were investigated [68]. In contrast to the LDHs synthesized by co-precipitation method, which typically require extensive ageing to have similar characteristics, the urea hydrolysis can provide particle size with large, thin platelets distributions [69].

Hydrothermal synthesis has been used to control the particle size and its distribution when soluble magnesium and aluminium salts were used together with alkali solution to prepare Mg/Al-carbonate LDHs [70]. Hydrothermal treatment can be used to compensate for the required residual water that is lost in the previous stages of the LDH development. When co-precipitation for preparing LDHs fails, a combined co-precipitated and hydrothermal synthesis can be proposed to improve the crystallization. The hydrothermal crystallization is usually carried out at temperatures up to 200 °C under autogenous pressure for a time ranging from hours to days [71]. This method has influence on the surface area and the growth of LDHs crystals. Improved crystalline structures can be obtained by hydrothermal treatment in the presence of water vapour at temperatures not exceeding the decomposition

temperature of the LDHs. While heating the reactants in a pressurized aqueous media improves the crystallinity of the resulting LDHs, however, the hydrothermal synthesis may require additional effort and time. This method can also result in a decrease of surface area and growth of hydrotalcite crystals [55].

The anion-exchange method is especially useful when the co-precipitation method is inapplicable. For example, when the divalent or trivalent metal cations or the anions involved are unstable in alkaline solution, or the direct reaction between metal ions and interlayer anions is more favourable (Fig.3.) [72]. In this anion-exchange method, the guests are exchanged with the anions in the interlayer regions of LDHs.

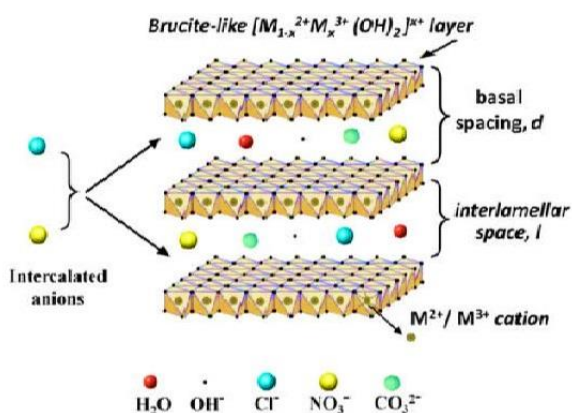


Fig. 3. Scheme of anion-exchange method<sup>72</sup>.

As was already mentioned, the intercalation of different anions in LDH, usually can be performed when the introduced anion has higher affinity with the LDH layer than the host anion. Small anions with relatively high charge density are generally the most preferable. However, the LDHs can be intercalated also with low charge large anions (including organic species) [73, 74]. LDHs containing  $\text{NO}_3^-$  anions are the most suitable precursors for anion exchange due to the easy displacement from the interlayer [42, 75]. Intercalation by smaller guests using anion exchange method is an effective way to enlarge the interlayer space of LDH host, so that it is possible to introduce large or low charge target guests into the interlayer of LDH regions.

The preparation of Mg/Al hydrotalcite-like compounds by combustion, electrochemical and microwave irradiation syntheses has also been reported. The drawbacks of these proposed techniques are the materials have a poor



crystallinity, time-consuming and rather expensive processes. Besides, high number of surface-defective sites could be induced [56].

### 1.5. Memory effect

The layered double hydroxides can be designed to have a “structural memory effect”. After calcination at temperatures from 200 to 600 °C, LDH is converted to mixed metal oxides (MMO) [76, 77], which have high adsorption capacity and other interesting physical features. Thermal treatment of LDHs up to about 200°C induces dehydration. Treatment up to 600°C induces dehydroxylation and loss of vaporizable anions such as carbonate, nitrate, oxalate, and acetate. Heating at up to 900°C leads to the formation of  $MgAl_2O_4$  spinels. This LDHs procedure calls a “structural memory effect” or reformation [78-80]. The MMO into aqueous solution, in the presence of anions, is recovering to the layered structure with anions incorporated in the interlayer [81]. It is therefore important to choose anions that can be easily removed at elevated temperatures forming stable non-toxic decomposition products [82]. Carbonate is an ideal anion for this purpose. As a carbonate containing LDH decomposes, it releases carbon dioxide and water vapour which are both stable. LDHs also have a higher affinity for carbonate than any other anion and this can reduce of non-removable anions being exchanged during long term storage and eliminates the need for precautions to prevent non-carbonate containing LDHs from adsorbing carbonate from the atmosphere or dissolved in water [83]. Reformation of LDH can provide several advantages with new functional LDH materials.

### 1.6. Application of LDHs

LDHs are widely used in commercial products as adsorbents, catalyst support precursors, acid residue scavengers, flame retardants, osmosis membranes and sensors [84-87]. Furthermore, LDHs materials were successfully used as drug and gens delivery, cosmetics, cancer therapy and biosensing [88-94]. LDHs have been studied for their potential application to the removal of oxyanions, such as arsenate, chromate, selenite, borate, and nitrate from contaminated waters [95-100] and also toxic metals ions [101-112]. The removal of oxyanions by LDHs can be ascribed to three different mechanisms, including surface adsorption, interlayer anion-exchange and reformation effect [113-115].

Layered double hydroxides can be prepared with different divalent and trivalent cations in the structure serving as precursors for the preparation of mixed metal oxides used as catalysts for oxidation and hydrogenation/dehydrogenation reactions. The exact features, such as the nature of the cations in the brucite-like layers and the specific surface area may have a significant effect on their catalytic properties [116]. Heterogeneous catalysts including metal–organic frameworks [117-119] and layered double hydroxides [120-124] are new environmentally friendly catalysts, which can be easily removed from the reaction mixture and recycled.

Many inhibitors are intercalated into the LDH and their behaviour has been evaluated [125-128]. The hydrotalcite layers were demonstrated to offer an anticorrosion protection even when applied as a surface conversion films on Mg alloys [129]. The results showed that ZnAl-vanadate-LDH possesses the best anion-exchange and inhibition abilities. Some inorganic inhibitors, cerium, molybdates, phosphates [130] and lanthanum [131] have also been proposed for Al alloys. These inhibitors create a passive insoluble oxide layer that stops the oxygen diffusion from the aggressive environment to the surface.

One particular property of LDHs nanocomposites is their ability to incorporate large molecule as drugs. Furthermore, they can increase the drug solubility without the alteration of pharmaceutical therapeutic activity [132, 133]. The self-assembled gold nanoparticles (AuNPs) on LDHs matrix have been obtained [134]. The resulted hybrids were tested against hepatitis B virus (HBV). The results showed that the hybrids have an inhibitory effect on HBV proliferation and a good cytocompatibility. The Zn/Al LDH incorporated with polyacrylonitrile (PAN) synthesised by in situ polymerisation indicate that PAN material can be designed with enhanced thermal stability and antibacterial behaviour by the dispersion of small amount of LDH [135, 136]. The antibacterial activities of PAN and its composites containing different wt.% of Zn-Al-LDH against bacteria such as *B. subtilis*, *P. aeruginosa*, *E. coli* and *S. aureus* were tested [137, 138]. The polar and high surface area of LDH favours electrostatic interaction between the positive surface of the nanocomposite and negatively charged bacterial cells which subsequently lowers the charge density on bacterial surface causing decrease in cell viability [139, 140]

In recent years, inorganic-organic hybrid luminescence materials have been widely investigated

due to the novel properties to form stable compounds with lanthanides in the interlayer space of LDH [141, 142]. However, these LDHs show limitation due to the low intensity of emission which is caused by direct coordination of water molecules and hydroxyl groups to the RE centre in the layer. For then hybrid RE-organic LDH materials, intercalation of guest organic anions in the interlayer galleries influences the luminescence properties dramatically. The luminescence properties have been investigated of  $\text{Eu}^{3+}$ -doped LDHs intercalated with certain organic compounds, such as naphthalene-1,5-sulfonate, naphthalene-2,6-dicarboxylate [143] citrate, glutamate, picolinate, ethylenediaminetetraacetate [144], and many other compounds [145-148]. The lanthanide-doped luminescent materials have drawn increasing attention as potential phosphor materials for use in optical devices [149-151]. The rare-earth metal ions offer the possibility of obtaining blue, green and red colours, which are necessary for RGB devices [152].

## 2. EXPERIMENTAL

### 2.1. Materials

The following starting materials were used: aluminium (III) nitrate nonahydrate ( $\text{Al}(\text{NO}_3)_3 \cdot 9\text{H}_2\text{O}$ , 98.5%, Chempur); magnesium (II) nitrate hexahydrate ( $\text{Mg}(\text{NO}_3)_2 \cdot 6\text{H}_2\text{O}$ , 99%, Chempur); cerium (III) nitrate hexahydrate ( $\text{Ce}(\text{NO}_3)_3 \cdot 6\text{H}_2\text{O}$ , 99.9%, Sigma-Aldrich), neodymium (III) nitrate hexahydrate ( $\text{Nd}(\text{NO}_3)_3 \cdot 6\text{H}_2\text{O}$ , 99.9%, Sigma-Aldrich), europium (III) nitrate hexahydrate ( $\text{Eu}(\text{NO}_3)_3 \cdot 6\text{H}_2\text{O}$ , 99.9%, Sigma-Aldrich), terbium (III) nitrate pentahydrate ( $\text{Tb}(\text{NO}_3)_3 \cdot 5\text{H}_2\text{O}$ , 99.9%, Sigma-Aldrich); cerium dioxide ( $\text{CeO}_2$ ,  $\geq 99.9\%$ , Sigma-Aldrich), ethylene glycol ( $\text{C}_2\text{H}_6\text{O}_2$ , 99.5%, Roth); citric acid ( $\text{C}_6\text{H}_8\text{O}_7$ , 99.5%, Chempur); benzoic acid ( $\text{C}_7\text{H}_6\text{CO}_2$ , 99.5%, Sigma-Aldrich), oxalic acid ( $\text{C}_2\text{H}_2\text{CO}_4$ , 98%, Sigma-Aldrich), lauric acid ( $\text{C}_{12}\text{H}_{24}\text{O}_2$ , 99%, Sigma-Aldrich), malonic acid ( $\text{C}_3\text{H}_4\text{O}_4$ , 99%, Sigma-Aldrich), succinic acid ( $\text{C}_4\text{H}_6\text{O}_4$ , 99%, Sigma-Aldrich), tartaric acid ( $\text{C}_4\text{H}_6\text{O}_6$ , 99.5%, Sigma-Aldrich), 1,3,5-benzentricarboxylic acid ( $\text{C}_9\text{H}_6\text{O}_6$ , 98%, Sigma-Aldrich), 4-methylbenzoic acid ( $\text{C}_8\text{H}_8\text{O}_2$ , 98%, Sigma-Aldrich), 4-dimethylaminobenzoic acid ( $\text{C}_9\text{H}_{11}\text{NO}_2$ , 98%, Sigma-Aldrich), 4-biphenylacetic acid ( $\text{C}_{14}\text{H}_{12}\text{O}_2$ , 98%, Sigma-Aldrich), terephthalic acid ( $\text{C}_6\text{H}_4$ -1,4-( $\text{CO}_2\text{H}$ )<sub>2</sub>, 98%, Sigma-Aldrich), sodium hydrogen carbonate ( $\text{NaHCO}_3$ , 99.7%, Sigma-Aldrich), sodium hydroxide ( $\text{NaOH}$ , 98%, Sigma-Aldrich), hydrochloric acid ( $\text{HCl}$ , 37%, Sigma-Aldrich), nitric acid ( $\text{HNO}_3$ , 68%, Sigma-Aldrich), polyvinyl alcohol (PVA,  $M_w$  89,000-98,000, Sigma-Aldrich).

### 2.2. Synthesis of Mg-Al non-substituted and lanthanide-substituted LDHs by co-precipitation method

LDH samples were synthesized by adding a mixture of  $\text{Mg}(\text{NO}_3)_2 \cdot 6\text{H}_2\text{O}$  and  $\text{Al}(\text{NO}_3)_3 \cdot 9\text{H}_2\text{O}$  (with molar ratio of 3:1) drop by drop to the solution of  $\text{NaHCO}_3$  (1.5 M). pH of the resulting solution was measured and kept at 8-9 using  $\text{NaOH}$  (2 M) under continuous stirring. To separate the slurry from the solution, the mixture was centrifuged at 3000 rpm for 2 min. The precipitated LDH was washed with distilled water and centrifuged again. Process was repeated four times depending on the sample. The formed LDH was dried at 75-80 °C for 12 h. Synthesis of  $\text{Mg}_3\text{Al}_{1-x}\text{Ce}_x$  compounds was performed in the same way as  $\text{Mg}_3\text{Al}$  LDH, keeping the pH of the solution about 10 during the synthesis and using  $\text{Ce}(\text{NO}_3)_3 \cdot 6\text{H}_2\text{O}$  as cerium source.

### 2.3. Synthesis of Mg-Al non-substituted and lanthanide-substituted LDHs by sol-gel method

The  $\text{Mg}_3\text{Al}$  and  $\text{Mg}_3\text{Al}_{1-x}\text{Nd}_x$ ,  $\text{Mg}_3\text{Al}_{1-x}\text{Eu}_x$ , and  $\text{Mg}_3\text{Al}_{1-x}\text{Tb}_x$  LDH specimens were prepared by sol-gel technique using metal nitrates  $\text{Mg}(\text{NO}_3)_2 \cdot 6\text{H}_2\text{O}$ ,  $\text{Al}(\text{NO}_3)_3 \cdot 9\text{H}_2\text{O}$ ,  $\text{Nd}(\text{NO}_3)_3 \cdot 6\text{H}_2\text{O}$ ,  $\text{Eu}(\text{NO}_3)_3 \cdot 6\text{H}_2\text{O}$ , and  $\text{Tb}(\text{NO}_3)_3 \cdot 5\text{H}_2\text{O}$  dissolved in 50 mL of deionized water as starting materials. To the obtained mixture, the 0.2 M solution of citric acid was added. The resulted solution was additionally stirred for 1 h at 80 °C. Finally, 2 mL of ethylene glycol was added with continued stirring at 150 °C. During the evaporation of solvent, the transformations from sols to the gels occurred. The synthesized precursor gels were dried at 105 °C for 24 h. The mixed metal oxides (MMO) were obtained by heating the gels at 650 °C for 4 h. LDHs were fabricated by reconstruction of MMO in deionized water at 80 °C for 6 h. The commercial hydroxide PURAL MG63HT powder (Brunsbüttel, Germany) which is chemically  $\text{Mg}_3\text{Al}$  LDH intercalated with  $\text{CO}_3^{2-}$  was also analysed for comparison.

### 2.4. Modification of Mg-Al non-substituted and lanthanide - substituted LDHs anions

The inorganic anions were exchanged according to the following [153, 154] experiments. The decarbonation of  $\text{CO}_3$ -LDHs was conducted as described in [153]. The 0.5 g of  $\text{CO}_3$ -LDH was added into 500 mL NaCl-HCl mixed solution (concentration: 1M for NaCl and 3.3 mM for HCl). The 0.048 mol  $\text{HNO}_3$  was mixed with 200 ml decarbonated water at 65°C then 0.024 mol  $\text{Mg}_3\text{Al}$  LDH was added [154]. After purging with  $\text{N}_2$ , the vessel was sealed and stirred for 24 h at ambient temperature. The suspension was filtered, washed with decarbonated water and acetone for several times, the product was dried at 40°C for 12 h.

$\text{Mg}_3\text{Al}$  and  $\text{Mg}_3\text{Al}_{1-x}\text{Eu}_x$ , benzoate, oxalate, laurate, malonate, succinate, tartrate, terephthalate, 1,3,5-benzentricarboxylate (BTC), 4-methylbenzoate (MB), 4-dimethylaminobenzoate (DMB) and 4-biphenylacetate (BPhAc), further,  $\text{Mg}_3\text{Al}$  and  $\text{Mg}_3\text{Al}_{1-x}\text{Eu}_x$ ,  $\text{Mg}_3\text{Al}_{1-x}\text{Tb}_x$  terephthalate were synthesized using anion exchange technique. For this, 2 mmol of  $\text{Mg}_3\text{Al}$  or  $\text{Mg}_3\text{Al}_{1-x}\text{Eu}_x$ ,  $\text{Mg}_3/\text{Al}_{1-x}\text{Tb}_x$  was immersed in the solution of disodium/sodium organic compounds with 1.5 molar excess amounts in comparison with LDHs. Next, the solution was stirred at room temperature for 24 h. After filtration and washing with deionized water and acetone, the synthesis product was dried at 40 °C for 12 h.

## 2.5. Preparation of sol LDH suspension for dip-coating

Mg<sub>3</sub>Al LDH coatings were synthesised using sol-gel method in different solutions. 0.5 g of LDH was mixed with 1 g of PVA in distilled water. LDH suspensions were deposited on silicon and stainless-steel substrates using the dip-coating technique by a single dipping process and the deposited film was dried before new layer is added.

## 2.6. Characterization techniques

X-ray diffraction analysis of synthesized compounds was performed with MiniFlex II diffractometer (Rigaku) using a primary beam Cu K $\alpha$  radiation ( $\lambda = 1.541838 \text{ \AA}$ ). The  $2\theta^\circ$  angle of the diffractometer was graduated from 8 to  $80^\circ$  in steps of  $0.02^\circ$ , with the measuring time of 0.4 s per step. Fourier-transform infrared spectroscopy (FT-IR) spectra were recorded using Bruker-Alpha FT-IR spectrometer in the range of  $4000\text{--}400 \text{ cm}^{-1}$ . The surface morphological features were characterized using a scanning electron microscope (SEM) Hitachi SU-70. The luminescent properties were investigated using Edinburgh Instruments FLS 980 spectrometer. The spectrometer was equipped with VUV monochromator VM504 from Acton Research Corporation (ARC) and deuterium lamp as an excitation source. Thermal analysis was carried out using a simultaneous thermal analyzer 6000 (Perkin-Elmer) in air atmosphere at scan rate of  $10 \text{ }^\circ\text{C}/\text{min}$  and the temperature range from  $30 \text{ }^\circ\text{C}$  up to  $900 \text{ }^\circ\text{C}$ . The particle and anion dimension sizes were calculated using the ImageJ and Avogadro programmes. The phase identification data, as well as crystal structure has been taken from databases using Match! software, version 3.8.1.143. The amount of carbonate in the synthesized samples was calculated from the  $\text{M}^{2+}/\text{M}^{3+}$  atomic ratios, assuming that carbonate is the only charge balancing interlayer anion. The water content in the formula was determined from the results of TG analyses. The chemical composition was defined to be  $[\text{Mg}_{0.75}\text{Al}_{0.25}(\text{OH})_2] (\text{CO}_3)_{0.125} \cdot 4\text{H}_2\text{O}$ . Dip-coating procedure was completed using instrument KSV D, KSV Instruments Ltd. Dip-coating parameter were set at immersion speed of  $85 \text{ mm}/\text{min}$ , keeping in solution for 30 second and withdrawing from solution at a speed of  $40 \text{ mm}/\text{min}$ . The roughness of Mg<sub>3</sub>Al LDH films was estimated using atomic force microscope (AFM) BioscopeII/Catalyst. The scan asyst based on peak force tapping mode equipped with a wafer of silicon nitride probe asyst at air AFM tip was used for imaging. Surface root mean square (RMS) values were calculated using MATLAB R2015b software.

### 3. RESULTS AND DISCUSSION

3.1. A comparative study of co-precipitation and sol-gel synthetic approaches to fabricate cerium-substituted Mg-Al layered double hydroxides

First step in this study was to investigate and to compare the  $Mg_3Al$  and  $Mg_3Al_{1-x}Ce_x$  LDHs synthesized by co-precipitation and sol-gel methods. In this novel aqueous sol-gel processing route, the LDHs were obtained as a result of decomposition of the precursor gels at 650 °C followed by reconstruction of the intermediate crystalline MMO powders in distilled water. These synthesis methods were successfully applied for the production of cerium-substituted  $Mg_3Al_{1-x}Ce_x$  LDHs with the substitution rate from 0.05 to 10 mol%.

#### 3.1.1. Synthesis and characterization by co-precipitation method

The  $Mg_3Al$  and  $Mg_3Al_{1-x}Ce_x$  LDHs samples were characterized by X-ray diffraction (XRD) measurements. The XRD pattern of the  $Mg_3Al$  LDH synthesized by co-precipitation method was found to be essentially similar to that of the commercial hydrotalcite PURAL MG63HT (Fig. 4).

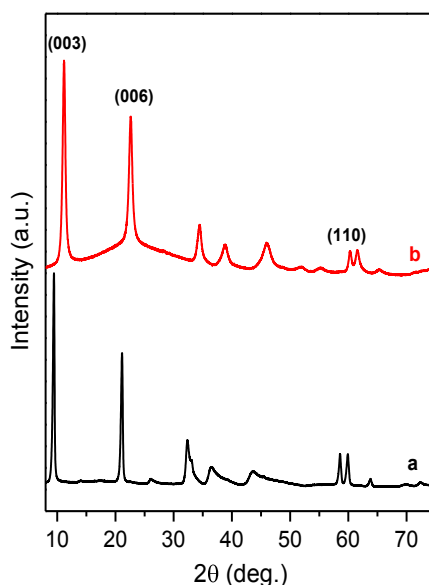


Fig. 4. XRD patterns of the (a)  $Mg_3Al$  LDH synthesized by co-precipitation method with comparison of commercial hydrotalcite (b) PURAL MG63HT.

In the XRD patterns of all  $Mg_3Al$  and  $Mg_3Al_{1-x}Ce_x$  LDHs phases are indexed on a hexagonal unit cell with a 3R rhombohedral symmetry and the most intensive diffraction lines are determined at  $2\theta$  angle of about  $10^\circ$  (003),  $23^\circ$  (006) and  $60.2^\circ$  (110). The XRD patterns of cerium substituted LDHs represented at Fig. 5 showing that the intensity of the peaks increases with the 5 mol% cerium amount and decreases at higher amount of cerium ( $Mg_3Al_{1-x}Ce_x$  10 mol%).

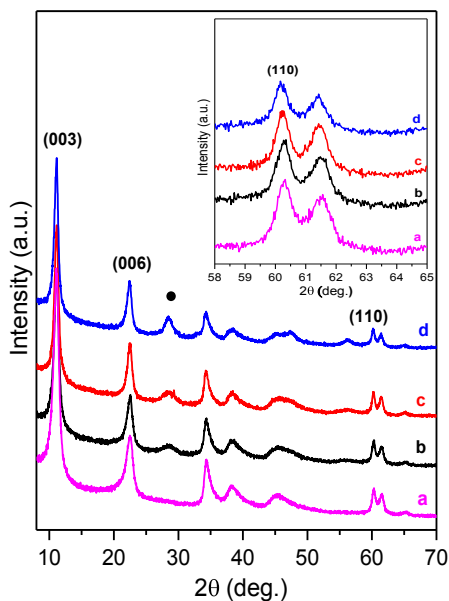


Fig. 5. XRD patterns of the  $Mg_3Al$  (a) and  $Mg_3Al_{1-x}Ce_x$  LDHs synthesized by co-precipitation method: (b) 5 mol% of Ce, (c) 7.5 mol% of Ce, (d) 10 mol% of Ce. Inset: the XRD patterns in the range of (110) diffraction reflections. The impurity phase is marked: ● -  $CeO_2$ .

The shift of the (110) reflection peak to a lower  $2\theta$  range certainly suggests incorporation of  $Ce^{3+}$  ion in metal hydroxide layers of the LDHs. Furthermore, at the same time, the broad diffraction peaks at  $2\theta \approx 29.5^\circ$  that can be attributed to a  $CeO_2$  phase are seen in the XRD patterns of the cerium-substituted LDHs.

The lattice parameters of  $M_3Al$  and  $Mg_3Al_{1-x}Ce_x$  LDH synthesised by co-precipitation method are listed in Table 2. The lattice parameter  $a = 2d$  (110) corresponds to an average cation-cation distance calculated from 110 reflections in brucite – like layers, the  $c$  parameter  $3/2 [d(003) + 2d(006)]$  corresponds to three times the thickness of  $d_{003}$  parameter, and can be affected



by amount of interlayer water and anions, metal molar ratio and the crystallinity of the samples. As seen, the lattice parameter values ( $a$  and  $c$ ) are slightly different for different samples. The large ionic radius of  $\text{Ce}^{3+}$  (1.01 Å) related an expansion in the cation-cation distance, which replace  $\text{Al}^{3+}$  ions (0.53 Å) [155] in the brucite-like layers.

Table 2. Lattice parameters of  $\text{Mg}_3\text{Al}$  and  $\text{Mg}_3\text{Al}_{1-x}\text{Ce}_x$  LDH synthesised by co-precipitation method.

Sample	d (003), Å	d (006), Å	d (110), Å	Lattice parameters (Å)	
				$a$	$c$
$\text{Mg}_3\text{Al}$	7.9627	3.9482	1.5344	3.067	23.878
$\text{Mg}_3\text{Al}_{1-x}\text{Ce}_x$ 5mol%	7.9463	3.9479	1.5347	3.068	23.838
$\text{Mg}_3\text{Al}_{1-x}\text{Ce}_x$ 7.5mol%	7.9541	3.9510	1.5356	3.070	23.852
$\text{Mg}_3\text{Al}_{1-x}\text{Ce}_x$ 10mol%	7.9634	3.9609	1.5376	3.074	23.880

The XRD analysis of heat-treated samples revealed formation of poorly crystalline magnesium oxide with peaks at  $2\theta = 36^\circ$ ,  $43^\circ$  and  $63^\circ$ . This is a consequence of the incorporation of aluminium in the MgO framework appears at above  $400^\circ\text{C}$ , resulting in formation of a mixed-metal oxide (MMO). During the calcination of LDH, the temperature should be higher than that of the layer collapse but lower than that of formation of cubic spinel phase ( $\text{MgAl}_2\text{O}_4$ ) appears near  $1000^\circ\text{C}$ . Calcination temperature is usually set between  $200$ - $600^\circ\text{C}$  [5]. The XRD patterns of the  $\text{Mg}_3\text{Al}$  (Fig. 6) and the  $\text{Ce}^{3+}$ -substituted (Fig. 4) LDHs calcined at  $650^\circ\text{C}$  show the formation of poorly crystalline MgO. However, the XRD patterns of the samples containing cerium exhibited also reflections of a  $\text{CeO}_2$  phase.

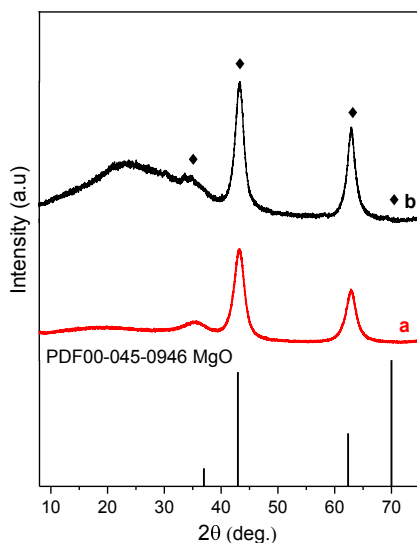


Fig. 6. XRD patterns of MMO of  $Mg_3Al$  and commercial etalon sample – Pural MG63HT both calcined at  $650^\circ C$ ; ◆ MgO.

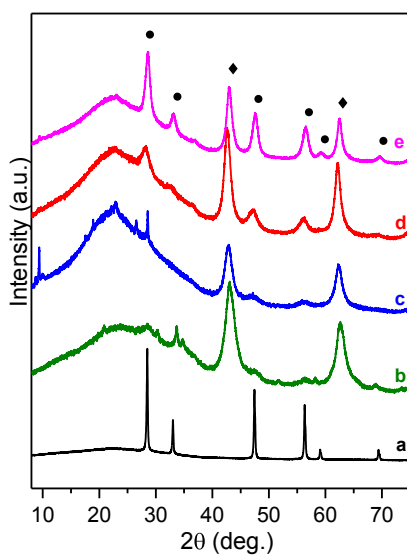


Fig. 7. XRD patterns of  $Mg_3Al_{1-x}Ce_x$  LDHs synthesized by co-precipitation method and calcined at  $650^\circ C$ : (a)  $CeO_2$ , (b) 1 mol% of Ce, (c) 5 mol% of Ce, (d) 7.5 mol% of Ce, (e) 10 mol% of Ce. The crystalline phases are marked: ◆ - MgO; ● -  $CeO_2$ .

The LDH are well known for their ability to regenerate the original layered structure when put in contact with pure water or an anion containing aqueous solution. This property of LDH is known as memory effect [77, 156]. The XRD patterns of  $Mg_3Al$  and  $Mg_3Al_{1-x}Ce_x$  LDH obtained after the hydration process at 80 °C for 6 h under stirring are shown in Figs. 8 and 9, respectively. It is possible to note that the recovered sample shows the typical LDH structure (memory effect), which indicates that the predominant phase in aqueous media is the highly hydroxylated LDH structure. The XRD patterns of reconstructed  $Mg_3Al_{1-x}Ce_x$  samples (Fig. 9) confirm transformation of mixed-metal oxides into LDH. The calcined LDH with a higher concentration of cerium, however, demonstrate less regeneration. The XRD patterns clearly show the formation of partially amorphous reaction products. The considerable amount of the amorphous part of the MMO product which contribute to a very broad peak of the XRD background remains uncrystallised. Furthermore, additional broad diffraction lines could be seen in these XRD patterns.

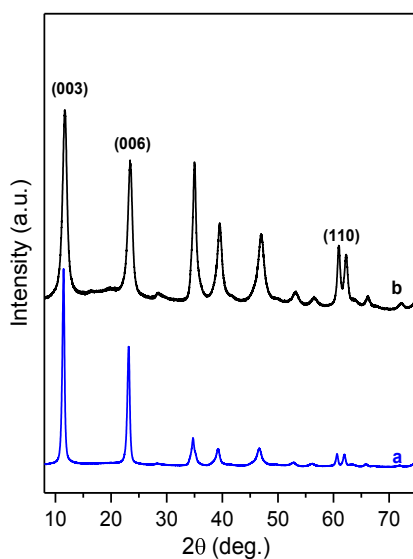


Fig. 8. XRD patterns of reconstructed of  $Mg_3Al$  LDH (a) and commercial etalon sample – Pural MG63HT (b).

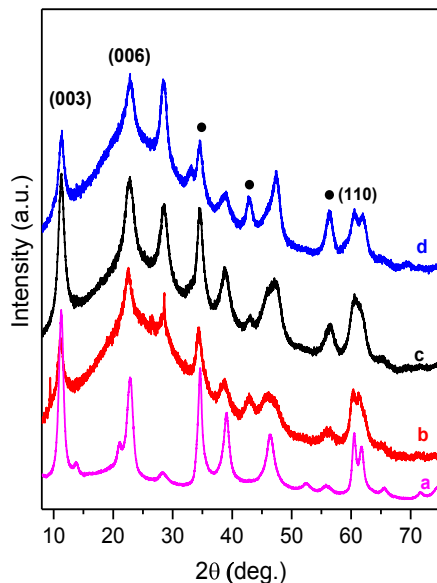


Fig. 9. XRD patterns of  $Mg_3Al_{1-x}Ce_x$  LDHs synthesized by co-precipitation method and Reconstructed from MMO: (a) 1 mol% of Ce, (b) 5 mol% of Ce, (c) 7.5 mol% of Ce, (d) 10 mol% of Ce; ● -  $CeO_2$ .

### 3.1.2. Synthesis and characterization by sol-gel method

The XRD patterns of sol-gel derived  $Mg_3Al$  and  $Mg_3Al_{1-x}Ce_x$  samples are shown in Figs. 10 and 11, respectively.

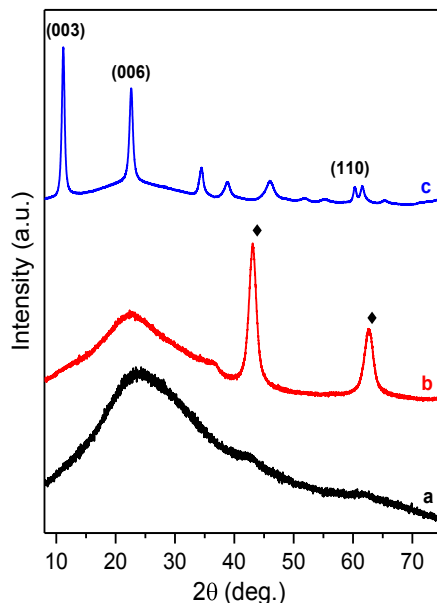


Fig. 10. XRD patterns of Mg-Al-O precursor gel (a), MMO obtained at 650 °C (b) and sol-gel derived Mg<sub>3</sub>Al LDH (c). The crystalline phases are marked: ◆ - MgO.

Evidently, only amorphous Mg-Al-O gel has formed during the initial stage of sol-gel processing of LDHs. After heat-treatment of Mg-Al-O precursor gel at 650 °C, a high crystalline MMO has formed (Fig. 10). The obtained MMO powdered samples were treated in water at 80 °C for 6 h under stirring. The XRD patterns of obtained specimens confirmed the formation of monophasic Mg<sub>3</sub>Al LDH during the reconstruction process in distilled water.

The formation of Mg<sub>3</sub>Al<sub>1-x</sub>Ce<sub>x</sub> LDH from the sol-gel derived powders does not depend on the Ce concentration in the samples (Fig. 11). The XRD patterns of the reconstructed LDHs powders demonstrate the sharp diffraction lines associated with an LDH crystalline phase only. No other crystalline phases have been detected. The (110) reflections of the LDHs are regularly shifted to a lower 2θ range as the cerium content is increased. The observed shift of the (110) reflections displacement signal toward lower values of 2θ containing different concentration of Ce<sup>3+</sup> can be an evidence of isomorphic incorporation of lanthanide ion in LDH.

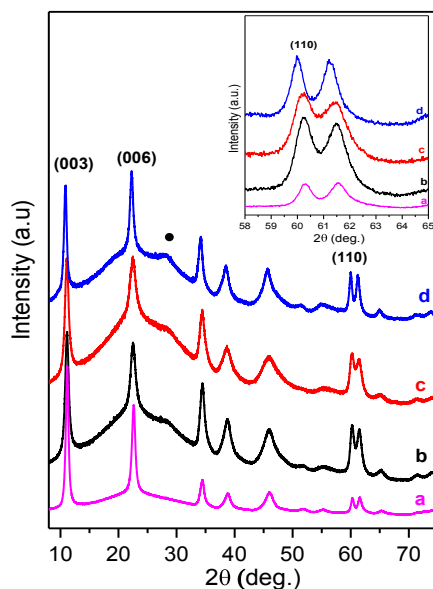


Fig. 11. XRD patterns of the  $Mg_3Al_{1-x}Ce_x$  LDHs synthesized by sol-gel method using reconstruction approach: (a)  $Mg_3Al$ , (b) 5 mol% of Ce, (c) 7.5 mol% of Ce, (d) 10 mol% of Ce. Inset: the XRD patterns in the range of (110) diffraction reflections. The impurity phase is marked: ● -  $CeO_2$ .

The lattice parameters of  $Mg_3Al$  and  $Mg_3Al_{1-x}Ce_x$  samples were also calculated (Table 3). As a result of the cerium substitution, the  $a$  parameter grows. Besides, the  $c$  parameter increases as well. The effect of increase of both lattice parameters induced by this isovalent Al-to-Ce substitution is qualitatively the same as that in the case of an increase of the  $Mg_3Al$  cation ratio since  $Mg^{2+}$  is bigger than  $Al^{3+}$ .

It is evident from XRD results that the co-precipitation and the sol-gel methods provide a gradual Al-to-Ce substitution, although some amount of Ce does not incorporate into the LDH layers and crystallize as cerium oxide. Also, the sol-gel method of the LDH preparation provides higher substitution rates. In the case of small-rate substitutions, both methods give similar results.

Table 3. Lattice parameters of  $Mg_3Al$  and  $Mg_3Al_{1-x}Ce_x$  LDH synthesised by sol-gel method.

Sample	d (003), Å	d (006), Å	d (110), Å	Lattice parameters (Å)	
				<i>a</i>	<i>c</i>
$Mg_3Al$	7.9181	3.9300	1.5346	3.067	23.744
$Mg_3Al_{1-x}Ce_x$ 5mol%	7.9476	3.9483	1.5351	3.069	23.832
$Mg_3Al_{1-x}Ce_x$ 7.5mol%	7.9683	3.9499	1.5376	3.070	23.894
$Mg_3Al_{1-x}Ce_x$ 10mol%	8.1418	3.9897	1.5411	3.080	24.415

### 3.1.3. Characterization of synthesized LDHs

The results of the thermogravimetric (TG) analysis of the LDHs synthesized by two different methods are shown in Figs. 12-15.

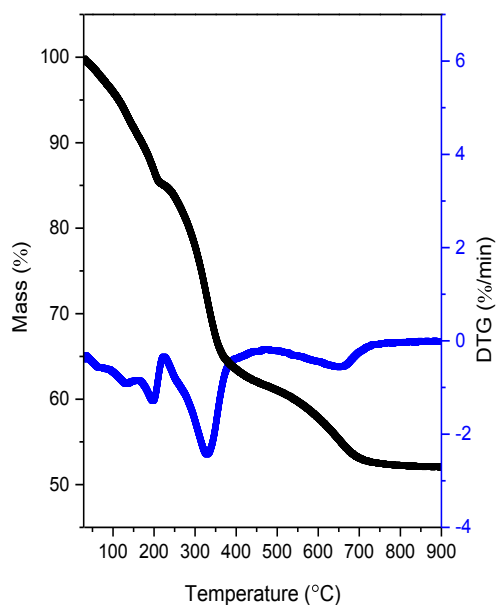


Fig. 12. TG-DTG curves of the  $Mg_3Al$  LDH synthesised by co-precipitation method.

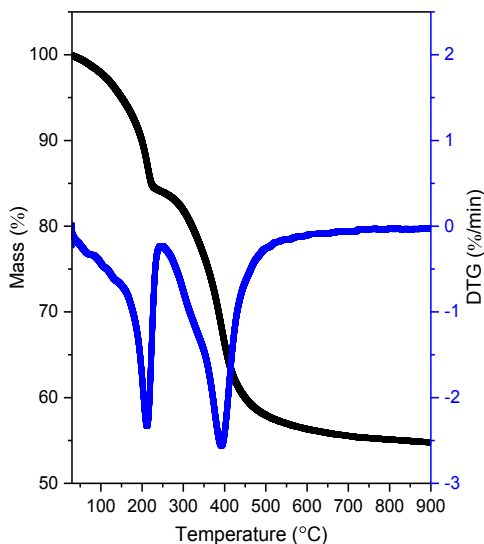


Fig. 13. TG-DTG curves of the  $Mg_3Al$  LDH synthesised by sol-gel method.

The initial mass loss was observed in the temperature ranges of 30-220 °C (16%) for  $Mg_3Al$  synthesised by co-precipitation method and 30-210 °C (15%) for the  $Mg_3Al$  prepared by sol-gel because of evolution of the adsorbed water. The mass loss in the temperature range of 340 – 650 °C for both samples (27% for co-precipitation and 30% sol-gel synthesised  $Mg_3Al$  LDHs) is due to dehydroxylation of the layers of the layered structure. Above 650 °C the brucite-type structure collapses and a solid solution of mixed spinel ( $MgAl_2O_4$ ) and  $MgO$ , or  $Al_2O_3$  and  $MgO$  is formed.

The TG-DTA curves of synthesised  $Mg_3Al_{1-x}Ce_x$  10 mol% LDHs are shown in Figs. 14 and 15, respectively. The initial two steps mass loss about 10% and 20% was observed in the temperature range of 30-200 °C for the  $Mg_3Al_{1-x}Ce_x$  10 mol% LDH prepared by co-precipitation method and one step mass loss about 16% is observed for of  $Mg_3Al_{1-x}Ce_x$  10 mol% LDH synthesised by sol-gel method. These changes in mass are also due to of evolution of adsorbed water. The main decomposition of LDHs appears in the temperature range of 318-470 °C (the mass loss 24-46%). The last mass loss step (470-650 °C) is due to the dehydroxylation and decomposition of the impurities of interlayer anions. As seen, the thermal behaviour of synthesized LDH is not dependent on the cerium substitution in the structure.



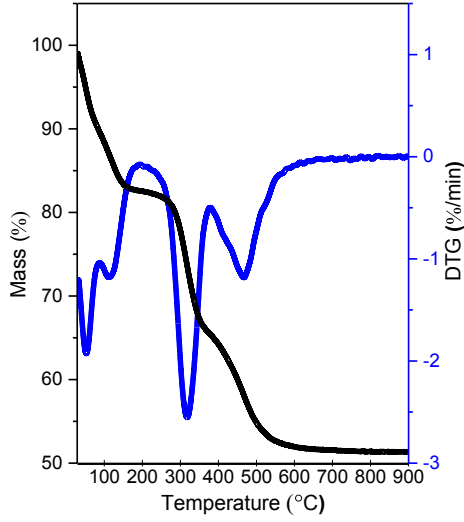


Fig. 14. TG-DTG curves of  $Mg_3Al_{1-x}Ce_x$  10 mol% LDH synthesised by coprecipitation method.

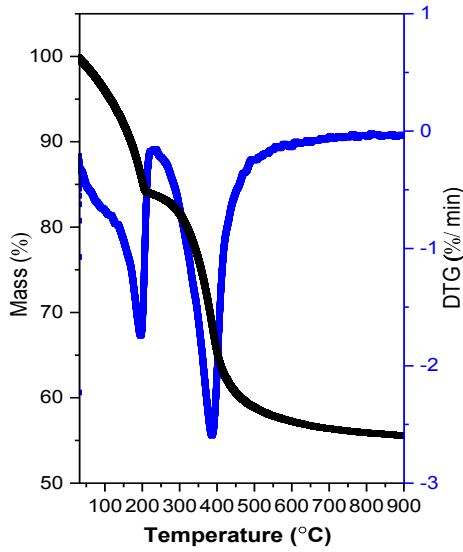


Fig. 15. TG-DTG curves of  $Mg_3Al_{1-x}Ce_x$  10 mol% LDH synthesised by sol-gel method.

The morphology of the  $Mg_3Al$  and  $Mg_3Al_{1-x}Ce_x$  LDHs synthesized by co-precipitation and sol-gel methods were examined using scanning electron microscopy (SEM) (Figs. 16-18).

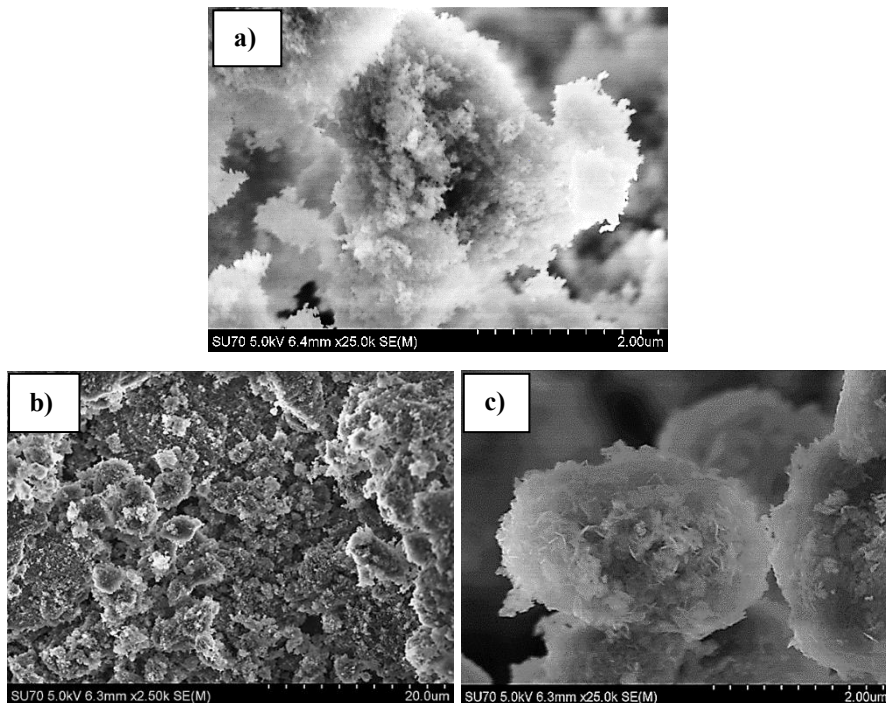


Fig. 16. SEM micrographs of  $Mg_3Al$  LDH(a), MMO (b) synthesized by co-precipitation method and  $Mg_3Al$  LDH (c) synthesized using sol-gel method.

The SEM micrographs of the  $Mg_3Al$  LDHs synthesized by co-precipitation and sol-gel methods (Fig. 16) demonstrate that the surfaces of both samples are composed of the agglomerated small plate-like particles of  $\sim 50$ - $100$  nm in length. After calcination of  $Mg_3Al$  LDH at  $650$  °C, the network of spherical nanoparticles has formed. Reconstruction of these powders results in formation of plate-like particles. The surface morphology of the  $Ce^{3+}$ -substituted samples is very similar for all the specimens independent of the substitution rate. The representative SEM micrographs of the  $Mg_3Al_{1-x}Ce_x$  1 mol% and  $Mg_3Al_{1-x}Ce_x$  10 mol% samples are presented in Figs. 17 and 18. The  $Mg_3Al_{1-x}Ce_x$  synthesized by co-precipitation method are composed of aggregated small fibrous plate-like particles. The sol-gel derived  $Mg_3Al_{1-x}Ce_x$  LDHs consist of the hexagonally shaped particles varying in size from

approximately 150 to 270 nm. The good connectivity between the grains has been also observed. These nanograins show tendency to form larger agglomerates. Overall, nanocrystalline nature of powders with the narrow size distribution of crystallites is observed for all the obtained LDH samples. The characteristic feature of synthesized LDHs is the formation of plate-like particles with hexagonal shape.

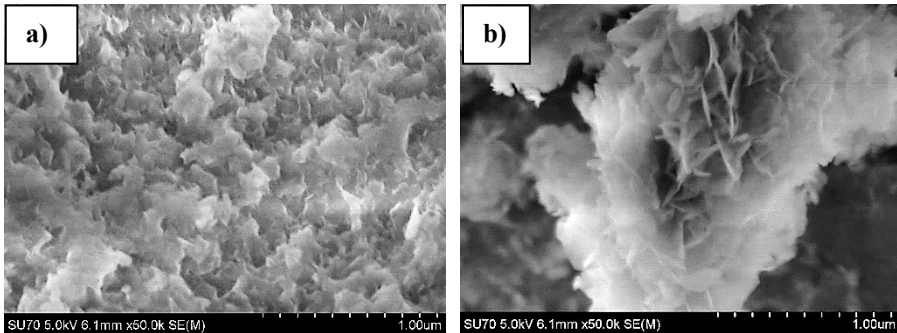


Fig. 17. SEM micrographs of Mg<sub>3</sub>Al<sub>1-x</sub>Ce<sub>x</sub>1 mol% LDHs synthesized by co-precipitation (a) and sol-gel (b) methods.

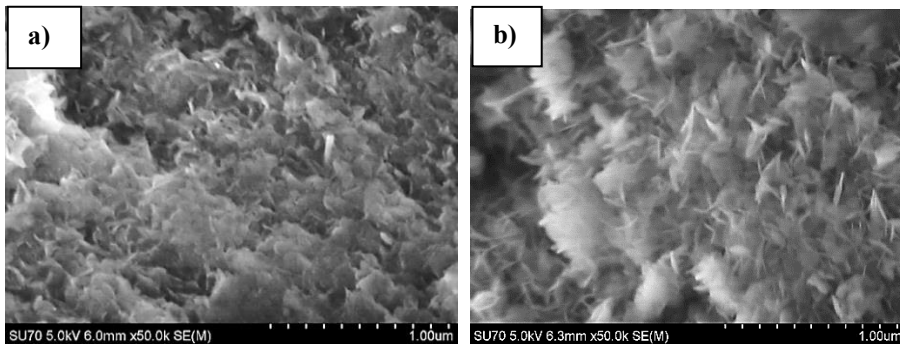


Fig. 18. SEM micrographs of Mg<sub>3</sub>Al<sub>1-x</sub>Ce<sub>x</sub>10 mol% LDHs synthesized by co-precipitation (a) and sol-gel (b) methods.

### 3.1.4. Luminescent properties

The fluorescence spectra of  $\text{Mg}_3\text{Al}_{1-x}\text{Ce}_x$  LDHs synthesized by and sol-gel methods are presented in Figs. 19 and 20, respectively. All powders were excited at 340 nm for taking the emission spectra. The major emission lines for the samples obtained by co-precipitation method are peaked at  $\sim 370$ - $390$  nm. The broad bands are attributed to  $[\text{Xe}]5d^1$ - $[\text{Xe}]5f^1$  transition of  $\text{Ce}^{3+}$  ions [157]. Surprisingly, the highest intensity of  $^5\text{D}_0 \rightarrow ^7\text{F}_2$  transition was observed for  $\text{Mg}_3\text{Al}_{1-x}\text{Ce}_x$  0.05 mol% specimen. It turned out that emission intensity decreases with increasing concentration of  $\text{Ce}^{3+}$  up to 1 mol%. The emission maximum was also slightly shifted towards a red spectral region when more  $\text{Ce}^{3+}$  was introduced into the host lattice.

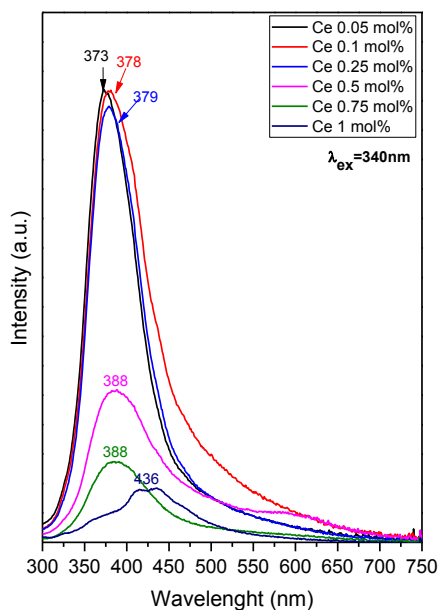


Fig. 19. Emission spectra for  $\text{Mg}_3\text{Al}_{1-x}\text{Ce}_x$  LDHs synthesized by co-precipitation method.

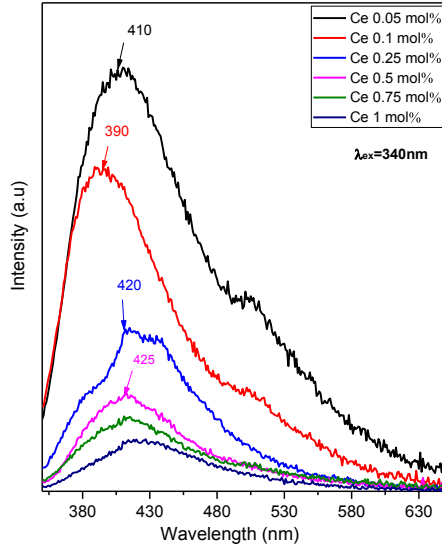


Fig. 20. Emission spectra for  $\text{Mg}_3\text{Al}_{1-x}\text{Ce}_x$  LDHs synthesized by sol-gel method.

This is in a good agreement with the results obtained in the  $\text{Ce}^{3+}$ -doped garnet-type phosphors. In the emission spectra of the sol-gel derived  $\text{Mg}_3\text{Al}_{1-x}\text{Ce}_x$  samples (Fig. 20), the bands are broader and more intensive. Moreover, the maximum of the emission of the LDHs synthesized using sol-gel technique is red shifted (390-430 nm) in comparison with the LDH phosphors prepared by co-precipitation method. The excitation and emission band positions depend on the dopant composition and concentration and affected by the host material and its stoichiometry, crystallinity, particle size, surface defects [158].

Summarizing, the novel an aqueous sol-gel synthesis approach for the fabrication of LDHs was developed. It was found that the conversion during the reconstruction of sol-gel derived MMO into LDH does not depend on the concentration of cerium. The proposed sol-gel synthesis route for LDHs has some benefits over the co-precipitation method such as simplicity, high homogeneity and good crystallinity of the end synthesized products.

## 3.2. Sol-gel synthesis and characterization of europium-substituted Mg-Al layered double hydroxides

### 3.2.1. Modification of LDH and characterization

All synthesized europium-substituted Mg-Al-O gels were amorphous powders. The XRD patterns of sol-gel derived and calcined at 650 °C  $\text{Mg}_3\text{Al}$  and  $\text{Mg}_3\text{Al}_1\text{Eu}_x$  (1–10 mol%) samples are shown in Fig. 21. According to the XRD patterns the heat-treated  $\text{Mg}_3\text{Al}_1\text{Eu}_x$  gels resulted in high crystalline MMO samples. The mixed-metal oxides transformed fully to LDH structures during reconstruction independent on the  $\text{Eu}^{3+}$  substitutional level (Fig. 22). However, the monophasic  $\text{Mg}_3\text{Al}_{1-x}\text{Eu}_x$  LDHs were obtained with amount of Eu less than 5 mol%. With increasing concentration of europium till 10 mol% the amount of side  $\text{Eu}(\text{OH})_3$  phase (PDF96-403-1477) has formed. The formation of  $\text{Eu}(\text{OH})_3$  is mainly due to the larger ionic radius of  $\text{Eu}^{3+}$  ions (1.08 Å) in comparison of ionic radius of  $\text{Al}^{3+}$  ions (0.53 Å) [155]. The  $\text{Eu}^{3+}$  ions taking up the octahedral positions of  $\text{Al}^{3+}$  ions led to the deformation of crystal lattice, and the excess  $\text{Eu}^{3+}$  ions in high basic condition crystallized as  $\text{Eu}(\text{OH})_3$ .

The shift of the (110) reflections displacement signal toward lower values of  $2\theta$  containing different concentration of  $\text{Eu}^{3+}$  lanthanide ion in LDH was observed. The calculated lattice parameters represented at Table 4. The values of parameter  $a$  confirm the  $\text{Al}^{3+}$  ions substitution by  $\text{Eu}^{3+}$  ions in the LDH host lattice.

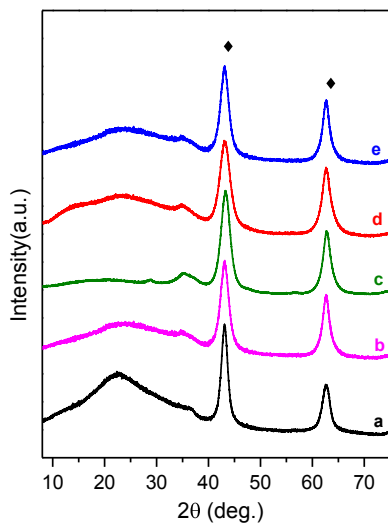


Fig. 21. XRD patterns of  $Mg_3Al_{1-x}Eu_x$  LDHs synthesized by sol-gel method and calcined at 650 °C: (a)  $Mg_3Al$ , (b) 1 mol% of Eu, (c) 5 mol% of Eu, (d) 7.5 mol% of Eu, (e) 10 mol% of Eu. The crystalline phase are marked: ♦ - MgO.

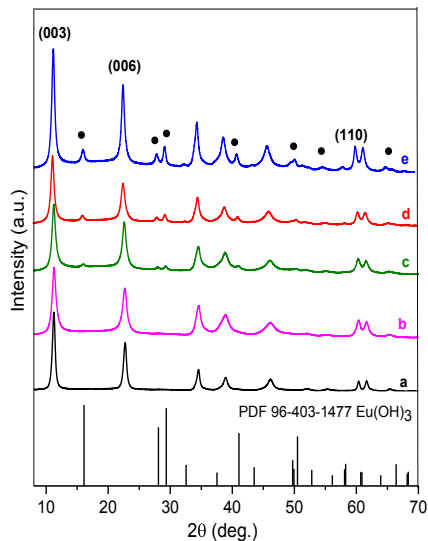


Fig. 22. XRD patterns of  $Mg_3Al_{1-x}Eu_x$  LDHs synthesized by sol-gel method using reconstruction approach: (a)  $Mg_3Al$ , (b) 1 mol% of Eu, (c) 5 mol% of Eu, (d) 7.5 mol% of Eu, (e) 10 mol% of Eu. The impurity phase is marked: • -  $Eu(OH)_3$ .

Table 4. Lattice parameters of  $M_3Al$  and  $Mg_3Al_{1-x}Eu_x$  LDH synthesised by sol-gel method.

Sample	d (003), Å	d (006), Å	d (110), Å	Lattice parameters (Å)	
				a	c
$Mg_3Al$	7.8431	3.9187	1.5331	3.065	23.519
$Mg_3Al_{1-x}Eu_x$ 1mol%	7.8667	3.9109	1.5327	3.064	23.590
$Mg_3Al_{1-x}Eu_x$ 5mol%	7.9483	3.9510	1.5346	3.068	23.834
$Mg_3Al_{1-x}Eu_x$ 7.5mol%	7.9811	3.9501	1.5398	3.070	23.890
$Mg_3Al_{1-x}Eu_x$ 10mol%	8.1221	3.9810	1.5402	3.080	24.420

The surface morphology of  $\text{Eu}^{3+}$  substituted LDH samples is very similar for all specimens independent of the substitutional level. Fig. 23 shows the representative SEM micrographs of sol-gel synthesized  $\text{Mg}_3\text{Al}_{1-x}\text{Eu}_x$  1mol% (Fig. 23a) and  $\text{Mg}_3\text{Al}_{1-x}\text{Eu}_x$  10mol% (Fig. 23b) samples. As seen, the  $\text{Mg}_3\text{Al}_{1-x}\text{Eu}_x$  LDHs are composed of small fibrous plate-like particles with hexagonal shape which are highly agglomerated. The particle size varies from approximately 300 to 700 nm. The surface morphological features of sample with higher europium content are more pronounced also consisting of hexagonally shaped nanostructures in LDHs.

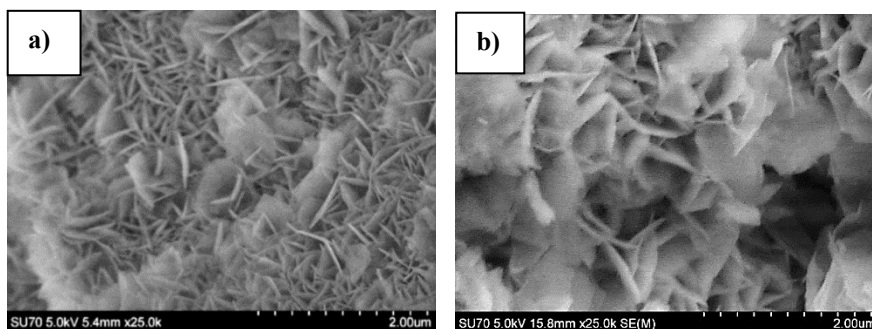


Fig. 23. SEM micrographs of  $\text{Mg}_3\text{Al}_{1-x}\text{Eu}_x$  1mol% (a) and  $\text{Mg}_3\text{Al}_{1-x}\text{Eu}_x$  10mol% (b) LDHs.

Thus, the XRD analysis results let us to conclude that the synthesized  $\text{Mg}_3\text{Al}_{1-x}\text{Eu}_x$  LDHs with low concentration of europium are high crystalline materials, since the XRD patterns contain very sharp diffraction lines attributable only to LDH phase. Interestingly, the formation of sol-gel based LDHs depends on the concentration of europium in the samples.

### 3.2.2. Modification of $\text{Mg}_3\text{Al}_1$ and $\text{Mg}_3\text{Al}_{1-x}\text{Eu}_x$ LDH

During the reconstruction of calcined sol-gel derived LDH precursors the main problem is the ionic carbonate which arising from atmospheric  $\text{CO}_2$ . Although the carbonate anion is adhesive held in the interlayer galleries and does not generally undergo direct anion-exchange, it is possible to replace it by treatment with an appropriate acid, which leads to liberation of carbon dioxide and incorporation of the conjugate base of the acid [159, 160]. In this work, we tried to exchange  $\text{CO}_3^{2-}$  to  $\text{OH}^-$ ,  $\text{Cl}^-$ ,  $\text{NO}_3^-$  anions and after this to intercalate terephthalate (TAL) [161] in to the LDH host of  $\text{Mg}_3\text{Al}$  and europium-containing  $\text{Mg}_3\text{Al}_{1-x}\text{Eu}_x$  by anion-exchange method. The XRD results are presented in Figs. 24-27.



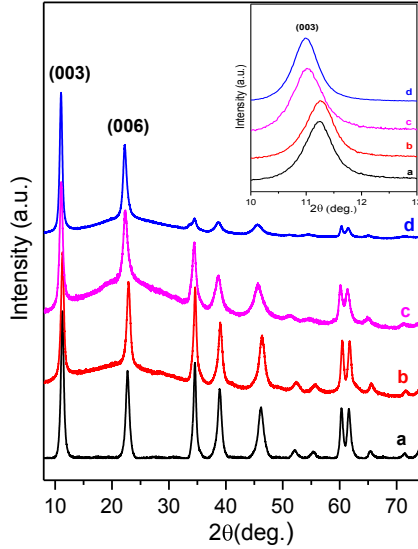


Fig. 24. XRD patterns of (a)  $\text{Mg}_3\text{Al-CO}_3$ , (b)  $\text{Mg}_3\text{Al-OH}$ , (c)  $\text{Mg}_3\text{Al-Cl}$  and (d)  $\text{Mg}_3\text{Al-NO}_3$  LDHs.

The diffraction reflections typical of LDH structure are seen in all the XRD patterns. The main compositions correspond to the single-phase  $\text{Mg}_3\text{Al-CO}_3$ ,  $\text{Mg}_3\text{Al-OH}$ ,  $\text{Mg}_3\text{Al-Cl}$  and  $\text{Mg}_3\text{Al-NO}_3$  layered double hydroxides. The XRD patterns of LDH phases obtained as a result of the anion exchanged reactions are shifted to the lower  $2\theta$  angle indicating a considerable increase in the basal spacing values as compared with the respective values for the main  $\text{Mg}_3\text{Al-CO}_3$ . As we can see the anion-exchanges for  $\text{Mg}_3\text{Al-CO}_3$  to  $\text{Mg}_3\text{Al-OH}$  has been not completed.

The XRD patterns of the  $\text{Mg}_3\text{Al-CO}_3$ ,  $\text{Mg}_3\text{Al-OH}$ ,  $\text{Mg}_3\text{Al-Cl}$ ,  $\text{Mg}_3\text{Al-NO}_3$  anion exchanged to TAL compound were prepared and characterized. The reflections in the XRD patterns (Figs. 25 and 26) are also in most of the cases shifted to the lower  $2\theta$  angle in comparison with non-exchanged samples. The calculated cell parameters are presented in Table 5.

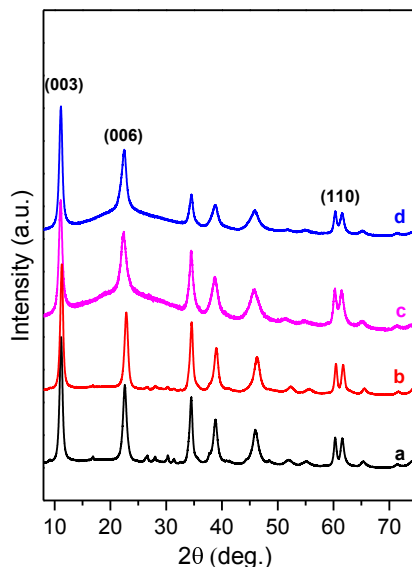


Fig. 25. XRD patterns of (a)  $\text{Mg}_3\text{Al-CO}_3\text{-TAL}$ , (b)  $\text{Mg}_3\text{Al-OH-TAL}$ , (c)  $\text{Mg}_3\text{Al-Cl-TAL}$  and (d)  $\text{Mg}_3\text{Al-NO}_3\text{-TAL}$  LDHs.

As seen from Fig. 26 the nitrate in  $\text{Mg}_3\text{Al-NO}_3$  is not exchanged by TAL like was observed in the rest cases. The (003) reflection is not shifted to the region of lower  $2\theta$  angle. The  $\text{CO}_3^{2-}$  and the  $\text{NO}_3^-$  anions have identical symmetry in free state, but their behavior as interlayer anions in LDHs is very different. The carbonate anion kept the orientation parallel to the hydroxide layers and this is more favorable of three oxygen atoms of the  $\text{CO}_3^{2-}$  anion. It can properly interact with hydroxyl groups of hydroxide layers by forming hydrogen bonds [85]. Unlike the  $\text{NO}_3^-$  has its molecular plane tilted orientation, which is making disorder of the 3R rhombohedral symmetry [43] within a hexagonal unit cell in LDH crystal structure. For this reason, probably it was more difficult to undergo inside of LDH host of terephthalate anion.

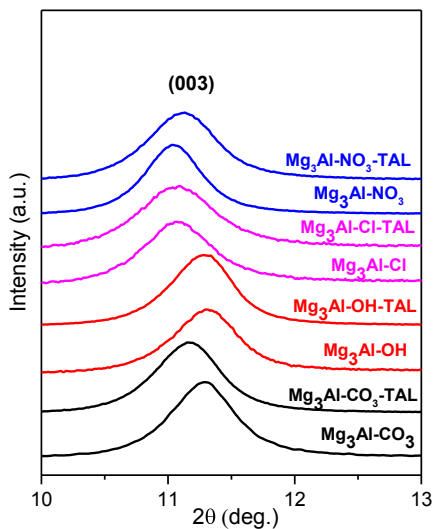


Fig. 26. The fragments of XRD patterns of LDHs with different intercalated anions.

Table 5. Lattice parameters of  $\text{Mg}_3\text{Al-CO}_3$  and exchanged with  $\text{OH}^-$ ,  $\text{Cl}^-$ ,  $\text{NO}_3^-$  inorganic anions following the intercalation of TAL LDHs.

Sample	d (003), Å	d (006), Å	d (110), Å	Lattice parameters (Å)	
				<i>a</i>	<i>c</i>
$\text{Mg}_3\text{Al-CO}_3$	7.9733	3.9718	1.5398	3.077	23.909
$\text{Mg}_3\text{Al-OH}$	7.9314	3.9621	1.5372	3.073	23.784
$\text{Mg}_3\text{Al-Cl}$	8.0444	4.0042	1.5353	3.069	24.123
$\text{Mg}_3\text{Al-NO}_3$	8.1191	4.0595	1.5415	3.083	24.345
$\text{Mg}_3\text{Al-CO}_3\text{-TAL}$	8.1326	4.0175	1.5431	3.085	24.387
$\text{Mg}_3\text{Al-OH-TAL}$	7.9770	3.9742	1.5378	3.074	23.921
$\text{Mg}_3\text{Al-Cl-TAL}$	7.9916	3.9637	1.5352	3.069	23.964
$\text{Mg}_3\text{Al-NO}_3\text{-TAL}$	7.9936	3.9968	1.5355	3.071	23.981

Next, europium-substituted  $Mg_3Al_{1-x}Eu_x$ -TAL LDHs with different amount of europium were synthesized and investigated. The XRD patterns of  $Mg_3Al_{1-x}Eu_x$ -TAL LDHs are shown in Fig. 27. As seen, the monophasic  $Mg_3Al_{1-x}Eu_x$ -TAL LDHs having different amount of europium were obtained.

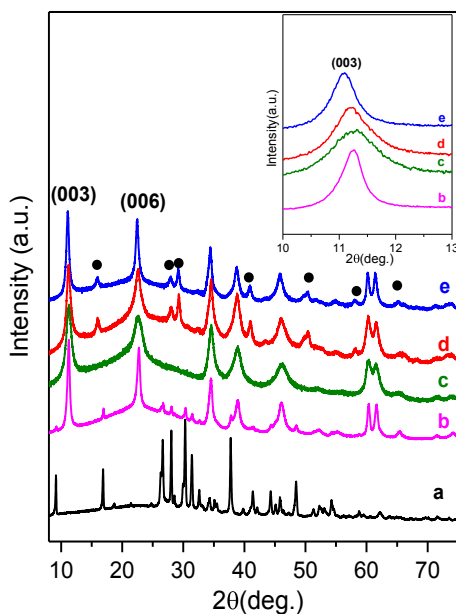


Fig. 27. XRD patterns of (a) TAL powders and  $Mg_3Al_{1-x}Eu_x$ -TAL LDHs: (b) 1 mol% of Eu, (c) 5 mol% of Eu, (d) 7.5 mol% of Eu and (e) 10 mol% of Eu. The impurity phase is marked: •-  $Eu(OH)_3$ .

With increasing concentration of europium till 7.5 mol% the impurity peak of  $Eu(OH)_3$  crystalline phase (PDF [96-403- 1477]) appeared in the XRD pattern of  $Mg_3Al_{1-x}Eu_x$ -TAL LDHs. As we can see from all XRD patterns the terephthalate successfully exchange the carbonate ion with lower concentration of europium. Furthermore, the negligible size of the parameter  $a$  in the products doped with  $Eu^{3+}$  suggesting that  $Eu^{3+}$  ions were doped in the brucite-like layers of LDHs and TAL - anion adsorbed on the surface of LDHs with the higher concentration of europium (Table 6).

Table 6. Lattice parameters of  $Mg_3Al_{1-x}Eu_x$  LDHs with intercalated TAL anion.

Sample	d (003), Å	d (006), Å	d (110), Å	Lattice parameters (Å)	
				a	c
$Mg_3Al_{1-x}Eu_x$ 1mol%- TAL	7.8647	3.9119	1.5332	3.065	23.579
$Mg_3Al_{1-x}Eu_x$ 5mol%- TAL	7.8537	3.9304	1.5336	3.066	23.550
$Mg_3Al_{1-x}Eu_x$ 7.5mol%- TAL	7.9780	3.9599	1.5368	3.065	23.824
$Mg_3Al_{1-x}Eu_x$ 10mol%- TAL	7.9447	3.9572	1.5334	3.072	23.924

FT-IR spectra in the region of 4000-500  $cm^{-1}$  of  $Mg_3Al_{1-x}Eu_x$ -TAL LDH samples with different concentration of europium are shown in Fig. 28. FT-IR spectra data also suggest that TAL-anions possibly are intercalated in LDHs.

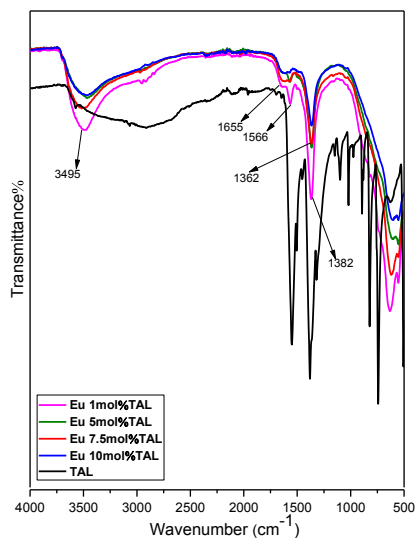


Fig. 28. FT-IR spectra of TAL and  $Mg_3Al_{1-x}Eu_x$ -TAL LDHs with different europium concentration.

The spectra recorded for all samples are very similar to each other with some small important differences. The absorption bands observed at around  $3495\text{-}3000\text{ cm}^{-1}$  and weak band at  $1655\text{ cm}^{-1}$  are ascribed to the stretching vibrations of hydroxyl (-OH) groups from the hydroxyl layers and from intercalated water molecules [162]. The strong absorption band visible at  $1362\text{ cm}^{-1}$  is attributed to the asymmetric vibration's modes of  $(\text{-CO}_3^{2-})$ . Two intensive absorption bands are present at  $1566\text{ cm}^{-1}$  and  $1382\text{ cm}^{-1}$ , and could be attributed to the asymmetric and symmetric stretching vibrations of carbon-oxygen bonds in  $(\text{-COO}^-)$  group [163], which correspond to terephthalate. The intensity of strongest absorption of TAL in the FT-IR spectra increases with decreasing europium concentration in the LDH.

The TG-DTA curves of synthesised  $\text{Mg}_3\text{Al-TAL}$  and  $\text{Mg}_3\text{Al}_{1-x}\text{Eu}_x$  1 mol%-TAL LDHs (Figs. 29 and 30, respectively) indicate three general steps of mass loss.

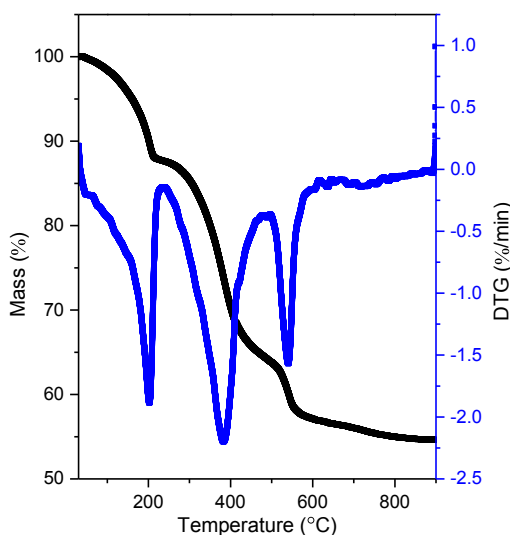


Fig. 29. TG-DTG curves of  $\text{Mg}_3\text{Al-TAL}$  LDH.

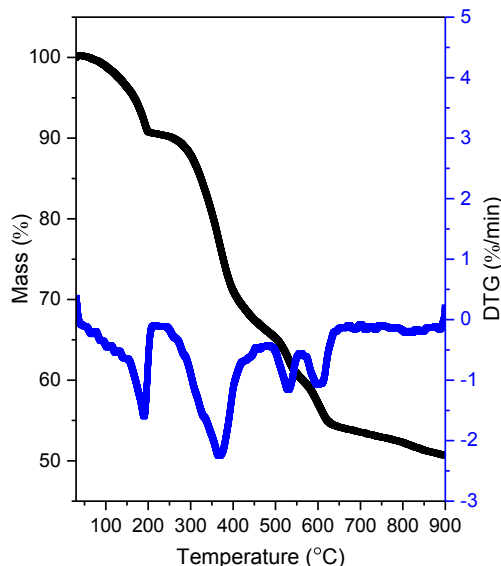


Fig. 30. TG-DTG curves of  $\text{Mg}_3\text{Al}_{1-x}\text{Eu}_x$  1 mol%- TAL LDH.

The first mass loss (10 %) corresponds to the removal of adsorbed water and interlayer water of LDH, and is present for all samples in the temperature range of 30-200 °C. The second mass loss observed in the range of 368-382 °C follows the dehydroxylation of the lattice. In the case of  $\text{Mg}_3\text{Al}$ -TAL mass loss is about 27 % and in the case of  $\text{Mg}_3\text{Al}_{1-x}\text{Eu}_x$  1 mol%- TAL is 19 %. The third mass loss (8 and 10 % for  $\text{Mg}_3\text{Al}$ -TAL and  $\text{Mg}_3\text{Al}_{1-x}\text{Eu}_x$  1 mol%- TAL LDHs) visible above 500 °C corresponds to the combustion and evaporation of the terephthalate anion.

The SEM micrographs of the synthesized  $\text{Mg}_3\text{Al-CO}_3$ ,  $\text{Mg}_3\text{Al-TAL}$  and  $\text{Mg}_3\text{Al}_{1-x}\text{Eu}_x$  1 mol%,  $\text{Mg}_3\text{Al}_{1-x}\text{Eu}_x$  1 mol%-TAL LDHs are depicted in Fig. 31.

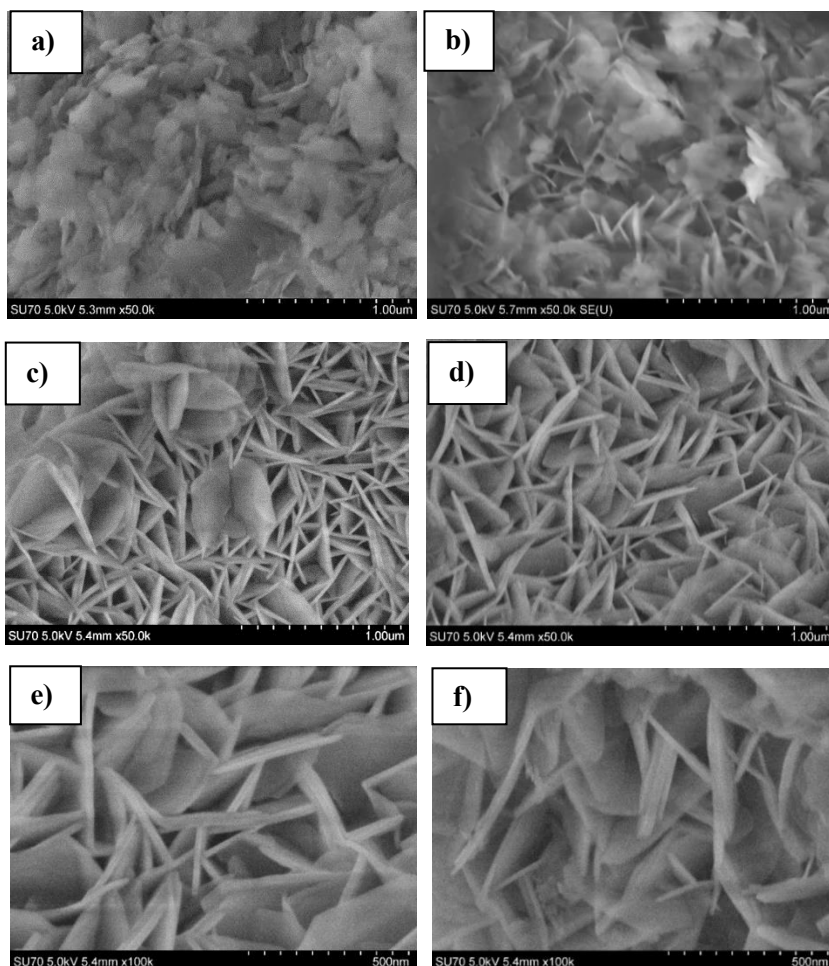


Fig. 31. SEM micrographs of (a)  $\text{Mg}_3\text{Al-CO}_3$ , (b)  $\text{Mg}_3\text{Al-TAL}$ , (c, e)  $\text{Mg}_3\text{Al}_{1-x}\text{Eu}_x$  1 mol% and (d, f)  $\text{Mg}_3\text{Al}_{1-x}\text{Eu}_x$  1 mol%- TAL LDHs.

The characteristic formation of plate-like particles with hexagonal shape of synthesized LDHs is clearly visible. The surface of  $\text{Mg}_3\text{Al-CO}_3$  LDHs is composed of the agglomerated plate-like particles about 400 nm in length. Such an agglomeration suggests an increased electrostatic interaction between crystallites-hexagons. The particle size of  $\text{Mg}_3\text{Al-TAL}$  LDHs is about 600 nm. The introduction of europium to LDHs had no influence on particle size ( $\text{Mg}_3\text{Al}_{1-x}\text{Eu}_x\text{-CO}_3$  and  $\text{Mg}_3\text{Al}_{1-x}\text{Eu}_x\text{-TAL}$  ~330–720 nm).



### 3.1.4. Luminescent properties

The excitation spectrum of  $\text{Mg}_3\text{Al}_{1-x}\text{Eu}_x$  0.05-1 mol% LDHs are represented at Fig. 32. The sharp peaks may arise from direct excitation of the  $\text{Eu}^{3+}$  ground state into higher levels in the  $4f^6$  configuration, and which can be ascribed to  ${}^7\text{F}_0 \rightarrow {}^5\text{D}_4$  (361 nm),  ${}^7\text{F}_0 \rightarrow {}^5\text{G}_2$  (375 nm),  ${}^7\text{F}_0 \rightarrow {}^5\text{L}_6$  (393 nm),  ${}^7\text{F}_0 \rightarrow {}^5\text{D}_2$  (469.4 nm), respectively.

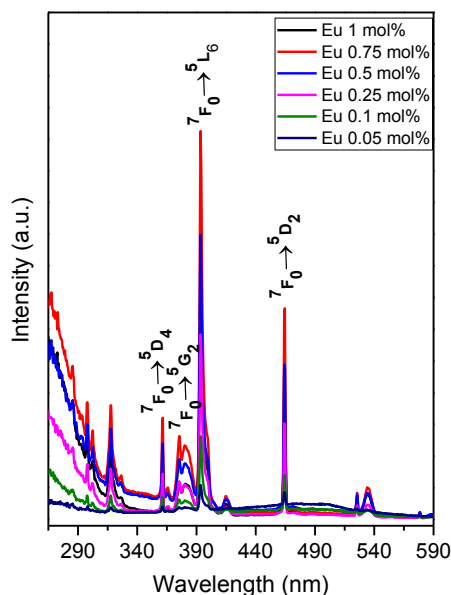


Fig. 32. Excitation spectra of  $\text{Mg}_3\text{Al}_{1-x}\text{Eu}_x$  0.05-1 mol% LDHs.

The emission spectra obtained at room temperature of all the  $\text{Mg}_3\text{Al}_{1-x}\text{Eu}_x$  0.05-1 mol% LDH samples under excitation at 320 nm are presented in Fig. 33. As seen, all samples share similar emission profiles. The emission spectra of  $\text{Mg}_3\text{Al}_{1-x}\text{Eu}_x$  LDHs show three main emissions in the wavelength range of 540–740 nm. In all spectra, the emission bands characteristic for  ${}^5\text{D}_0 \rightarrow {}^7\text{F}_j$  ( $J=1, 2, 3, 4$ ) transitions of  $\text{Eu}^{3+}$  ions were observed. The emission peaks are referred to the typical three  ${}^5\text{D}_0 \rightarrow {}^7\text{F}_1$  (591 nm)  ${}^5\text{D}_0 \rightarrow {}^7\text{F}_2$  (615 nm) and  ${}^5\text{D}_0 \rightarrow {}^7\text{F}_4$  (700) transitions of  $\text{Eu}^{3+}$  ion. The emission due to  ${}^5\text{D}_0 \rightarrow {}^7\text{F}_2$  transition is the strongest, indicating that  $\text{Eu}^{3+}$  ions occupy a low-symmetry site.  ${}^5\text{D}_0 \rightarrow {}^7\text{F}_2$  transition called as a hypersensitive transition. This can be caused by the addition of another molecule, in this case double hydroxide from brucite-like layer and carbonate from LDH structure. The presence of the low-symmetry structure containing the  $\text{Eu}^{3+}$  can only be observed in the nanocrystal line

products, the results allow to exclude the adsorption of  $\text{Eu}^{3+}$  on the surface of LDHs [164]. When  $\text{Eu}^{3+}$  ions occupy the sites with inversion symmetry, the  ${}^5\text{D}_0 \rightarrow {}^7\text{F}_1$  transition, typical magnetic dipole transition, should be relatively dominant; while, if there is no inversion symmetry at the sites of  $\text{Eu}^{3+}$  ions,  ${}^5\text{D}_0 \rightarrow {}^7\text{F}_2$  transition should be relatively dominant [165].

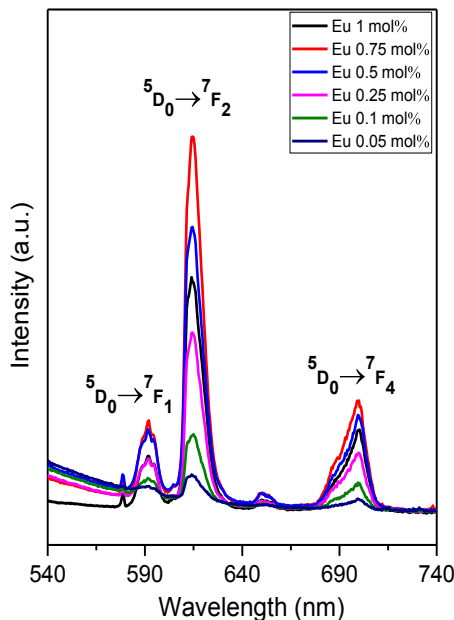


Fig. 33. Emission spectra of  $\text{Mg}_3\text{Al}_{1-x}\text{Eu}_x$  0.05-1 mol% LDHs.

The red strong emission of  ${}^5\text{D}_0 \rightarrow {}^7\text{F}_2$  were observed in the  $\text{Mg}_3\text{Al}_{1-x}\text{Eu}_x$  LDH phase. It is clear that the photoluminescence intensity increases with increasing the  $\text{Eu}^{3+}$  concentration to 0.75 mol%. With further increasing amount of europium the intensity of emission decreases due to the concentration quenching. As the concentration of  $\text{Eu}^{3+}$  increases, the distances between  $\text{Eu}^{3+}$  ions in the layers will be shortened, which dramatically increases the interaction of ions and causes serious concentration quenching already in  $\text{Mg}_3\text{Al}_{1-x}\text{Eu}_x$  1mol% LDH sample. This fact additionally confirms that  $\text{Eu}^{3+}$  ions replace  $\text{Al}^{3+}$  in the host lattice.

Fig. 34 shows the excitation spectra of  $\text{Mg}_3\text{Al}_{1-x}\text{Eu}_x$  1-10 mol%-TAL LDHs (along with  $\text{Mg}_3\text{Al}_{1-x}\text{Eu}_x$  1-10 mol% for comparison), which are composed to a large broad band in the ultraviolet spectral region from 200-320 nm and a sharp peak around 394 nm. This broad band is ascribed to transitions from the

ground state  $S_0$  to the first excited state  $S_1$  ( $\pi, \pi^*$ ) of the ligands from organic terephthalate anions.

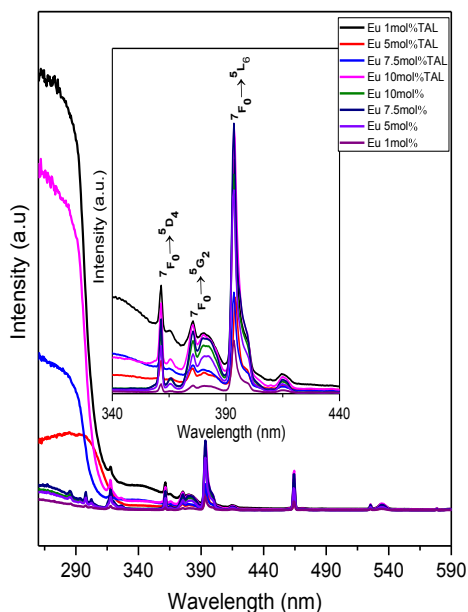


Fig. 34. Excitation spectra of  $Mg_3Al_{1-x}Eu_x$  1-10 mol%-TAL and  $Mg_3Al_{1-x}Eu_x$  1-10 mol% LDHs.

The emission spectra of  $Mg_3Al_{1-x}Eu_x$  1-10 mol%-TAL LDHs (Fig. 35) shows four main emissions in the wavelength range of 540–740 nm. The maximum photoluminescence intensity in the  $Mg_3Al_{1-x}Eu_x$ -TAL LDHs is observed for the sample with 5 mol%  $Eu^{3+}$  substitution. Again, concentration quenching could be observed, however, the results indicate that the organic terephthalate ligand transfers the excitation energy to the  $Eu^{3+}$  ion and thus improve the photoluminescence intensity of the LDH samples. Contrary, the  $Mg_3Al_{1-x}Eu_x$  samples show very pure emission in comparison with  $Mg_3Al_{1-x}Eu_x$ -TAL ones.

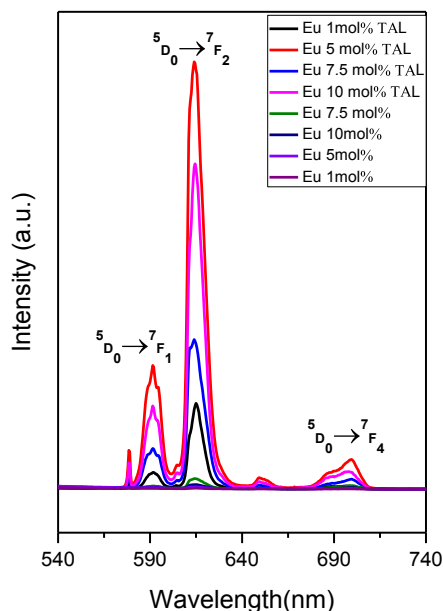


Fig. 35. Emission spectra of Mg<sub>3</sub>Al<sub>1-x</sub>Eu<sub>x</sub> 1-10 mol%-TAL and Mg<sub>3</sub>Al<sub>1-x</sub>Eu<sub>x</sub> 1-10 mol% LDHs.

Therefore, the ability to absorb the light energy dominates for the anions which characterize the strong basicity of the terephthalate, then carbonate anion. Carbonate is a weaker base and has weaker affinity to protons, correspondingly showing weaker interaction with hydrogen atoms of layer hydroxyl groups, thus transferring less energy to Eu<sup>3+</sup>. The intercalation of TAL into Mg<sub>3</sub>Al<sub>1-x</sub>Eu<sub>x</sub> LDH remarkably enhanced the intensity of  $^5D_0$ - $^7F_2$  transition compared with Mg<sub>3</sub>/Al<sub>1-x</sub>Eu<sub>x</sub>-CO<sub>3</sub>. The interlayer TAL anions located in a proximity to the Eu<sup>3+</sup> ions in the brucite-like layer act as an energy antenna for the red emission of Eu<sup>3+</sup> ions. Moreover, no obvious emission bands from the organic ligand are observed, indicating that the organic TAL ligand transfers the excitation energy efficiently to the Eu<sup>3+</sup> ion thus improve the luminescence intensity of samples.

### 3. 3. Induced neodymium luminescence in the sol-gel derived Mg-Al layered double hydroxides

The XRD patterns of  $Mg_3Al_{1-x}Nd_x$  1–10 mol% LDHs synthesized by sol-gel method is shown in Fig. 36. The LDH phases indexed on a hexagonal unit cell with a 3R rhombohedral symmetry and the diffraction lines in their patterns are determined at  $2\theta$  angle of about  $10^\circ$  (003),  $23^\circ$  (006) and  $60.2^\circ$  (110). The monophasic  $Mg_3Al_{1-x}Nd_x$  LDHs were obtained with amount of Nd less than 5 mol%. With increasing concentration of neodymium till 10 mol%, however, the impurity  $Nd(OH)_3$  phase ([PDF [00-070-0215]]) is forming.

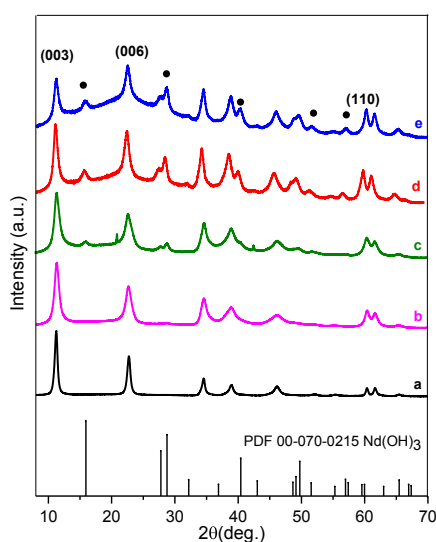


Fig. 36. XRD patterns of (a)  $Mg_3Al$  and  $Mg_3Al_{1-x}Nd_x$  LDHs synthesized by sol-gel method using reconstruction approach: (b) 1 mol% of Nd, (c) 5 mol% of Nd, (d) 7.5 mol% of Nd and (e) 10 mol% of Nd. The impurity phase is marked: •-  $Nd(OH)_3$ .

The XRD patterns of  $Mg_3Al_{1-x}Nd_x$ -TAL LDHs are presented in Fig. 37. These results confirm the formation of monophasic  $Mg_3Al_{1-x}Nd_x$ -TAL LDHs. However, with increasing concentration of neodymium till 10 mol% the impurity peak of  $Nd(OH)_3$  phase also appeared in the XRD pattern. As we can see from all XRD patterns the terephthalate successfully exchange the carbonate ion in the LDHs with lower concentration of neodymium.

Fig. 38 shows the SEM micrographs of  $Mg_3Al_{1-x}Nd_x$  5 mol% and  $Mg_3Al_{1-x}Nd_x$  10 mol% LDH powders. The  $Mg_3Al_{1-x}Nd_x$  LDHs consist of the

hexagonally shaped particles varying in size from approximately 400 to 600 nm. The formation of cloud-like agglomerates from these nanoparticles was also observed.

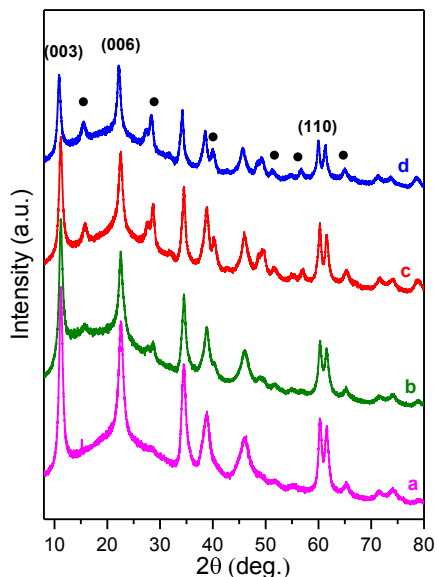


Fig. 37. XRD patterns of  $Mg_3Al_{1-x}Nd_x$ -TAL LDHs: (a) 1 mol% of Nd, (b) 5 mol% of Nd, (c) 7.5 mol% of Nd, (d) 10 mol% of Nd. The impurity phase is marked: •-  $Nd(OH)_3$ .

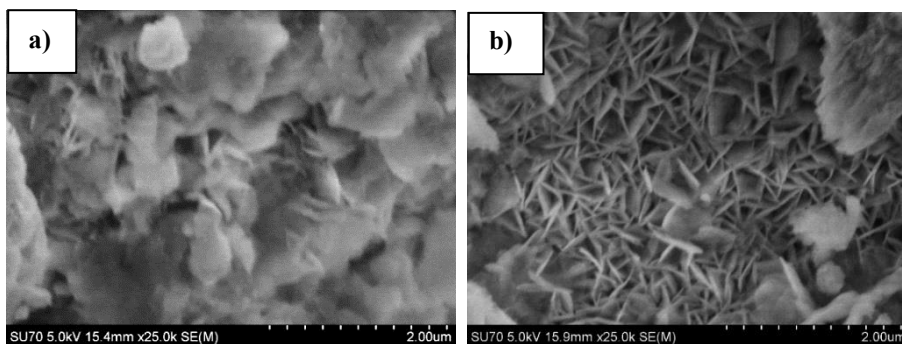


Fig. 38. SEM micrographs of (a)  $Mg_3Al_{1-x}Nd_x$  5 mol% and (b)  $Mg_3Al_{1-x}Nd_x$  10 mol% LDHs.

The luminescent properties of the obtained  $Mg_3Al_{1-x}Nd_x$  LDHs were investigated. Unfortunately, these neodymium-substituted layered double hydroxides as prepared did not demonstrate any luminescence, even though

XRD patterns and SEM morphology have been showed the monophasic  $\text{Mg}_3\text{Al}_{1-x}\text{Nd}_x$  LDH formation. The attempt to generate the luminescence by intercalating terephthalate in these LDH samples was made. The emission spectra of  $\text{Mg}_3\text{Al}_{1-x}\text{Nd}_x$  1-10 mol%- TAL LDH samples in the near-red region given by excitation at 580 nm are shown in Fig. 39.

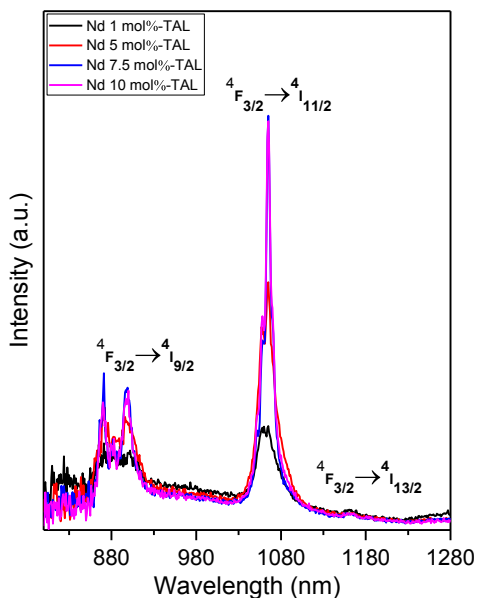


Fig. 39. Emission spectra of  $\text{Mg}_3\text{Al}_{1-x}\text{Nd}_x$  1-10 mol%-TAL LDHs (Ex=580 nm).

The emission spectra contain several bands located at 900 and 1065 nm, which arise due to the  ${}^4\text{F}_{3/2} \rightarrow {}^4\text{I}_{9/2}$  and  ${}^4\text{F}_{3/2} \rightarrow {}^4\text{I}_{11/2}$  transitions of  $\text{Nd}^{3+}$ . Bands near 1165 nm are assigned to the  ${}^4\text{F}_{3/2} \rightarrow {}^4\text{I}_{13/2}$  transitions of  $\text{Nd}^{3+}$ . The photoluminescence intensity of the  $\text{Mg}_3\text{Al}_{1-x}\text{Nd}_x$  – TAL LDH phase reaches its maximum at the  $\text{Nd}^{3+}$  concentration of 7.5 mol%. A further growth of the neodymium amount leads to a slight decrease in the emission intensity due to the concentration quenching. The interlayer TAL anions act as an energy antenna to the central  $\text{Nd}^{3+}$  ions enhancing the luminescence.

### 3.4. Sol-gel synthesis and characterization of terbium-substituted Mg-Al layered double hydroxides

#### 3.4.1. Modification of LDH and characterization

The attempts to incorporate  $Tb^{3+}$  into the brucite-like octahedral layers of  $Mg_3Al$  LDH and  $Mg_3Al$ -TAL with possible strong green emission of  $Tb^{3+}$  ion was also done. The XRD patterns of  $Tb^{3+}$ -substituted  $Mg_3Al_{1-x}Tb_x$  LDHs are shown in Fig. 40.

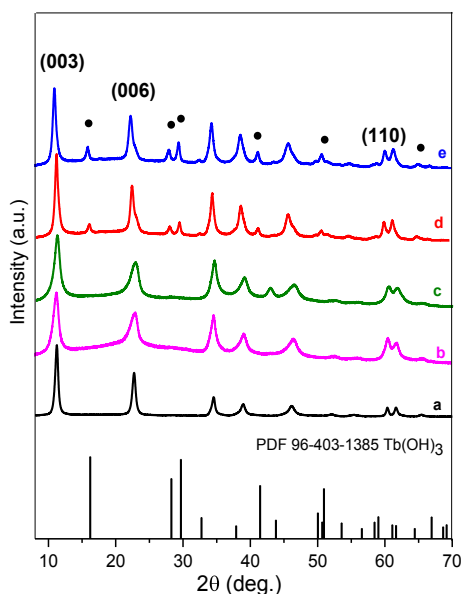


Fig. 40. XRD patterns of (a)  $Mg_3Al$  and  $Mg_3Al_{1-x}Tb_x$  LDHs synthesized by sol-gel method using reconstruction approach: (b) 1 mol% of Tb, (c) 5 mol% of Tb, (d) 7.5 mol% of Tb and (e) 10 mol% of Tb. The impurity phase is marked: •-  $Tb(OH)_3$ .

The monophasic  $Mg_3Al_{1-x}Tb_x$  LDHs were obtained with amount of terbium less than 7.5 mol%. With increasing concentration of terbium till 10 mol% the impurity peak of  $Tb(OH)_3$  (PDF [96-403-1385]) phase appears in the XRD patterns. The formation of  $Tb(OH)_3$  is due to the larger ionic radius of  $Tb^{3+}$  ions (1.06 Å) in comparison of ionic radius of  $Al^{3+}$  ions (0.53 Å) [155]. The  $Tb^{3+}$  ions taking up the octahedral positions of  $Al^{3+}$  ions led to the deformation of crystal lattice, and the excess  $Tb^{3+}$  ions in high basic condition crystallized as  $Tb(OH)_3$ . The observed shift of the (110) reflections toward lower values of  $2\theta$  containing different concentration of  $Tb^{3+}$



confirms partial substitution of  $\text{Al}^{3+}$  by  $\text{Tb}^{3+}$ . The calculated lattice parameters are presented at Table 7.

Terbium substitution effect in  $\text{Mg}_3\text{Al-TAL}$  LDH has been also investigated. For this reason,  $\text{Mg}_3\text{Al}_{1-x}\text{Tb}_x\text{-TAL}$  LDHs with different amount of terbium have been prepared. The XRD patterns of  $\text{Mg}_3\text{Al}_{1-x}\text{Tb}_x\text{-TAL}$  LDHs are shown in Fig. 41. The monophasic  $\text{Mg}_3\text{Al}_{1-x}\text{Tb}_x\text{-TAL}$  LDHs were obtained with amount of terbium less than 7.5 mol%. With increasing concentration of terbium till 10 mol% the peak of  $\text{Tb}(\text{OH})_3$  crystalline phase appeared in the XRD patterns.

Table 7. Lattice parameters of  $\text{M}_3\text{Al}$  and  $\text{Mg}_3\text{Al}_{1-x}\text{Tb}_x$  LDH synthesised by sol-gel method.

Sample	d (003), Å	d (006), Å	d (110), Å	Lattice parameters (Å)	
				<i>a</i>	<i>c</i>
$\text{Mg}_3\text{Al}$	7.8431	3.9187	1.5331	3.065	23.519
$\text{Mg}_3\text{Al}_{1-x}\text{Tb}_x$ 1mol%	7.8262	3.8739	1.5283	3.055	23.468
$\text{Mg}_3\text{Al}_{1-x}\text{Tb}_x$ 5mol%	7.8904	3.9008	1.5310	3.060	23.661
$\text{Mg}_3\text{Al}_{1-x}\text{Tb}_x$ 7.5mol%	7.9714	3.9635	1.5368	3.072	23.904
$\text{Mg}_3\text{Al}_{1-x}\text{Tb}_x$ 10mol%	8.0241	3.9756	1.5385	3.075	24.062

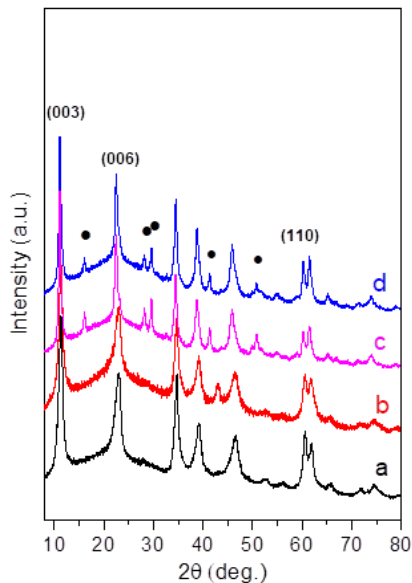


Fig. 41. XRD patterns of  $Mg_3/Al_{1-x}Tb_x$  - TAL LDHs: (a) 1 mol% of Tb, (b) 5 mol% of Tb, (c) 7.5 mol% of Tb, (d) 10 mol% of Tb; The impurity phase is marked: ● –  $Tb(OH)_3$ .

It is seen from Table 8 that the calculated interlayer distances values of TAL intercalate samples are  $d_{003}=7.84 - 8.02 \text{ \AA}$ , which are larger than those of  $Mg_3Al-CO_3$  LDHs in consideration of the different ionic radii of  $CO_3^{2-}$  ( $1.74 \text{ \AA}$ ). Subtracting the brucite-like layer spacing is  $4.8 \text{ \AA}$  and the gallery height is  $9.6 \text{ \AA}$  [12], given that size of the TAL anion is approximately  $9.8 \text{ \AA}$ , this value has been ascribed to the presence of the terephthalate anion adopting a vertical arrangement.

Table 8. Lattice parameters of  $Mg_3Al_{1-x}Tb_x$  LDHs with intercalated TAL anion.

Sample	d (003), Å	d (006), Å	d (110), Å	Lattice parameters (Å)	
				<i>a</i>	<i>c</i>
$Mg_3Al_{1-x}Tb_x$ 1mol%- TAL	7.8428	3.8892	1.5293	3.057	23.518
$Mg_3Al_{1-x}Tb_x$ 5mol%- TAL	7.8594	3.9044	1.5299	3.058	23.568
$Mg_3Al_{1-x}Tb_x$ 7.5mol%- TAL	7.9894	3.9651	1.5385	3.075	23.958
$Mg_3Al_{1-x}Tb_x$ 10mol%- TAL	8.0227	3.9746	1.5389	3.076	24.058

FT-IR spectra of  $Mg_3Al_{1-x}Tb_x$ -TAL LDHs samples recorded in the region of 4000-500  $cm^{-1}$  are shown in Fig. 42.

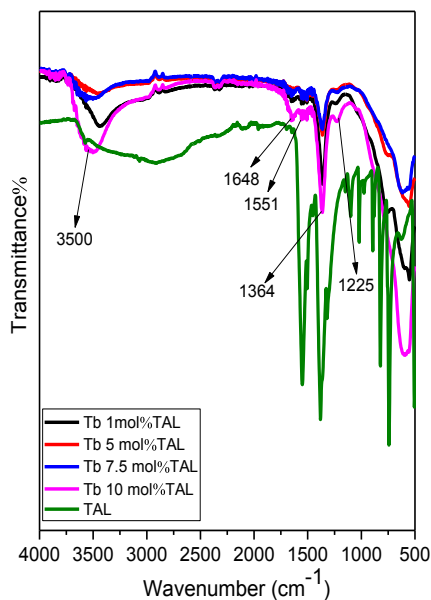


Fig. 42. FT-IR spectra of  $Mg_3Al_{1-x}Tb_x$ -TAL LDHs with different terbium concentration.

The absorption bands observed at around  $3500\text{-}3000\text{ cm}^{-1}$  and weak band at  $1648\text{ cm}^{-1}$  ascribed to the stretching vibrations of hydroxyl (-OH) groups from the hydroxyl layers and from intercalated water molecules. The strong absorption band visible at  $1364\text{ cm}^{-1}$  is attributed to the asymmetric vibration's modes of ionic carbonate ( $\text{-CO}_3^{2-}$ ). Furthermore, two main bands are also corresponding to terephthalate anion and present at  $1551\text{ cm}^{-1}$  and  $1225\text{ cm}^{-1}$ , which are assigned to the asymmetric and symmetric stretching vibrations of carbon-oxygen bonds of ( $\text{-COO}^-$ ) group. These FT-IR spectra data suggest that TAL-anions are intercalated in all  $\text{Mg}_3\text{Al}_{1-x}\text{Tb}_x$ -TAL LDHs samples.

The morphology of the synthesized  $\text{Mg}_3\text{Al}_{1-x}\text{Tb}_x$  and  $\text{Mg}_3\text{Al}_{1-x}\text{Tb}_x$ -TAL LDHs (Fig. 43) samples were examined using scanning electron microscopy. The surface of hybrid inorganic-organic  $\text{Mg}_3\text{Al}_{1-x}\text{Tb}_x$ -TAL LDHs contains very resolved plate-like particles with hexagonal shape. The particle size of  $\text{Mg}_3\text{Al}_{1-x}\text{Tb}_x$  5 mol% varies in the range of  $\sim 150\text{-}280\text{ nm}$  in length, and for the  $\text{Mg}_3\text{Al}_{1-x}\text{Tb}_x$  5mol%-TAL sample the particle size was determined about  $\sim 300\text{ nm}$ .

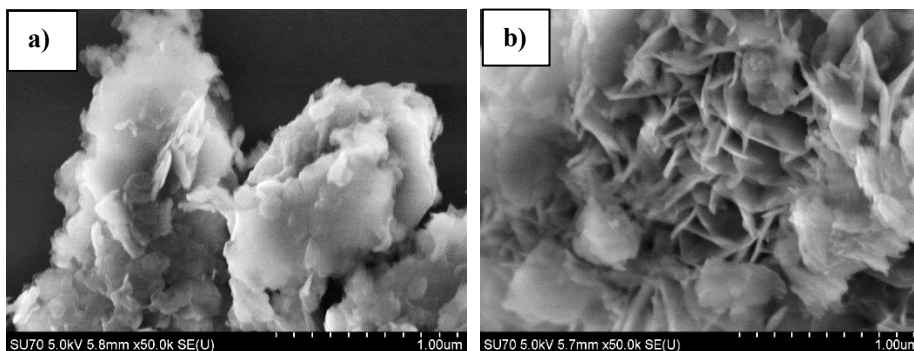


Fig. 43. SEM micrographs of (a)  $\text{Mg}_3\text{Al}_{1-x}\text{Tb}_x$  5 mol% and (b)  $\text{Mg}_3\text{Al}_{1-x}\text{Tb}_x$  5 mol%-TAL LDHs.

### 3.4.2. Luminescent properties

The excitation spectra obtained at room temperature of all  $\text{Mg}_3\text{Al}_{1-x}\text{Tb}_x$  and  $\text{Mg}_3\text{Al}_{1-x}\text{Tb}_x$ -TAL LDHs samples are presented in Fig. 44. The excitation spectra are composed of a large broad band in the ultraviolet spectral region from  $250\text{-}300\text{ nm}$ . The large broad band is ascribed to transitions from the ground state  $S_0$  to the first excited state  $S_1$  ( $\pi, \pi^*$ ) of the ligands from organic terephthalate anions. Some excitation bands appeared at  $350, 380$  and  $486\text{ nm}$ , assigned  ${}^7\text{F}_6 \rightarrow {}^5\text{G}_4$ ,  ${}^7\text{F}_6 \rightarrow {}^5\text{L}_{10}$  and  ${}^7\text{F}_6 \rightarrow {}^5\text{G}_6$  electronic transitions, respectively

[166, 167]. The emission spectra of  $\text{Mg}_3\text{Al}_{1-x}\text{Tb}_x$  and  $\text{Mg}_3\text{Al}_{1-x}\text{Tb}_x$ -TAL LDHs (Fig. 45) shows four main emissions in the wavelength range of 475–650 nm. The green emission bands characteristic for  $^5\text{D}_4$ – $^7\text{F}_J$  ( $J=3, 4, 5, 6$ ) transitions of  $\text{Tb}^{3+}$  ions correspond to 621, 584, 542, 488 nm. The intensity of photoluminescence in the  $\text{Mg}_3\text{Al}_{1-x}\text{Tb}_x$  and  $\text{Mg}_3\text{Al}_{1-x}\text{Tb}_x$ -TAL LDHs phase increases with the 5 mol% $\text{Tb}^{3+}$  concentration and decreasing with further increasing amount of terbium due to the concentration quenching.

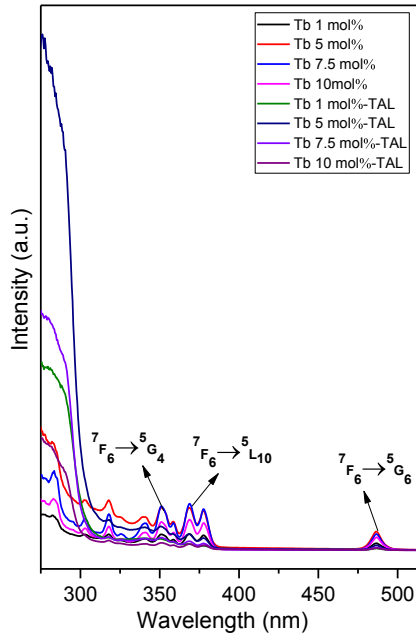


Fig. 44. Excitation spectra of  $\text{Mg}_3\text{Al}_{1-x}\text{Tb}_x$  and  $\text{Mg}_3\text{Al}_{1-x}\text{Tb}_x$ -TAL LDHs.

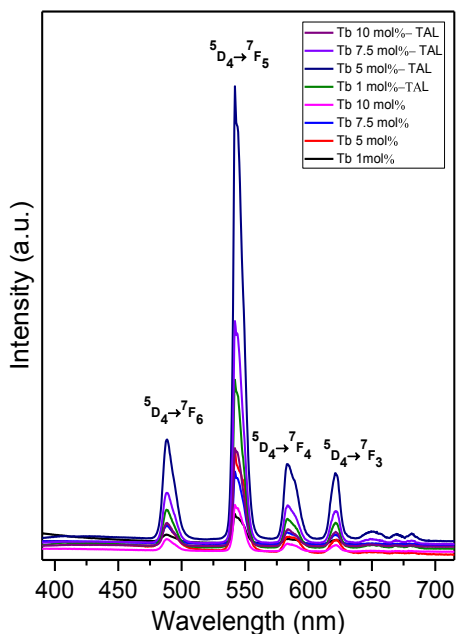


Fig. 45. Emission spectra of  $Mg_3Al_{1-x}Tb_x$  and  $Mg_3Al_{1-x}Tb_x$  - TAL LDHs.

The organic terephthalate ligand transfers the excitation energy to the  $Tb^{3+}$  ion and thus improved the photoluminescence intensity of the samples. The intercalation of TAL into  $Mg_3Al_{1-x}Tb_x$  LDH remarkably enhanced the intensity of  ${}^5D_4-{}^7F_5$  transition compared with  $Mg_3Al_{1-x}Tb_x$ . The green  ${}^5D_4-{}^7F_5$  emission of  $Tb^{3+}$  in  $Mg_3Al_{1-x}Tb_x$ -TAL showed a roughly 4 times enhancement, which had more excellent sensitizing ability. The interlayer TAL anions located in a proximity to the  $Tb^{3+}$  ions in the brucite-like layer act as an energy antenna for the green emission of  $Tb^{3+}$  ions [168].

### 3.5. Layered double hydroxides: Peculiarities of intercalation of organic anions

LDHs with photoluminescence function can have practical application in optical devices. However, it is limited by the low emission intensity arising from the direct coordination of water molecules and hydroxyl groups to the layer of lanthanoids centre. As we already observed, the hybrid lanthanide-substituted LDH materials with organic anions intercalated in the interlayer galleries show enhanced luminescence properties. For this reason, we synthesized several hybrids inorganic-organic LDHs using

anion exchange method and investigated their structural properties and ability to act as energy transfer agents.

### 3.5.1. Modification of LDH with organic anions and characterization

The intercalated organic anions were arranged by anions size in the interlayer space and by the charge to compensate of the hydroxide layer in LDHs, such as short-long carbon chains (oxalate, laurate, malonate, succinate, tartrate) and benzoic (benzoate, 1,3,5-benzentricarboxylate, 4-methylbenzoate, 4-dimethylaminobenzoate and 4-biphenylacetate) carboxyl acid groups. The XRD patterns of  $Mg_3Al-CO_3$  intercalated with organic anions are presented in Figs. 46 and 47. The reflections in the XRD patterns are shifted to the lower  $2\theta$  angle indicating a considerable increase in the basal spacing values  $c$  as compared with the respective values for the main  $Mg_3Al-CO_3$  LDH. The positions of diffraction peaks (003) of short-long chains as a  $Mg_3Al$ -oxalate,  $Mg_3Al$ -laurate,  $Mg_3Al$ -succinate (Fig. 46) and benzoic (Fig. 47) carboxylates as a 4-biphenylacetate, benzoate, 1,3,5-benzentricarboxylate LDHs moved small  $2\theta$  angle integrally corresponding to the increase of interlayer spacing (see the calculated values of the lattice parameters  $c$  in Table 9). The determined values of the lattice parameters  $c$  were monotonically increased from  $c = 23.613 \text{ \AA}$  for the  $Mg_3Al-CO_3$  to  $c = 24.375 \text{ \AA}$  for the  $Mg_3Al$ -oxalate and  $c = 24.261 \text{ \AA}$  for the  $Mg_3Al$ -laurate (in the case of short-long chains intercalation) also, to  $c = 24.492 \text{ \AA}$  for the  $Mg_3Al$ -4-biphenylacetate and  $c = 24.252 \text{ \AA}$  for the  $Mg_3Al$ -benzoate (in the case of derivatives of aromatic hydrocarbons). These results let us to conclude that all anions studied have been successfully intercalated to the  $Mg_3Al$  LDHs structure.

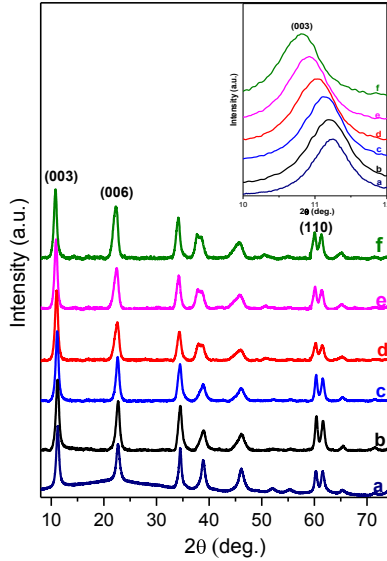


Fig. 46. XRD patterns of  $\text{Mg}_3\text{Al-CO}_3$  (a) and  $\text{Mg}_3\text{Al-CO}_3$  intercalated with organic anions:  $\text{Mg}_3\text{Al-succinate}$  (b),  $\text{Mg}_3\text{Al-malonate}$  (c),  $\text{Mg}_3\text{Al-tartrate}$  (d),  $\text{Mg}_3\text{Al-laurate}$  (e) and  $\text{Mg}_3\text{Al-oxalate}$  (f) LDHs.

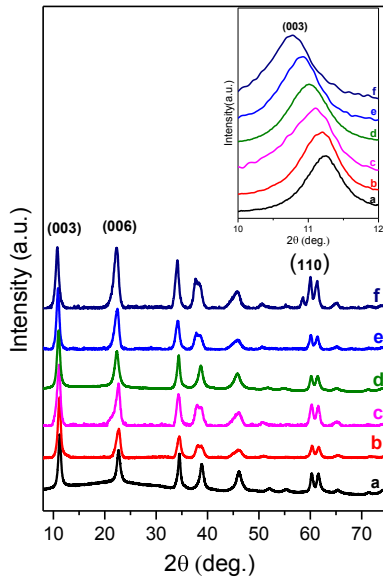


Fig. 47. XRD patterns of  $\text{Mg}_3\text{Al-CO}_3$  (a) and  $\text{Mg}_3\text{Al-CO}_3$  intercalated with organic anions  $\text{Mg}_3\text{Al-4-dimethylaminobenzoate}$  (b),  $\text{Mg}_3\text{Al-4-dimethylaminobenzoate}$  (c),  $\text{Mg}_3\text{Al-4-dimethylaminobenzoate}$  (d),  $\text{Mg}_3\text{Al-4-dimethylaminobenzoate}$  (e) and  $\text{Mg}_3\text{Al-4-dimethylaminobenzoate}$  (f) LDHs.



methylbenzoate (c), Mg<sub>3</sub>Al-1,3,5-benzentricarboxylate (d) Mg<sub>3</sub>Al-benzoate (e) and Mg<sub>3</sub>Al-4-biphenylacetate (f) LDHs.

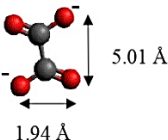
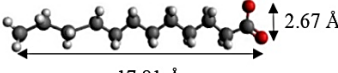
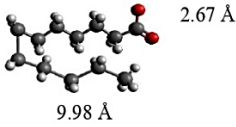
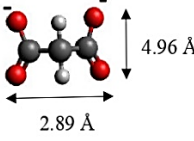
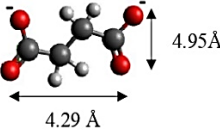
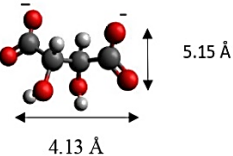
Table 9. The determined values of *d* spacing and lattice parameters *c* of anion-intercalated in Mg<sub>3</sub>Al LDHs.

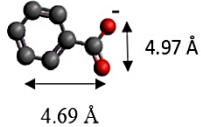
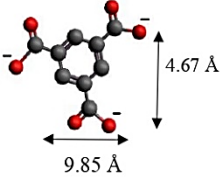
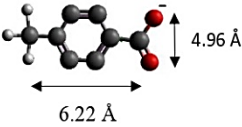
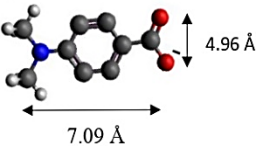
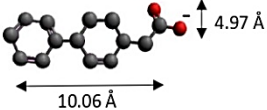
Sample	Basal spacing/Å d(003)	Cell parameter/Å		
		d(110)	a	c
Mg <sub>3</sub> Al-CO <sub>3</sub>	7.8744	1.5350	3.068	23.613
Mg <sub>3</sub> Al-oxalate	8.1286	1.5385	3.076	24.375
Mg <sub>3</sub> Al-laurate	8.0905	1.5380	3.075	24.261
Mg <sub>3</sub> Al-tartarate	7.9970	1.5359	3.070	23.981
Mg <sub>3</sub> Al-malonate	7.9568	1.5343	3.067	23.860
Mg <sub>3</sub> Al-succinate	7.9454	1.5333	3.065	23.826
Mg <sub>3</sub> Al-4-biphenylacetate	8.1675	1.5396	3.078	24.492
Mg <sub>3</sub> Al-benzoate	8.0875	1.5384	3.075	24.252
Mg <sub>3</sub> Al-4-methylbenzoate	8.0564	1.5383	3.075	24.159
Mg <sub>3</sub> Al-1,3,5-benzentricarboxylate	8.0328	1.5373	3.073	24.088
Mg <sub>3</sub> Al-4-dimethylaminobenzoate	7.8907	1.5324	3.063	23.662

The anions dimensions are listed in Table 10. The oxalate anion intercalated to LDH was the smallest by length 1.94 Å and width 5.01Å, and the laurate anion compared with oxalate is longest in dimension (17.81 Å). The laurate anion might have special orientation which existed at the certain angle between carbon chains and laminate of LDHs. In this case, the laurate anion was flexible to the position of better orientation in to the LDH host. Moreover, for the rest organic carboxylates, the intercalation in to the LDH structure could be problematic due to their spherical energetic interferences between -CH<sub>3</sub> groups and M-OH hydroxide layers. The Mg<sub>3</sub>Al-oxalate and the Mg<sub>3</sub>Al-4-biphenylacetate two phases with different basal spacings (Fig. 48) correspond to two vertical and horizontal particular orientations, which are grafting into the hydroxide layers. The hydrogen energy arises from the

formation of hydrogen bonds between the interlayer water molecules, the hydroxide layers, the interlayer anions, and among the H<sub>2</sub>O molecules themselves. The orientation of oxalate anion depends on ability of H<sub>2</sub>O molecules to form more compact structures around the two -COO<sup>-</sup> groups than around the hydrophobic ends of the monocarboxylate species. Four oxalate -COO<sup>-</sup> groups lie perpendicular to the layers, with two O-atoms coordinated to different hydroxide layers and for 4-biphenylacetate and benzoate, the -COO<sup>-</sup> groups are orientationally more disordered, and the O-atoms of its -COO<sup>-</sup> groups that lie parallel to the layers tend to occupy M-OH sites along the H-H vectors, whereas those -COO<sup>-</sup> tend to occupy the centres of the M-OH triangles. The ordered structure of MgAl-4-biphenylacetate LDH may be due to larger 4-biphenylacetate anions to accommodate them with the layers.

Table 10. Formula and dimensions of anions.

Anion	Chemical formula	Structural formula and dimensions
Oxalate	$(C_2H_4)^{2-}$	
Laurate	$(C_{12}H_{23}O_2)^{2-}$	 
Malonate	$(C_3H_2O_4)^{2-}$	
Succinate	$(C_4H_4O_4)^{2-}$	
Tartrate	$(C_4H_4O_6)^{2-}$	

Benzoate	$(C_7H_5O_2)^-$	 <p>4.69 Å</p> <p>4.97 Å</p>
1,3,5-benzentricarboxylate	$(C_9H_5O_6)^{3-}$	 <p>9.85 Å</p> <p>4.67 Å</p>
4-methylbenzoate	$(C_8H_7O_2)^-$	 <p>6.22 Å</p> <p>4.96 Å</p>
4-dimethylaminobenzoate	$(C_9H_{10}O_2)^-$	 <p>7.09 Å</p> <p>4.96 Å</p>
4-biphenylacetate	$(C_{14}H_{11}O_2)^-$	 <p>10.06 Å</p> <p>4.97 Å</p>

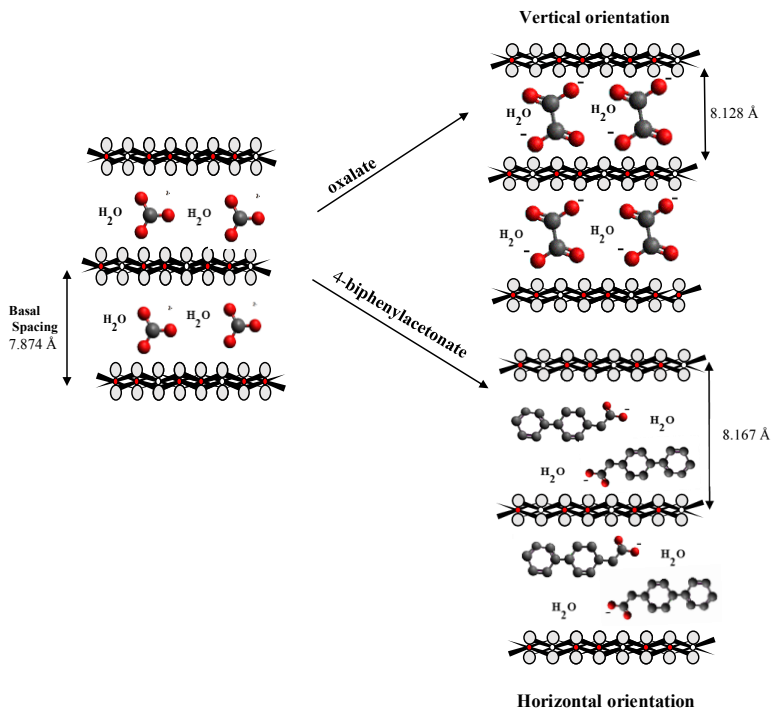


Fig. 48. A schematic structure of LDHs with interlayer carbonate anion and the specific orientation of oxalate and 4-biphenylacetate anions between the layers.

Europium substitution effects in Mg<sub>3</sub>Al-organic anions LDH have been investigated. The Mg<sub>3</sub>Al<sub>1-x</sub>Eu<sub>x</sub> with Eu 1mol% and LDHs intercalated with different organic carboxylates have been synthesized. The XRD patterns of the synthesized intercalated Mg<sub>3</sub>Al<sub>1-x</sub>Eu<sub>x</sub> LDH are depicted in Figs. 49 and 50.

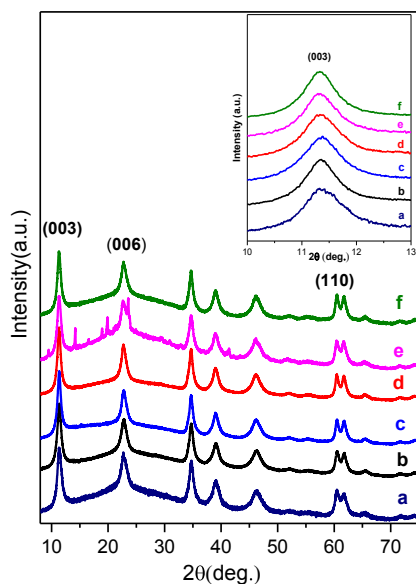


Fig. 49. XRD patterns of  $\text{Mg}_3\text{Al}_1\text{Eu} 1 \text{ mol}\%-\text{CO}_3$  (a) and hybrid inorganic-organic LDHs:  $\text{Mg}_3\text{Al}_{1-x}\text{Eu}_x$ -succinate (b),  $\text{Mg}_3\text{Al}_{1-x}\text{Eu}_x$ -malonate (c),  $\text{Mg}_3\text{Al}_{1-x}\text{Eu}_x$ -tartrate (d),  $\text{Mg}_3\text{Al}_{1-x}\text{Eu}_x$ -laurate (e) and  $\text{Mg}_3\text{Al}_{1-x}\text{Eu}_x$ -oxalate (f).

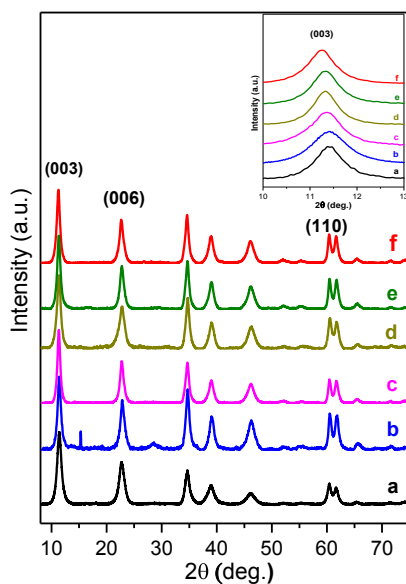


Fig. 50. XRD patterns of  $\text{Mg}_3\text{Al}_1\text{Eu} 1 \text{ mol}\%-\text{CO}_3$  (a) and hybrid inorganic-organic LDHs:  $\text{Mg}_3\text{Al}_{1-x}\text{Eu}_x$ -4-dimethylaminobenzoate (b),  $\text{Mg}_3\text{Al}_{1-x}\text{Eu}_x$ -4-4-4-trifluoromethylbenzoate (c),  $\text{Mg}_3\text{Al}_{1-x}\text{Eu}_x$ -4-4-4-trifluorophenylborate (d),  $\text{Mg}_3\text{Al}_{1-x}\text{Eu}_x$ -4-4-4-trifluorophenylborate (e) and  $\text{Mg}_3\text{Al}_{1-x}\text{Eu}_x$ -4-4-4-trifluorophenylborate (f).

methylbenzoate (c),  $Mg_3Al_{1-x}Eu_x$ -1,3,5-benzentricarboxylate (d),  $Mg_3Al_{1-x}Eu_x$ -benzoate (e) and  $Mg_3Al_{1-x}Eu_x$ -4-biphenylacetate (f).

It seems that interlayer distances are most increased in the case of oxalate and 4-biphenylacetate incorporated europium-substituted  $Mg_3Al$  LDHs.

FT-IR spectra of organic anion intercalated  $Mg_3Al_1Eu$  1 mol% LDHs in the region of 4000-500  $cm^{-1}$  are shown in Figs. 51 and 52. The absorption bands observed at around 3500-3000  $cm^{-1}$  (-OH) groups originated from the hydroxyl layers and from intercalated water molecules. The strong absorption band visible at 1360  $cm^{-1}$  is attributed to the asymmetric vibration's modes of ( $-CO_3^{2-}$ ), which still exist in the interlayer of intercalated LDHs. The bands in range of 1570-1627  $cm^{-1}$  are assigned to the asymmetric and symmetric stretching vibrations of carbon-oxygen bonds of ( $-COO^-$ ) group. The peaks observed in the range of 2850-2937  $cm^{-1}$  reflect the C-H stretching vibrations of ( $-CH_2-$ ) in the organic compounds. These data demonstrate the formation of the composites and interactions of the organic guests with the LDH layers.

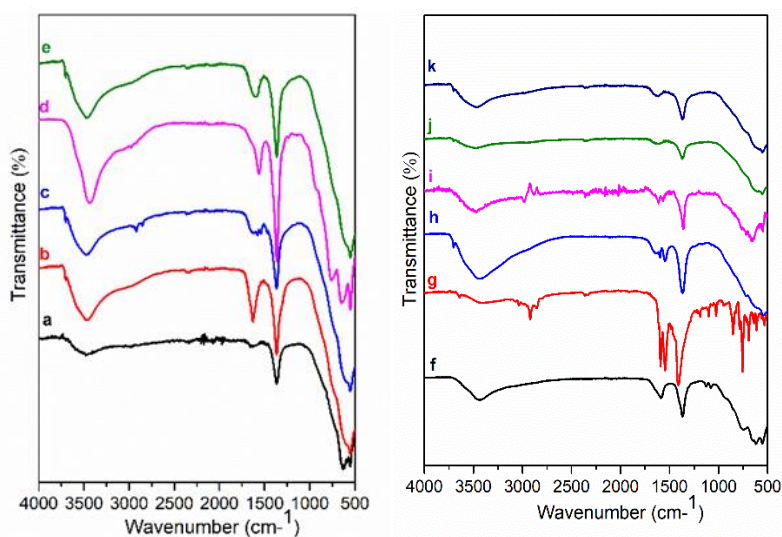


Fig. 51. FT-IR spectra of  $Mg_3Al-CO_3$  (a) and hybrid inorganic-organic LDHs:  $Mg_3Al$ -oxalate (b),  $Mg_3Al$ -laurate (c),  $Mg_3Al$ -succinate (d),  $Mg_3Al$ -malonate (e),  $Mg_3Al$ -tartrate (f),  $Mg_3Al$ -4-biphenylacetate (g),  $Mg_3Al$ -benzoate (h),  $Mg_3Al$ -1,3,5-benzentricarboxylate (i),  $Mg_3Al$ -4-methylbenzoate (j) and  $Mg_3Al$ -4-dimethylaminobenzoate (k).

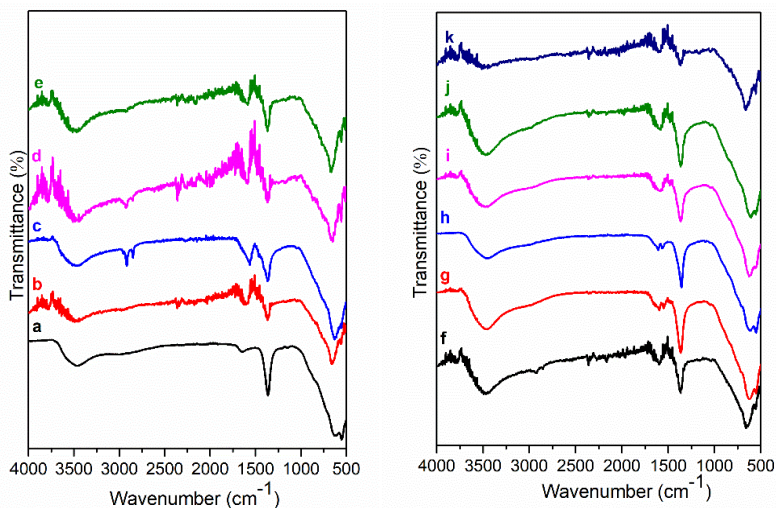


Fig. 52. FT-IR spectra of of  $Mg_3Al_1Eu$  1mol%- $CO_3$  (a) and hybrid inorganic-organic LDHs:  $Mg_3Al_{1-x}Eu_x$ -oxalate (b),  $Mg_3Al_{1-x}Eu_x$ -laurate (c),  $Mg_3Al_{1-x}Eu_x$ -succinate (d),  $Mg_3Al_{1-x}Eu_x$ -malonate (e),  $Mg_3Al_{1-x}Eu_x$ -tartrate (f),  $Mg_3Al_{1-x}Eu_x$ -benzoate (g),  $Mg_3Al_{1-x}Eu_x$ -1,3,5-benzentricarboxylate (h),  $Mg_3Al_{1-x}Eu_x$ -1-4-biphenylacetate (i),  $Mg_3Al_{1-x}Eu_x$ -4-methylbenzoate (j) and  $Mg_3Al_{1-x}Eu_x$ -4-dimethylaminobenzoate (k).

The SEM micrographs of representative  $Mg_3Al$ -oxalate,  $Mg_3Al$ -4-biphenylacetate (BPhAc),  $Mg_3Al_{1-x}Eu_x$  1mol%-tartrate and  $Mg_3Al_{1-x}Eu_x$  1mol%-benzoate LDHs samples are presented in Figs. 53 and 54. The particle sizes of  $Mg_3Al$ -BPhAc and  $Mg_3Al$ -oxalate LDHs (Fig. 53) is about 600 nm and 500 nm, respectively.

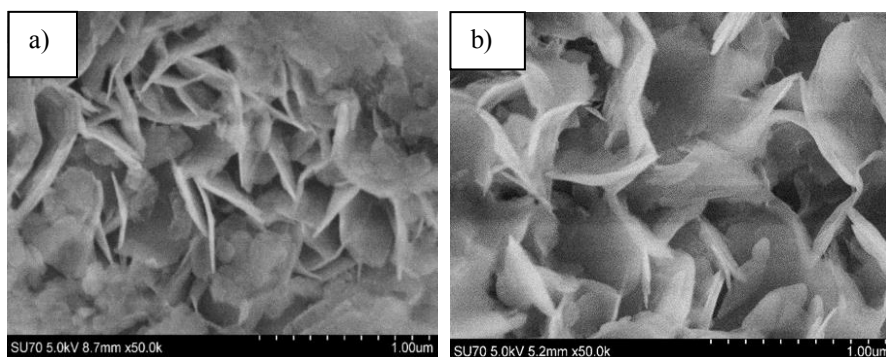


Fig. 53. SEM micrographs of (a)  $Mg_3Al$ -oxalate and (b)  $Mg_3Al$ -4-biphenylacetate (BPhAc) LDHs.



The formation of same hexagonally shaped particles with the size of ~400–450 nm were observed and for the  $\text{Mg}_3\text{Al}_{1-x}\text{Eu}_x$  1 mol%-tartrate and  $\text{Mg}_3\text{Al}_{1-x}\text{Eu}_x$  1 mol%- benzoate specimens (Fig. 54). The plate-shaped morphology remains visible and became smoother after the intercalation of organic anions.

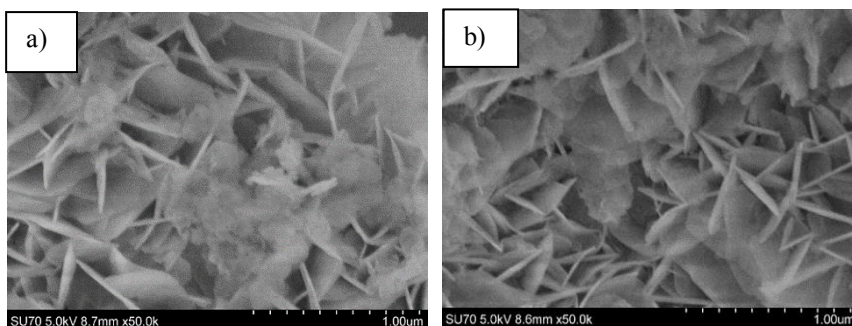


Fig. 54. SEM micrographs of (a)  $\text{Mg}_3\text{Al}_{1-x}\text{Eu}_x$  1 mol%-tartrate and (b)  $\text{Mg}_3\text{Al}_{1-x}\text{Eu}_x$  1 mol%-benzoate LDHs.

### 3.5.2. Luminescent properties

The emission spectra obtained at room temperature of  $\text{Mg}_3\text{Al}_{1-x}\text{Eu}_x$  1 mol%- benzoate, oxalate, laurate, malonate, succinate, tartrate, 1,3,5-benzentricarboxylate (BTC), 4-methylbenzoate (MB), 4-dimethylaminobenzoate (DMB) and 4-biphenylacetate (BPhAc) samples under excitation at 394 nm are presented in Fig. 55. The emission spectra of  $\text{Mg}_3\text{Al}_{1-x}\text{Eu}_x$  1 mol%- organic anions LDHs shows four main emissions in the wavelength range of 550–740 nm. In all spectra, the emission bands characteristic for  ${}^5\text{D}_0\text{--}{}^7\text{F}_J$  ( $J=1, 2, 3, 4$ ) transitions of  $\text{Eu}^{3+}$  ions were observed. The emission peaks are referred to the typical four  ${}^5\text{D}_0\text{--}{}^7\text{F}_1$  (590 nm),  ${}^5\text{D}_0\text{--}{}^7\text{F}_2$  (613 nm),  ${}^5\text{D}_0\text{--}{}^7\text{F}_3$  (650 nm) and  ${}^5\text{D}_0\text{--}{}^7\text{F}_4$  (697 nm) transitions of  $\text{Eu}^{3+}$  ion. The emission due to  ${}^5\text{D}_0\text{--}{}^7\text{F}_2$  transition is the strongest, indicating that  $\text{Eu}^{3+}$  ions occupy a low-symmetry site. Moreover, indicating that the organic anion ligands transfer the excitation energy to the  $\text{Eu}^{3+}$  ion and thus improved the photoluminescence intensity of the samples.

Two mechanisms of energy transfer between rare earth ions and organic molecules are known as intramolecular and intermolecular energy transfer. The potency to absorb the UV radiation is by interlayer organic anions, this energy is then transferred to the  $\text{Eu}^{3+}$  center by the interaction between the

carboxyl oxygen of the intercalated anions with the hydrogen of the  $M(OH)_6$  octahedra via a hydrogen bond and the  $Eu^{3+}$  reemits the radiation as red visible light.

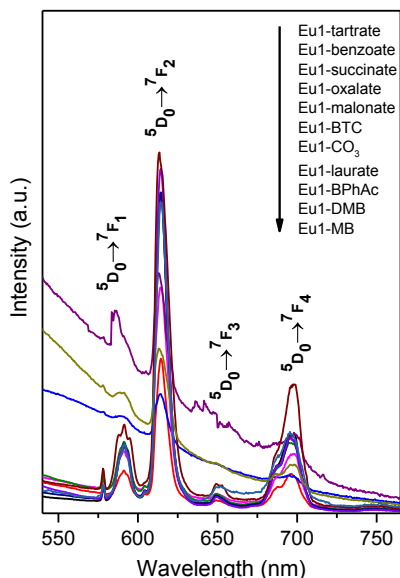


Fig. 55. Emission spectra of  $Mg_3Al_{1-x}Eu_x$  1 mol% - benzoate, oxalate, laurate, malonate, succinate, tartrate, 1,3,5-benzentricarboxylate (BTC), 4-methylbenzoate (MB), 4-dimethylaminobenzoate (DMB) and 4-biphenylacetate (BPhAc) intercalated compounds ( $Ex=394$  nm).

Therefore, the ability to absorb the light energy dominates for the anions which characterize the strong basicity of the tartrate and benzoate, then carbonate - anion. The aromatic ring structure itself can strongly affect the resonant energy levels of rare earth ions. As we can see from emission spectra the  $Mg_3Al_{1-x}Eu_x$  1 mol% -tartrate and  $Mg_3Al_{1-x}Eu_x$  1 mol% -benzoate LDH shows the highest intensity to compare with other organic ligands. Carboxylic acid and carbonyl group on aromatic ring generally inhibits fluorescence since the energy of the  $n \rightarrow \pi^*$  transition is less than  $\pi \rightarrow \pi^*$  transition. In this case the strongest luminescence light appears with  $Mg_3Al_{1-x}Eu_x$  1 mol% -tartrate and  $Mg_3Al_{1-x}Eu_x$  1 mol% -benzoate LDHs due to methylene groups leads decrease in the interaction between the two parts of the molecule having a common system of delocalized  $\pi$  electron orbitals. The  $-CH_2-$  bridge breaking up the system of conjugated  $\pi$ -electron bonds [169]. The europium LDH compounds formed with oxalate, laurate, malonate, succinate, BTC, MB,

DMB and BPhAc have lower brightness of luminescence primarily for this reason. The emission intensity strongly depends on the coordinative environment such as size of organic molecules (see Table 10).

### 3.6. Sol-gel synthesis and characterization of thin films of Mg-Al layered double hydroxides

Dip-coating technique was used for the fabrication of thin films of Mg-Al layered double hydroxides [170]. The substrate should be immersed in the sol-gel solution and dwell in it for a period of time and lifted from the chemical solution with a low redrawing speed. The substrate is further dry/heated to improve the thin film layer. LDHs appear to be a favorable alternative to the traditional chromate conversion coatings due to their characteristic structure and capability of ion exchange intercalation. The LDH films could be more compact and uniform due to the elimination of incompatibility between the LDH particles and the corresponding films. This coating is suitable for anticorrosion application, however, the known LDH films are still too thin to be applied in practice.

#### 3.6.1. Synthesis on Si and stainless-steel substrates and characterization

The same sol-gel synthesis method was applied for the fabrication of thin films of the Mg<sub>3</sub>Al LDHs on different substrates, namely silicon and stainless steel using dip-coating technique. The XRD patterns of Mg<sub>3</sub>Al LDHs obtained on silicon and steel substrates are presented in Figs. 56 and 57, respectively.

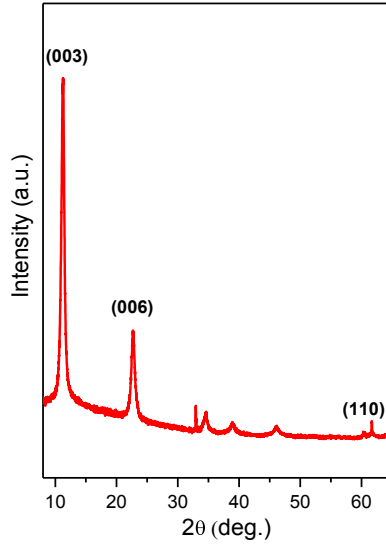


Fig. 56. XRD pattern of the  $Mg_3Al$  LDH coating on silicon substrate using 15 layers of precursor at 70 °C.

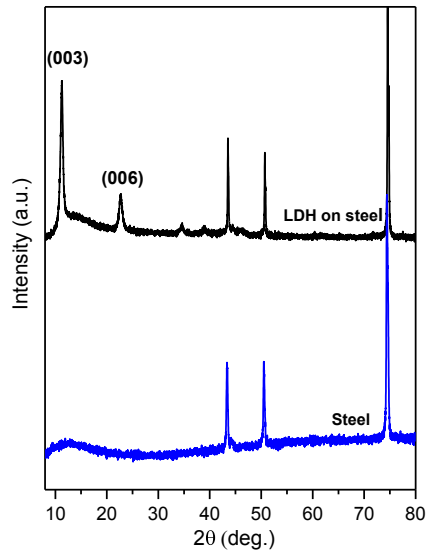


Fig. 57. XRD pattern of the  $Mg_3Al$  LDH coating on stainless-steel substrate using 15 layers of precursor at 70 °C.

Evidently, the intensity of Si reflection originated from the substrate is much higher in comparison to the main reflection of LDH samples. However, eliminating silicon reflection from the XRD patterns (see insertion in Fig. 56), the main reflections clearly represent the formation of LDH structure after 15 dipping procedures. The formation of  $Mg_3Al$  LDHs thin films on stainless steel substrate (Fig. 57) was also observed. The diffraction lines of  $Mg_3Al$  LDHs thin films are sharper and more intensive for the sample obtained on the silicon, confirming higher crystallinity of synthesized  $Mg_3Al$  LDH. In both cases, the single-phase crystalline LDHs have formed.

The surface morphology of  $Mg_3Al$  LDH film obtained on Si substrate is presented in the SEM images (Fig. 58). The surface of substrate is covered with monolithic layer of agglomerated plate-like particles 5-10  $\mu m$  in size. However, the SEM micrographs obtained at higher magnification clearly show that these plate-like particles are composed of hexagonally shaped nanoparticles which are characteristic for the LDH structures.

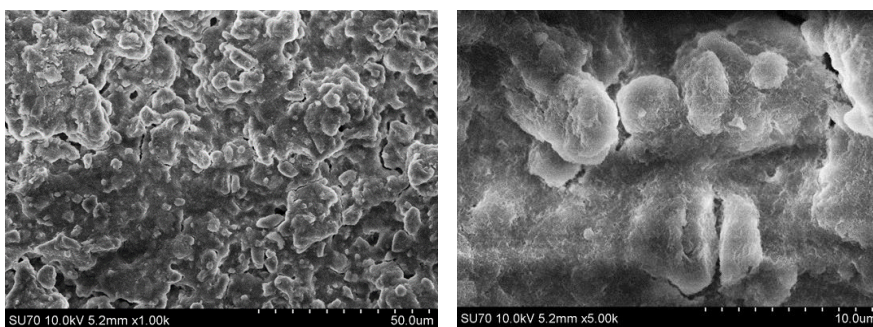


Fig. 58. SEM micrographs of  $Mg_3Al$  LDH film on silicon substrate obtained at different magnifications.

### 3.6.2. Modification of sol-gel processing

To enhance the sol-gel processing, the temperature of drying was raised and viscosity of precursor gel was increased by adding PVA (poly (vinyl alcohol)) solution. The XRD patterns of LDHs coatings obtained on Si (Fig. 59) and stainless-steel (Fig. 60) substrates, however, were almost the same as without addition of PVA. The XRD patterns show the formation of poorly crystalline LDH phase on Si substrate. The dip-coating in PVA solution and drying at 300 °C temperature (the PVA melting point is about 266°C) the LDH phase has not formed. The LDH sample with higher crystallinity was obtained on the steel substrate.

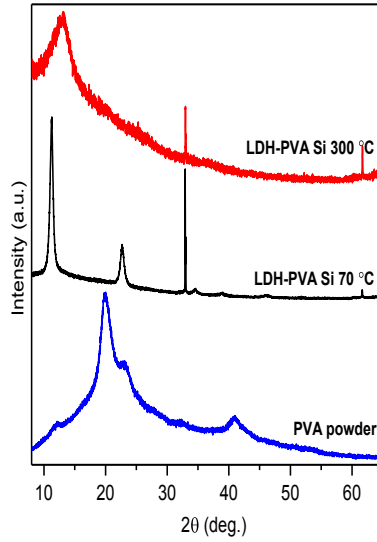


Fig. 59. XRD patterns of the  $Mg_3Al$  LDH coatings on silicon substrate using 15 layers of precursor with PVA solution obtained at 70 °C and 300 °C.

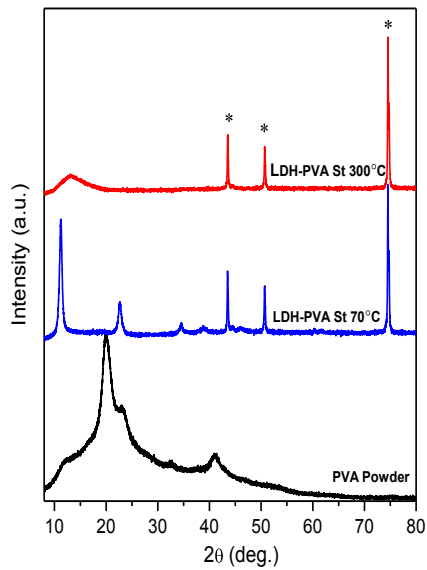


Fig. 60. XRD patterns of the  $Mg_3Al$  LDH coatings on stainless-steel substrate using 15 layers of precursor in PVA solution obtained at 70 °C and 300 °C temperatures. Reflections of stainless steel are marked: \*.

The SEM micrographs of  $Mg_3Al$  LDH films obtained on Si substrate using precursor in the PVA solution are shown in Fig. 61. The formation of nanograins of LDH is evident when PVA solution was used in the sol-gel processing. Moreover, these nanograins show tendency to form cloudy agglomerates when synthesis was performed at 300 °C.

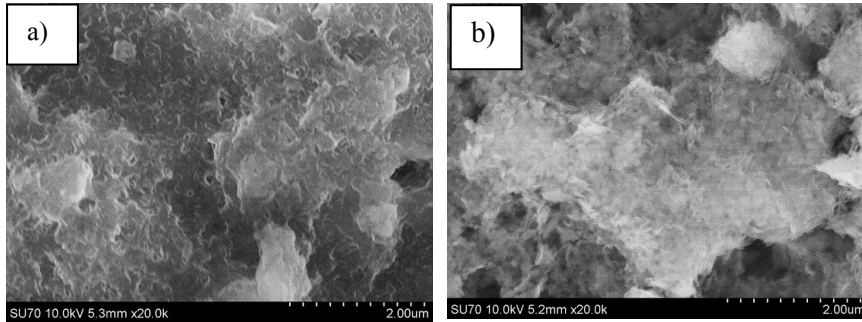


Fig. 61. SEM micrographs of  $Mg_3Al$  LDH films obtained on silicon substrate in PVA solution at (a) 70 °C and (b) 300 °C.

Atomic force microscopy (AFM) is a material characterization technique, which can evaluate the topology of the materials. The results of the analysis of topographic images obtained using this method allow to obtain detailed information on the state of the surface. One of the basic advantages of AFM from the point of view is the possibility of imaging with a very large magnification surfaces of nanomaterials. Other one important advantage of AFM is the ability to describe quantitative surface quality by determining roughness coefficients. The quantitative analysis of the surface topography of layers is carried out based on surface unevenness parameters. The basic parameters describing surface topographies are RMS (rough mean square) [171].

In Figs. 62-65 AFM micrographs of different  $Mg_3Al$  LDH films before and after modification on silicon and stainless-steel plates are represented. The AFM data of LDH profiles have been filtered with a mathematical procedure implemented in the MATLAB software. Such a software computes several roughness parameters at different „walk“ of axes x (vertical) and y (horizontal) positions (see Table 11). For this reason, the AFM images has been reduced and cut off from middle  $10 \mu m^2$  square for better comparison. Figs. 62 and 63 show the  $Mg_3Al$  LDH films dip-coated on the silicon and stainless substrates, respectively. The average RMS parameter obtained by AFM was determined to be 186.14 nm for the  $Mg_3Al$  LDH surface on the

silicon substrate and 352.62 nm for the Mg<sub>3</sub>Al LDH surface on the stainless-steel substrate.

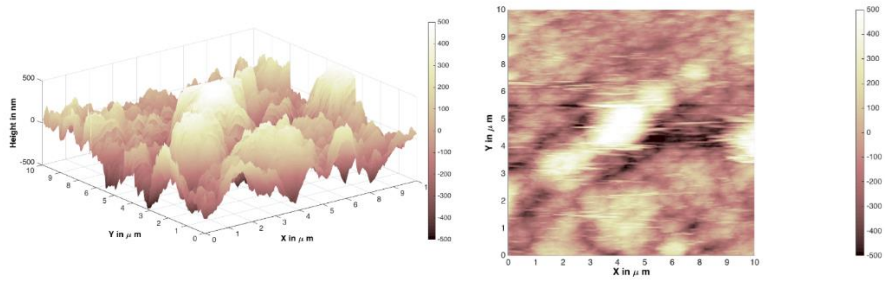


Fig. 62. Surface topography of Mg<sub>3</sub>Al LDH film on silicon substrate at 70 °C.

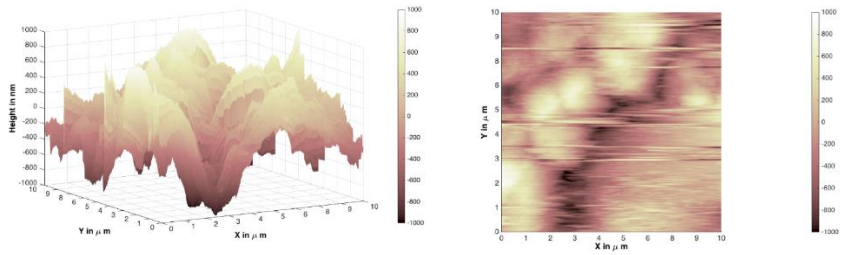


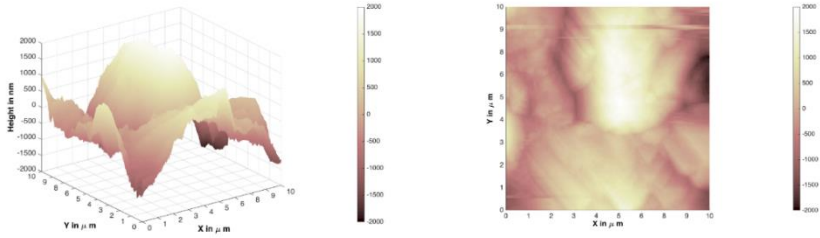
Fig. 63. Surface topography of Mg<sub>3</sub>Al LDH film on stainless-steel substrate at 70 °C.

Table 11. The RMS calculated parameters of AFM images.

AFM Images	Average RMS X (nm)	Average RMS Y (nm)	Average RMS (nm)	Min Height (nm)	Max Height (nm)	Average Heights (nm)
62	172.78	170.99	186.14	-500	500	-43.48
63	334.26	345.86	352.62	-1000	1000	-67.55
64	398.66	691.39	733.30	-2000	2000	135.03
65	774.36	778.69	1181.12	-2000	2000	-858.89



However, using the PVA (Figs. 64 and 65) solution for the modification of the  $Mg_3Al$  LDH the roughness increased to 733.30 and 1181.12 nm on the silicon and stainless-steel substrates, respectively.



**Fig. 64.** Surface topography of  $Mg_3Al$  LDH on silicon substrate in PVA solution at 70 °C.

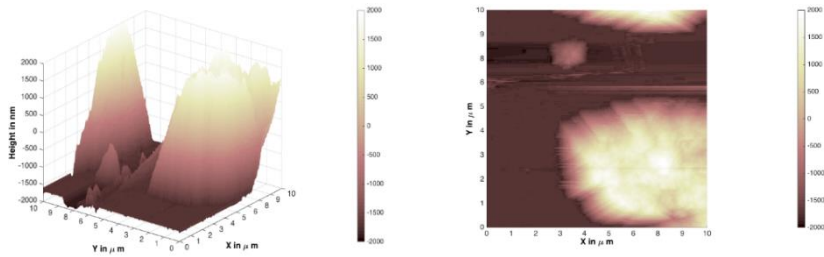


**Fig. 65.** Surface topography of  $Mg_3Al$  LDH on stainless substrate in PVA solution at 70 °C.

This might be because the higher concentration of polymers resulted in the formation of larger micelles of the monomer in the solution and the larger polymer aggregates on the surface. As we can see from the AFM images and the RMS calculated values results the synthesized LDHs coatings can be characterized as nanometer-size thin films. Its has been observed that the  $Mg_3Al$  LDH film formed on silicon substrate in the distilled water had the most smooth surface what can be applied for future work for the anti-corrosion properties.

## 4. CONCLUSIONS

1. The  $\text{Mg}_3\text{Al}$  LDHs were successfully synthesized by co-precipitation method and for the first time using aqueous sol-gel chemistry approach. This novel sol-gel processing route for LDHs is based on the decomposition of the precursor gels at  $650\text{ }^\circ\text{C}$  followed by reconstruction of the intermediate crystalline MMO powders in water. The proposed sol-gel synthesis route for LDHs has some benefits over the co-precipitation method such as simplicity, high homogeneity and good crystallinity of the end synthesized products.
2. The same synthesis methods were successfully applied for the synthesis of cerium-substituted LDHs ( $\text{Mg}_3\text{Al}_{1-x}\text{Ce}_x$ ) with the substitution rate from 0.05 to 10 mol%. It was found that the conversion during the reconstruction of sol-gel derived MMO into  $\text{Mg}_3\text{Al}_{1-x}\text{Ce}_x$  LDHs does not depend on the concentration of cerium. The sol-gel derived  $\text{Mg}_3\text{Al}_{1-x}\text{Ce}_x$  LDHs consisted of the hexagonally shaped particles varying in size from approximately 150 to 270 nm.
3. The luminescent properties of the obtained  $\text{Mg}_3\text{Al}_{1-x}\text{Ce}_x$  LDHs showed the major emission lines attributed to the  $[\text{Xe}]5d^1-[\text{Xe}]5f^1$  transition of  $\text{Ce}^{3+}$  ions were peaked at  $\sim 370\text{--}390\text{ nm}$  prepared by co-precipitation method. The maximum of the emission of the LDHs synthesized using sol-gel technique is red shifted ( $390\text{--}430\text{ nm}$ ).
4. The monophasic europium-substituted  $\text{Mg}_3\text{Al}_{1-x}\text{Eu}_x$  LDHs were obtained with amount of Eu less than 5 mol%. With increasing concentration of Eu till 10 mol% the amount of side  $\text{Eu}(\text{OH})_3$  phase has formed. Inorganic  $\text{CO}_3^{2-}$  to  $\text{OH}^-$ ,  $\text{Cl}^-$ ,  $\text{NO}_3^-$  anions has been exchanged and intercalated with terephthalate (TAL) in to the  $\text{Mg}_3\text{Al}$  and  $\text{Mg}_3\text{Al}_{1-x}\text{Eu}_x$  LDH hosts. The hexagonally shaped particles of  $\text{Mg}_3\text{Al}_{1-x}\text{Eu}_x\text{-CO}_3$  and  $\text{Mg}_3\text{Al}_{1-x}\text{Eu}_x\text{-TAL}$  LDHs with the size of  $\sim 330\text{--}720\text{ nm}$  have formed.
5. The red emission of  ${}^5\text{D}_0 \rightarrow {}^7\text{F}_2$  in the  $\text{Mg}_3\text{Al}_{1-x}\text{Eu}_x$  LDH phase with the maximum of intensity at the  $\text{Eu}^{3+}$  concentration of 0.75 mol% was determined. The intensity of photoluminescence in the  $\text{Mg}_3\text{Al}_{1-x}\text{Eu}_x\text{-TAL}$  LDHs increased significantly due to intercalation of terephthalate ligand which transfers the excitation energy to the  $\text{Eu}^{3+}$  ion.
6. The monophasic neodymium-substituted  $\text{Mg}_3\text{Al}_{1-x}\text{Nd}_x$  1–10 mol% LDHs were synthesized by sol-gel method with amount of Nd less than 5 mol%. The obtained  $\text{Mg}_3\text{Al}_{1-x}\text{Nd}_x$  LDHs did not demonstrate any

luminescence. However, neodymium luminescence in the  $\text{Mg}_3\text{Al}_{1-x}\text{Nd}_x$  was induced by intercalation of terephthalate ligand. The emission spectra of  $\text{Mg}_3\text{Al}_{1-x}\text{Nd}_x$  1-10 mol%- TAL LDHs contained several emission bands located at 900 and 1065 nm, which arise due to the  ${}^4\text{F}_{3/2} \rightarrow {}^4\text{I}_{9/2}$  and  ${}^4\text{F}_{3/2} \rightarrow {}^4\text{I}_{11/2}$  transitions of  $\text{Nd}^{3+}$  ion.

7. The monophasic  $\text{Tb}^{3+}$ -substituted  $\text{Mg}_3\text{Al}_{1-x}\text{Tb}_x$  and  $\text{Mg}_3\text{Al}_{1-x}\text{Tb}_x$ -TAL LDHs were obtained with amount of terbium less than 7.5 mol%. The particle size for the  $\text{Mg}_3\text{Al}_{1-x}\text{Tb}_x$  5mol%-TAL was determined about  $\sim 300$  nm. The intercalation of TAL remarkably enhanced the intensity of  ${}^5\text{D}_4 \rightarrow {}^7\text{F}_5$  transition in the emission spectra of  $\text{Mg}_3\text{Al}_{1-x}\text{Tb}_x$  LDHs.
8. The  $\text{Mg}_3\text{Al-CO}_3$  and  $\text{Mg}_3\text{Al}_{1-x}\text{Eu}_x$  LDHs intercalated with benzoate, oxalate, laurate, malonate, succinate, tartrate, 1,3,5-benzentricarboxylate, 4-methylbenzoate, 4-dimethylaminobenzoate and 4-biphenylacetate were prepared by sol-gel processing. The emission bands characteristic for  ${}^5\text{D}_0 \rightarrow {}^7\text{F}_J$  ( $J=1, 2, 3, 4$ ) transitions of  $\text{Eu}^{3+}$  ions with intercalated organic compounds were observed. The emission spectra of  $\text{Mg}_3\text{Al}_{1-x}\text{Eu}_x$  1 mol% -tartrate and  $\text{Mg}_3\text{Al}_{1-x}\text{Eu}_x$  1 mol% -benzoate LDH showed the highest intensity to compare with other organic ligands.
9. The  $\text{Mg}_3\text{Al}$  LDH coatings have been successfully fabricated on the silicon and stainless-steel substrates using the dip-coating processing route. The XRD patterns demonstrated high crystallinity of synthesized  $\text{Mg}_3\text{Al}_1$  LDH. The SEM micrographs obtained at higher magnification clearly showed that the plate-like particles formed on the surface are composed of hexagonally shaped nanoparticles which are characteristic for the LDH structures.
10. The average RMS parameter obtained by AFM was determined to be 186.14 nm for the  $\text{Mg}_3\text{Al}$  LDH surface on the silicon substrate and 352.62 nm for the  $\text{Mg}_3\text{Al}$  LDH surface on the stainless-steel substrate. The roughness of coatings increased to 733.30 and 1181.12 nm on the silicon and stainless-steel substrates, respectively, using the PVA solution for the modification of the  $\text{Mg}_3\text{Al}$  LDH.

## 5. LIST OF PUBLICATIONS AND CONFERENCES PARTICIPATION

### 5.1. Publications included in the thesis

#### 5.1.1. Articles in journals

1. A. Smalenskaite, L. Pavasaryte, Thomas C.K. Yang, A. Kareiva, Undoped and  $\text{Eu}^{3+}$  doped magnesium-aluminium layered double hydroxides: peculiarities of intercalation of organic anions and investigation of luminescence properties, *Materials*, 12, 736 (2019) 1-14.
2. A. Smalenskaite, A.N. Salak, M.G.S. Ferreira, R. Skaudzius, A. Kareiva, Sol-gel synthesis and characterization of hybrid inorganic-organic Tb(III)-terephthalate containing layered double hydroxides, *Optical Materials*, 80 (2018) 186–196.
3. A. Smalenskaite, A.N. Salak, A. Kareiva, Induced neodymium luminescence in sol-gel derived layered double hydroxides, *Mendeleev Communications*, 28 (2018) 493-494.
4. A. Smalenskaite, S. Şen, A.N. Salak, M.G.S. Ferreira, A. Beganskiene, A. Kareiva, Sol-gel derived lanthanide-substituted layered double hydroxides  $\text{Mg}_3/\text{Al}_{1-x}\text{Ln}_x$ , *Acta Physica Polonica A*, 133 (2018) 884-886.
5. A. Smalenskaite, D.E.L. Vieira, A.N. Salak, M.G.S. Ferreira, A. Katelnikovas, A. Kareiva, A comparative study of co-precipitation and sol-gel synthetic approaches to fabricate cerium-substituted MgAl layered double hydroxides with luminescence properties, *Applied Clay Science*, 143 (2017) 175–183.
6. A. Smalenskaite, S. Şen, A.N. Salak, M.G.S. Ferreira, R. Skaudzius, A. Katelnikovas, A. Kareiva, Sol-gel synthesis and characterization of non-substituted and europium-substituted layered double hydroxides  $\text{Mg}_3/\text{Al}_{1-x}\text{Eu}_x$ , *Current Inorganic Chemistry*, 6 (2016) 149-154.

#### 5.1.2. Attended conferences

1. A. Smalenskaitė, A.N. Salak, M.G.S. Ferreira, A. Kareiva, Synthesis and characterization of hybrid inorganic-organic Tb(III)- terephthalate containing layered double hydroxides, *International conference ACIN 2018: fourth international conference on advanced complex inorganic nanomaterials*, July 15-20, 2018, Namur, Belgium.

2. A. Smalenskaitė, A. Beganskienė, R. Skaudžius, A. Kareiva, Synthesis and characterization of hybrid inorganic (LDH)-organic (terephthalate) nanostructures, *International conference Nanotechnology and nanomaterials (NANO-2018)* August 27-30, 2018, Kijev, Ukraine.
3. A. Smalenskaitė, A.N. Salak, M.G.S Ferreira, A. Katelnikovas, A. Kareiva, On the synthesis and characterization of cerium-substituted layered double hydroxides  $Mg_3Al_{1-x}Ce_x$ , *International conference ISIC 19: 19th edition of the international symposium on intercalation compounds*, 2017, May 28-June 1, Assisi, Italy.
4. A. Kareiva, A. Smalenskaitė, S. Sen, A.N. Salak, M.G.S Ferreira, A. Beganskienė, Sol-gel derived lanthanide-substituted layered double hydroxides  $Mg_3/Al_{1-x}Ln$ , *International conference on oxide materials for electronic engineering - fabrication, properties and applications, OMEE-2017*, May 29 - June 2, 2017 Lviv, Ukraine.
5. A. Smalenskaitė, A.N. Salak, M.G. Ferreira, A. Kareiva, Cerium-substituted Mg-Al layered double hydroxides synthesised by sol-gel method with luminescence properties, *There is no future without the past“ : science on the interface of XIX-XXI centuries : the international conference dedicated to the 215-th birth anniversary of Ignacy Domeyko*, 2017, Vilnius, Lithuania.
6. A. Smalenskaitė, S. Sen, A.N. Salak, M.G.S. Ferreira, A. Kareiva, A novel approach for the synthesis of layered double hydroxides  $Mg_3/Al_{1-x}Eu_x$ , *Chemistry and chemical technology 2017 : proceedings of the international conference*, April 28th, 2017, Kaunas, Lithuania.
7. A. Smalenskaitė, A.N. Salak, M.G.S. Ferreira, A. Kareiva, Reconstruction peculiarity in co-precipitated Mg/Al and Mg/Al/Ce layered double hydroxides, *International conference nanoPT 2016 - International Conference on Nanoscience and Nanotechnology*, 16-19 February, Braga, Portugal.
8. A. Smalenskaitė, A. Kareiva, Synthesis and characterization of Mg/Al and Mg/Al/Ce layered double hydroxides by co-precipitation method, *International conference Nanochemistry and nanomaterials 2015: 2nd international conference of chemists*, 2015, Vilnius, Lithuania.

## 5.2. Publications not included in the thesis

### 5.2.1. Articles in journals

1. D.E.L. Vieira, D. Sokol, A. Smalenskaite, A. Kareiva, M.G.S. Ferreira, J.M. Vieira, A.N. Salak, Cast iron corrosion protection with chemically modified Mg/Al layered double hydroxides synthesized using a novel approach, *Surface & Coatings Technology*, 375 (2019) 158–163.
2. B. Buckus, G. Brimas, A. Stašinskas, A. Smalenskaitė, S. Tautkus, A. Beganskienė, A. Kareiva, Analytical characterization of adipose tissue structure and composition: A novel approach towards diagnosis of metabolic disturbances in human body. *Chemija*, 26 (2015) 98-106.

### 5.2.2. Attended conferences

1. D. Sokol, A. Smalenskaitė, A. Kareiva, V.V. Rubanik, A.D. Shilin, V.V. Rubanik, D.E.L. Vieira, A.N. Salak, M.G.S. Ferreira, Ultrasound-assisted formation of multifunctional layered double hydroxides, *Ultrasonics 2016 : 2nd international conference on ultrasonic- based applications: from analysis to synthesis*, 6-8th June 2016, Caparica, Portugal.
2. B. Buckus, G. Brimas, Z. Juodeikis, A. Smalenskaitė, A. Beganskiene, A. Kareiva, Evaluation of adipose tissue composition by  $^1\text{H}$  NMR and its relationship to ultrasonoscopic measurements in obese patients. *8<sup>th</sup> Congress of the Baltic Association of Surgeons. Tallinn, Estonia, September 10-12, (2015)*.
3. B. Buckus, G. Brimas, A. Smalenskaitė, A. Beganskiene, A. Kareiva, Evaluation of adipose tissue composition by  $^1\text{H}$  NMR and it's relationship to ultrasonoscopic measurements in obese patients. *20<sup>th</sup> World Congress "IFSO15". Vienna, Austria, August 26-29, (2015)*.
4. A. Smalenskaite, B. Buckus, S. Tautkus, A. Beganskiene, G. Brimas, A. Kareiva, Determination of fatty acid composition of adipose tissue by  $^1\text{H}$  NMR spectroscopy. *International Conference of Lithuanian Chemical Society „Chemistry and Chemical Technology 2015“ Vilnius, Lithuania, January 23, (2015)*.
5. A. Smalenskaite, B. Buckus, S. Tautkus, A. Beganskiene, G. Brimas, A. Kareiva, Analytical characterization of adipose structure and composition: A novel approach towards diagnostics and therapeutics. *19<sup>th</sup> International Scientific Conference "EcoBalt 2014". Riga, Latvia, October 8-10, (2014)*.

## 6. ACKNOWLEDGEMENTS

I want to thank my supervisors first of all Prof. Aivaras Kareiva for great knowledge, encourage and support all those study years starting from Master degree. Thank you so much of thrust and believe in me as a scientist and as a person, I am very grateful of having opportunity to work, communicate together and to get experience from such brilliant person. Thank you for showing me directions and always being the best example. Also, I am thankful for Prof. Aldona Beganskienė that was my supervisor and adviser, for being a great helper in all situations.

I would also like say thanks to Dr. Andrei Salak from Department of Materials and Ceramic Engineering, CICECO – Aveiro Institute of Materials for knowledge, help and collaboration during the PhD secondment at Aveiro University.

I am grateful and thankful for Prof. Vladas Gefenas from Department of Chemistry and Technology, Lithuanian University of Educational Science for the first knowledge of chemistry science's secrets and encouragement of further studies at Vilnius University.

I am thankful for all colleges at the Department of Inorganic Chemistry for the help and assistant during different measurements. I would like to thank my college Dr. Andrius Laurikėnas for the help, advices and being a good teacher in difficulties of scientific work procession and for the friendship.

I am thankful to my amazing Mother of giving me opportunity to study and to become educated person, also for support in all cases of life. Thank you for giving me wisdom, strength and faith.

## 7. REFERENCES

1. A. I. Khan, D. O'Hare, *Journal of Materials Chemistry*, 12 (2002) 3191-3198.
2. X. Duan, D.G. Evans, Springer-Verlag Berlin Heidelberg, Germany, 119 (2006) 1-234.
3. X. Wenlei, P. Hong, L. Chen, *Journal of Molecular Catalysis A*, 246 (2006) 24-32.
4. K. Klemkaite-Ramanauske, A. Zilinskas, R. Taraskevicius, A. Khinsky, A. Kareiva, *Polyhedron* 68 (2014) 340-345.
5. V. Rives, *Layered Double Hydroxides: Present and Future*. Nova Science Publishers, New York, 2001.
6. M. Meyn, K. Beneke, G. Lagaly, *Inorganic Chemistry*, 29 (26) (1990) 5201-5206.
7. V. Mas, G. Baronetti, N. Amadeo, M. Laborde, *Chemical Engineering Journal* 138 (2008) 602-607.
8. J. Bauer, P. Behrens, M. Speckbacher, H. Langhals, *Advance Functional Materials*, 13 (2003) 241- 248.
9. G.W. Walter, *Corrosion Science*, 26 (1986) 27-38.
10. A. M. Fogg, V. M Green, H. G. Harvey, D. O'Hare, *Advance Materials*, 11 (1999) 1466-1469.
11. F. Li, X. Duan, *Applications of Layered Double Hydroxides Structure Bonding (Berlin)* 119 (2006) 193-223.
12. K. Binnemans, *Chemical Reviews*, 109 (2009) 4283-4374.
13. N. H. Gutmann, L. Spiccia, T. W. Turney, *Journal of Materials Chemistry*, 10 (2000) 1219-1224.
14. K. A. Tarasov, D. O'Hare, V. P. Isupov, *Inorganic Chemistry* 42 (2003) 1919-1927.



15. D. Ananias, M. Kostova, F. A. A. Paz, A. Ferreira, L. D. Carlos, J. Klinowski, J. Rocha, *Journal of the American Chemical Society*, 126 (2004) 10410-10417.
16. D. W. Dong, S. C. Jiang, Y. F. Men, X. L. Ji, B. Z. Jiang, *Advance Materials*, 12 (2000) 646-649.
17. A. Katelnikovas, J. Plewa, S. Sakirzanovas, D. Dutczak, D. Enseling, F. Baur, H. Winkler, A. Kareiva, T. Jüstel, *Journal of Materials Chemistry*, 22 (2012a) 22126–22134.
18. A. Katelnikovas, J. Plewa, S. Sakirzanovas, D. Dutczak, D. Enseling, F. Baur, H. Winkler, A. Kareiva, T. Jüstel, *Optical Materials*, 34 (2012b) 1195–1201.
19. W.J. Zhang, Y.L. Li, H.X. Fan, *Optical Materials*, 51 (2016) 78–83.
20. V.I. Tsaryuk, K.P. Zhuravlev, V.F. Zolin, V.A. Kudryashova, J. Legendziewicz, R. Szostak, *Journal of Applied Spectroscopy*, 74 (1) (2007) 51–59.
21. X. Y. Xue, Q. Y. Gu, G. H. Pan, J. Liang, G. L. Huang, G. B. Sun, S. L. Ma, X. J. Yang, *Inorganic Chemistry*, 53 (3) (2014) 1521 –1529.
22. N. K. Chu, Y. H. Sun, Y. S. Zhao, X.X. Li, G. B. Sun, S.L. Ma, X. J. Yang, *Dalton Transaction* 41 (2012) 7409–7414.
23. A. Kareiva, *Materials Science (Medžiagotyra)* 17 (2011) 428–437.
24. D. Sokol, A. N. Salak, M. G. S. Ferreira, A. Beganskiene, A. Kareiva, *Jornal of Sol-Gel Science Technology*, 85 (2018) 221-230.
25. D. Sokol, M. Ivanov, A. N. Salak, R. Grigalaitis, J. Banyś, A. Kareiva, *Material Science-Poland*, 37(2) (2019), 190-195.
26. R. M. M. Santos, J. Tronto, V. Briois and C. V. Santilli, *Journal of Materials Chemistry A*, 5 (2017) 9998-10009.
27. F. Cavani, F. Trifirò, A. Vaccari, *Catalysis today*, Elsevier Science Publishers B.V., Amsterdam., 11 (1991) 173-301.
28. H. R. Oswald, R. Asper Riedel Publishing Company, Dordrecht, The Netherlands (1977) 71- 140.

29. A. S. Bookin, V. A. Drits, *Clays and Clay Minerals* 41 (1993) 551-557.
30. T. N. Ramesh, P. V. Kamath, C. Shivakumara, *Journal of Electrochemical Society*, 152 (2005) A806-A810.
31. S. J. Palmer, R. L. Frost, T. Nguyen, *Coordination Chemistry Reviews*, 253 (2009) 250–267.
32. S. Zaneva, T. Stanimirova, Geological Society, Annual Scientific Conference "Geology 2004", House of Science and Technology, Sofia, Bulgaria, Sofia University (2004) 110–112.
33. Z.P. Xu, H.C. Zeng, *The Journal of Physical Chemistry B*, 105 (2001), 1743–1749.
34. M. del Arco, S. Gutiérrez, C. Martin, V. Rives, J. Rocha, *Journal of Solid State Chemistry* 151 (2000) 272-280.
35. V. Rives, *Materials Chemistry and Physics* 75 (2002) 19–25.
36. F. Trifiro, A. Vaccari, *Comprehensive Supramolecular Chemistry*, Oxford, 7 (1996) 251-291.
37. M. Szabados, Z. Konya, A. Kukovecz, P. Sipos, I. Palinko, *Applied Clay Science*, 174 (2019) 138-145
38. C.C.L. Pereira, J.C. Lima, A.J. Moro, B. Monterio, *Applied Clay Science*, 146 (2017) 216–222.
39. P. Vincente, M.E.P. Bernall, R.J.R. Casero, D. Ananias, F.A.A. Paz, J. Rocha, V. Rives, *Microporous and Mesoporous Materials*, 226 (2016) 209–220.
40. M. Karmaoui, L. Mafra, R. A. Sa Ferreira, J. Rocha, L. D. Carlos, N. Pinna, *Journal of Physical Chemistry C*, 111 (2007) 2539-2544.
41. F. Geng, Y. Matsushita, R. Ma, H. Xin, M. Tanaka, F. Izumi, N. Iyi, T. Sasaki, *Journal of American Chemistry Society*, 130 (2008) 16344–16350.
42. S. Miyata, *Clays and Clay Minerals*, 31 (1983) 305–311.
43. D.G. Costa, A.B. Rocha, W.F. Souza, S.S.X. Chiaro A.A. Leitao, *Journal of Physics and Chemistry*, 114 (2010) 14133–14140.
44. N. Kim, A. Harale, T.T. Tsotsis, M. Sahimi, *Journal of Chemical Physics* 127 (2007) 224701.
45. J. Wang, G.K.R.J. Kirkpatrick, X. Hou, *Chemistry Materials*, 14 (2002) 2078–2085.

46. Z.P. Xu, Y. Jin, S. Liu, Z. Hao, G.Q.M. Lu, *Journal of Colloid and Interface Science*, 326 (2008) 522–529.
47. M. Pavlovic, R. Huber, M. Adok-Sipiczki, C. Nardina, I. Szilagyi, *Soft Matter*, 12 (2016) 4024–4033.
48. M. Pavlovic, P. Rouster, T. Oncsik, I. Szilagyi, *ChemPlusChem*, 82 (2017) 121–131.
49. S. S. Ray, D. Mosangi, S. Pillai, *The Chemical Record* 18 (2018) 913-927.
50. T. Sato, H. Fujita, T. Endo, M. Shimada, A. Tsunashima, *Reactivity of Solids*, 5 (1988) 219-228.
51. M. Jitianu, M. Zaharescu, M. Bălăsoiu, A. Jitianu, *Journal of Sol-Gel Science and Technology*, 26 (2003) 217-221.
52. A. Inayat, M. Klumpp, W. Schwieger, *Applied Clay Science*, 51 (2011) 452-459.
53. Z. P. Xu, G. Q. (Max) Lu, *Journal of Materials Chemistry*, 17 (2005) 1055-1062.
54. H.W. Olf, L.O. Torres-Dorante, R. Eckelt, H. Kosslick, *Applied Clay Science*, 43 (2009) 459-464.
55. M. R. Othman, Z. Helwani, Martunus, W. J. N. Fernando, *Applied Organometallic Chemistry*, 23 (2009) 335-346.
56. L. A. Utracki, M. Sepehr, E. Boccaleri *Synthetic, Polymer Advance Technology*, 18 (2007) 1-37.
57. K. Klemkaite, I. Prosycevas, R. Taraskevicius, A. Khinsky, A. Kareiva, *Central European Journal of Chemistry*, 9 (2011) 275-282;
58. A.N. Salak, J. Tedim, A.I. Kuznetsova, J.L. Ribeiro, L.G. Vieira, M.L. Zheludkevich, M.G.S. Ferreira, *Chemical Physics*, 397 (2012) 102–108.
59. K. Parida, M. Satpathy, L. Mohapatra, *Journal of Materials Chemistry*, 22 (2012) 7350–7357.
60. H. S. Panda, R. Srivastava, D. Bahadur, *Bulletin of Materials Science*, 34 (2011) 1599–1604.
61. L. F. Theiss, G. A. Ayoko, R. L. Frost, *Applied Surface Science*, 383 (2016) 200-213.
62. M. Meyen, K. Beneke, G. Lagaly, *Inorganic Chemistry*, 32 (1993) 1209-1215.
63. C. J. Brinker, G.W. Scherer, *The Physics and Chemistry of Sol-Gel Processing*. Academic Press, San Diego, 1990.

64. A. Katelnikovas, J. Barkauskas, F. Ivanauskas, A. Beganskiene, A. Kareiva, *Journal of SolGel Science and Technology* 41 (2007) 193 – 201.
65. F. Prinetto, G. Ghiotti, P. Graffin, D. Tichit, *Microporous and Mesoporous Materials*, 39 (2000) 229-247.
66. U. Costantino, F. Marmottini, M. Nocchetti, R. Vivani, *European Journal of Inorganic Chemistry*, 10 (1998) 1439-1446.
67. J.M. Oh, S.H. Hwang, J.H. Choy, *Solid State Ionics*, 151 (2002) 285-291.
68. S. Naseem, B. Gevers, R. Boldt, F. J. W. J. Labuschagn, A. Leuteritz, *RSC Advances*, 9 (2019) 3030-3040.
69. K. Parida, M. Satpathy, L. Mohapatra, *Journal of Materials Chemistry*, 22 (2012) 7350 -7357.
70. F. Kovanda, D. Kolousek, Z. Cilova, V. Hulinsky, *Applied Clay Science*, 28 (2005) 101-109.
71. J. He, M. Wei, B. Li, Y. Kang, D. G. Evans, X. Duan, *Structure Bonding*, 119 (2006) 89-119.
72. D. Scarpellini, C. Falconi, P. Gaudio, A. Mattocchia, P.G. Medaglia, A. Orsini, R. Pizzoferrato, M. Richetta, *Microelectronic Engineering*, 126 (2014) 129–133.
73. S.P. Newman, W. Jones, *New Journal of Chemistry*, 22 (1998) 105–115.
74. C. Jaubertie, M.J. Holgado, M.S. San Román, V. Rives, *Chemistry of Materials*, 18 (2006) 3114–3121.
75. M. Richetta, A. Mattocchia, A. Medaglia, P.G. Montanari, R. Pizzoferrato, D. Scarpellini, A. Varone, S. Kaciulis, A. Mezzi, P. Soltania, A. Orsini, *Surface and Interface Analysis*, 48 (2016) 514-518.
76. J. S. Valente, M. S. Cantu, M. Lima, F. Figueras, *Chemistry of Materials*, 21 (2009) 5809–5818.
77. A. C. Teixeira, A. F. Morais, I. G. N. Silva, E. Breynaert, D. Mustafa, *Crystals*, 9 (2019) 153.
78. Z. Gao, K. Sasaki, X. Qiu, *Langmuir*, 34 (19) (2018) 5386-5395.
79. J.M. Fernandez, M.A. Ulibarri, F.M. Lbajos, V. Rives, *Journal of Materials Chemistry*, 8 (11) (1998) 2507–2514.
80. S. Jamil, A. R. Alvi, S. R. Khan, M. R. S. A. Janjua, *Progress in Chemistry*, 31 (2019) 394-412.

81. F. Winter, X. Xia, B. P. C. Hereijgers, J. H. Bitter, A. J. van Dillen, M. Muhler, K. P. J. de Jong, *The Journal of Physical Chemistry, B* 110 (2006) 9211–9218.
82. H. Wang, J. Chen, Y. Cai, J. Ji, L. Liu, H. H. Teng, *Applied Clay science*, 35 (1-2) (2007) 59-66.
83. S. Palmer, J.A. Soisonard, R. L. Frost, *Journal of Colloid Interface Science*, 329(2) (2009) 404-409.
84. A.N. Salak, A.D. Lisenkov, M.L. Zheludkevich, M.G.S. Ferreira, *ECS Electrochemistry Lett.* 3 (2014) C9–C11.
85. M. Serdechnova, A.N. Salak, F.S. Barbosa, D.E.L. Vieira, J. Tedim, M.L. Zheludkevich, M.G.S. Ferreira, *Journal of Solid State Chemistry*, 233 (2016) 158–165.
86. H.J. Li, X.Y. Su, C.H. Bai, Y.Q. Xu, Z.C. Pei, S.G. Sun, *Sensors and Actuators. B- Chemical*, 225, (2016) 109–114.
87. P. Lu, S. Liang, L. Qiu, Y.S. Gao, Q. Wang, *Journal of Membrane Science*, 504 (2016) 196–205.
88. E. F. Grosu, D. Simiuc, R. Froidevaux, *Biomedical Journal Scientific and Technical Research*, 2 (2018) 2747-2752.
89. N. B. Allou, P. Saikia, A. Borah, R. L. Goswamee, *Colloid and Polymer Science*, 295 (5) (2017) 725-747.
90. V. R. Rodrigues Cunha, R. Barbosa de Souza, A. M. C. Rebello Pinto da Fonseca Martins, I. Hong Jun Koh, V. R. Leopoldo Constantino, *Histological and Microcirculation Evaluation Scientist Reports* 6 (2016) Art. No. 30547.
91. H. Hu, K. M. Xiu, S. L. Xu, W. T. Yang, F. J. Xu, *Bioconjugate Chemistry*, 24 (6) (2013) 968-978.
92. Z. Cao, N. N. M. Adnan, G. Wang, A. Rawal, B. Shi, R. Liu, K. Liang, L. Zhao, J. J. Gooding, C. Boyer, Z. Gu, *Journal of Colloid and Interference Science* 521 (2018) 242-251.
93. K. Zhang, Z. P. Xu, J. Lu, Z. Y. Tang, H. J. Zhao, D. A. Good, M. Q. Wei, *International Journal of Molecular Science*, 15 (5) (2014) 7409-7428.
94. A. C. Luca, L. D. Duceac, G. Mitrea, M. I. Ciuhodaru, D. L. Ichim, G. Baciuc, E. A. Banu, A. C. Iordache, *Materiale Plastice* 55 (2018) 552-554.
95. Y. You, G.F. Vance, H. Zhao, *Applied Clay Science*, 20 (2001)13–25.

96. S. K. Yun, V. R. L. Constantino, T. J. Pinnavaia, *Clays and Clay Minerals*, 43, (1995) 503-510.
97. S. Tezuka, R. Chitrakar, A. Sonoda, K. Ooi, T. Tomida, *Green Chemistry*, 6 (2004) 104-109.
98. N.K. Lazaridis, T.A. Pandi, K.A. Matis, *Industrial and Engineering Chemistry Research*, 43 (2004) 2209-2215.
99. G.P. Gillman, *Science of The Total Environment*, 336 (2006) 926-931.
100. R.L. Frost, A.W. Musumeci, *Journal of Colloid and Interface Science*, 302 (2006) 203-206.
101. S. Chen, Y. Huang, X. Han, Z. Wu, C. Lai, J. Wang, Q. Deng, Z. Zeng, S. Deng, *Chemistry Engineering Journal*, 352 (2018), 306-315.
102. P. Koilraj, K. Sasaki, *Chemistry Selection*, 2 (2017) 10459-10469.
103. B. Zhang, L. Luan, R. Gao, F. Li, Y. Li, T. Wu, *Colloids and Surfaces A*, 520 (2017), 399-408.
104. L. Ma, S.M. Islam, H. Liu, J. Zhao, G. Sun, H. Li, S. Ma, M.G. Kanatzidis, *Chemistry of Materials*, 29 (2017), 3274-3284.
105. K. Zhu, Y. Gao, X. Tan, C. Chen, *ACS Sustainable Chemistry and Engineering*, 4 (2016), 4361-4369.
106. X. He, X. Qiu, J. Chen, *Colloids and Surfaces A: Physicochemical and Engineering Aspects*, 516 (2017), 362-374.
107. L. Alidokht, S. Oustan, A. Khataee, M. Neyshabouri, A. Reyhanitabar, *Research on Chemical Intermediates*, 44 (2018) 2319-2331.
108. X. Wang, X. Zhu, X. Meng, *RSC Advance*, 7 (2017) 34984-34993.
109. G. Sheng, J. Hu, H. Li, J. Li, Y. Huang, *Chemosphere*, 148 (2016) 227-232.
110. M. Laipan, H. Fu, R. Zhu, L. Sun, J. Zhu, H. He, *Scientific Reports*, 7: 7277 (2017) 1-11.
111. D. Park, Y.S. Yun, J.M. Park, *Chemosphere*, 60 (2005) 1356-1364.
112. X. Song, Y. Wu, *Bulletin Korean Chemistry Sociate*, 35 (2014) 1817-1824.
113. F. Li and X. Duan, *Structure and Bonding*, 119 (2005) 193-223.
114. R.L. Frost, A.W. Musumeci, M.O. Adebajo, W. Martens, *Journal of Thermal Analysis Calorimetry*, 89 (2007) 95-99.
115. K. Schulze, W. Makowski, R. Chyży, R. Dziembaj, G. Geismar, *Applied Clay Science*, 18 (2001) 59-69.

116. L. P. Wang, B. Xiao, G. Y. Wang, J. Q. Wu, *Chine Science Chemistry*, 54 (2011) 1468–1473.
117. A. M. Rasero-Almansa, M. Iglesias and F. Sanchez, *RSC Advances*, 6 (2016) 106790–106797.
118. A. Taher, D. W. Kim, I. M. Lee, *RSC Advance*, 7 (2017) 17806–17812.
119. R. Chitrakar, S. Tezuka, A. Sonoda, K. Sakane and T. Hirotsu, *Industrial and Engineering Chemistry Research*, 47 (2008) 4905–4908.
120. M. X. Gao, M. H. Zhang, Y. H. Li, *RSC Advance*, 7 (2017) 11929–11937.
121. A. Zazoua, K. Saadi, D. Bachari, C. Halliche, Rabia, *Research on Chemical Intermediates*, 40 (2014) 931–946.
122. M. Sipiczki, E. Kuzmann, Z. Homonnay, J. Megyeri, K. Kovacs, I. Palinko, P. Sipos, *Hyperfine Interactions*, 217:(1-3) (2013) 145–149.
123. K. Hosni, O. Abdelkarim, N. Frini-Srasra, E. Srasra, *Korean Journal of Chemistry Engineering*, 32 (2015) 104–112.
124. T.T.X. Hang, T.A. Truc, N.T. Duong, P.G. Vu, T. Hoang, *Applied Clay Science*, 67 (2012) 18-25.
125. M.F. Montemor, D.V. Snihirova, M.G. Taryba, S.V. Lamaka, I.A. Kartsonakis, A.C. Balaskas, *Electrochimica Acta*, 60 (2012), 31-40.
126. M.L. Zheludkevich, S.K. Poznyak, L.M. Rodrigues, D. Raps, T. Hack, L.F. Dick, *Corrosion Science*, 52 (2) (2010) 602-611.
127. M.L. Zheludkevich, J. Tedim, C.S.R. Freire, S.C.M. Fernandes, S. Kallip, A. Lisenkov, *Journal of Materials Chemistry*, 21 (2011) 4805-4812.
128. L. Guo, F. Zhang, J.C. Lu, R.C. Zeng, S.Q. Li, L. Song, J.M. Zeng, *Frontiers of Materials Science*, 12(2) (2018) 198–206.
129. M.L. Zheludkevich, R. Serra, M.F. Montemor, K.A. Yasakau, I.M. Miranda Salvado, M.G.S. Ferreira, *Electrochimica Acta*, 51 (2005) 208–217.
130. A. K. Mishra, R. Balasubramaniam, *Corrosion Science*, 49 (2007) 1027-1044.
131. L. Perioli, P. Mutascio, C. Pagano, *Pharmaceutical Research*, 30 (2013) 156-166.

132. M.A. Djebbi, Z. Bouaziz, A. Elabed, M. Sadiki, S. Elabed, *International Journal of Pharmaceutics*, 506 (2016) 438-448.
133. G. Carja, E.F. Grosu, C. Petrarean, N. Nichita, *Nano Research*, 11 (2015) 3512-3523.
134. C.T. Gore, S. Omwoma, W. Chen, *Chemical Engineering Journal*, 284 (2016) 794–801.
135. A. Wang, Y. Bao, Z. Weng, *Chinese Journal of Chemical Engineering*, 16 (2008) 938–943.
136. Y. Shi, Y. Li, J. Zhang, Z. Yu, D. Yang, *Materials Science and Engineering C*, 51 (2015) 346–355.
137. P. Govindaraj, B. Kandasubramanian, K. M. Kodam, *Materials Chemistry and Physics*, 147 (2014) 934–941.
138. A. Mukherjee, I.M. Sadiq, T.C. Prathna, *Formatex: Extremadura* (2011) 245–251.
139. A. Sirelkhatim, S. Mahmud, A. Seeni, *Nano-Micro Letters*, 7 (2015) 219–242.
140. T. Posati, F. Costantino, L. Latterini, M. Nocchetti, M. Paolantoni, L. Tarpani, *Inorganic Chemistry*, 51 (2012), 13229-13236.
141. Y. Zhao, J.G. Li, F. Fang, N. Chu, H. Ma, X. Yang, *Dalton Transactions*, 41 (2012) 12175–1218.
142. X. Hu, X. Gao, *Physical Chemistry Chemical Physics*, 13 (2011) 10028–10035.
143. C. Li, L. Wang, D.G. Evans, X. Duan, *Industrial and Engineering Chemistry Research*, 48 (2009) 2162–2171.
144. Y. Sohn, *Ceramics International*, 40 (2014) 13803-13811.
145. P.V. Jyothy, K.A. Amrutha, J. Gijo, N.V. Unnikrishnan, *Journal of Fluorescence*, 19 (2009) 165-168.
146. H.N. Tran, C. Lin, S.H. Woo, H.P. Chao, *Applied Clay Science*, 154 (2018) 17–27.
147. S. Li, H. Qin, R. Zuo, Z. Bai, *Applied Surface Science*, 353 (2015) 643–650.
148. M. Maqbool, *The European Physical Journal Applied Physics*, 34 (2006) 31–34.
149. M. Maqbool, I. Ahmad, H.H. Richardson, M.E. Kordesch, *Applied Physics Letters* 91 (193511) (2007) 1–3.
150. R. Skaudzius, T. Juestel, A. Kareiva, *Materials Chemistry and Physics*, 170 (2016) 229–238.



151. K. Okamoto, T. Yoshimi, S. Miura, *Applied Physics Letters*, 53 (1988) 678–680.
152. A. Zabaliute, S. Butkute, A. Zukauskas, P. Vitta, A. Kareiva, *Applied Optics*, 53 (2014) 907-914.
153. Z. Hong, W. Winson, L. Tianxi, *Journal of Applied Polymer Science* 122 (2011) 273–281.
154. B. Kutlu, A. Leuteritz, R. Boldt, D. Jehnichen, G. Heinrich, *Chemical Engineering Journal*, 243 (2014) 394-404.
155. R.D. Shannon, *Acta Crystallographica*, 32 (1976) 751-767.
156. J. Perez-Ramirez, S. Abello, N.M. Van der Pers, *Journal of Physics and Chemistry C*, 111(2007) 3642-3650.
157. K. Kömpe, H. Borchert, J. Storz, A. Lobo, S. Adam, T. Möller, M. Haase, *Angewandte Chemie International Edition*, 42 (2003) 5513-5516.
158. F.Y. Li, Z.Q. Xia, S.P. Yang, S.Y. Gao, *Materials Science*, 39 (2004) 4711–4713.
159. S. Carlino, M. J. Hudson, S. W. Husain, *Solid State Ionics*, 84 (1996) 117-129.
160. S. Carlino, M. J. Hudson, S. W. Husain, *Materials Chemistry*, 4 (1994) 99-104.
161. N. K. Chu, Y. H. Sun, Y. S. Zhao, X. X. Li, G. B. Sun, S. L. Ma, X. J. Yang, *Dalton Transactions*, 41 (2012) 7409–7414.
162. L. Liu, Q. Wang, C. Gao, H. Chen, W. Liu, Y. Tang, *The Journal of Physical Chemistry C*, 118 (2014) 14511–14520.
163. P. Kovar, M. Pospisil, M. Nocchetti, P. Capkova, K. Melanova, *Journal of Molecular Modelling*, 13 (2007) 937–942.
164. S. Gago, M. Pillinger, R.A.S. Ferreira, L.D. Carlos, T.M. Santos, I.S. Goncalves, *PhD Thesis Chemistry Materials*, 2005, 5803–5809.
165. T. Posati, F. Bellezza, A. Cipiciani, F. Costantino, M. Nocchetti, L. Tarpani, L. Latterini, *Journal of Crystals Growth*, 10 (2010) 2847-2850.
166. P.V. Jyothy, K.A. Amrutha, J. Gijo, N.V Unnikrishnan, *Journal of Fluorescence*, 19 (2009) 165-168.
167. Q.Y. Gu, Y.H. Sun, N.K. Chu, S.L. Ma, Z.Q. Jia, X.J. Yang, *European Journal of Inorganic Chemistry* (2012) 4407-4412.

168. L.L. Liu, Q. Wang, C.J. Gao, H. Chen, W.S. Liu, Y. Tang, *The Journal of Physical Chemistry* 118 (2014) 14511-14520.
169. V.I. Tsaryuk, K.P. Zhuravlev, V.F. Zolin, V.A. Kudryashova, J. Legendziewicz, R. Szostak, *Journal of Applied Spectroscopy*, 74 (2007) 51-59.
170. A. Mahmood, A. Naeem, *Recent Applications in Sol-Gel Synthesis*, 2017.
171. P. Antonio, M. Lasalvia, G. Perna, V. Capozzi, *Biochimica et Biophysica Acta*, 1818 (2012) 3141–3148.

## 8. SUMMARY IN LITHUANIAN

VILNIAUS UNIVERSITETAS  
FIZINIŲ IR TECHNOLOGIJOS MOKSLŲ CENTRAS

Aurelija  
SMALENSKAITĖ

Sluoksniuotieji dvigubi hidroksidai:  
sintezė, apibūdinimas, modifikavimas ir  
lantanoidų jonų pakaitų įtaka  
liuminescencinėms savybėms

**DAKTARO DISERTACIJA**

Gamtos mokslai  
Chemija N 003

---

VILNIUS 2019

Disertacija rengta 2015–2019 metais Vilniaus universitete.

**Moksliniai vadovai:**

**prof. habil. dr. Aivaras Kareiva** (Vilniaus universitetas, gamtos mokslai, chemija – P 003). Nuo 2015-10-01 iki 2017-10-05;

**prof. dr. Aldona Beganskienė** (Vilniaus Universitetas, gamtos mokslai, chemija – P 003). Nuo 2017-10-05 iki 2019-09-30.

Gynimo taryba:

Pirmininkas: **prof. dr. Henrikas Cesiulis** (Vilniaus universitetas, gamtos mokslai, chemija – N 003).

Nariai:

**prof. dr. Rasa Pauliukaitė** (Fizinių ir technologijos mokslų centras, gamtos mokslai, chemija – N 003);

**prof. dr. Sarah L. Stoll** (Georgetown universitetas, gamtos mokslai, chemija – N 003);

**prof. habil. dr. Sigitas Tamulevičius** (Kauno technologijos universitetas, technologijos mokslai, medžiagų inžinerija – T 008);

**prof. habil. dr. Sigitas Tumkevičius** (Vilniaus universitetas, gamtos mokslai, chemija – N 003).3.

Disertacija bus ginama viešame Chemijos mokslo krypties gynimo tarybos posėdyje 2020 m. sausio 17 d. 14 val. Vilniaus universiteto Chemijos ir geomokslų fakulteto Neorganinės chemijos auditorijoje.

Adresas: Naugarduko g. 24, LT-03225 Vilnius, Lietuva. Tel.: 2193108. Faksas: 2330987.

Disertaciją galima peržiūrėti Vilniaus universiteto, Fizinių ir technologijos mokslų centro bibliotekose ir VU interneto svetainėje adresu: <https://www.vu.lt/naujienos/ivykiu-kalendorius>

VILNIUS UNIVERSITY  
CENTRE OF PHYSICAL SCIENCES AND TECHNOLOGY

Aurelija  
SMALENSKAITĖ

# Layered Double Hydroxides: synthesis, characterization, modification and lanthanide ions substitution effects on luminescent properties

**DOCTORAL DISSERTATION**

Natural sciences  
Chemistry N 003

---

VILNIUS 2019

This dissertation was written between 2015 and 2019 at Vilnius University.

**Academic supervisors:**

**Prof. Habil. Dr. Aivaras Kareiva** (Vilnius University, Natural Sciences, Chemistry – N 003) (From 2015-10-01 to 2017-10-05).

**Prof. Dr. Aldona Beganskienė** (Vilnius University, Natural Sciences, Chemistry – N 003) (From 2017-10-05 to 2019-09-30).

This doctoral dissertation will be defended in a public meeting of the Dissertation Defence Panel:

**Chairman – Prof. Dr. Henrikas Cesiulis** (Vilnius University, Natural Sciences, Chemistry – N 003).

**Members:**

**Prof. Dr. Rasa Pauliukaitė** (Centre of Physical Sciences and Technology, Natural Sciences, Chemistry – N 003);

**Prof. Dr. Sarah L. Stoll** (Georgetown University, Natural Sciences, Chemistry – N 003);

**Prof. Habil. Dr. Sigitas Tamulevičius** (Kaunas University of Technology, Technology Science, Material Engineering– T 008);

**Prof. Habil. Dr. Sigitas Tumkevičius** (Vilnius University, Natural Sciences, Chemistry – N 003).

The dissertation shall be defended at a public meeting of the Dissertation Defence Panel at 2 pm on January 17, 2020 in Inorganic Chemistry auditorium 141 of the Chemistry and Geoscience Faculty, Vilnius University.

Address: Naugarduko g. 24, LT-03225 Vilnius, Lithuania. Tel.: 2193108. Fax: 2330987.

The text of this dissertation can be accessed at the libraries of (name of the institutions granted the right to conduct doctoral studies in alphabetical order), as well as on the website of Vilnius University:

[www.vu.lt/lt/naujienos/ivykiu-kalendorius](http://www.vu.lt/lt/naujienos/ivykiu-kalendorius)

## IVADAS

Sluoksniuoti dvigubi hidroksidai (SDH) – tai junginiai, susidedantys iš teigiamą krūvį turinčių brusito ( $\text{Mg}(\text{OH})_2$ ) tipo kristalinės gardelės sluoksnių su tarp sluoksniuose esančiais krūvį kompensuojančiais anijonais bei vandens molekulėmis. Bendra SDH cheminė formulė gali būti išreikšta taip:  $[\text{M}^{2+}_{1-x}\text{M}^{3+}_x(\text{OH})_2]^{x+}(\text{A}^{m-})_{x/m} \cdot n\text{H}_2\text{O}$ . SDH gali būti sintetiniai keičiant katijono arba anijono tipą, gaunant naujas funkcines medžiagas, turinčias skirtingas fizikines-chemines savybes. SDH gali būti gaunami skirtingais sintezės metodais. Dažniausias paruošimo būdas yra bendro nusodinimo metodas sumaišant tirpias metalų druskas. Kaitinant 200–600 °C temperatūroje, SDH paverčiamas mišriu metalo oksidu (MMO), pasižyminčiu dideliu savituoju paviršiaus plotu ir galimybe, vadinama „atminties efektu“, atkurti originalią sluoksniuotąją struktūrą. Kitas būdas gauti SDH yra atliekant anijonų mainus. Anijonai yra įterpiami tarp sluoksnių, kad būtų išlaikytas junginio elektroneutralumas. Dėl tokio palankaus SDH modifikavimo galima gauti daug įvairių daugiafunkcinių SDH medžiagų, kurios gali būti naudojamos katalizėje, optikoje, korozijos inhibitoriuose, fotochemijoje ir elektrochemijoje.

Pastaruoju metu didelis dėmesys skiriamas skirtingų metalų jonų įterpimui į SDH pagrindinius sluoksnius, taip sukuriant naujas funkcines medžiagas. Į SDH įvesta daugybė pereinamųjų metalų jonų bei metalų anijoninių kompleksinių junginių su organiniais ligandais. Retųjų žemių elementai buvo išsamiai ištirti dėl jų intensyvių emisijos juostų, atsirandančių dėl f-f perėjimų. Retųjų žemių metalų jonai suteikia galimybę gauti mėlyną, žalią ir raudoną spalvas, būtinas gauti RGB prietaisams. Taigi, naujų SDH, legiruotų įvairiais lantanoidais (Ce, Eu, Nd, Tb), sintezė ir liuminescencinių savybių tyrimas sudaro šio disertacinio darbo aktualumą.

**Šios daktaro disertacijos tikslas** buvo ištirti lantanoidais pakeistų Mg-Al SDH liuminescencines savybes. Pirmą kartą lantanoidais pakeisti sluoksniuotieji dvigubi hidroksidai buvo susintetinti naudojant zolių-gelių sintezės procesą. Šiam tikslui įgyvendinti buvo suformuluoti tokie disertacijos uždaviniai:

1. Susintetinti  $\text{Ce}^{3+}$  jonais legiruotus Mg-Al SDH, ištirti jų liuminescencines savybes ir palyginti bendrojo nusodinimo ir zolių-gelių sintezės metodus šiems junginiams gauti.
2. Pirmą kartą zolių-gelių metodu susintetinti  $\text{Eu}^{3+}$  jonais legiruotą Mg-Al SDH.



3. Ištirti  $\text{Nd}^{3+}$  jonų luminescencijos savybes sluoksniuotose dvigubuose hidroksiduose.
4. Pirmą kartą zolių-gelių metodu susintetinti  $\text{Tb}^{3+}$  jonais legiruotą Mg-Al SDH.
5. Ištirti organinių anijonų ypatumus SDH struktūroje.
6. Sukurti naujus sintezės metodus plonomis Mg-Al SDH plėvelėms gaminti.

## IŠVADOS

1.  $\text{Mg}_3\text{Al}$  sluoksniuoti dvigubi hidroksidai (SDH) buvo sėkmingai susintetinti bendrojo nusodinimo ir pirmą kartą vandeniniu zolių-gelių sintezės metodais. Naujas SDH zolių-gelių sintezės metodas pagrįstas gelių kaitinimu  $650\text{ }^\circ\text{C}$  temperatūroje ir SDH rekonstravimu iš gautų mišrių metalų oksidų (MMO) vandenyje.
2. Šie sintezės metodai buvo sėkmingai pritaikyti 0,05 iki 10 mol% ceriu pakeistiems SDH ( $\text{Mg}_3\text{Al}_{1-x}\text{Ce}_x$ ) sintetinti. Nustatyta, kad rekonstruojant iš zolių-gelių gautus MMO į  $\text{Mg}_3\text{Al}_{1-x}\text{Ce}_x$  SDH virsmas nepriklauso nuo cerio koncentracijos. Gauti  $\text{Mg}_3\text{Al}_{1-x}\text{Ce}_x$  SDH sudarė šešiakampės formos daleles, kurių dydis buvo maždaug nuo 150 iki 270 nm. SDH zolių-gelių sintezės metodas yra paprastesnis už bendro nusodinimo metodą, leidžiantis susintetinti grynesnius, homogeniškesnius, aukšto kristališkumo galutinius sintezės produktus.
3. Gautų bendrojo nusodinimo metodu  $\text{Mg}_3\text{Al}_{1-x}\text{Ce}_x$  SDH liuminescencinės savybės parodė, kad  $\text{Ce}^{3+}$  jonų  $[\text{Xe}] 5d^1 - [\text{Xe}] 5f^1$  perėjimui priskiriamos pagrindinės emisijos linijos buvo stebimos 370-390 nm bangos ilgių intervale. O SDH, susintetintų zolių-gelių metodu, emisijos maksimumas buvo pasislinkęs į didesnių bangos ilgių sritį (390-430 nm).
4. Zolių-gelių metodu susintetinti vienfaziai europiu pakeisti iki 5 mol%  $\text{Mg}_3\text{Al}_{1-x}\text{Eu}_x$  SDH. Didėjant Eu koncentracijai iki 10 mol% susidarė Eu  $(\text{OH})_3$  pašalinė fazė. Taip pat,  $\text{CO}_3^{2-}$ ,  $\text{OH}^-$ ,  $\text{Cl}^-$ ,  $\text{NO}_3^-$  neorganiniai anijonai buvo pakeisti įterpiant tereftalatą (TAL) į  $\text{Mg}_3\text{Al}$  ir  $\text{Mg}_3\text{Al}_{1-x}\text{Eu}_x$  SDH tarpsluoksnius. Susidarė šešiakampės formos ir  $\sim 330\text{--}720$  nm dydžio  $\text{Mg}_3\text{Al}_{1-x}\text{Eu}_x\text{-CO}_3$  ir  $\text{Mg}_3\text{Al}_{1-x}\text{Eu}_x\text{-TAL}$  SDH dalelės.
5. Nustatyta, kad intensyviausia  ${}^5\text{D}_0 \rightarrow {}^7\text{F}_2$  emisija pasižymėjo  $\text{Mg}_3\text{Al}_{1-x}\text{Eu}_x$  SDH su 5 mol%  $\text{Eu}^{3+}$  koncentracija. Susintetinto  $\text{Mg}_3\text{Al}_{1-x}\text{Eu}_x\text{-TAL}$  SDH fotoluminescencijos intensyvumas žymiai padidėjo dėl tereftalato ligando sužadavimo energijos į  $\text{Eu}^{3+}$  joną perdavimo.

6. Neodimiu pakeisti  $Mg_3Al_{1-x}Nd_x$  1–10 mol% SDH taip pat buvo susintetinti zolių-gelių metodu. Vienfaziai SDH junginiai gauti, kai Nd pakeitimo kiekis buvo mažesnis nei 5 mol%. Tačiau gauti  $Mg_3Al_{1-x}Nd_x$  SDH neparodė jokios liuminescencijos. Neodimio liuminescenciją  $Mg_3Al_{1-x}Nd_x$  paskatino tereftalato ligando interkaliacija į SDH struktūrą.  $Mg_3Al_{1-x}Nd_x$  1-10 mol% - TAL SDH emisijos spektrai turėjo keletą emisijos juostų, esančių ties 900 ir 1065 nm, kurios atsiranda dėl  ${}^4F_{3/2} \rightarrow {}^4I_{9/2}$  ir  ${}^4F_{3/2} \rightarrow {}^4I_{11/2}$   $Nd^{3+}$  jonų perėjimų.
7. Zolių-gelių metodu susintetinti vienfaziai  $Tb^{3+}$  jonais legiruoti iki 7,5 mol%  $Mg_3Al_{1-x}Tb_x$  ir  $Mg_3Al_{1-x}Tb_x$ -TAL SDH.  $Mg_3Al_{1-x}Tb_x$  5 mol% -TAL SDH dalelių dydis buvo apie 300 nm.  $Mg_3Al_{1-x}Tb_x$ -TAL SDH emisijos intensyvumas žymiai padidėjo dėl tereftalato interkaliacijos.
8.  $Mg_3Al-CO_3$  ir  $Mg_3Al_{1-x}Eu_x$  SDH anijonai buvo sėkmingai pakeisti benzoatu, oksalatu, lauratu, malonatu, sukcinatu, tartratu, 1,3,5-benzenstrikarboksilatu, 4-metilbenzoatu, 4-dimetilaminobenzoatu ir 4-bifenilacetanatu.  $Mg_3Al_{1-x}Eu_x$  1 mol% -tartrato ir  $Mg_3Al_{1-x}Eu_x$  1 mol% - benzoato SDH emisijos pasižymėjo didžiausiu intensyvumu.
9. Zolių-gelių metodu buvo sėkmingai susintetintos  $Mg_3Al$  SDH dangos ant silicio ir nerūdijančio plieno padėklų. Gautos aukšto kristališkumo  $Mg_3Al_1$  SDH dangos. SEM mnuotraukos parodė, kad ant paviršiaus susidariusios plokštelės pavidalo dalelės yra sudarytos iš šešiakampės formos nanodalelių, būdingų SDH struktūrai.
10. Nustatytas  $Mg_3Al$  SDH paviršiaus šiurkštumo RMS parametras ant silicio padėklo buvo lygus 186,14 nm, o ant nerūdijančio plieno pagrindo - 352,62 nm. Naudojant PVA tirpalą  $Mg_3Al$  SDH modifikavimui dangų ant silicio ir nerūdijančio plieno padėklų šiurkštumas padidėjo iki 733,30 nm ir 1181,12 nm.

MOKSLINIŲ PUBLIKACIJŲ DISERTACIJOS TEMA SĄRAŠAS IR  
JŲ KOPIJOS

Straipsniai recenzuojamuose žurnaluose:

1. A. Smalenskaite, L. Pavasaryte, Thomas C.K. Yang, A. Kareiva, Undoped and  $\text{Eu}^{3+}$  doped magnesium-aluminium layered double hydroxides: peculiarities of intercalation of organic anions and investigation of luminescence properties, *Materials*, 12, 736 (2019) 1-14.
2. A. Smalenskaite, A.N. Salak, M.G.S. Ferreira, R. Skaudzius, A. Kareiva, Sol-gel synthesis and characterization of hybrid inorganic-organic Tb(III)-terephthalate containing layered double hydroxides, *Optical Materials*, 80 (2018) 186–196.
3. A. Smalenskaite, A.N. Salak, A. Kareiva, Induced neodymium luminescence in sol-gel derived layered double hydroxides, *Mendeleev Communications*, 28 (2018) 493-494.
4. A. Smalenskaite, S. Şen, A.N. Salak, M.G.S. Ferreira, A. Beganskiene, A. Kareiva, Sol-gel derived lanthanide-substituted layered double hydroxides  $\text{Mg}_3/\text{Al}_{1-x}\text{Ln}_x$ , *Acta Physica Polonica A*, 133 (2018) 884-886.
5. A. Smalenskaite, D.E.L. Vieira, A.N. Salak, M.G.S. Ferreira, A. Katelnikovas, A. Kareiva, A comparative study of co-precipitation and sol-gel synthetic approaches to fabricate cerium-substituted  $\text{MgAl}$  layered double hydroxides with luminescence properties, *Applied Clay Science*, 143 (2017) 175–183.
6. A. Smalenskaite, S. Şen, A.N. Salak, M.G.S. Ferreira, R. Skaudzius, A. Katelnikovas, A. Kareiva, Sol-gel synthesis and characterization of non-substituted and europium-substituted layered double hydroxides  $\text{Mg}_3/\text{Al}_{1-x}\text{Eu}_x$ , *Current Inorganic Chemistry*, 6 (2016) 149-154.

Pranešimų mokslinėse konferencijose tezės:

1. A. Smalenskaitė, A.N. Salak, M.G.S. Ferreira, A. Kareiva, Synthesis and characterization of hybrid inorganic-organic Tb(III)-terephthalate containing layered double hydroxides, *International conference ACIN 2018: fourth international conference on advanced complex inorganic nanomaterials*, July 15-20, 2018, Namur, Belgium.

2. A. Smalenskaitė, A. Beganskienė, R. Skaudžius, A. Kareiva, Synthesis and characterization of hybrid inorganic (LDH)-organic (terephthalate) nanostructures, *International conference Nanotechnology and nanomaterials (NANO-2018)* August 27-30, 2018, Kijev, Ukraine.
3. A. Smalenskaitė, A.N. Salak, M.G.S Ferreira, A. Katelnikovas, A. Kareiva, On the synthesis and characterization of cerium-substituted layered double hydroxides  $Mg_3Al_{1-x}Ce_x$ , *International conference ISIC 19: 19th edition of the international symposium on intercalation compounds*, 2017, May 28-June 1, Assisi, Italy.
4. A. Kareiva, A. Smalenskaitė, S. Sen, A.N. Salak, M.G.S Ferreira, A. Beganskienė, Sol-gel derived lanthanide-substituted layered double hydroxides  $Mg_3/Al_{1-x}Ln$ , *International conference on oxide materials for electronic engineering - fabrication, properties and applications, OMEE-2017*, May 29 - June 2, 2017 Lviv, Ukraine.
5. A. Smalenskaitė, A.N. Salak, M.G. Ferreira, A. Kareiva, Cerium-substituted Mg-Al layered double hydroxides synthesised by sol-gel method with luminescence properties, *There is no future without the past“ : science on the interface of XIX-XXI centuries : the international conference dedicated to the 215-th birth anniversary of Ignacy Domeyko*, 2017, Vilnius, Lithuania.
6. A. Smalenskaitė, S. Sen, A.N. Salak, M.G.S. Ferreira, A. Kareiva, A novel approach for the synthesis of layered double hydroxides  $Mg_3/Al_{1-x}Eu_x$ , *Chemistry and chemical technology 2017 : proceedings of the international conference*, April 28th, 2017, Kaunas, Lithuania.
7. A. Smalenskaitė, A.N. Salak, M.G.S. Ferreira, A. Kareiva, Reconstruction peculiarity in co-precipitated Mg/Al and Mg/Al/Ce layered double hydroxides, *International conference nanoPT 2016 - International Conference on Nanoscience and Nanotechnology*, 16-19 February, Braga, Portugal.
8. A. Smalenskaitė, A. Kareiva, Synthesis and characterization of Mg/Al and Mg/Al/Ce layered double hydroxides by co-precipitation method, *International conference Nanochemistry and nanomaterials 2015: 2nd international conference of chemists*, 2015, Vilnius, Lithuania.

Article

# Undoped and Eu<sup>3+</sup> Doped Magnesium-Aluminium Layered Double Hydroxides: Peculiarities of Intercalation of Organic Anions and Investigation of Luminescence Properties

Aurelija Smalenskaite <sup>1,\*</sup>, Lina Pavasaryte <sup>2,3</sup>, Thomas C. K. Yang <sup>2,3</sup> and Aivaras Kareiva <sup>1</sup>

<sup>1</sup> Department of Inorganic Chemistry, Vilnius University, Naugarduko 24, LT 03225 Vilnius, Lithuania; aivaras.kareiva@chf.vu.lt

<sup>2</sup> Department of Chemical Engineering and Biotechnology, National Taipei University of Technology, 1, Sec. 3, Chung-Hsiao E. Road, Taipei 106, Taiwan; lina.pavasaryte@gmail.com (L.P.); ckyang@ntu.edu.tw (T.C.K.Y.)

<sup>3</sup> Center for Precision Analysis and Materials Research, National Taipei University of Technology, 1, Sec. 3, Zhongxiao E. Rd., Taipei 10608, Taiwan

\* Correspondence: aurelija.smalenskaite@chf.vu.lt

Received: 11 January 2019; Accepted: 28 February 2019; Published: 4 March 2019



**Abstract:** The Mg<sub>3</sub>/Al and Mg<sub>3</sub>/Al<sub>0.99</sub>Eu<sub>0.01</sub> layered double hydroxides (LDHs) were fabricated using a sol-gel chemistry approach and intercalated with different anions through ion exchange procedure. The influence of the origin of organic anion (oxalate, laurate, malonate, succinate, tartrate, benzoate, 1,3,5-benzentricarboxylate (BTC), 4-methylbenzoate (MB), 4-dimethylaminobenzoate (DMB) and 4-biphenylacetate (BPhAc)) on the evolution of the chemical composition of the inorganic-organic LDHs system has been investigated. The obtained results indicated that the type and arrangement of organic guests between layers of the LDHs influence Eu<sup>3+</sup> luminescence in the synthesized different hybrid inorganic-organic matrixes. For the characterization of synthesis products X-ray diffraction (XRD) analysis, infrared (FTIR) spectroscopy, fluorescence spectroscopy (FLS), and scanning electron microscopy (SEM), were used.

**Keywords:** LDHs; Eu doping effect; intercalation of organic species; size effect; luminescence

## 1. Introduction

A general chemical formula of layered double hydroxides (LDHs) is [M<sup>2+</sup><sub>1-x</sub>M<sup>3+</sup><sub>x</sub>(OH)<sub>2</sub>]<sup>x+</sup>(A<sup>y-</sup>)<sub>x/y</sub>·zH<sub>2</sub>O, here M<sup>2+</sup> and M<sup>3+</sup> are divalent and trivalent cations forming layered structure, respectively, and A<sup>y-</sup> is anion occupying interlayer space [1]. LDHs show hexagonal crystal structure that depends on different parameters of the intercalated species. Intercalation of different anions in LDH is a challenging topic because the anion-exchange could be performed mostly, when the introduced anion has higher affinity with the LDH layer than the host anion. Usually, the anions with small size and high charge density are used for such investigations. Nevertheless, the low-charge large organic anions could also be introduced to the LDH structure [2]. The possibility to substitute of monovalent anions in the Mg/Al LDH could be expressed by following order OH<sup>-</sup> > F<sup>-</sup> > Cl<sup>-</sup> > Br<sup>-</sup> > NO<sup>3-</sup>. More selective are anions with higher charge CO<sub>3</sub><sup>2-</sup> > SO<sub>4</sub><sup>2-</sup> [3]. The anion-exchange selectivity is usually related to the guest orientation. Two orientations are observed for the organic anion within the gallery either vertical perpendicular to the layers or horizontal. Whether a vertical or horizontal orientation exists, depends upon the charge on the layers and the degree of hydration of the sample. Moreover, the water molecules stabilize the LDH structure via formation of a hydrogen bond [4–6]. The organic anions can create negative charge

in the LDH particles, which can be associated to the micellization or formation of self-assembly of exchanged or adsorbed organic anions on the LDH surface [7]. Furthermore, interaction between LDHs carbonate and carboxylate-containing substances is an important aspect of the high affinity of these types of anions to the LDH surface. The adsorption of monovalent anions on the positively charged surface can proceed differently, which can be classified by the indirect Hofmeister series of the ions. Deviation from the series of the ions was observed only for the  $\text{HCO}_3^-$  ions due to pronounced very high affinity to the LDH materials. Multivalent anions exhibit also high affinity to the LDH surfaces neutralizing the charge of the surface or even making it reversal at higher concentrations. This feature is more pronounced for anions with higher negative charge and platelets of significant negative charge could be formed. These results allow one to design LDH-based ion-exchange systems for different applications [8–10]. Besides, LDH intercalated with amino, ethylenediaminetetraacetic, diethylenetriaminepentaacetic, citric and malic acids could be used as adsorbents to remove toxic cationic and anionic species from aqueous media [11]. Moreover, LDHs intercalated with succinic acid and lauric acid were used as lubricant additives [12].

In recent years, inorganic-organic hybrid luminescence materials have been widely investigated due to the novel properties to form stable compounds with lanthanides based on unique anion exchange ability in the interlayer space of LDH. New photoluminescence materials when LDHs were doped with rare-earth (RE) have been synthesized [13,14]. These multifunctional materials are useful in many fields such as medicine, photochemistry, catalysis, environmental applications [15,16]. However, these LDHs show limitation due to the low intensity of emission which is caused by direct coordination of water molecules and hydroxyl groups to the RE centre in the layer. For the hybrid RE-organic LDH materials, intercalation of guest organic anions in the interlayer galleries influences the luminescence properties dramatically. For example, the enhanced green luminescence for  $\text{Tb}^{3+}$  by terephthalate anions in Tb-doped LDH was observed [17]. It was determined the possible energy transfer from the excited state of the introduced anion to  $\text{Tb}^{3+}$  active centres. The organic anions or neutral molecules should be chemically stable and have good solubility, significant mobility and capability to form amorphous layers [18]. The organic groups which have different donor-acceptor capabilities, different size and different lability are introduced into the LDHs host position. In the previous reports, the luminescence properties of  $\text{Eu}^{3+}$ -doped LDHs intercalated by certain organic compounds, such as naphthalene-1,5-sulfonate, naphthalene-2,6-dicarboxylate [19] citrate, glutamate, picolinate, ethylenediaminetetraacetate [20], and many other compounds [21–24] have been investigated and discussed.

The goal of the present study was to investigate the luminescence properties of the  $\text{Eu}^{3+}$  doped LDHs containing organic anions. The influence of the origin of organic anion (oxalate, laurate, malonate, succinate, tartrate, benzoate, 1,3,5-benzentricarboxylate (BTC), 4-methylbenzoate (MB), 4-dimethylaminobenzoate (DMB) and 4-biphenylacetate (BPhAc)) on the evolution of the chemical composition of the inorganic-organic LDHs system has been investigated.

## 2. Experimental

### 2.1. Synthesis of LDHs

The  $\text{Mg}_3/\text{Al}$  and  $\text{Mg}_3/\text{Al}_{0.99}\text{Eu}_{0.01}$  LDH specimens were prepared by sol-gel technique using metal nitrates  $\text{Mg}(\text{NO}_3)_2 \cdot 6\text{H}_2\text{O}$ ,  $\text{Al}(\text{NO}_3)_3 \cdot 9\text{H}_2\text{O}$  and  $\text{Eu}(\text{NO}_3)_3 \cdot 6\text{H}_2\text{O}$ , dissolved in 50 mL of deionized water as starting materials. To the obtained mixture, the 0.2 M solution of citric acid was added. The resulted solution was additionally stirred for 1 h at 80 °C. Finally, 2 mL of ethylene glycol was added with continued stirring at 150 °C. During the evaporation of solvent, the transformations from sol to the gel occurred. The synthesized precursor gel was dried at 105 °C for 24 h and was used for the synthesis of LDHs. The  $\text{Mg}_3/\text{Al}$  and  $\text{Mg}_3/\text{Al}_{0.99}\text{Eu}_{0.01}$  LDHs were fabricated by reconstruction of mixed-metal oxides (MMO) in deionized water at 80 °C for 6 h, The MMO were formed during annealing the gels at 650 °C for 4 h.

## 2.2. Intercalation of $Mg_3/Al$ and $Mg_3/Al_{0.99}Eu_{0.01}$ LDHs with Organic Anions

$Mg_3/Al$  or  $Mg_3/Al_{0.99}Eu_{0.01}$  benzoate, oxalate, laurate, malonate, succinate, tartrate, 1,3,5-benzentricarboxylate (BTC), 4-methylbenzoate (MB), 4-dimethylaminobenzoate (DMB) and 4-biphenylacetate (BPhAc) were synthesized using anion exchange technique. For this, 2 mmol of  $Mg_3/Al$  or  $Mg_3/Al_{0.99}Eu_{0.01}$  was immersed in the solution of disodium/sodium organic compounds with 1.5 molar excess amounts in comparison with LDHs. Next, the solution was stirred at room temperature for 24 h. After filtration and washing with deionized water and acetone, the synthesis product was dried at 40 °C for 12 h.

## 2.3. Characterization

X-ray diffraction analysis (XRD, Rigaku Mini Flex, Rigaku, The Woodlands, TX, USA) of synthesized compounds were performed with MiniFlex II diffractometer (Rigaku) using a primary beam Cu K $\alpha$  radiation ( $\lambda = 1.541838 \text{ \AA}$ ). The  $2\theta$  angle of the diffractometer was graduated from 8 to 80° in steps of 0.02°, with the measuring time of 0.4 s per step. Fourier-transform infrared spectroscopy (FT-IR) spectra were recorded using Bruker-Alpha FT-IR spectrometer (Bruker, Ettlingen, Germany) in the range of 4000–400  $\text{cm}^{-1}$ . The luminescent properties were investigated using Edinburgh Instruments FLS 980 spectrometer (Edinburgh Instruments, Kirkton Campus, UK). The surface morphological features were characterized using a scanning electron microscope (SEM, Hitachi, Tokyo, Japan) Hitachi SU-70. The particle and anion dimension sizes were calculated using the ImageJ and Avogadro programmes (Jolla, CA, USA). The amount of carbonate in the synthesized samples was calculated from the  $M^{II}/M^{III}$  atomic ratios, assuming that carbonate is the only charge balancing interlayer anion. The water content in the formula was determined from the results of TG analyses. The chemical composition was defined to be  $[Mg_{0.75}Al_{0.25}(OH)_2](CO_3)_{0.125}\cdot 4H_2O$ .

## 3. Results and Discussion

It is reported [3] that LDH containing not only nitrates or chlorides, but also  $CO_3^{2-}$  could be used for intercalation of other inorganic anions. Free  $CO_3^{2-}$  and the  $NO_3^-$  anions show similar symmetry, however, behave differently as interlayer anions in LDHs structure. The  $CO_3^{2-}$  is orientated parallel to the hydroxide layers. It can easily interact with hydroxyl groups of hydroxide layers by forming hydrogen bonds [25]. The  $NO_3^-$  has molecular plane tilted orientation, which makes disorder of the 3R rhombohedral symmetry [26] within a hexagonal unit cell of LDH crystal structure. Previously, the LDHs were obtained using the anion-exchanged method showing that values of basal spacing  $c$  increased significantly in comparison with starting carbonate containing LDH [11]. The parameter  $c$  depends on the size, charge and orientation of the intercalated species.

In this work, the intercalated organic anions, such as short-long carbon chains (oxalate, laurate, malonate, succinate, tartrate) and benzoic (benzoate, 1,3,5-benzentricarboxylate, 4-methylbenzoate, 4-dimethylaminobenzoate and 4-biphenylacetate) carboxyl acid groups could be arranged by anions size in the interlayer and by the charge to compensate the hydroxide layer. In the XRD patterns of the LDH phases obtained by the anion exchanged reactions the diffraction peaks were shifted to the lower values of  $2\theta$  angle proving that values of the basal spacing  $c$  increased. The positions of diffraction peaks (003) of LDHs intercalated with short-long chains ( $Mg_3/Al$ -succinate,  $Mg_3/Al$ -malonate,  $Mg_3/Al$ -tartrate,  $Mg_3/Al$ -laurate and  $Mg_3/Al$ -oxalate (see Figure 1)) are shifted to smaller  $2\theta$  angle values. The similar shift was observed and for the LDHs modified with benzoic carboxylates (Figure 2). The determined values of the lattice parameters  $c$  (see Table 1) were monotonically increased from  $c = 23.613 \text{ \AA}$  for the  $Mg_3/Al$ - $CO_3$  to  $c = 24.375 \text{ \AA}$  for the  $Mg_3/Al$ -oxalate (in the case of short-long chains intercalation) and to  $c = 24.492 \text{ \AA}$  for the  $Mg_3/Al$ -4-biphenylacetate (in the case of derivatives of aromatic hydrocarbons). These results led us to conclude that all anions studied have been successfully intercalated to the  $Mg_3/Al$  LDHs structure.

**Table 1.** The determined values of  $d$  spacing and lattice parameters of anion-intercalated  $Mg_3/Al$  LDHs. The standard deviations for all measurements do not exceed  $\pm 0.0005$ .

Sample	Basal Spacing/Å		Cell Parameter/Å	
	d(003)	d(110)	a	c
$Mg_3/Al-CO_3$	7.8744	1.5350	3.068	23.613
$Mg_3/Al$ -oxalate	8.1286	1.5385	3.076	24.375
$Mg_3/Al$ -laurate	8.0905	1.5380	3.075	24.261
$Mg_3/Al$ -tartarate	7.9970	1.5359	3.070	23.981
$Mg_3/Al$ -malonate	7.9568	1.5343	3.067	23.860
$Mg_3/Al$ -succinate	7.9454	1.5333	3.065	23.826
$Mg_3/Al$ -4-biphenylacetate	8.1675	1.5396	3.078	24.492
$Mg_3/Al$ -benzoate	8.0875	1.5384	3.075	24.252
$Mg_3/Al$ -4-methylbenzoate	8.0564	1.5383	3.075	24.159
$Mg_3/Al$ -1,3,5-benzotricarboxylate	8.0328	1.5373	3.073	24.088
$Mg_3/Al$ -4-dimethylaminobenzoate	7.8907	1.5324	3.063	23.662

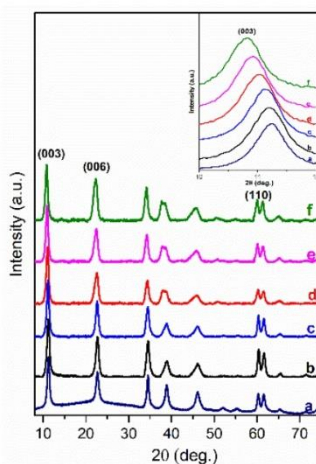


**Figure 1.** XRD patterns of  $Mg_3/Al-CO_3$  layered double hydroxides (LDH) (a) and  $Mg_3/Al-CO_3$  intercalated with organic anions:  $Mg_3/Al$ -succinate (b),  $Mg_3/Al$ -malonate (c),  $Mg_3/Al$ -tartrate (d),  $Mg_3/Al$ -laurate (e), and  $Mg_3/Al$ -oxalate (f).



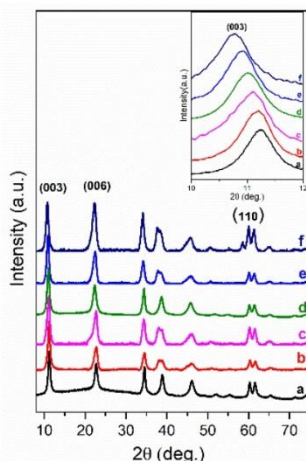


**Figure 2.** XRD patterns of  $Mg_3/Al-CO_3$  LDH (a) and  $Mg_3/Al-CO_3$  intercalated with organic anions  $Mg_3/Al-4$ -dimethylaminobenzoate (b),  $Mg_3/Al-4$ -methylbenzoate (c),  $Mg_3/Al-1,3,5$ -benzentricarboxylate (d),  $Mg_3/Al$ -benzoate (e) and  $Mg_3/Al-4$ -biphenylacetate (f).

The dimensions of anions (Table 2) show that the oxalate anion of intercalated LDH was the smallest by length (1.94 Å) and having the highest height (5.01 Å). Since the determined  $c$  parameter for the  $Mg_3/Al$ -oxalate modified LDH is the largest between short-long chains intercalation, it can be deduced that the oxalate anion has specific vertical orientation in the LDHs (see Figure 3). In the case of aromatic hydrocarbons, the height of all anions is very similar. Therefore, the 4-biphenylacetate which has a largest length (10.06 Å) has horizontal orientation in the LDH structure (Figure 3). The  $Mg_3/Al$ -oxalate and the  $Mg_3/Al-4$ -biphenylacetate LDHs having similar basal spacings correspond to the intercalated LDHs with vertical and horizontal anion orientations in which they are grafting into the hydroxide layers. There are spherical energetic interferences between  $-CH_3$  groups of anions and M-OH hydroxide layers what cause difficult intercalation in the LDH structure. The formation of hydrogen bonds between water molecules in the layers, the hydroxide layers, the interlayer anions, and among the  $H_2O$  molecules themselves is possible. The orientation of oxalate anion possibly is related to the formation of  $H_2O$  molecules more compact structures with the two  $-COO^-$  groups than with the hydrophobic ends of the monocarboxylate. Four oxalate  $-COO^-$  groups are distributed perpendicular to the layers, with two O-atoms coordinated to different hydroxide layers. In the case of 4-biphenylacetate, the  $-COO^-$  groups are orientated differently, and the O-atoms of its  $-COO^-$  groups that situated parallel to the layers can occupy M-OH sites along the H-H vectors, whereas those  $-COO^-$  tend to occupy the centers of the M-OH triangles.

Table 2. Formula and dimensions of anions.

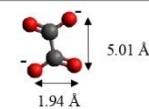
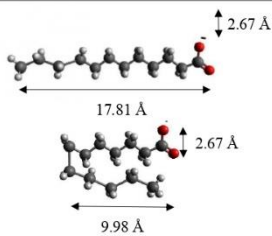
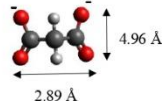
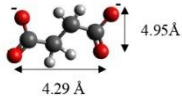
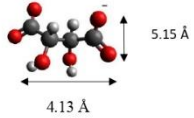
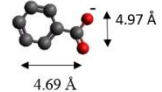
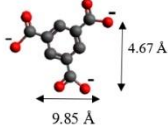
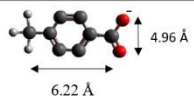
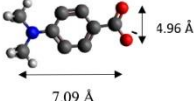
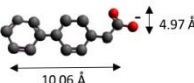
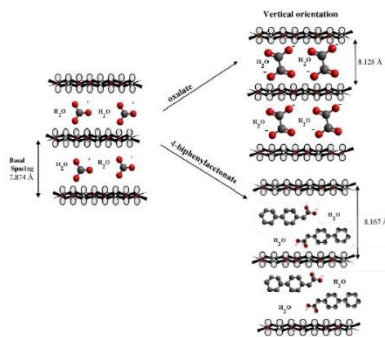
Anion	Chemical Formula	Structural Formula and Dimensions
Oxalate	$(C_2H_4)^{2-}$	
Laurate	$(C_{12}H_{23}O_2)^{2-}$	
Malonate	$(C_3H_2O_4)^{2-}$	
Succinate	$(C_3H_4O_4)^{2-}$	
Tartrate	$(C_4H_4O_6)^{2-}$	
Benzoate	$(C_7H_5O_2)^-$	
1,3,5-benzentricarboxylate	$(C_9H_5O_6)^{3-}$	

Table 2. Cont.

Anion	Chemical Formula	Structural Formula and Dimensions
4-methylbenzoate	$(C_8H_7O_2)^-$	
4-dimethylaminobenzoate	$(C_9H_{10}O_2)^-$	
4-biphenylacetate	$(C_{14}H_{11}O_2)^-$	



**Figure 3.** A schematic structure of LDHs with interlayer carbonate anion and the specific orientation of oxalate and 4-biphenylacetate anions between the layers.

Europium substitution effects incorporating  $Eu^{3+}$  at the  $Al^{3+}$  positions in  $Mg_3Al$ -organic anion LDHs have been investigated. According to [27], the  $Mg_3/Al_{0.99}Eu_{0.01}$  (with 1 mol% of Eu) have been prepared and intercalated with different organic anions. The XRD patterns (Figures 4 and 5) for the hybrid inorganic-organic  $Mg_3/Al_{0.99}Eu_{0.01}$  LDHs showed, that the position of the (003) diffraction line is relevant to the interlayer distance and depends on the size of the intercalated organic anion. Surprisingly, the shift of the diffraction lines in the XRD patterns of intercalated with different organic anions of  $Eu^{3+}$ -substituted LDHs is less pronounced in comparison with the samples without europium. This might be due to the reason, that the electrostatic attraction between mixed-metal cations and anions is weaker influencing on the distance of interlayer.

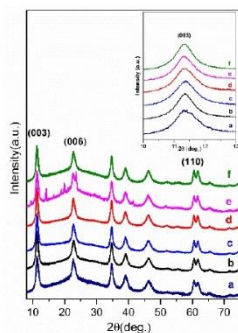


**Figure 4.** XRD patterns of  $Mg_3/Al_{0.99}Eu_{0.01}-CO_3$  (a) and hybrid inorganic-organic LDHs:  $Mg_3/Al_{0.99}Eu_{0.01}$ -succinate (b),  $Mg_3/Al_{0.99}Eu_{0.01}$ -malonate (c),  $Mg_3/Al_{0.99}Eu_{0.01}$ -tartrate (d),  $Mg_3/Al_{0.99}Eu_{0.01}$ -laurate (e) and  $Mg_3/Al_{0.99}Eu_{0.01}$ -oxalate (f).

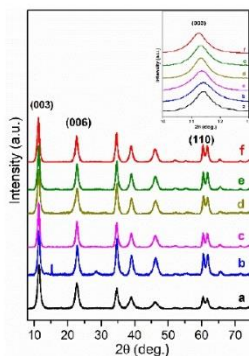


**Figure 5.** XRD patterns of  $Mg_3/Al_{0.99}Eu_{0.01}-CO_3$  (a) and hybrid inorganic-organic LDHs:  $Mg_3/Al_{0.99}Eu_{0.01}$ -4-dimethylaminobenzoate (b),  $Mg_3/Al_{0.99}Eu_{0.01}$ -4-methylbenzoate (c),  $Mg_3/Al_{0.99}Eu_{0.01}$ -1,3,5-benzentricarboxylate (d),  $Mg_3/Al_{0.99}Eu_{0.01}$ -benzoate (e) and  $Mg_3/Al_{0.99}Eu_{0.01}$ -4-biphenylacetate (f).

FT-IR spectra of  $Mg_3/Al$ ,  $Mg_3/Al_{0.99}Eu_{0.01}$  and hybrid inorganic-organic LDHs are shown in Figures 6 and 7. The spectra of all samples are almost identical with very little differences. The broad absorptions visible at  $3500-3000\text{ cm}^{-1}$  are characteristic vibrations of (-OH) groups [11]. The most intensive absorption bands detectable at  $1360\text{ cm}^{-1}$  could be assigned to the asymmetric vibrations of  $CO_3^{2-}$ , which still exists in the interlayer of intercalated LDHs along with intercalated organic anions. The absorption bands in the range of  $1570-1627\text{ cm}^{-1}$  are assigned to the carbon-oxygen bonds of (-COO<sup>-</sup>) group. The first absorption band is related to the asymmetric vibration of the carboxylate group ( $\nu_{as}, COO^-$ ) and the second is attributable to the symmetric

vibration of the carboxylate group ( $\nu_s$ ,  $\text{COO}^-$ ), demonstrating the coordination of carboxylates to  $\text{Mg}_3/\text{Al}$ -benzoate (h),  $\text{Mg}_3/\text{Al}$ -1,3,5-benzentricarboxylate (i),  $\text{Mg}_3/\text{Al}$ -4-methylbenzoate (Figure 6) and  $\text{Mg}_3/\text{Al}_{0.99}\text{Eu}_{0.01}$ -benzoate (g),  $\text{Mg}_3/\text{Al}_{0.99}\text{Eu}_{0.01}$ -1,3,5-benzentricarboxylate (h) (Figure 7). The absorption bands visible at  $2850\text{--}2937\text{ cm}^{-1}$  are due to the C-H stretching vibrations of methylene ( $-\text{CH}_2-$ ) of the organic compounds. Thus, the FT-IR results prove the formation of the inorganic-organic hybrids and interactions of the introduced organic species with the LDH layers.

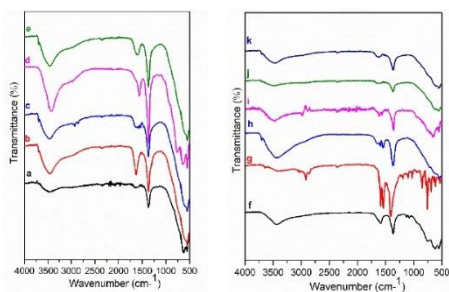


**Figure 6.** FT-IR spectra of  $\text{Mg}_3/\text{Al}\text{-CO}_3$  (a) and hybrid inorganic-organic LDHs:  $\text{Mg}_3/\text{Al}$ -oxalate (b),  $\text{Mg}_3/\text{Al}$ -laurate (c),  $\text{Mg}_3/\text{Al}$ -succinate (d),  $\text{Mg}_3/\text{Al}$ -malonate (e). FT-IR spectra of  $\text{Mg}_3/\text{Al}$ -tartrate (f),  $\text{Mg}_3/\text{Al}$ -4-biphenylacetate (g),  $\text{Mg}_3/\text{Al}$ -benzoate (h),  $\text{Mg}_3/\text{Al}$ -1,3,5-benzentricarboxylate (i),  $\text{Mg}_3/\text{Al}$ -4-methylbenzoate (j) and  $\text{Mg}_3/\text{Al}$ -4-dimethylaminobenzoate (k).

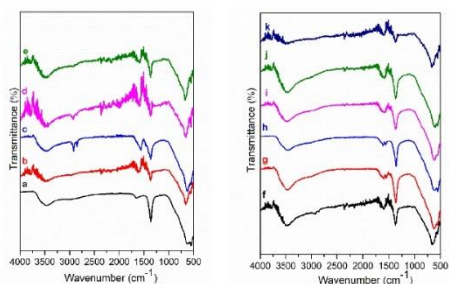


**Figure 7.** FT-IR spectra of  $\text{Mg}_3/\text{Al}_{0.99}\text{Eu}_{0.01}\text{-CO}_3$  (a) and hybrid inorganic-organic LDHs:  $\text{Mg}_3/\text{Al}_{0.99}\text{Eu}_{0.01}$ -oxalate (b),  $\text{Mg}_3/\text{Al}_{0.99}\text{Eu}_{0.01}$ -laurate (c),  $\text{Mg}_3/\text{Al}_{0.99}\text{Eu}_{0.01}$ -succinate (d),  $\text{Mg}_3/\text{Al}_{0.99}\text{Eu}_{0.01}$ -malonate (e). FT-IR spectra of  $\text{Mg}_3/\text{Al}_{0.99}\text{Eu}_{0.01}$ -tartrate (f),  $\text{Mg}_3/\text{Al}_{0.99}\text{Eu}_{0.01}$ -benzoate (g),  $\text{Mg}_3/\text{Al}_{0.99}\text{Eu}_{0.01}$ -1,3,5-benzentricarboxylate (h),  $\text{Mg}_3/\text{Al}_{0.99}\text{Eu}_{0.01}$ -4-biphenylacetate (i),  $\text{Mg}_3/\text{Al}_{0.99}\text{Eu}_{0.01}$ -4-methylbenzoate (j) and  $\text{Mg}_3/\text{Al}_{0.99}\text{Eu}_{0.01}$ -4-dimethylaminobenzoate (k).

The emission spectra obtained at room temperature of  $\text{Mg}_3/\text{Al}_{0.99}\text{Eu}_{0.01}$  and  $\text{Mg}_3/\text{Al}_{0.99}\text{Eu}_{0.01}$  samples intercalated with benzoate, oxalate, laurate, malonate, succinate, tartrate, 1,3,5-benzentricarboxylate (BTC), 4-methylbenzoate (MB), 4-dimethylaminobenzoate (DMB) and 4-biphenylacetate (BPhAc) anions ( $\lambda_{\text{ex}} = 394\text{ nm}$ ) are presented in Figure 8. The emission spectra

of  $Mg_3/Al_{0.99}Eu_{0.01}$ —organic anion LDHs show four main emission lines between 550 nm and 740 nm. All observed emission bands are due to  ${}^5D_0-{}^7F_J$  ( $J = 1, 2, 3, 4$ ) transitions of  $Eu^{3+}$  ions. According to the literature, the emissions are  ${}^5D_0-{}^7F_1$  (590 nm),  ${}^5D_0-{}^7F_2$  (613 nm),  ${}^5D_0-{}^7F_3$  (650 nm) and  ${}^5D_0-{}^7F_4$  (697 nm) transitions typical of  $Eu^{3+}$  ion [28]. The  $Eu^{3+}$  ions occupy a low-symmetry site, since the emission due to  ${}^5D_0-{}^7F_2$  transition is the strongest. Moreover, the results obtained indicate that the excitation energy to the  $Eu^{3+}$  ion in most of the cases is transferring from the organic anion ligands increasing the intensity of emission of the LDHs. Two mechanisms of intramolecular and intermolecular energy transfer between lanthanide ions and organic molecules have been suggested [29]. As was stated in [29], the intensity of emission of lanthanide distributed in host matrixes is affected by the energy matching degree between organic ligands and lanthanide ions. Evidently, when the energy matching degree is better, the energy transfer efficiency is higher and, consequently, the emission intensity of the compound is higher. The potency to absorb the UV radiation by interlayer organic anions and possible transfer this energy to the  $Eu^{3+}$  center by the interaction between the carboxyl oxygen of the intercalated anions with the hydrogen of the  $M(OH)_6$  octahedra via a hydrogen bond was suggested. The tartrate and benzoate having the strong basicity, showed higher ability to absorb the light [30]. Carbonate is a weaker base, thus transferring less energy to  $Eu^{3+}$  ions. The aromatic ring in the benzene can also influence the levels of resonant energy of lanthanide ions. As we can see from emission spectra the  $Mg_3/Al_{0.99}Eu_{0.01}$ -tartrate and  $Mg_3/Al_{0.99}Eu_{0.01}$ -benzoate LDHs show the highest emission intensity to compare with LDHs containing other organic ligands. Carboxylate and carbonyl groups connected with aromatic ring usually decrease the intensity of emission. The energy matching degree in the benzoate and  $Eu(III)$  complex obviously should be enhanced influencing the intensity of emission [31]. Moreover, the bridge of methylene groups  $-CH_2-$  can break up the conjugated  $\pi$ -electron system [18].

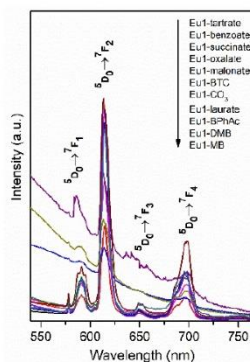


**Figure 8.** Emission spectra of  $Mg_3/Al_{0.99}Eu_{0.01}$  and LDHs intercalated with tartrate, benzoate, succinate, oxalate, malonate, 1,3,5-benzentricarboxylate, laurate, 4-biphenylacetate, 4-dimethylaminobenzoate and 4-methylbenzoate. (Ex = 394 nm).

The SEM micrographs depicted in Figure 9 represent the microstructure of  $Mg_3/Al-CO_3$  and  $Mg_3/Al_{0.99}Eu_{0.01}-CO_3$  layered double hydroxides. As seen, the solids are composed of particles having plate form and size about of 200–400 nm. The representative SEM micrographs of LDHs intercalated with different organic anions are shown in Figure 10. The surface microstructure still represents the characteristic features of LDHs [32], however, the particle sizes increased considerably

(500–600 nm). Finally, the SEM micrographs of the samples which showed the most intensive emission  $Mg_3/Al_{0.99}Eu_{0.01}$ -tartrate and  $Mg_3/Al_{0.99}Eu_{0.01}$ -benzoate are presented in Figure 11. Evidently, the surface microstructure of these two samples is almost identical. The hexagonally shaped particles with the size of ~450–500 nm have formed.

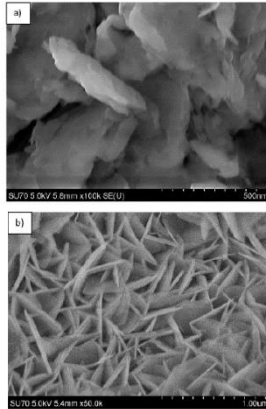


Figure 9. SEM micrographs of  $Mg_3/Al-CO_3$  (a) and  $Mg_3/Al_{0.99}Eu_{0.01}-CO_3$  (b) LDHs.

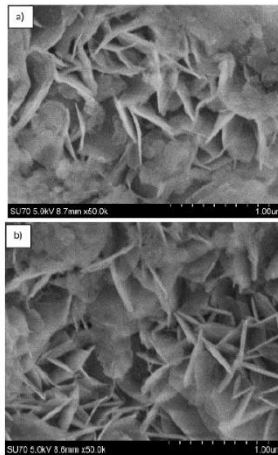


Figure 10. SEM micrographs of  $Mg_3/Al$ -oxalate (a) and  $Mg_3/Al$ -4-biphenylacetate (b) LDHs.

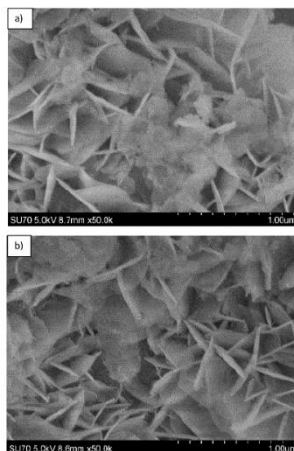


Figure 11. SEM micrographs of  $Mg_3/Al_{0.99}Eu_{0.01}$ -tartrate (a) and  $Mg_3/Al_{0.99}Eu_{0.01}$ -benzoate (b) LDHs.

#### 4. Conclusions

$Mg_3/Al-CO_3$  and  $Mg_3/Al_{0.99}Eu_{0.01}$  LDHs intercalated with benzoate, oxalate, laurate, malonate, succinate, tartrate, 1,3,5-benzentricarboxylate (BTC), 4-methylbenzoate (MB), 4-dimethylaminobenzoate (DMB) and 4-biphenylacetate (BPhAc) were prepared by sol-gel processing. The XRD analysis results clearly showed that the positions of diffraction peaks (003) of LDHs intercalated with anions were shifted to smaller  $2\theta$  angle values. However, the shift of the diffraction lines in the XRD patterns of intercalated with different organic anions of  $Eu^{3+}$ -substituted LDHs was less pronounced in comparison with the samples without europium. The FT-IR results demonstrated once again the formation of the inorganic-organic hybrids and interaction of the organic ions with the LDH layers. The obtained results let us to conclude that depending on the size of anions these species could have specific vertical or horizontal orientations in the LDH structure. The microstructure of  $Mg_3/Al-CO_3$ ,  $Mg_3/Al_{0.99}Eu_{0.01}-CO_3$  and  $Mg_3/Al_{0.99}Eu_{0.01}$ -organic anion was typical for LDH samples. The SEM images showed the formation of hexagonally shaped plate-like particles of LDHs of 200–600 nm in size with high degree of agglomeration. The room temperature luminescence of  $Mg_3/Al_{0.99}Eu_{0.01}$  and  $Mg_3/Al_{0.99}Eu_{0.01}$  samples intercalated with benzoate, oxalate, laurate, malonate, succinate, tartrate, 1,3,5-benzentricarboxylate (BTC), 4-methylbenzoate (MB), 4-dimethylaminobenzoate (DMB) and 4-biphenylacetate (BPhAc) anions under excitation at 394 nm was investigated. In all spectra, the typical four emission bands due to transitions of  ${}^3D_0 \rightarrow {}^7F_1$  (590 nm),  ${}^3D_0 \rightarrow {}^7F_2$  (613 nm),  ${}^3D_0 \rightarrow {}^7F_3$  (650 nm) and  ${}^3D_0 \rightarrow {}^7F_4$  (697 nm) of  $Eu^{3+}$  ion were determined. The  $Mg_3/Al_{0.99}Eu_{0.01}$ -tartrate and  $Mg_3/Al_{0.99}Eu_{0.01}$ -benzoate LDHs showed the highest emission intensity to compare with LDHs containing other organic ligands.

**Author Contributions:** Conceptualization, A.S. and A.K.; methodology, A.S.; software, A.S.; validation, T.C.K.Y., L.P. and A.K.; formal analysis, A.K.; investigation, A.S.; resources, L.P.; data curation, T.C.K.Y.; writing—original draft preparation, A.S.; writing—review and editing, A.K.; visualization, T.C.K.Y.; supervision, A.K.; project administration, A.K.; funding acquisition, A.K.

**Funding:** This research received no external funding.



**Acknowledgments:** L. Pavasaryte is thankful for the Post-Doctoral Fellowship administrated through the National Taipei University of Technology.

**Conflicts of Interest:** The authors declare no conflict of interest.

## References

1. Evans, D.E.; Slade, R.C.T. *Layered Double Hydroxides*; Springer-Verlag: Berlin, Germany, 2005; Volume 119, pp. 1–87.
2. Khan, A.I.; O'Hare, D. Intercalation chemistry of layered double hydroxides: recent developments and applications. *J. Mater. Chem.* **2002**, *12*, 3191–3198. [[CrossRef](#)]
3. Miyata, S. Anion-exchange properties of hydrotalcite-like compounds. *Clays Clay Miner.* **1983**, *31*, 305–311. [[CrossRef](#)]
4. Costa, D.G.; Rocha, A.B.; Souza, W.F.; Chiaro, S.S.X.; Leitao, A.A. Structural model proposition and thermodynamic and vibrational analysis of hydrotalcite-like compounds by DFT calculations. *J. Phys. Chem.* **2010**, *114*, 14133–14140. [[CrossRef](#)]
5. Kim, N.; Harale, A.; Tsotsis, T.T.; Sahimi, M. Atomistic simulation of nanoporous layered double hydroxide materials and their properties. II. Adsorption and diffusion. *J. Chem. Phys.* **2007**, *127*, 224701. [[CrossRef](#)] [[PubMed](#)]
6. Wang, J.; Kirkpatrick, G.K.R.J.; Hou, X. Interlayer Structure and Dynamics of  $\text{Cl}^-$ – $\text{LiAl}_2$ -Layered Double Hydroxide:  $^{35}\text{Cl}$  NMR Observations and Molecular Dynamics Modeling. *Chem. Mater.* **2002**, *14*, 2078–2085.
7. Pavlovic, M.; Adok-Sipiczki, M.; Nardin, C.; Pearson, S.; Bourgeat-Lami, E.; Prevot, V.; Szilagy, I. Effect of MacroRAFT Copolymer Adsorption on the Colloidal Stability of Layered Double Hydroxide Nanoparticles. *Langmuir* **2015**, *31*, 12609–12617. [[CrossRef](#)] [[PubMed](#)]
8. Xu, Z.P.; Jin, Y.; Li, S.; Hao, Z.; Lu, G.Q. Surface charging of layered double hydroxides during dynamic interactions of anions at the interfaces. *J. Colloid Interface Sci.* **2008**, *326*, 522–529. [[CrossRef](#)] [[PubMed](#)]
9. Pavlovic, M.; Huber, R.; Adok-Sipiczki, M.; Nardina, C.; Szilagy, I. Ion specific effects on the stability of layered double hydroxide colloids. *Soft Matter* **2016**, *12*, 4024–4033. [[CrossRef](#)] [[PubMed](#)]
10. Pavlovic, M.; Rouster, P.; Oncsik, T.; Szilagy, I. Tuning Colloidal Stability of Layered Double Hydroxides: from Monovalent Ions to Polyelectrolytes. *ChemPlusChem* **2017**, *82*, 121–131. [[CrossRef](#)]
11. Liu, L.; Wang, Q.; Gao, C.; Chen, H.; Liu, W.; Tang, Y. Dramatically Enhanced Luminescence of Layered Terbium Hydroxides as Induced by the Synergistic Effect of  $\text{Gd}^{3+}$  and Organic Sensitizers. *J. Phys. Chem. C* **2014**, *118*, 14511–14520. [[CrossRef](#)]
12. Kovar, P.; Pospisil, M.; Nocchetti, M.; Capkova, P.; Melanova, K. Molecular modeling of layered double hydroxide intercalated with benzoate, modeling and experiment. *J. Mol. Model.* **2007**, *13*, 937–942. [[CrossRef](#)] [[PubMed](#)]
13. Posati, T.; Costantino, F.; Latterini, L.; Nocchetti, M.; Paolantoni, M.; Tarpani, L. New insights on the incorporation of lanthanide ions into nanosized layered double hydroxides. *Inorg. Chem.* **2012**, *51*, 13229. [[CrossRef](#)] [[PubMed](#)]
14. Zhao, Y.; Li, J.G.; Fang, E.; Chu, N.; Ma, H.; Yang, X. Structure and luminescence behaviour of as-synthesized, calcined, and restored  $\text{MgAlEu-LDH}$  with high crystallinity. *Dalton Trans.* **2012**, *41*, 12175–12184. [[CrossRef](#)] [[PubMed](#)]
15. Salak, A.N.; Tedim, J.; Kuznetsova, A.I.; Ribeiro, J.L.; Vieira, L.G.; Zheludkevich, M.L.; Ferreira, M.G.S. Comparative X-ray diffraction and infrared spectroscopy study of Zn-Al layered double hydroxides: Vanadate vs nitrate. *Chem. Phys.* **2012**, *397*, 102–108. [[CrossRef](#)]
16. Constantino, U.; Constantino, F.; Elisei, F.; Latterini, L.; Nocchetti, M. Coupling physical chemical techniques with hydrotalcite-like compounds to exploit their structural features and new multifunctional hybrids with luminescent properties. *Phys. Chem. Chem. Phys.* **2013**, *32*, 13254–13269. [[CrossRef](#)] [[PubMed](#)]
17. Smalenskaite, A.; Salak, A.N.; Ferreira, M.G.S.; Skaudzius, R.; Kareiva, A. Sol-gel synthesis and characterization of hybrid inorganic-organic Tb(III)-terephthalate containing layered double hydroxides. *Opt. Mater.* **2018**, *80*, 186–196.
18. Tsaryuk, V.I.; Zhuravlev, K.P.; Zolin, V.F.; Kudryashova, V.A.; Legendziewicz, J.; Szostak, R. Luminescence efficiency of aromatic carboxylates of europium and terbium when methylene bridges and nitro groups are present in the ligands. *J. Appl. Spectrosc.* **2007**, *74*, 51–59. [[CrossRef](#)]

19. Hu, X.; Gao, X. Multilayer coating of gold nanorods for combined stability and biocompatibility. *Phys. Chem. Chem. Phys.* **2011**, *13*, 10028–10035.
20. Li, C.; Wang, L.; Evans, D.G.; Duan, X. Thermal Evolution and Luminescence Properties of Zn-Al-Layered Double Hydroxides Containing Europium(III) Complexes of Ethylenediaminetetraacetate and Nitrilotriacetate. *Ind. Chem. Res.* **2009**, *48*, 2162–2171. [CrossRef]
21. Sohn, Y. Structural and spectroscopic characteristics of terbium. hydroxide/oxide nanorods and plates. *Ceram. Int.* **2014**, *40*, 13803. [CrossRef]
22. Jyothy, P.V.; Amrutha, K.A.; Gijo, J.; Unnikrishnan, N.V. Fluorescence enhancement in Tb<sup>3+</sup>/CdS nanoparticles doped silica xerogels. *J. Fluoresc.* **2009**, *19*, 165. [CrossRef] [PubMed]
23. Tran, H.N.; Lin, C.; Woo, S.H.; Chao, H.P. Efficient removal of copper and lead by Mg/Al layered double hydroxides intercalated with organic acid anions: adsorption kinetics, isotherms, and thermodynamics. *Appl. Clay Sci.* **2018**, *154*, 17–27. [CrossRef]
24. Li, S.; Qin, H.; Zuo, R.; Bai, Z. Tribological performance of Mg/Al/Ce layered double hydroxides nanoparticles and intercalated products as lubricant additives. *Appl. Surf. Sci.* **2015**, *353*, 643–650. [CrossRef]
25. Costa, D.G.; Rocha, A.B.; Souza, W.F.; Chiaro, S.S.; Leita, A.A. Comparative Structural, thermodynamic and electronic analyses of ZnAlAn– hydrotalcite-like compounds (An = Cl<sup>-</sup>, F<sup>-</sup>, Br<sup>-</sup>, OH<sup>-</sup>, CO<sub>3</sub><sup>2-</sup> or NO<sub>3</sub><sup>-</sup>): An ab initio study. *Appl. Clay Sci.* **2012**, *56*, 16–22. [CrossRef]
26. Serdechnova, M.; Salak, A.N.; Barbosa, F.S.; Vieira, D.E.L.; Tedim, J.; Zheludkevich, M.L.; Ferreira, M.G.S. Interlayer intercalation and arrangement of 2-mercaptobenzothiazolate and 1,2,3 benzotriazolate anions in layered double hydroxides: *In situ* X-ray diffraction study. *J. Solid State Chem.* **2016**, *233*, 158–165. [CrossRef]
27. Smalenskaite, A.; Sen, S.; Salak, A.N.; Ferreira, M.G.S.; Skaudzius, R.; Katelnikovas, A.; Kareiva, A. Sol-gel Synthesis and Characterization of Non-Substituted and Europium-Substituted Layered Double Hydroxides Mg<sub>3</sub>/Al<sub>1-x</sub>Eu<sub>x</sub>. *Curr. Inorg. Chem.* **2016**, *6*, 149–154. [CrossRef]
28. Gago, S.; Pillinger, M.; Ferreira, R.A.S.; Carlos, L.D.; Santos, T.M.; Goncalves, I.S. Immobilization of lanthanide ions in a pillared layered double hydroxide. *Chem. Mater.* **2005**, *17*, 5803–5809. [CrossRef]
29. Yan, B.; Wang, W.-J.; Song, Y.-S. Photophysical properties of praseodymium complexes with aromatic carboxylic acids: double light conversion both in ultraviolet and visible region. *Spectrochim. Acta Part A* **2007**, *66*, 1115–1121. [CrossRef] [PubMed]
30. Bryce-Smith, D.; Gilbert, A.; Orger, B.; Twitchett, P. Photoaddition of ethylenes and acetylenes to hexafluorobenzene. *Chem. Soc.* **1978**, *1*, 241–245. [CrossRef]
31. Hilder, M.; Junk, P.C.; Kynast, U.H.; Lezhnina, M.M. Spectroscopic properties of lanthanoid benzene carboxylates in the solid state: Part 1. *J. Photochem. Photobiol. A* **2009**, *202*, 10–20. [CrossRef]
32. Xu, Z.P.; Braterman, P.S. Synthesis, structure and morphology of organic layered double hydroxide (LDH) hybrids: Comparison between aliphatic anions and their oxygenated analogs. *Appl. Clay Sci.* **2010**, *48*, 235–242. [CrossRef]



© 2019 by the authors. Licensee MDPI, Basel, Switzerland. This article is an open access article distributed under the terms and conditions of the Creative Commons Attribution (CC BY) license (<http://creativecommons.org/licenses/by/4.0/>).



## Sol-gel synthesis and characterization of hybrid inorganic-organic Tb(III)-terephthalate containing layered double hydroxides

A. Smalenskaite<sup>a,\*</sup>, A.N. Salak<sup>b</sup>, M.G.S. Ferreira<sup>b</sup>, R. Skaudzius<sup>a</sup>, A. Kareiva<sup>b</sup>

<sup>a</sup> Department of Inorganic Chemistry, Institute of Chemistry, Vilnius University, Naugarduko 24, LT 03225, Vilnius, Lithuania

<sup>b</sup> Department of Materials and Ceramic Engineering, CICECO – Aveiro Institute of Materials, 3810-193 Aveiro, Portugal



### ARTICLE INFO

#### Keywords:

Layered double hydroxides  
Sol-gel processing  
Terbium substitution effects  
Intercalation of terephthalate  
Luminescent properties

### ABSTRACT

Mg<sub>3</sub>/Al<sub>1</sub> and Mg<sub>3</sub>/Al<sub>1-x</sub>Tb<sub>x</sub> layered double hydroxides (LDHs) intercalated with terephthalate anion were synthesized using sol-gel method. The obtained materials were characterized by X-ray diffraction (XRD) analysis, infrared (FTIR) spectroscopy, fluorescence spectroscopy (FLS) and scanning electron microscopy (SEM). The Tb<sup>3+</sup> substitution effects in the Mg<sub>3</sub>/Al<sub>1-x</sub>Tb<sub>x</sub> LDHs were investigated by changing the Tb<sup>3+</sup> concentration in the cation layers. The study indicates that the organic guest-terephthalate in the interlayer spacing of the LDH host influences the luminescence of the hybrid inorganic-organic materials.

### 1. Introduction

Layered double hydroxides (LDHs) are compounds composed of positively charged brucite-like layers with an interlayers containing anions and water molecules  $(M_1^{2+}M_2^{2+}(\text{OH})_2)^+(A^-)_{x/y}z\text{H}_2\text{O}$ , where M<sup>2+</sup> and M<sup>3+</sup> are divalent and trivalent metal cations and A<sup>n-</sup> is an intercalated anion). In the composition of LDH materials the M<sup>2+</sup> and M<sup>3+</sup> cations can be substituted or partly replaced by other cations and the interlayer anion can also be replaced by other anions, modifying their chemical and physical properties. The commonly found M<sup>2+</sup> and M<sup>3+</sup> cations in the LDH structure are Mg<sup>2+</sup>, Zn<sup>2+</sup>, Co<sup>2+</sup>, Ni<sup>2+</sup>, Cu<sup>2+</sup> or Mn<sup>2+</sup> and Al<sup>3+</sup>, Cr<sup>3+</sup>, Co<sup>3+</sup>, Fe<sup>3+</sup>, V<sup>3+</sup> or Y<sup>3+</sup>, respectively. Small anions with relatively high charge density are generally the most preferable. However, the LDHs can be intercalated also with low-charge large anions (including organic species) [1–3]. The ease of exchange of monovalent anions is in the order of OH<sup>-</sup> > F<sup>-</sup> > Cl<sup>-</sup> > Br<sup>-</sup> > NO<sub>3</sub><sup>-</sup>. Divalent anions, such as SO<sub>4</sub><sup>2-</sup> > CO<sub>3</sub><sup>2-</sup> have higher selectivity than monovalent anions. LDHs containing NO<sub>3</sub><sup>-</sup> anions are the most suitable precursors for anion exchange due to the easy displacement from the interlayer [4]. LDHs are widely used in commercial products as adsorbents, catalyst support precursors, anion exchangers, acid residue scavengers, flame retardants, osmosis membranes and sensors [5–9]. The formation and exploitation of new types of layered double hydroxide (LDH)/polymer NC hydrogels with high performance has been also investigated [10].

LDHs can be fabricated by different synthesis methods. However, the most common preparation technique is co-precipitation method starting from soluble salts of the metals [11,12]. Sol-gel synthesis route

for the mixed metal oxides and related compounds have some benefits over other methods such as simplicity, synthesis at low temperatures, effectiveness, suitability for different systems and cost efficiency [13–16]. Recently we showed, that the synthesis products obtained by reformation of the sol-gel derived mixed metal oxides (MMO) show the typical LDH structure [17,18].

Considerable attention has been focused on incorporating rare earth elements into LDH host layers to develop new functional materials, which resemble designed optical properties [19,20]. Many investigations of luminescent materials based on aromatic carboxylates of lanthanides have related to their use in analytical chemistry, biology, medical diagnostics, and environmental monitoring. LDHs doped with Tb<sup>3+</sup> ions in the brucite-like layers were prepared by a simple one-step co-precipitation method with incorporation of 4-biphenylacetate anion in the interlayer space of the LDH [21]. The luminescence study indicated that energy transfer from the excited state of the intercalated anion guest molecules to Tb<sup>3+</sup> centres in the host layers takes place. The influence of pyridine-2,6-dicarboxylic acid (H<sub>2</sub>dpic) for the luminescence of rare earth ions have been discussed. The substitution effects of 2,20-biphenyldicarboxylic, 1,3,5-benzenetri-carboxylic, quinalic, terephthalic, and 2,5-pyridinedicarboxylic acids, phenylalanine and tyrosine were also investigated [22–25].

The main aim of this study was to investigate Tb<sup>3+</sup> substitution effects in the hybrid inorganic-organic Mg<sub>3</sub>/Al<sub>1-x</sub>Tb<sub>x</sub> terephthalate (TAL) system fabricated for the first time to the best of our knowledge by sol-gel synthesis route. The results on the influence of TAL addition on the luminescence of Tb<sup>3+</sup> in the LDH matrix will be presented herein.

\* Corresponding author.

E-mail address: aurelija.smalenskaite@ch.vu.lt (A. Smalenskaite).

<https://doi.org/10.1016/j.optmat.2018.04.048>

Received 14 March 2018; Received in revised form 23 April 2018; Accepted 24 April 2018  
0925-3467 / © 2018 Published by Elsevier B.V.

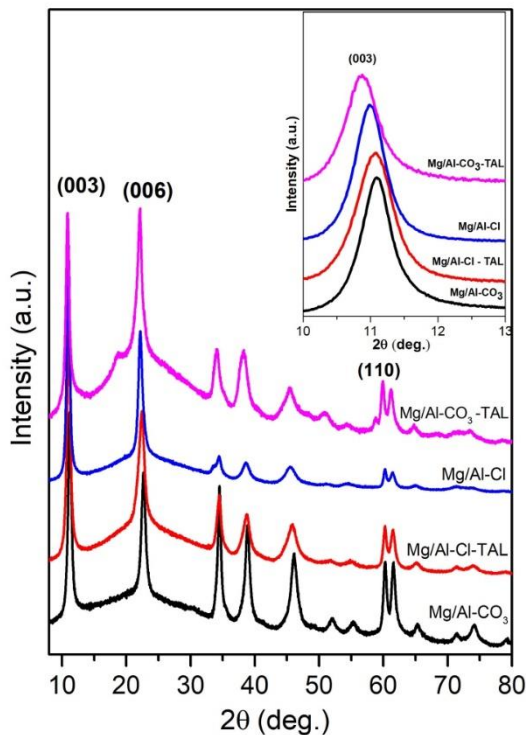


Fig. 1. XRD patterns of  $Mg_3/Al-CO_3$ ,  $Mg_3/Al-Cl$  and exchanged with TAL LDH. The characteristic diffraction peaks of LDH are indexed.

## 2. Experimental

Aluminium (III) nitrate nonahydrate ( $Al(NO_3)_3 \cdot 9H_2O$ , 98.5%, Hempur); magnesium (II) nitrate hexahydrate ( $Mg(NO_3)_2 \cdot 6H_2O$ , 99%, Hempur); terbium (III) nitrate pentahydrate ( $Tb(NO_3)_3 \cdot 5H_2O$ , 99.9%, Sigma-Aldrich); ethylene glycol ( $C_2H_4O_2$ , 99.5%, Roth); citric acid ( $C_6H_8O_7$ , 99.5%, Hempur); terephthalic acid ( $C_8H_6O_4$ , 98%, Sigma-Aldrich), sodium hydroxide (NaOH, 98%, Sigma-Aldrich) were used as starting materials.

The  $Mg_3/Al_{1-x}Tb_x$  LDH samples were synthesized using an aqueous sol-gel method from the solution of metal nitrates dissolved in 50 ml of deionised water. To this solution 0.2 M citric acid was added and obtained solution was stirred for 1 h at 80 °C. Next, 2 ml of ethylene glycol have been added to the resulted mixture with continues stirring at

150 °C until the complete evaporation of solvent. The obtained gel was dried at 105 °C for 24 h. The mixed metal oxides were obtained by heating the gels at 650 °C for 4 h. The  $Mg_3/Al_{1-x}Tb_x$  LDH specimens were obtained by reformation of mixed metal oxide powders in deionised water at 50 °C for 6 h under stirring. For comparison, the  $Mg_3/Al$  hydroxalite was also synthesized and analyzed. The terephthalic acid intercalated  $Mg_3/Al_{1-x}Tb_x$ -TAL hybrid inorganic-organic specimens were synthesized by anion exchange method. 2 mmol of  $Mg_3/Al_{1-x}Tb_x$  powders were dispersed in a 1.5-fold molar excess solution of disodium terephthalate (TAL) and the mixture was stirred at ambient temperature for 24 h. The solid product was isolated by filtration, washed thoroughly with deionised water and acetone, and dried in oven at 40 °C for 12 h.

X-ray diffraction patterns of the obtained synthesis products were

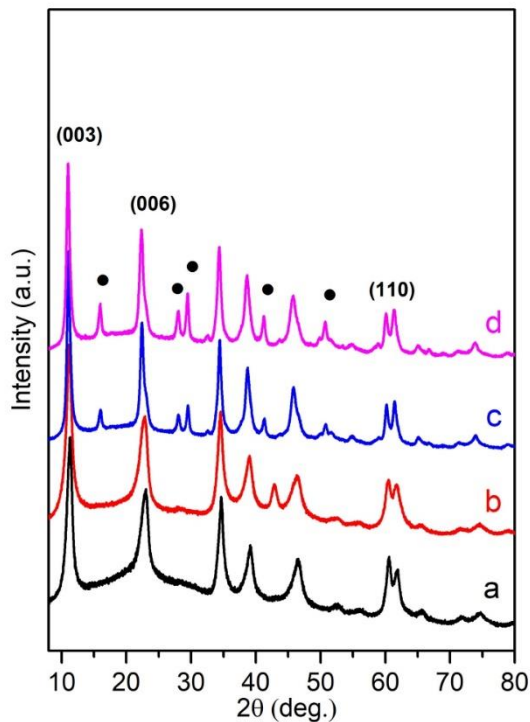


Fig. 2. XRD patterns of  $Mg_5/Al_{1-x}Tb_x-CO_3$  LDHs with different substitution level of terbium: (a) 1 mol%, (b) 5 mol%, (c) 7.5 mol% and (d) 10 mol%. The crystalline side phase is marked: ● –  $Tb(OH)_3$ .

recorded with MiniFlex II diffractometer (Rigaku) using a primary beam  $Cu K\alpha$  radiation ( $\lambda = 1.541838 \text{ \AA}$ ). The  $2\theta$  angle of the diffractometer was graduated from  $8$  to  $80^\circ$  in steps of  $0.02^\circ$ , with the measuring time of  $0.4 \text{ s}$  per step. FT-IR analysis of compounds was conducted using Perkin-Elmer FT-IR spectrometer. All spectra were recorded at ambient temperature in the range of  $4000\text{--}400 \text{ cm}^{-1}$ . Thermal analysis was carried out using a simultaneous thermal analyzer 6000 (Perkin-Elmer) in air atmosphere at scan rate of  $10^\circ \text{C}/\text{min}$  and the temperature range from  $30^\circ \text{C}$  up to  $900^\circ \text{C}$ . Excitation and emission spectra were recorded on an Edinburg Instruments FLS 900 spectrometer. The morphology of particles was investigated using a scanning electron microscope (SEM) Hitachi SU-70. The particle size was calculated using the ImageJ programme.

### 3. Results and discussion

The most suitable LDH precursors for the anion-exchange is the sample containing nitrate or chloride. During the sol-gel processing the LDH precursor containing the carbonate is forming [17]. Although the carbonate anion is adhesive held in the interlayer galleries and does not generally undergo direct anion-exchange, it is possible to replace it by treatment with an appropriate acid, which leads to liberation of carbon dioxide and incorporation of the conjugate base of the acid [26–28]. In this study, the  $CO_3^{2-}$  in the LDH was exchanged by  $Cl^-$  following with intercalation of terephthalate in to the terbium-containing LDH matrix. The XRD patterns of the synthesized  $Mg_5/Al$ ,  $Mg_5/Al-Cl$  exchanged by TAL and  $Mg_5/Al-CO_3$  exchanged by TAL are shown in Fig. 1. The diffraction reflections typical of LDH structure are seen in all the XRD

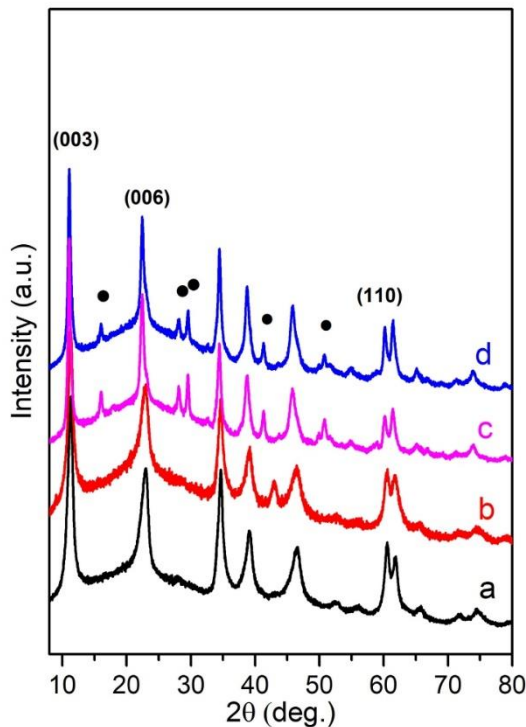


Fig. 3. XRD patterns of  $Mg_3/Al_{1-x}Tb_x$ -TAL LDHs with different substitution level of terbium: (a) 1 mol%, (b) 5 mol%, (c) 7.5 mol% and (d) 10 mol%. The side crystalline phase is marked: ● –  $Tb(OH)_3$ .

patterns. The main compositions correspond to the single-phase  $Mg_3/Al-CO_3$ ,  $Mg_3/Al-Cl$ ,  $Mg_3/Al-Cl-TAL$  and  $Mg_3/Al-TAL$  layered double hydroxides. LDHs phases indexed on a hexagonal unit cell with a 3 R rhombohedral symmetry and the most intensive diffraction lines in their patterns are determined at  $2\theta$  angle of about  $10^\circ$  (003),  $23^\circ$  (006) and  $60.2^\circ$  (110). The (003) and (110) peaks of all samples represent the layered structure, and cell parameters  $c$  and  $a$  reflect the interlayer anions and cation-cation distances in the LDHs. The calculated values of the lattice parameters were  $c = 2.3744$  nm and  $a = 0.3068$  nm ( $Mg_3/Al-CO_3$ ),  $c = 2.4123$  nm and  $a = 0.3069$  nm ( $Mg_3/Al-Cl$ ),  $c = 2.3964$  nm and  $a = 0.3069$  nm ( $Mg_3/Al-Cl-TAL$ ) and  $c = 2.4387$  nm and  $a = 0.3085$  nm ( $Mg_3/Al-TAL$ ). The LDH phases obtained as a result of the anion exchanged reactions, therefore the

XRD patterns should be shifted to the lower  $2\theta$  angle indicating a considerable increase in the basal spacing values as compared with the respective values for the main  $Mg_3/Al-CO_3$  LDH. As we can see from the XRD data, the anion-exchanges for  $Mg_3/Al-Cl$  to  $Mg_3/Al-Cl-TAL$  did not proceed fully. On the other hand, the value of unit cell  $c$  parameter increased in the  $Mg_3/Al-TAL$  after complete reformation of  $Mg_3/Al-CO_3$ .

Next, terbium substitution effect incorporating  $Tb^{3+}$  at  $Al^{3+}$  positions in  $Mg_3/Al-TAL$  LDH has been investigated. For this reason, series of  $Mg_3/Al_{1-x}Tb_x$  and  $Mg_3/Al_{1-x}Tb_x-TAL$  LDHs with different amount of terbium have been prepared. The XRD patterns of  $Mg_3/Al_{1-x}Tb_x$  and  $Mg_3/Al_{1-x}Tb_x-TAL$  LDHs are shown in Figs. 2 and 3, respectively. The monophase  $Mg_3/Al_{1-x}Tb_x$  LDHs were obtained with amount of terbium

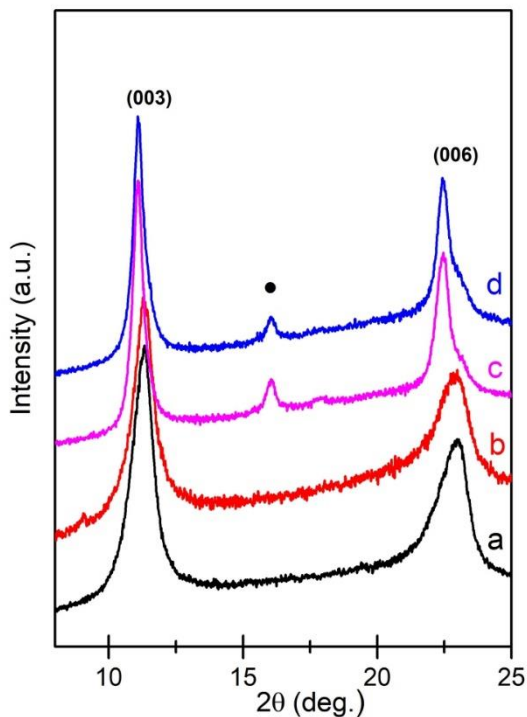


Fig. 4. The fragments of XRD patterns of  $Mg_3/Al_{1-x}Tb_x$ -TAL LDHs with different substitutional level of terbium: (a) 1 mol%, (b) 5 mol%, (c) 7.5 mol% and (d) 10 mol%. The side crystalline phase is marked: ● -  $Tb(OH)_3$ .

**Table 1**  
Basal spacing  $d$  values and cell parameters ( $a$ ,  $c$ ) of  $Mg_3/Al_{1-x}Tb_x$ -TAL LDHs.

Sample	Basal spacing/Å		Cell parameter/Å	
	$d_{003}$	$d_{110}$	$a$	$c$
Mg/Al/Tb 1 mol%-TAL	7.8428	1.5293	3.057	23.518
Mg/Al/Tb 5 mol%-TAL	7.8594	1.5299	3.058	23.568
Mg/Al/Tb 7.5 mol%-TAL	7.9894	1.5385	3.075	23.958
Mg/Al/Tb 10 mol%-TAL	8.0227	1.5389	3.076	24.058

less than 7.5 mol%. With increasing concentration of terbium till 7.5 mol% the impurity peak of  $Tb(OH)_3$  crystalline phase (PDF [00-019-1325]) appeared in the XRD pattern of  $Mg_3/Al_{1-x}Tb_x$  LDH. The  $Tb^{3+}$

ions taking up the positions of  $Al^{3+}$  ions led to the deformation of crystal lattice [29], and the excess  $Tb^{3+}$  ions in high basic condition crystallized as  $Tb(OH)_3$ . However, in the case of  $Mg_3/Al_{1-x}Tb_x$  with lower concentration of  $Tb^{3+}$  than 7.5 mol% the observed shift of the (110) and (003) reflections toward lower values of  $2\theta$  suggests incorporation of  $Tb^{3+}$  in LDH lattice. For the  $Mg_3/Al_{1-x}Tb_x$ -TAL LDHs, with increasing amount of terbium the position of (003) and (006) diffraction lines are clearly shifted to the region of lower  $2\theta$  values (see Fig. 4). Basal spacing  $d$  values and cell parameters ( $a$ ,  $c$ ) of  $Mg_3/Al_{1-x}Tb_x$ -TAL LDHs are summarized in Table 1. The obtained lattice parameters are in a good agreement with those determined for  $Mg_3/Al_1$  LDH samples [17,30,31]. It is also seen from Table 1 that the obtained all lattice parameters increase with increasing amount of terbium in the specimens indicating that  $Tb^{3+}$  ions were incorporated in the brucite-

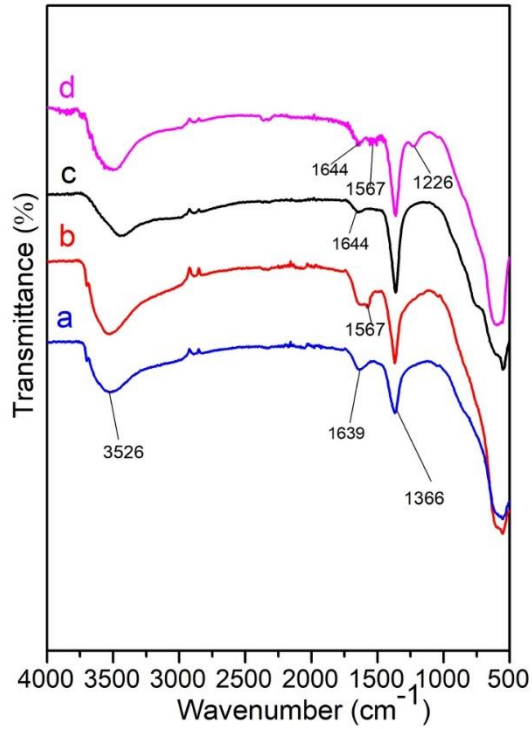


Fig. 5. FT-IR spectra of  $Mg_2/Al-CO_2$  (a),  $Mg_2/Al-TAL$  (b),  $Mg_3/Al_{1.3}Tb_x-CO_2$  (c) and  $Mg_3/Al_{1.3}Tb_x-TAL$  (d) LDHs.

like layers of LDHs [32].

FT-IR spectra of  $Mg_2/Al-CO_2$ ,  $Mg_2/Al-TAL$ ,  $Mg_3/Al_{1.3}Tb_x-CO_2$  and  $Mg_3/Al_{1.3}Tb_x-TAL$  LDH samples recorded in the region of  $4000-500\text{ cm}^{-1}$  are shown in Fig. 5. The obtained FT-IR spectra are very similar for all samples. The broad absorption bands observed at around  $3500-3000\text{ cm}^{-1}$  and weak bands at  $1641-1644\text{ cm}^{-1}$  could be attributed to the stretching vibrations of hydroxyl (-OH) groups from the hydroxyl layers and from intercalated water molecules [29]. The strong absorption band visible at  $1366\text{ cm}^{-1}$  corresponds to the asymmetric vibrations modes of ionic carbonate ( $CO_3^{2-}$ ). The FT-IR spectra of terephthalic acid intercalated LDHs show additional absorption bands at  $1567\text{ cm}^{-1}$  and  $1223\text{ cm}^{-1}$ , which are assigned to the asymmetric and symmetric stretching vibrations of carboxylate (-COO)

group [33,34]. These FT-IR spectra results suggest that TAL-anion is successfully intercalated in  $Mg_2/Al$  and  $Mg_3/Al_{1.3}Tb_x$  LDHs.

The excitation spectra obtained at room temperature of all  $Mg_2/Al_{1.3}Tb_x-CO_2$  and  $Mg_2/Al_{1.3}Tb_x-TAL$  LDHs are presented in Fig. 6. The excitation spectra are composed of a large broad band in the ultraviolet spectral region from 250 to 300 nm. This broad band is ascribed to transitions from the ground state  $S_0$  to the first excited state  $S_1$  ( $\pi, \pi^*$ ) of the ligands from organic terephthalate anions. Some excitation bands appeared at 350, 380 and 486 nm, assigned  ${}^7F_6 \rightarrow {}^5G_4$ ,  ${}^7F_6 \rightarrow {}^5L_{10}$  and  ${}^7F_6 \rightarrow {}^5G_6$  electronic transitions, respectively [35,36]. The emission spectra of  $Mg_2/Al_{1.3}Tb_x-CO_2$  and  $Mg_2/Al_{1.3}Tb_x-TAL$  LDHs (Fig. 7) show four main emissions in the wavelength range of 475–650 nm. The green emission bands observed at 621, 584, 542, 488 nm are



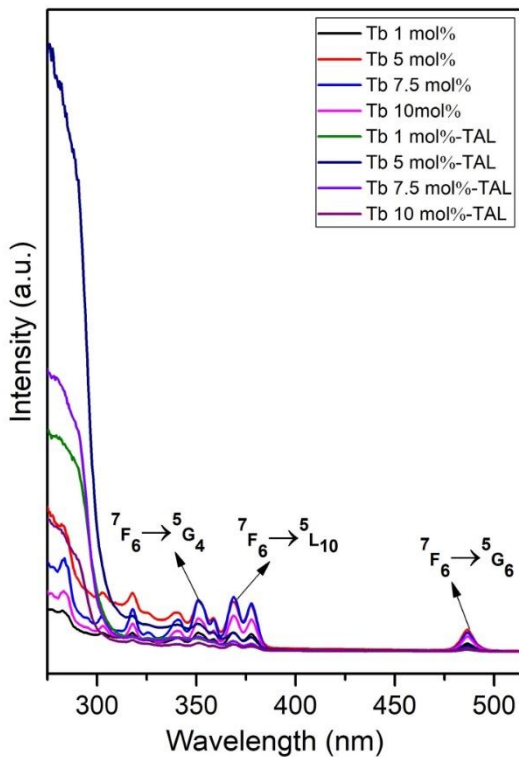


Fig. 6. Excitation spectra of  $\text{Mg}_2/\text{Al}_{1-x}\text{Tb}_x\text{-CO}_3$  and  $\text{Mg}_2/\text{Al}_{1-x}\text{Tb}_x\text{-TAL}$  LDHs.

characteristic for  ${}^5\text{D}_4\text{-}{}^7\text{F}_j$  ( $j = 3, 4, 5, 6$ ) transitions of  $\text{Tb}^{3+}$  ions. The maximum photoluminescence intensity in the  $\text{Mg}_2/\text{Al}_{1-x}\text{Tb}_x\text{-CO}_3$  and  $\text{Mg}_2/\text{Al}_{1-x}\text{Tb}_x\text{-TAL}$  LDHs is observed for the samples with the 5 mol% of  $\text{Tb}^{3+}$ . The intensity of emission decreases with further increasing amount of terbium up to 7.5–10 mol%  $\text{Tb}^{3+}$ , probably due to the presence of  $\text{Tb}(\text{OH})_3$  impurity phase in the samples or due to the concentration quenching. The results presented in this study indicate that the organic terephthalate ligand transfers the excitation energy to the  $\text{Tb}^{3+}$  ion and thus improves the photoluminescence intensity of the LDH samples. Therefore, the ability to absorb the light energy dominates for the terephthalate that shows stronger basicity in comparison with the carbonate anion. Carbonate is a weaker base and has weaker

affinity to protons, correspondingly showing weaker interaction with hydrogen atoms of layer hydroxyl groups, thus transferring less energy to  $\text{Tb}^{3+}$ . The intercalation of TAL into  $\text{Mg}_2/\text{Al}_{1-x}\text{Tb}_x$  LDH remarkably enhanced the intensity of  ${}^5\text{D}_4\text{-}{}^7\text{F}_5$  transition compared with  $\text{Mg}_2/\text{Al}_{1-x}\text{Tb}_x\text{-CO}_3$ . The green  ${}^5\text{D}_4\text{-}{}^7\text{F}_5$  emission of  $\text{Tb}^{3+}$  in  $\text{Mg}_2/\text{Al}_{1-x}\text{Tb}_x\text{-TAL}$  showed roughly 4 times enhancement indicating excellent sensitizing ability. The interlayer TAL anions located in the proximity to the  $\text{Tb}^{3+}$  ions in the brucite-like layer act as an energy antenna for the green emission of  $\text{Tb}^{3+}$  ions [37–39].

The morphology of the synthesized  $\text{Mg}_2/\text{Al-CO}_3$ ,  $\text{Mg}_2/\text{Al-TAL}$ ,  $\text{Mg}_2/\text{Al}_{1-x}\text{Tb}_x\text{-CO}_3$  and  $\text{Mg}_2/\text{Al}_{1-x}\text{Tb}_x\text{-TAL}$  LDHs samples were examined using scanning electron microscopy. The SEM micrographs of  $\text{Mg}_2/\text{Al-}$

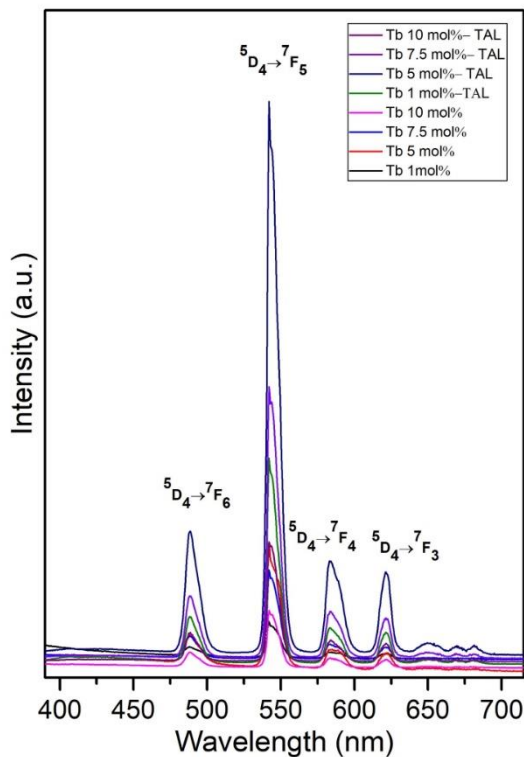


Fig. 7. Emission spectra of  $\text{Mg}_3/\text{Al}_{1-x}\text{Tb}_x-\text{CO}_3$  and  $\text{Mg}_3/\text{Al}_{1-x}\text{Tb}_x-\text{TAL}$  LDHs.

$\text{CO}_3$  and  $\text{Mg}_3/\text{Al}-\text{TAL}$  LDHs are shown in Fig. 8. As seen, the surface of the  $\text{Mg}_3/\text{Al}-\text{CO}_3$  LDH sample is composed of agglomerated small plate-like particles. These plate-shaped particles became smoother after intercalation process (see Fig. 8b). The characteristic morphological feature of LDH is the formation of plate-like particles with hexagonal shape [40,41]. The agglomeration of  $\text{Mg}_3/\text{Al}-\text{CO}_3$  particles suggests an increased electrostatic interaction between crystallites-hexagons. The surface morphology of hybrid inorganic-organic  $\text{Mg}_3/\text{Al}-\text{TAL}$  LDHs differs having very resolved plate-like particles with hexagonal shape. The particle size of modified LDH with TAL was determined about ~150–270 nm in length. Almost identical SEM results were observed

for the terbium-doped  $\text{Mg}_3/\text{Al}_{1-x}\text{Tb}_x-\text{CO}_3$  and  $\text{Mg}_3/\text{Al}_{1-x}\text{Tb}_x-\text{TAL}$  LDH samples (Fig. 9). The particle size of these LDHs varies in the range of ~150–300 nm. The fabrication of luminescent ordered multilayer transparent ultrathin films based on these inorganic-organic hybrid materials is possible [42] and currently is under investigation.

#### 4. Conclusions

$\text{Mg}_3/\text{Al}-\text{CO}_3$  and  $\text{Mg}_3/\text{Al}/\text{Tb}-\text{CO}_3$  LDHs intercalated with anion terephthalate (TAL) have been produced by sol-gel method. The XRD analysis results confirmed successful intercalation of the LDH layers

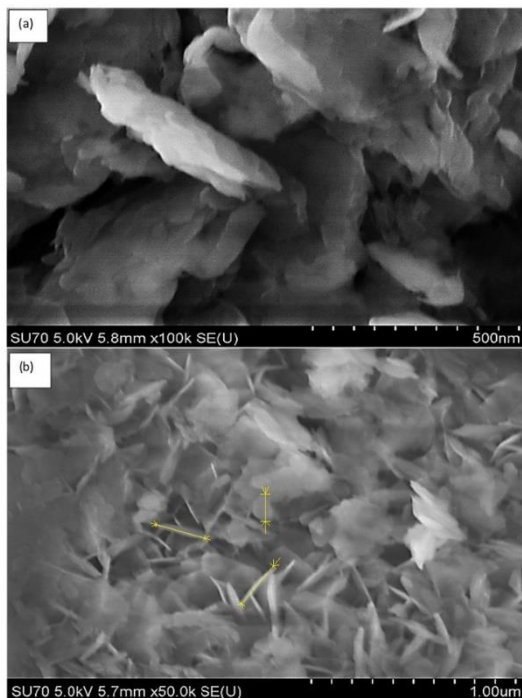


Fig. 8. SEM images of  $Mg_2+/Al-CO_2$  (a) and  $Mg_2+/Al-TAL$  (b) LDHs.

with organic molecules indicating the significant growth of interlayer space from 2.3744 nm to 2.4387 nm for the  $Mg_2+/Al-CO_2$  and  $Mg_2+/Al-TAL$ , respectively. The FT-IR spectra of terephthalic acid intercalated LDHs showed absorption bands at  $1567\text{ cm}^{-1}$  and  $1223\text{ cm}^{-1}$ , which were assigned to the asymmetric and symmetric stretching vibrations of carboxylate ( $-COO$ ) group. These results additionally proved the formation of LDH structure with organic functional groups. The emission spectra of  $Mg_2+/Al_{1-x}Tb_x-CO_2$  and  $Mg_2+/Al_{1-x}Tb_x-TAL$  LDHs showed four main emissions in the wavelength range of 475–650 nm. The maximum photoluminescence intensity in the  $Mg_2+/Al_{1-x}Tb_x-CO_2$  and  $Mg_2+/Al_{1-x}Tb_x-TAL$  LDHs was observed for the samples with the 5 mol% of  $Tb^{3+}$ . The luminescence of  $Tb^{3+}$  ions in all prepared LDH materials were enhanced by intercalation with terephthalic anion due to the sensitization effect. Thus, we can conclude that the obtained inorganic–organic hybrid material can improve the luminescence of  $Tb^{3+}$

ions in comparison with the LDHs matrix. The typical LDH microstructure was observed for all synthesized LDH samples. The size of the surfactant anions may be a potential factor that influences stacking and growth of the metal hydroxide layers during the reformation process. The surfaces of the LDHs were composed of agglomerated small plate-like particles of approximately 150–300 nm in size.

#### Acknowledgment

This work was supported by a grant SEMAT (No. SEN-02/2016) of National Research Programme „Healthy ageing“ from the Research Council of Lithuania. This work has been also partially done in frame of the project TUMOCS. This project has received funding from the European Union's Horizon 2020 research and innovation programme under the Marie Skłodowska-Curie grant agreement No 645660.

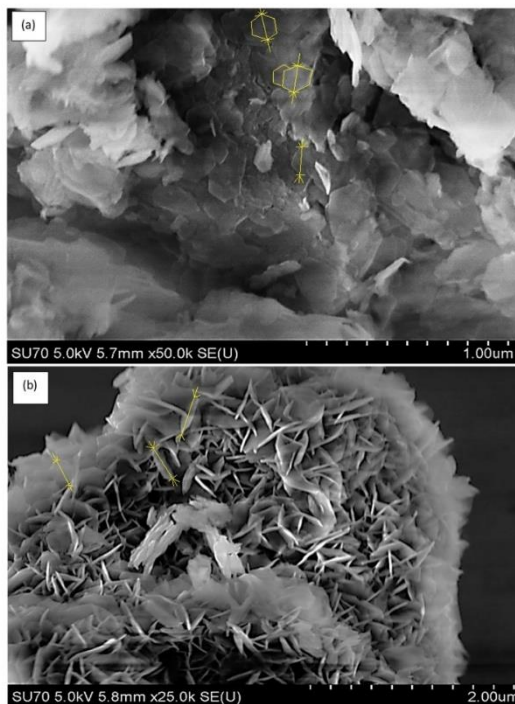


Fig. 9. SEM images of  $Mg_9/Al_{13}Tb_2CO_3$  (a) and  $Mg_9/Al_{13}Tb_2TAL$  (b) LDHs.

## References

- [1] A.I. Khan, D. O'Hare, *J. Mater. Chem.* 12 (2002) 3191–3198.
- [2] S.P. Newman, W. Jones, *New J. Chem.* 22 (1998) 105–115.
- [3] C. Joubertie, M.J. Hojgado, M.S. San Román, V. Rives, *Chem. Mater.* 18 (2006) 3114–3121.
- [4] S. Miyata, *Clay Miner.* 31 (1983) 305–311.
- [5] A.N. Salak, J. Tedim, A.I. Kuznetsova, J.L. Ribeiro, L.G. Vieira, M.L. Zheludkevich, M.G.S. Ferreira, *Chem. Phys.* 397 (2012) 102–108.
- [6] J. Carneiro, A.F. Caetano, A. Kuznetsova, F. Mota, A.N. Salak, J. Tedim, N. Schamagl, M.L. Zheludkevich, M.G.S. Ferreira, *RSC Adv.* 5 (2015) 39916–39929.
- [7] H.J. Li, X.Y. Su, C.H. Bai, Y.Q. Xu, Z.C. Pei, S.G. Sun, *Sens. Actuators B Chem.* 225 (2016) 109–114.
- [8] P. Liu, S. Liang, L. Qiu, Y.S. Gao, Q. Wang, *J. Membr. Sci.* 504 (2016) 96–205.
- [9] M. Serdechnova, A.N. Salak, F.S. Barbosa, D.E.L. Vieira, J. Tedim, M.L. Zheludkevich, M.G.S. Ferreira, *J. Solid State Chem.* 233 (2016) 158–165.
- [10] Z. Hu, G. Chen, *Adv. Mater.* 26 (2014) 5950–5956.
- [11] K. Klemkaite-Ramanauskė, A. Žilinskis, R. Taraskevicius, A. Khinsky, A. Kareiva, *Polyhedron* 68 (2014) 340–345.
- [12] D. Sokol, K. Klemkaite-Ramanauskė, A. Khinsky, K. Baltakys, A. Beganskiene, A. Baltauskas, J. Finkas, A. Kareiva, *Mat. Sci. (Medžiagotyra)* 23 (2017) 144–149.
- [13] C.J. Brinker, G.W. Sherer, *Academic Press*, San Diego, (1990).
- [14] A. Kareiva, Aqueous sol-gel synthesis methods for the preparation of garnet crystal structure compounds, *Mat. Sci. (Medžiagotyra)* 17 (2011) 428–437.
- [15] T. Li, H.F. He, T. Zhang, B. Zhao, Z.Q. Chen, H.Y. Dai, R.Z. Xue, Z.P. Chen, *J. Allergy Comp.* 684 (2016) 315–321.
- [16] S. Rutkaitė, E. Gaigalas, A. Beganskiene, F. Ivanauskas, R. Ramanauskas, A. Kareiva, *Allegory Comp.* 739 (2018) 504–509.
- [17] A. Smalenskaite, D.E.L. Vieira, A.N. Salak, M.G.S. Ferreira, A. Katelnikovas, A. Kareiva, *Appl. Clay Sci.* 143 (2017) 175–183.
- [18] D. Sokol, A.N. Salak, M.G.S. Ferreira, A. Beganskiene, A. Kareiva, *J. Sol. Gel Sci. Technol.* 85 (2018) 221–230.
- [19] K. Binnemans, *Chem. Rev.* 109 (2009) 4283–4374.
- [20] T. Yagami, M. Hagiwara, S. Fujihara, *J. Sol. Gel. Technol.* 82 (2017) 380–389.
- [21] P. Gunawan, R.J. Xu, *Phys. Chem. C* 113 (2009) 17206–17214.
- [22] V.I. Tsaryuk, K.P. Zhuravlev, V.F. Zoln, V.A. Kudryashova, J. Legendziewicz, R. Szotak, *J. Appl. Spectrosc.* 74 (1) (2007) 51–59.
- [23] J. Albertson, *Acta Chem. Scand.* 26 (1972) 1023–1044.
- [24] Q.Y. Gu, N.K. Chu, G.H. Pan, G.B. Sun, S.L. Ma, X.J. Yang, *Eur. J. Inorg. Chem.* 3 (2014) 559–556.
- [25] N.K. Chu, Y.H. Sun, Y.S. Zhao, X.X. Li, G.B. Sun, S.L. Ma, X.J. Yang, *Dalton Trans.* 41 (2012) 7409–7414.
- [26] S. Carlino, M.J. Hudson, S.W. Ho, *Inorg. Solid State Ionics* 84 (1996) 117–129.
- [27] S. Carlino, M.J. Hudson, *J. Mater. Chem.* 4 (1994) 99–104.
- [28] Z. Hong, W. Wilson, L. Tianxi, *J. Appl. Polym. Sci.* 122 (2011) 273–281.
- [29] R.D. Shannon, *Acta Crystallogr.* 32 (1976) 751–767.
- [30] X.R. Gao, L.X. Lei, C.G. Lv, Y.M. Sun, H.G. Zheng, Y.P. Cui, *J. Solid State Chem.* 181 (2008) 1776–1781.
- [31] F. Kooli, I.C. Chisem, M. Uccidic, W. Jones, *Chem. Mater.* 8 (1996) 1969–1977.
- [32] X. Gao, L. Lei, L. Kang, Y. Wang, Y. Lian, K. Jiang, *J. Allergy C SSS* (2014) 703–707.
- [33] L. Liu, Q. Wang, C. Gao, H. Chen, W. Liu, Y. Tang, *J. Phys. Chem. C* 118 (2014) 14511–14520.
- [34] P. Kovar, M. Pospisil, M. Neechitai, P. Capkova, K. Melanova, *J. Mol. Model.* 13 (2007) 937–942.
- [35] Y. Sohn, *Ceram. Int.* 40 (2014) 13803–13811.
- [36] F. Vicente, M.E. Perez-Bernal, R.J. Ruano-Castro, Duarte Ananias, F.A. Almeida Fur, J. Rocha, V. Rives, *Microporous Mesoporous Mater.* 226 (2016) 209–220.
- [37] Q.Y. Gu, Y.H. Sun, N.K. Chu, S.L. Ma, Z. Jia, X.J. Yang, *Eur. J. Inorg. Chem.* (2012) 4407–4412.
- [38] L.L. Liu, Q. Wang, C.J. Gao, H. Chen, W.S. Liu, Y. Tang, *J. Phys. Chem.* 118 (2014) 14511–14520.
- [39] L.L. Liu, M.H. Yu, J. Zhang, B.K. Wang, W.S. Liu, Y.J. Tang, *Mater. Chem. C* 3 (2015) 2326–2333.
- [40] Z.P. Xu, P.S. Braterman, *Appl. Clay Sci.* 48 (2010) 235–242.
- [41] K. Klemkaite, I. Prosycevas, R. Taraskevicius, A. Khinsky, A. Kareiva, *Cent. Eur. J. Chem.* 9 (2011) 275–282.
- [42] W.J. Zhang, Y.L. Li, H.X. Fan, *Opt. Mater.* 51 (2016) 78–83.

Proceedings of the International Conference on Oxide Materials for Electronic Engineering, May 29–June 2, 2017, Lviv

## Sol–Gel Derived Lanthanide-Substituted Layered Double Hydroxides $Mg_3/Al_{1-x}Ln_x$

A. SMALENSKAITE<sup>a</sup>, S. ŠEŅ<sup>b</sup>, A. N. SALAK<sup>c</sup>, M. G. S. FERREIRA<sup>c</sup>, A. BEGANSKIENE<sup>g</sup>  
AND A. KAREIVA<sup>a,\*</sup>

<sup>a</sup>Department of Inorganic Chemistry, Institute of Chemistry, Vilnius University,  
Naugarduko 24, LT-03225 Vilnius, Lithuania

<sup>b</sup>Department of Chemistry, Faculty of Arts and Sciences, Dumlunar University, 43820 Kütahya, Turkey

<sup>c</sup>Department of Materials and Ceramic Engineering and CICECO — Aveiro Institute of Materials,  
3810-193 Aveiro, Portugal

Mg/Al/Ln (Ln = Nd, Sm, Eu) layered double hydroxides (LDHs) were synthesized using sol–gel method for the first time to the best our knowledge. The obtained materials were characterized by X-ray diffraction analysis and fluorescence spectroscopy. The phase composition and luminescent properties of these LDHs were investigated and discussed. The  $Ln^{3+}$  substitution effects were investigated in the  $Mg_3Al_{1-x}Ln_x$  LDHs by changing the  $Ln^{3+}$  concentration in the metal cation layers up to 10 mol%. It was demonstrated that only  $Mg_3Al_{1-x}Eu_x$  LDHs showed luminescence properties, however, no any light emission was observed for the  $Mg_3Al_{1-x}Nd_x$  and  $Mg_3Al_{1-x}Sm_x$  LDH samples.

DOI: 10.12693/APhysPolA.133.884

PACS/topics: 78.66.Fd, 82.70.Gg, 82.33.Ln, 71.20.Eh, 78.55.Hx

### 1. Introduction

LDHs are compounds with a general chemical formula of  $[M_{1-x}^{2+}M_x^{3+}(\text{OH})_2]^{x+}(A^{y-})_{x/y} \cdot z\text{H}_2\text{O}$ , where  $M^{2+}$  and  $M^{3+}$  are divalent and trivalent metal cations and  $A^y$  is an intercalated anion which compensates the positive charge created by the partial substitution of  $M^{2+}$  by  $M^{3+}$  in a brucite-type  $M^{2+}(\text{OH})_2$  hydroxide [1]. LDHs are widely used in commercial products as adsorbents, catalyst support precursors, anion exchangers, acid residue scavengers, flame retardants, osmosis membranes, sensors and other [2–4].

Considerable attention has been focused on incorporating of rare earth elements into LDHs host layers to develop new functional materials, which resemble designed optical properties [5–11]. The rare earth doped luminescent materials have drawn increasing attention as potential phosphor materials for use in optical devices [12]. The main aim of this study was to investigate  $Nd^{3+}$ ,  $Sm^{3+}$  and  $Eu^{3+}$  substitution effects in the  $Mg/Al_{1-x}Ln_x$  systems (the  $Ln^{3+}$  concentration in the crystal lattice was changed from 0.05 to 10 mol%) fabricated for the first time to the best our knowledge by sol–gel synthesis route.

### 2. Experimental

The Mg/Al and Mg/Al/Ln (Ln = Nd, Sm, Eu) LDH samples were synthesized from solutions of  $Mg(\text{NO}_3)_2 \cdot 6\text{H}_2\text{O}$ ,  $Al(\text{NO}_3)_3 \cdot 9\text{H}_2\text{O}$  (with molar ratio of 3:1),  $Nd(\text{NO}_3)_3 \cdot 6\text{H}_2\text{O}$ ,  $Sm(\text{NO}_3)_3 \cdot 6\text{H}_2\text{O}$  and

$Eu(\text{NO}_3)_3 \cdot 6\text{H}_2\text{O}$ . The metal nitrates were dissolved in 50 ml of distilled water, then a 0.2 M citric acid solution was added and the mixture was stirred for 1 h at 80 °C. Next, 2 ml of ethylene glycol have been added to the resulted mixture with continuous stirring at 150 °C until the complete evaporation of solvent. The obtained gels were dried at 105 °C for 24 h. The mixed metal oxides (MMO) were obtained by calcination of the gels at 650 °C for 4 h. The Mg/Al and  $Mg_3/Al_{1-x}Ln_x$  LDH specimens were obtained by reconstruction of MMO powders in water at 50 °C for 6 h under stirring.

X-ray diffraction (XRD) patterns were recorded using a MiniFlex II diffractometer (Rigaku) in  $\text{Cu } K_\alpha$  radiation in the  $2\theta$  range from 8 to 80° (step of 0.02°) with the exposition time of 0.4 s per step. Excitation and emission spectra were recorded on an Edinburgh Instruments FLS 900.

### 3. Results and discussion

The XRD patterns of synthesized by sol–gel method Mg/Al/Nd 1–10 mol% LDHs are shown in Fig. 1. The LDHs synthesized by sol–gel method were found to be essentially similar to that of standard hydroxalcite. Three basal reflections typical of an LDH structure were observed at  $2\theta$  of about 11.5° (003), 23° (006) and 35° (009). Besides, two characteristic LDH peaks were clearly seen at about 60.2° and 61.5° which correspond to the reflections from the (110) and (113) planes. However, the XRD patterns of the Mg/Al/Nd 5 mol% sample exhibited also reflections of a  $Nd(\text{OH})_3$  phase. As seen from Fig. 1, with increase of amount of neodymium the intensity of these diffraction peaks monotonically also increases. XRD patterns of synthesized by sol–gel method

\*corresponding author; e-mail: aivaras.kareiva@chf.vu.lt

Mg/Al/Sm 1–10 mol.% LDHs are shown in Fig. 2. Interestingly, the XRD patterns confirm formation of almost single phase Mg/Al/Sm LDH. Only at higher concentrations of samarium (> 7 mol.%) the synthesized samples contained also reflections attributable to the  $\text{Sm}(\text{OH})_3$  phase. The monophasic Mg/Al/Eu LDHs were also obtained with amount of Eu less than 5 mol.%. With increase of concentration of europium till 7.5 mol.% the negligible amount of side  $\text{Eu}(\text{OH})_3$  phase has formed. Thus, these results confirmed that highly crystalline lanthanide-substituted LDHs could be synthesized during hydroxylation of sol-gel derived crystalline MMO samples in aqueous media. The lattice parameters of the Mg/Al/Ln LDH samples prepared by sol-gel method were also determined. The lattice parameters grow from about 3.065 to 3.076 Å (*a*-parameter) and from about 23.699 to 23.899 Å (*c*-parameter) with increase of amount of lanthanide elements was observed. The obtained crystallographic data suggest that the observed variation in the lattice parameters of the Mg/Al/Ln LDHs are caused by substitution of aluminium by lanthanide elements in the host layers.

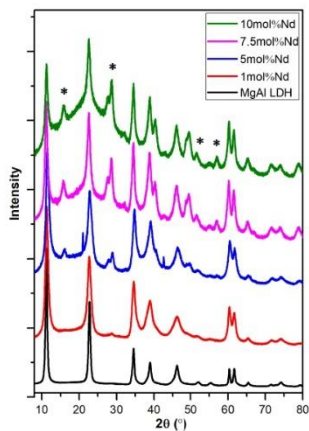


Fig. 1. XRD patterns of synthesized by sol-gel method Mg/Al/Nd 1–10 mol.% LDHs. The  $\text{Nd}(\text{OH})_3$  phase is marked as \*.

The luminescent properties of the obtained LDHs were also investigated. The emission spectra obtained at room temperature of all the Mg/Al/Eu LDH samples under excitation at 320 nm are presented in Fig. 3. The emission spectra of Mg/Al/Eu LDHs shows three main emissions in the wavelength range of 500–740 nm. The emis-

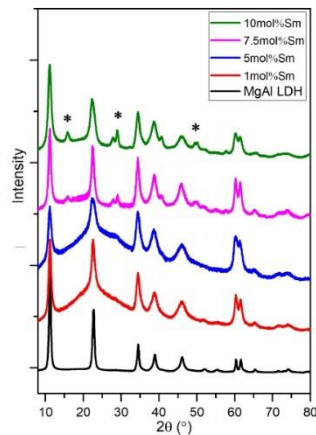


Fig. 2. XRD patterns of synthesized by sol-gel method Mg/Al/Sm 1–10 mol.% LDHs. The  $\text{Sm}(\text{OH})_3$  phase is marked as \*.

sion peaks are referred to the typical three  ${}^5D_0 \rightarrow {}^7F_1$  (591 nm)  ${}^5D_0 \rightarrow {}^7F_2$  (615 nm) and  ${}^5D_0 \rightarrow {}^7F_4$  (703 nm) transitions of  $\text{Eu}^{3+}$  ion. The emission due to  ${}^5D_0 \rightarrow {}^7F_2$  transition is the strongest, indicating that  $\text{Eu}^{3+}$  ions occupy a low-symmetry site. It is clear that the photoluminescence intensity in the Mg/Al/Eu LDH phase increases with increase of the  $\text{Eu}^{3+}$  concentration, and reaches the maximum when the concentration of  $\text{Eu}^{3+}$  is 7.5%. With further increasing amount of europium the intensity of emission decreases due to the concentration quenching. Surprisingly, the Mg/Al/Nd and Mg/Al/Sm LDH samples did not show any luminescence. Recently, the organic-inorganic hybrid phosphors have been designed and assembled by the intercalation of organic compounds, as sensitizer, into the layered lanthanide hydroxides or by changing the doping concentration of the activator ions [13–17]. This approach is currently under investigation to stimulate light emission in the Mg/Al/Nd and Mg/Al/Sm LDH samples.

#### 4. Conclusions

The  $\text{Mg}/\text{Al}_{1-x}\text{Ln}_x$  ( $\text{Ln}^{3+} = \text{Nd}^{3+}$ ,  $\text{Sm}^{3+}$  and  $\text{Eu}^{3+}$ ) layered double hydroxides (LDHs) with the substitution rate from 0.05 to 10 mol.% were successfully synthesized by sol-gel preparation technique. In this novel aqueous sol-gel processing route, the LDHs were obtained as a result of decomposition (calcination) of the precursor gels at 650 °C followed by rehydration of the intermediate crystalline MMO powders in water. The luminescent prop-

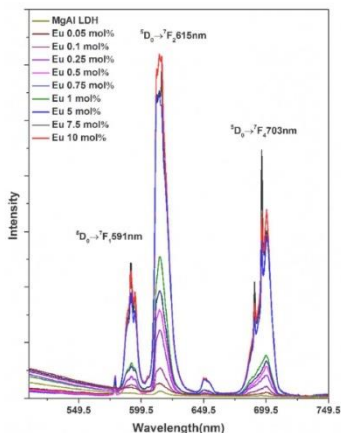


Fig. 3. Photoluminescence emission spectra of Mg/Al/Eu<sup>3+</sup> LDHs ( $\lambda_{ex} = 320$  nm).

erties of the obtained LDHs were also investigated. The emission spectra of Mg/Al/Eu LDHs showed three main emissions in the wavelength range of 500–740 nm corresponding to the typical  $^5D_0 \rightarrow ^7F_1$  (591 nm)  $^5D_0 \rightarrow ^7F_2$  (615 nm) and  $^5D_0 \rightarrow ^7F_4$  (703 nm) transitions of Eu<sup>3+</sup> ion. However, the Mg/Al/Nd and Mg/Al/Sm LDH samples did not show any luminescence.

#### Acknowledgments

The work has been done in frame of the project TU-MOCS. This project has received funding from the European Union's Horizon 2020 research and innovation programme under the Marie Skłodowska-Curie grant agreement No. 645660.

#### References

- [1] J. Wu, Z.Y. Ren, S.C. Du, L.J. Kong, B.W. Liu, W. Xi, J.Q. Zhu, H.G. Fu, *Nano Res.* **9**, 713 (2016).
- [2] M. Serdechnova, A.N. Salak, F.S. Barbosa, D.E.L. Vieira, J. Tedim, M.L. Zheludkevich, M.G.S. Ferreira, *J. Solid State Chem.* **233**, 158 (2016).
- [3] P. Lu, S. Liang, L. Qiu, Y.S. Gao, Q. Wang, *J. Membr. Sci.* **504**, 196 (2016).
- [4] H.J. Li, X.Y. Su, C.H. Bai, Y.Q. Xu, Z.C. Pei, S.G. Sun, *Sensors Actuat. B Chem.* **225**, 109 (2016).
- [5] K. Binnemans, *Chem. Rev.* **109**, 4283 (2009).
- [6] P. Gunawan, R. Xu, *J. Phys. Chem. C* **113**, 17206 (2009).
- [7] P. Vicente, M.E. Perez-Bernal, R.J. Ruano-Casero, D. Ananias, P.A.A. Paz, J. Rocha, V. Rives, *Micropor. Mesopor. Mater.* **226**, 209 (2016).
- [8] T. Posati, F. Costantino, L. Latterini, M. Nocchetti, M. Paolantoni, L. Tarpani, *Inorg. Chem.* **51**, 13229 (2012).
- [9] M. Domiguez, M.E. Perez-Bernal, R.J. Ruano-Casero, C. Barriga, V. Rives, R.A.S. Ferreira, L.D. Carlos, J. Rocha, *Chem. Mater.* **23**, 1993 (2011).
- [10] Z. Zhang, G.M. Chen, J.G. Liu, *RSC Adv.* **4**, 7991 (2014).
- [11] X.R. Gao, L.X. Lei, L.W. Kang, Y.Q. Wang, Y.W. Lian, K.L. Jiang, *J. Alloys Comp.* **585**, 703 (2014).
- [12] R. Skaudzius, T. Juestel, A. Kareiva, *Mater. Chem. Phys.* **170**, 229 (2016).
- [13] S. Yi, Z.H. Yang, S.W. Wang, W.W. Chi, *J. Appl. Polym. Sci.* **119**, 2620 (2011).
- [14] D.R.M. Vargas, M.J. Oviedo, F.D. Lisboa, F. Wypych, G.A. Hirata, *J. Nanomater.* **730**, 153 (2013).
- [15] L.L. Liu, D. Xia, W.S. Liu, Y. Tang, *Chin. J. Inorg. Chem.* **29**, 1663 (2013).
- [16] A.H. Tamboli, A.R. Jadhav, W.J. Chung, H. Kim, *Energy* **93**, 955 (2015).
- [17] W.J. Zhang, Y.L. Li, H.X. Fan, *Opt. Mater.* **51**, 78 (2016).



## Research paper

## A comparative study of co-precipitation and sol-gel synthetic approaches to fabricate cerium-substituted Mg–Al layered double hydroxides with luminescence properties



A. Smalenskaite<sup>a,\*</sup>, D.E.L. Vieira<sup>b</sup>, A.N. Salak<sup>b</sup>, M.G.S. Ferreira<sup>b</sup>, A. Katelnikovas<sup>c</sup>, A. Kareiva<sup>a</sup>

<sup>a</sup> Department of Inorganic Chemistry, Vilnius University, Naugarduko 24, LT 03225, Vilnius, Lithuania

<sup>b</sup> Department of Materials and Ceramic Engineering, CICECO – Aveiro Institute of Materials, 3810-193 Aveiro, Portugal

<sup>c</sup> Department of Analytical and Environmental Chemistry, Vilnius University, Naugarduko 24, LT 03225, Vilnius, Lithuania

## ARTICLE INFO

## Keywords:

Layered double hydroxides  
Co-precipitation, sol-gel processing  
Cerium substitution effects  
Luminescent properties

## ABSTRACT

Mg/Al/Ce layered double hydroxides (LDHs) intercalated with carbonate and hydroxide anions were synthesized using co-precipitation and sol-gel method. The obtained materials were characterized by thermogravimetric (TG) analysis, X-ray diffraction (XRD) analysis, fluorescence spectroscopy (FLS) and scanning electron microscopy (SEM). The chemical composition, microstructure and luminescent properties of these LDHs were investigated and discussed. The Ce<sup>3+</sup> substitution effects were investigated in the Mg<sub>3</sub>Al<sub>1-x</sub>Ce<sub>x</sub> LDHs by changing the Ce<sup>3+</sup> concentration in the metal cation layers from 0.05 to 10 mol%. It was demonstrated, that luminescence properties of cerium-substituted LDHs depend on the morphological features of the host lattice.

## 1. Introduction

Layered double hydroxides (LDHs) are compounds composed of positively charged brucite-like layers with an interlayer gallery containing charge compensating anions and water molecules. The metal cations occupy the centres of shared oxygen octahedra whose vertices contain hydroxide ions that connect to form infinite two-dimensional sheets (Jayaraj and Vallabhan, 1991; Klemkaite et al., 2011a, 2011b; Bi et al., 2014; Wu et al., 2016). A general chemical formula of an LDH can be expressed as  $[M_1^{2+}_x M_2^{3+}_y(OH)_z]^{(A^-)_z} \cdot nH_2O$ , where M<sup>2+</sup> and M<sup>3+</sup> are divalent and trivalent metal cations and A<sup>z-</sup> is an intercalated anion which compensates the positive charge created by the partial substitution of M<sup>2+</sup> by M<sup>3+</sup> in a brucite-type M<sup>2+</sup>(OH)<sub>2</sub> hydroxide. The anions in the interlayer are not strictly limited to their nature. LDHs with many different anionic species have been reported: both inorganic anions (carbonate, chloride, nitrate, sulphate, molybdate, phosphate etc.) and organic anions (terephthalate, acrylate, lactate, etc.) (Miyata, 1983; Newman and Jones, 1998; Jaubertie et al., 2006; Klemkaite-Ramanauske et al., 2014; Kuwahara et al., 2016). The commonly found cations are Mg<sup>2+</sup>, Zn<sup>2+</sup>, Co<sup>2+</sup>, Ni<sup>2+</sup>, Cu<sup>2+</sup> or Mn<sup>2+</sup> as divalent cations and Al<sup>3+</sup>, Cr<sup>3+</sup>, Co<sup>3+</sup>, Fe<sup>3+</sup>, V<sup>3+</sup>, Y<sup>3+</sup> or Mn<sup>3+</sup> among the trivalent ones.

After calcination at temperatures from 300 to 600 °C, an LDH is converted to the mixed metal oxides (MMO) with high specific surface

area and basic properties. An ability of MMO to recover the original layered structure is a property known as „memory effect“ (Rives, 2001; Klemkaite et al., 2011a, 2011b; Cosano et al., 2016). When MMO is immersed into an aqueous solution which contains some anions, the layered structure can be recovered with those anions intercalated into the interlayer. A more irregular structure of agglomerated flake-like platelets or amorphous phase has been observed after such a reconstruction (Alvarez et al., 2013; Mascolo and Mascolo, 2015).

LDHs have a well-defined layered structure within nanometre scale (0.3–3 nm) interlayer and contain important functional groups in both the metal hydroxide layers and interlayers. LDHs are widely used in commercial products as adsorbents, catalyst support precursors, anion exchangers, acid residue scavengers, flame retardants, osmosis membranes, sensors (Salak et al., 2012; Carneiro et al., 2015; Li et al., 2016; Lu et al., 2016; Serdechnova et al., 2016). The formation and exploitation of new types of layered double hydroxide (LDH)/polymer NC hydrogels with high performance has been also investigated (Hu and Chen, 2014). Moreover, the LDHs have an HCl absorption capacity, and may be used as PVC thermal stabilizer (Lu et al., 2008). Recently, considerable attention has been focused on incorporating rare earth elements into LDH host layers to develop new functional materials, which resemble designed optical properties (Binnemans, 2009). LDHs doped with Tb<sup>3+</sup> ions in the brucite-like layers were prepared by a simple one-step co-precipitation method. When 4-biphenylacetate

\* Corresponding author.

E-mail address: [aurelija.smalenskaite@chf.vu.lt](mailto:aurelija.smalenskaite@chf.vu.lt) (A. Smalenskaite).

<http://dx.doi.org/10.1016/j.clay.2017.03.036>

Received 7 December 2016; Received in revised form 22 March 2017; Accepted 24 March 2017  
0169-1317/© 2017 Elsevier B.V. All rights reserved.



anions were intercalated in the interlayer space, a big amount of  $Tb^{3+}$  up to about 19 wt% was incorporated in the oxygen octahedral layers of the LDH. The luminescence study indicated that energy transfer from the excited state of the intercalated anion guest molecules to  $Tb^{3+}$  centres in the host layers takes place (Gunawan and Xu, 2009). The samples (both as-prepared and calcined) containing  $Tb^{3+}$  exhibited green fluorescence (William et al., 2006). Nanosize LDHs doped with  $Eu^{3+}$ ,  $Yb^{3+}$ ,  $Tb^{3+}$  and  $Nd^{3+}$  were prepared through the microemulsion method (Posati et al., 2012; Vicente et al., 2016). It was concluded that the lanthanide content in the LDH samples depends on the ionic radius of the lanthanide cation and on fabrication conditions.  $Eu^{3+}$  and  $Nd^{3+}$  were incorporated also into hydrocalumite and mayenite (Dominguez et al., 2011). The Zn/Al/Eu LDHs were reported as perspective and efficient luminescent materials (Zhang et al., 2014; Gao et al., 2014).

Rare earth doped luminescent materials have drawn increasing attention as potential phosphor materials for use in optical devices (Maqbool, 2006; Maqbool et al., 2007; Stanulis et al., 2014; Zabilute et al., 2014; Skaudzius et al., 2016). The rare-earth metal ions offer the possibility of obtaining blue, green and red colours, which are necessary for RGB devices (Okamoto et al., 1988; Katelnikovas et al., 2012a, 2012b). The organic-inorganic hybrid phosphors have been designed and assembled by the intercalation of salicylic acid, as sensitizer, into the layered lanthanide hydroxides with the compositions of Gd/Tb/Eu/OH/NO<sub>2</sub>/H<sub>2</sub>O through ion-exchange reaction under hydrothermal condition (Liu et al., 2013). The luminescence colour of a rare-earth doped LDH can be easily tuned from green to red due to the energy transfer from the  $Tb^{3+}$  to  $Eu^{3+}$  ions by changing the doping concentration of the activator ions. Luminescent ordered multilayer transparent ultrathin films based on inorganic rare earth elements doped layered double hydroxides Mg/Al/Eu nanosheets and organic ligand were recently fabricated via layer-by-layer assembly method (Zhang et al., 2016).

Vargas et al., 2013, has reported a doping of the layers of a Zn/Al LDH with  $Dy^{3+}$  ions. Photoluminescence spectra of the nitrate intercalated LDH showed a wide emission band with strong intensity in the yellow region (around 574 nm), originated from symmetry distortion of the octahedral coordination in dysprosium centres. The emission spectra of Ce-doped different inorganic matrixes are often characterized by a broad emission band with quite symmetric photoluminescence peak at around 530 nm, which is assigned to the  $5d^1(^2\tilde{D}_{3/2}) \rightarrow 4f^1(^2F_{5/2}$  and  $^2F_{7/2})$  transitions of  $Ce^{3+}$  (Katelnikovas et al., 2007, 2008, 2011; Misevicius et al., 2012; Katelnikovas et al., 2013). Cerium-doped hydroxalate-like precursors were recently synthesized by co-precipitation method (Tamboli et al., 2015). However, these compounds were studied only as efficient catalysts for hydrogen production. In this work, the LDHs with the metal cation composition of  $Mg_xAl_{1-x}Ce_z$  (with the  $Ce^{3+}$  substitution rate from 0.05 to 10 mol%) were synthesized using co-precipitation and sol-gel method. The main aim of this study was to investigate an effect of  $Ce^{3+}$  substitution on crystal structure of the obtained layered double hydroxides and estimate the maximal cerium-to-aluminium substitution rate. The luminescent properties of the  $Mg_xAl_{1-x}Ce_z$  LDH samples were also investigated in this study for the first time to the best of our knowledge.

## 2. Experimental

### 2.1. Synthesis by co-precipitation method

LDH samples were synthesized by adding a mixture of  $Mg(NO_3)_2 \cdot 6H_2O$  and  $Al(NO_3)_3 \cdot 9H_2O$  (with molar ratio of 3:1) drop by drop to the solution of  $NaHCO_3$  (1.5 M). pH of the resulting solution was measured and kept at 8–9 using NaOH (2 M) under continuous stirring. To separate the slurry from the solution, the mixture was centrifuged at 3000 rpm for 2 min. The precipitated LDH was washed with distilled water and centrifuged again. Process was repeated three

or four times depending on the sample. The formed LDH was dried at 75–80 °C for 12 h. The mixed-metal oxide (MMO) was achieved by heat treatment at 650 °C for 4 h. Synthesis of Mg/Al/Ce compounds was performed in the same way as Mg/Al LDH, keeping the pH of the solution about 10 during the synthesis and using  $Ce(NO_3)_3 \cdot 6H_2O$  as cerium source.

### 2.2. Synthesis by sol-gel method

The Mg/Al and Mg/Al/Ce LDH samples were synthesized from solutions of the same reagents as those used in the co-precipitation method. The metal nitrates were dissolved in 50 ml of distilled water, then a 0.2 M citric acid solution was added and the mixture was stirred for 1 h at 80 °C. At the next step, 2 ml of ethylene glycol have been added to the resulted mixture with continuous stirring at 150 °C until the complete evaporation of solvent. The obtained gel was dried at 105 °C for 24 h. The MMO was obtained by calcination of the gel at 650 °C for 4 h.

### 2.3. Rehydration/reconstruction

The MMO powders obtained by co-precipitation and sol-gel methods followed by heat treatment at 650 °C were reconstructed in water at 50 °C for 6 h under stirring (2 g of the powder per 40 ml of water). The commercial hydrotalcite PURAL MG63HT powder (Brunsbüttel, Germany) which is chemically a  $Mg_3Al$  LDH intercalated with  $CO_3^{2-}$  was also analysed for comparison.

### 2.4. Characterization

X-ray diffraction (XRD) patterns were recorded using a MiniFlex II diffractometer (Rigaku) in  $Cu K\alpha$  radiation in the  $2\theta$  range from 8 to 80° (step of 0.02°) with the exposition time of 0.4 s per step. Rietveld analysis of the XRD data was performed using the PANalytical HighScore Plus suite. Thermal analysis was carried out using a simultaneous thermal analyser 6000 (Perkin-Elmer) in air atmosphere at scan rate of 10 °C/min over the temperature range of 30 °C to 900 °C. Excitation and emission spectra were recorded on an Edinburgh Instruments FLS 900. Morphology of the LDH powders was investigated using a scanning electron microscope (SEM) Hitachi SU-70. The Fourier transform infrared (FT-IR) spectra were recorded using Perkin-Elmer spectrometer from the LDH samples dispersed in KBr and pressed into pellets.

## 3. Results and discussion

The XRD pattern of the Mg/Al LDH synthesized by co-precipitation method was found to be essentially similar to that of the commercial hydrotalcite PURAL MG63HT. Three basal reflections typical of an LDH structure were observed: at  $2\theta$  of about 10° (003), 23° (006) and 35° (009). Besides, two characteristic LDH peaks were clearly seen at about 60.2° and 61.5° which correspond to the reflections from the (110) and (113) planes. Evidently, that only amorphous Mg–Al–O gel has formed during the sol-gel preparation of LDH.

As seen from Fig. 1, increasing amount of cerium results in a monotonic decrease of the intensity of these diffraction peaks. In addition, the reflections are shifted to a lower  $2\theta$  range. The observed shift of the (110) and (113) reflections certainly suggests incorporation of this lanthanide ion in metal hydroxide layers of the LDHs prepared by co-precipitation. At the same time, the broad diffraction peaks that can be attributed to a  $CeO_2$  phase are seen in the patterns of the LDHs with a non-zero Ce content (Fig. 1). Intensities of these peaks slightly increase with increasing the nominal Ce content indicating that although the Al-to-Ce substitution rate grows, the difference between the nominal and actual rate grows as well.

Thermal treatment of an LDH at elevated temperatures results in

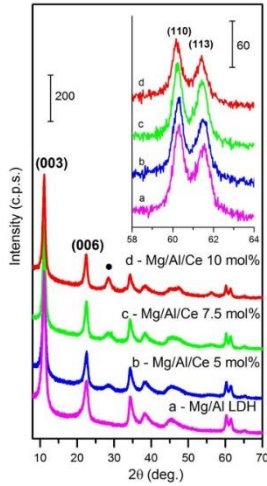


Fig. 1. XRD patterns of the Mg/Al/Ce LDHs synthesized by co-precipitation method: (a) cerium-free, (b) 5 mol% of Ce, (c) 7.5 mol% of Ce, (d) 10 mol% of Ce. The basal reflection is indicated. Inset: the XRD patterns in the range of (110) and (113) diffraction reflections. The crystalline phase is marked: ● -  $\text{CeO}_2$ .

loss of interlayer water molecules, charge-compensating anions and dehydroxylation of brucite-like layers. Mg/Al LDH decomposes followed by formation of MMO with a rock-salt like magnesium oxide as the only crystalline phase (Fig. 2) with Al atoms randomly dispersed throughout the solid, that is often described as an Mg(Al)O phase (Zhao et al., 2002).

The XRD patterns of the  $\text{Mg}_2\text{Al}$  LDHs (including the Ce-substituted ones) fabricated by co-precipitation method and calcined at  $650^\circ\text{C}$  are shown in Fig. 3. The formation of poorly crystalline magnesium oxide is evident in all cases. However, the XRD patterns of the samples containing cerium exhibited also reflections of a  $\text{CeO}_2$  phase. The XRD patterns of the Mg-Al-O precursor gels calcined at the same temperature are given in Fig. 4. Apparently, in comparison with the MMO obtained from LDHs prepared by co-precipitation method, the MMO from the sol-gel precursors have formed with higher crystallinity despite of no LDH phase formed during the sol-gel processing. In order to complete crystallization and obtain the material suitable for a quantitative XRD phase analysis (Salak et al., 2013; Carneiro et al., 2015) the formed MMO were heat-treated at higher temperature, namely at  $1000^\circ\text{C}$  for 6 h. Figs. 3 and 4 demonstrate the XRD patterns of the resulting products. It is seen that along with the diffraction reflections from MgO and  $\text{CeO}_2$ , the peaks attributed to the cubic spinel  $\text{MgAl}_2\text{O}_4$  phase are present. The Mg/(Al + Ce) molar ratios were estimated from the Rietveld analysis of the XRD data to be  $3.22 \pm 0.15$  and  $2.92 \pm 0.11$  for the MMO obtained from LDHs prepared by co-precipitation method and for the MMO from the sol-gel derived powders, respectively.

The ability of MMO to (re)form the LDH structure in water or water solutions was tested. The XRD patterns of the LDH samples formed as a result of hydration of the MMO obtained via co-precipitation and sol-gel

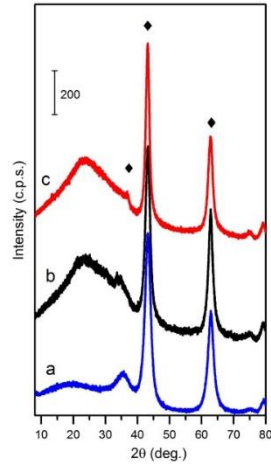


Fig. 2. XRD patterns of Mg/Al LDH calcined at  $650^\circ\text{C}$ : (a) commercial Purul MG63HT, (b) synthesized by co-precipitation and (c) sol-gel methods. The MgO phase is marked ◆.

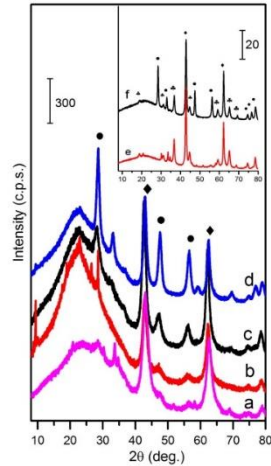


Fig. 3. XRD patterns of Mg/Al/Ce LDHs synthesized by co-precipitation method and calcined at  $650^\circ\text{C}$ : (a) 1 mol% of Ce, (b) 5 mol% of Ce, (c) 7.5 mol% of Ce, (d) 10 mol% of Ce. Calcined at  $1000^\circ\text{C}$ : (e) cerium-free, (f) 7.5 mol% of Ce. The crystalline phases are marked: ◆ - MgO; ● -  $\text{CeO}_2$ ; ▲  $\text{MgAl}_2\text{O}_4$ .

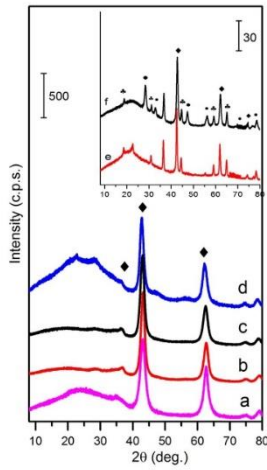


Fig. 4. XRD patterns of gels Mg/Al/Ce LDHs calcined at 650: (a) 1 mol% of Ce, (b) 5 mol % of Ce, (c) 7.5 mol% of Ce, (d) 10 mol% of Ce. Calcined at 1000 °C: (e) cerium-free, (f) 7.5 mol% of Ce. The crystalline phases are marked: ♦ - MgO; ● - CeO<sub>2</sub>; ◆ MgAl<sub>2</sub>O<sub>4</sub>.

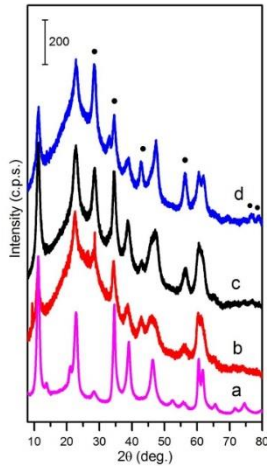


Fig. 5. XRD patterns of Mg/Al/Ce LDHs synthesized by co-precipitation method and reconstructed: (a) 1 mol% of Ce, (b) 5 mol% of Ce, (c) 7.5 mol% of Ce, (d) 10 mol% of Ce. ● - CeO<sub>2</sub>.

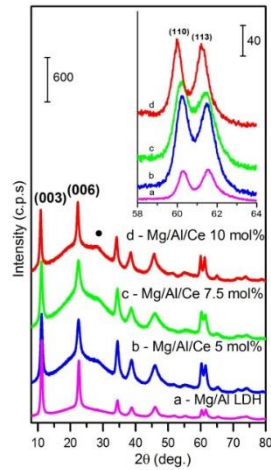


Fig. 6. XRD patterns of the Mg/Al/Ce LDHs synthesized by sol-gel method using reconstruction approach: (a) cerium-free, (b) 5 mol% of Ce, (c) 7.5 mol% of Ce, (d) 10 mol% of Ce. The basal reflection is indicated. Inset: the XRD patterns in the range of (110) and (113) diffraction reflections. The crystalline phase is marked: ● - CeO<sub>2</sub>.

methods are shown in Figs. 5 and 6, respectively.

The XRD patterns of the Mg/Al samples (cerium free) synthesized by co-precipitation, calcined and then immersed in water (Fig. 5) indicate a complete transformation of mixed-metal oxides into an LDH phase. Thus, the reconstruction of layered structure of LDH initially prepared by co-precipitation method occurs in water. The calcined LDHs with a non-zero cerium content demonstrate, however, a less complete regeneration: reflections of the CeO<sub>2</sub> phase are observed in the respective XRD patterns. Besides, it is clearly seen that the considerable amount of the amorphous part of the MMO product which contribute to a very broad peak of the XRD background remains uncrystallised.

The samples obtained by rehydration of the sol-gel derived samples show the typical LDH structure (Fig. 6), although no traces of an LDH phase has been detected at any stage of the sol-gel processing. Heat treatment of the sol-gels resulted in high crystalline MMO powders, which were hydroxylated in aqueous media providing well-crystallized LDH phase. According to the XRD patterns presented in Fig. 6, the mixed-metal oxides transformed fully to layered double hydroxides. Interestingly, the formation of LDH from the sol-gel derived powders does not depend on the Ce concentration in the samples. The XRD patterns of the reconstructed (hydroxylated) MMO powders demonstrate the sharp diffraction lines associated with an LDH crystalline phase only. No other crystalline phases have been detected. The (110) reflections of the LDHs are regularly shifted to a lower 2θ range as the cerium content is increased. Actually, the term "reconstruction" we use is not fully correct in the case of LDHs obtained from the sol-gel derived samples. In fact, this is a novel synthesis approach for the fabrication of LDHs, which is based on an aqueous sol-gel processing route.

The basal spacing (which are the distance between the adjacent hydroxide layers) and the lattice parameters of the LDH samples prepared by two different methods are listed in Table 1. The lattice

**Table 1**  
The basal spacings (*d*) and lattice parameters (*a*, *c*) of Mg/Al LDH and Mg/Al/Ce LDHs synthesized by co-precipitation and sol-gel methods.

The cation composition	$d_{(002)}$ (Å)	$d_{(004)}$ (Å)	$d_{(110)}$ (Å)	<i>a</i> (Å)	<i>c</i> (Å)
Co-precipitation method					
Mg/Al	7.9627	3.9482	1.5344	3.067	23.878
Mg/Al/Ce 5 mol%	7.9463	3.9479	1.5347	3.068	23.828
Mg/Al/Ce 7.5 mol%	7.9541	3.9510	1.5356	3.070	23.852
Mg/Al/Ce 10 mol%	7.9634	3.9609	1.5376	3.074	23.880
Sol-gel method					
Mg/Al	7.9181	3.9300	1.5346	3.068	23.744
Mg/Al/Ce 5 mol%	7.9476	3.9483	1.5351	3.069	23.832
Mg/Al/Ce 7.5 mol%	7.9683	3.9499	1.5376	3.074	23.894
Mg/Al/Ce 10 mol%	8.1418	3.9897	1.5411	3.081	24.415

parameter *a* reflects an average cation-cation distance and can be calculated as  $a = 2d_{(110)}$  from the interplanar distance corresponded to the (110) reflections in the brucite-like layers. Parameter *c* is a function of both size and ratio of cations  $M^{2+}$  and  $M^{3+}$ . Parameter *c* depends mainly on size, charge and orientation of the intercalated species: anions and water molecules (Salak et al., 2014). In order to minimize the experimental error caused by the 2θ scale shift, *c*-parameter is usually calculated using the interplanar distances of at least two basal reflections: typically, (003) and (006), as  $c = 3/2 [d_{(003)} + 2d_{(006)}]$ . The obtained crystallographic data (Table 1) suggest that the observed variation in the lattice parameters of the Mg/Al/Ce LDHs are caused by substitution of aluminium by cerium in the host layers.

Because of the relatively large ionic radius of  $Ce^{3+}$  (1.01 Å), substitution of  $Al^{3+}$  (0.53 Å) by  $Ce^{3+}$  is expected to lead to an expansion of the cation-cation distance in the brucite-like layers (Shannon, 1976). Therefore, as a result of the aluminium-to-cerium substitution, the *a*-parameter grows. Besides, the *c*-parameter increases as well, since because of such a substitution the layers become thicker. The effect of increase of both lattice parameters induced by this isoivalent Al-to-Ce substitution is qualitatively the same as that in the case of an increase of the Mg/Al cation ratio since  $Mg^{2+}$  is bigger than  $Al^{3+}$ . Dependences of lattice parameters of the carbonate-intercalated Mg/Al LDHs on the Mg/Al ratio have been reported (Newman and Jones, 2001). It has been shown that when the ratio is increased from 1:1 to 3.5:1, the lattice parameters grow from about 3.02 to 3.07 Å (*a*-parameter) and from about 22.6 to 23.7 Å (*c*-parameter). In this work, the Mg/Al/Ce LDHs prepared by co-precipitation were most likely intercalated with  $CO_3^{2-}$ , as the synthesis was conducted in a  $NaHCO_3$  solution (see Experimental). As regards of the Mg/Al/Ce layered double hydroxides formed via hydroxylation of the sol-gel derived MMO, these LDHs can be intercalated with  $OH^-$  and  $CO_3^{2-}$ , because the water used for the rehydration procedure was not specially decarbonized. Indeed, the presence of carbonate in the LDH samples prepared using either co-precipitation or via sol-gel method was confirmed by FT-IR study. A spectral band at about  $1360\text{ cm}^{-1}$  associated with  $\nu_s$  vibration of  $CO_3^{2-}$  was detected in the samples regardless of the preparation method used (Fig. S1). At the same time, the presence of intercalated  $OH^-$  cannot be unambiguously confirmed nor discarded by FT-IR, since one can hardly distinguish between the intercalated hydroxyl groups and those in the brucite-like layers.

In terms of the most compact (flat-laying) orientation, the anions  $OH^-$  and  $CO_3^{2-}$  give the same height of the interlayer gallery, which is equal to the double van der Waals radius of oxygen (Salak et al., 2014). Therefore, the values reported by Newman and Jones can be used as references for our LDHs. It is seen from Table 1 that the obtained lattice parameters of the Ce-substituted  $Mg_3Al$  LDHs are above the aforementioned ranges. The obtained values of both *a*- and *c*-parameters cannot be associated with any deviation in the Mg/Al ratio and certainly indicate the gradual substitution of aluminium by cerium in the brucite-like layers.

The Al-to-Ce isomorphous substitution rate in the obtained Mg/Al/Ce LDHs was estimated using the expression based on that proposed by Richardson (Richardson, 2012) for a case of substitution by two different trivalent cations:

$$a_{LDH} = a_{Mg(OH)_2} - \frac{1}{2} \sin\left(\frac{\alpha}{2}\right) [r(Mg^{2+}) - (1-x)r(Al^{3+}) - xr(Ce^{3+})]$$

Values of the parameter *a* for  $Mg(OH)_2$  and the angle  $\alpha$  were taken from the paper by Brindley and Kao (Brindley and Kao, 1984) and the Shannon's ionic radii (Shannon, 1976) were used. The calculated *a*-parameter value for the ideal Mg/Al/Ce 10 mol% LDH (3.089 Å) was compared with the experimentally obtained values. It was found that the real amount of cerium that substituted aluminium in the Mg/Al/Ce 10 mol% LDHs is about 8 and 6 mol% for the samples prepared by co-precipitation and through sol-gel, respectively.

Based on the obtained results, the methods of fabrication of the Mg/Al/Ce LDH applied in this work can be compared. As seen from Fig. 1 and Fig. 6, both the co-precipitation method and the sol-gel method provide a gradual Al-to-Ce substitution, although some amount of Ce does not incorporate into the LDH layers and crystallize as cerium oxide. It follows from a comparison of the lattice parameters of LDHs of the same nominal composition but prepared by different methods that when the nominal composition is 5–10 mol% of Ce, the sol-gel method of the LDH preparation provides higher substitution rates. At the same time, in the case of small-rate substitutions, both methods give similar results. Our idea was the following: if we prove that at least 5 mol% of Al can be substituted by Ce, it guarantees that smaller-rate substitutions are successful a fortiori. In the study of the luminescence properties, where LDHs with the small substitution rates (1 mol% and less) were used, we considered the LDHs of the same nominal composition but prepared by different methods as chemically equal.

The results of the thermogravimetric analysis of the LDHs synthesized by two different methods are shown in Figs. 7 and 8. The initial mass loss was observed in the temperature ranges of 30–150 °C (–18%) and 30–200 °C (–17%) for the Mg/Al/Ce 10 mol% LDH prepared by

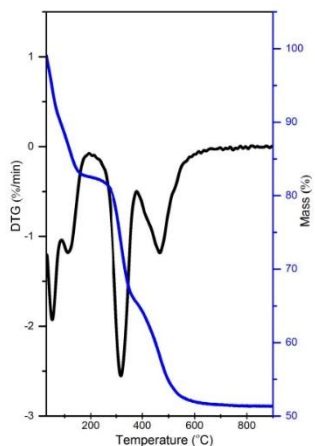


Fig. 7. TG-DTG curves recorded for the Mg/Al/Ce 10 mol% LDH sample synthesized by co-precipitation method.

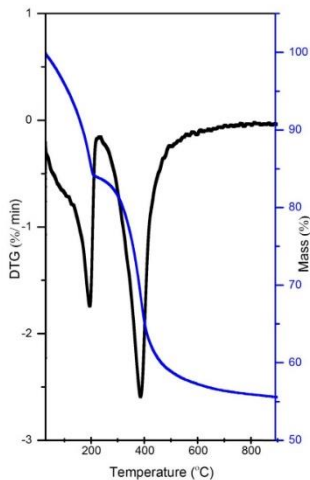


Fig. 8. TG-DTG curves recorded for the Mg/Al/Ce 10 mol% LDH sample synthesized by sol-gel method.

co-precipitation and sol-gel methods, respectively. Some decrease in mass occurs even below 100 °C because of evolution of the adsorbed water. (Yang et al., 2002). The main decomposition of Mg/Al/Ce 10 mol% sample prepared by co-precipitation method occurs via two steps in the temperature ranges of 290–350 °C and 350–600 °C. These thermal behaviours result from the loss of the coordinated water and the intercalated anions (in the lower temperature range) and dehydroxylation of the layers followed by collapse of the layered structure (in the higher temperature range). However, the main decomposition of Mg/Al/Ce 10 mol% sample prepared by sol-gel method occurs in one step by monotonic weight decrease in the temperature range of 200–600 °C.

The luminescent properties of the obtained LDHs were also investigated. The luminescence wavelengths of  $Ce^{3+}$  ions change widely from near UV to the red range depending on the nature of the host lattices (Kömpe et al., 2003; Li et al., 2004). The emission spectra of Mg/Al/Ce samples fabricated by co-precipitation method is shown in Fig. 9. All powders were excited at 340 nm for taking the emission spectra. The major emission lines are peaked at ~370–390 nm. The broad bands are attributed to  $[Xe]5d^1-[Xe]5f^3$  transition of  $Ce^{3+}$  ions (Katelnikovas et al., 2010). Surprisingly, the highest intensity of  $^3D_0 \rightarrow ^7F_2$  transition was observed for Mg/Al/Ce 0.05 mol% specimen. It turned out that emission intensity decreases with increasing concentration of  $Ce^{3+}$  up to 1 mol%. The emission maximum was also slightly shifted towards a red spectral region when more  $Ce^{3+}$  was introduced into the host lattice. This is in a good agreement with the results obtained in the  $Ce^{3+}$ -doped garnet-type phosphors. In the emission spectra of the sol-gel derived Mg/Al/Ce samples (Fig. 10), the bands are broader and more intensive. Moreover, the maximum of the emission of the LDHs synthesized using sol-gel technique is red shifted (390–430 nm) in comparison with the LDH phosphors prepared by co-precipitation method. Fig. 9 also shows the emission spectra of the Mg/Al/Ce LDHs synthesized by co-precipitation method, calcined and

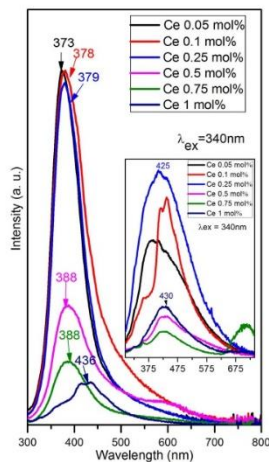


Fig. 9. Emission spectra of Mg/Al/Ce LDHs synthesized by co-precipitation method and reduced view of reconstruction.

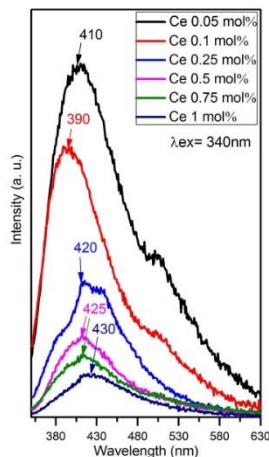


Fig. 10. Emission spectra of Mg/Al/Ce LDH synthesized by sol-gel method.

then reconstructed. It is interesting to note the light output is much stronger in the reconstructed cerium-doped LDHs. Moreover, the red-shift of the emission maximum of the reconstructed Mg/Al/Ce sample is

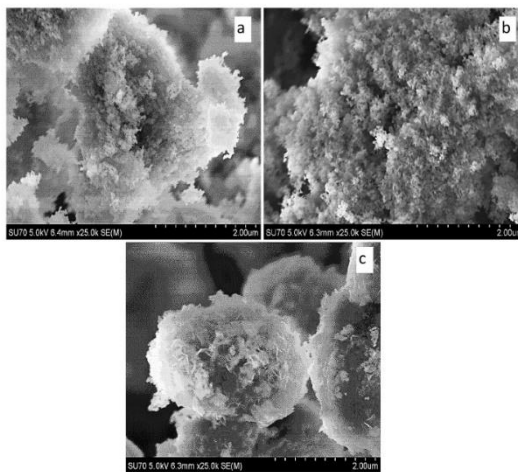


Fig. 11. SEM micrographs of a) Mg/Al LDH synthesized by co-precipitation method, b) Mg/Al LDH calcined at 650 °C and c) reconstructed Mg/Al LDH.

also evident. On the other hand, the highest intensity of  ${}^3D_0 \rightarrow {}^7F_2$  transition still is determined for Mg/Al/Ce 0.05 mol% specimen. With further increasing cerium content up to 1% the concentration quenching was observed (Devaraju et al., 2009).

The morphology of the synthesized Mg/Al and Mg/Al/Ce samples was examined using scanning electron microscopy. The characteristic feature of synthesized LDH should be formation of plate-like particles with hexagonal shape (Costa et al., 2008; Xu and Braterman, 2010). The rehydration results in (re)generation of the metal hydroxide sheets and the plate-like geometry of the primary particles. The SEM micrographs represent the cerium-free Mg/Al LDH powders synthesized by co-precipitation method (Fig. 11). The typical LDH microstructure is evident from this SEM micrograph. The surface is composed of the agglomerated small plate-like particles of 50–100 nm in diameter. After calcination of Mg/Al LDH at 650 °C, the network of spherical nanoparticles (50 to 100 nm) have formed. Rehydration of these nanoparticles results in formation of plate-like particles with hexagonal shape (Fig. 11c). However, after such a reconstruction, the average particle size of the LDHs increases to ~100–150 nm. The surface morphology of the Ce<sup>3+</sup>-substituted samples is very similar for all the specimens independent of the substitution rate. The representative SEM micrographs (Fig. 12) of the Mg/Al/Ce 1 mol% sample synthesized by co-precipitation method, calcined and then reconstructed show small fibrous plate-like particles that are aggregated as in the case of a cerium-free LDH sample. The SEM micrographs of the Mg/Al/Ce 1 mol% and Mg/Al/Ce 10 mol% LDHs fabricated by sol-gel method followed by hydration are shown in Fig. 12. It is seen that the sol-gel derived Mg/Al/Ce LDHs consist of the larger hexagonally shaped particles varying in size from approximately 150 to 200 nm. The good connectivity between the grains is also observed. These nanograins show tendency to form larger agglomerates. On the whole, nanocrystalline nature of powders with the narrow size distribution of crystallites is observed for all the obtained LDH samples.

The luminescence properties are expected to depend on the closest

coordination of Ce in the layer and hardly on the interlayer distance. The main difference between the LDHs prepared using either co-precipitation method or sol-gel-method is in size and regularity of the crystallites. It is known that the LDH crystallites obtained as a result of (re)hydration of the calcined powders are more irregular than those obtained by co-precipitation. Therefore we consider that the observed differences in the luminescence properties are caused by differences in morphology of the LDHs.

#### 4. Conclusions

The Mg/Al layered double hydroxides (LDHs) were successfully synthesized by co-precipitation method and using sol-gel preparation technique. To the best of our knowledge the latter was successfully applied for production of LDHs for the first time. In this novel aqueous sol-gel processing route, the LDHs were obtained as a result of decomposition (calcination) of the precursor gels at 650 °C followed by rehydration of the intermediate crystalline MMO powders in water. The same synthesis methods were successfully applied for production of cerium-substituted LDHs (Mg/Al/Ce) with the substitution rate from 0.05 to 10 mol%. It was found that in case of the Mg/Al/Ce LDHs prepared by co-precipitation followed by calcination, the regeneration rate decreases with increase of cerium content, while the conversion of the rehydrated sol-gel derived MMO into LDH does not depend on the concentration of cerium and is close to 100%. The proposed sol-gel synthesis route for LDHs has some benefits over conventional method such as simplicity, high homogeneity of the end products, effectiveness, suitability to study substitution effects for different multinary metal systems and cost efficiency.

The luminescent properties of the obtained LDHs were also investigated. The major emission lines attributed to the  $[Xe]5d^1-[Xe]5f^1$  transition of Ce<sup>3+</sup> ions were peaked at ~370–390 nm and 390–430 nm for the Mg/Al/Ce samples fabricated by co-precipitation and by sol-gel methods, respectively. The emission bands were broader, more inten-

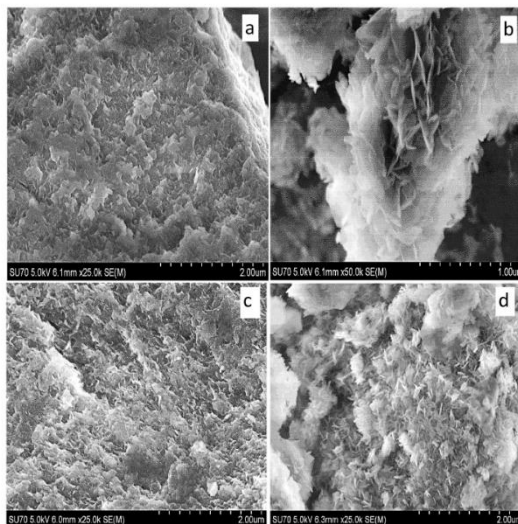


Fig. 12. SEM micrographs of a) Mg/Al/Ce 1 mol% LDH synthesized by co-precipitation method and b) reconstructed Mg/Al/Ce 1 mol% LDH c) Mg/Al/Ce 1 mol% LDH and d) Mg/Al/Ce 10 mol% LDH synthesized by sol-gel method.

sive and red-shifted in the case of the sol-gel derived LDHs.

The typical LDH microstructure was observed in all the obtained samples. The surfaces of the LDHs prepared by co-precipitation were composed of agglomerated small plate-like particles of 50–100 nm in diameter. After calcination followed by reconstruction (rehydration), the particle size of obtained LDH was observed to increase to 100–150 nm. Even larger particles formed in case of the LDHs prepared by hydration from the sol-gel derived MMO powders.

Luminescence properties of cerium doped LDHs were found to depend on the morphology of the host lattice. The observed compositional behaviours of lattice parameters and the luminescence characteristics indicate the successful isomorphous incorporation of  $Ce^{3+}$  into the brucite-like layers of the  $Mg_xAl_{1-x}Ce_x$  LDHs at least when  $x \leq 0.01$ .

Supplementary data to this article can be found online at <http://dx.doi.org/10.1016/j.clay.2017.03.036>.

#### Acknowledgements

The work has been done in frame of the project TUMOCs. This project has received funding from the European Union's Horizon 2020 – Research and innovation Framework Programme under the Marie Skłodowska-Curie grant agreement No 645660. The financial support of P2020 COMPETE and FCT-Portugal through project POCl-01-0145-FEDER-016686 - PTDC/CTM-NAN/2418/2014 (NANOCONCOR) is also acknowledged.

#### References

- Alvarez, M.G., Chimentao, R.J., Barrabes, N., Fottinger, K., Gisbert-Guirado, F., Klyemenov, E., Tichit, D., Medina, F., 2013. Structure evolution of layered double hydroxides activated by induced reconstruction. *Appl. Clay Sci.* 83–84, 1–11.
- Bi, X., Zhang, H., Dou, L., 2014. Layered double hydroxide-based nanocarriers for drug delivery. *Pharmaceutics* 6, 298–332.
- Binneman, K., 2009. Lanthanide-based luminescent hybrid materials. *Chem. Rev.* 109, 4283–4374.
- Bridley, G.W., Kuo, C.C., 1984. Structural and IR relations among brucite-like divalent metal hydroxides. *Phys. Chem. Minerals* 10, 187–191.
- Carneiro, J., Caetano, A.F., Kuznetsova, A., Maia, F., Salas, A.N., Tedim, J., Schamagl, N., Zhelezkovich, M.L., Ferreira, M.G.S., 2015. Polyelectrolyte-modified layered double hydroxide nanostainers as vehicles for combined inhibitors. *RSC Adv.* 5, 39916–39929.
- Cosano, D., Esquinas, C., Jimenez-Sanchidrian, C., Ruiz, J.R., 2016. Use of Raman spectroscopy to assess the efficiency of MgAl mixed oxides in removing cyanide from aqueous solutions. *Appl. Surf. Sci.* 364, 426–432.
- Costa, F., Leuteritz, A., Wagenknecht, U., Jehnichen, D., Häußler, L., Heinrich, G., 2008. Intercalation of Mg–Al layered double hydroxide by anionic surfactants: preparation and characterization. *Appl. Clay Sci.* 38, 153–164.
- Devaraju, M.K., Yin, S., Sato, T., 2009.  $Tm^{3+}$  doped  $V_2O_5$  nanocrystals: rapid hydrothermal synthesis and luminescence. *Eur. J. Inorg. Chem.* 29–30, 4441–4445.
- Dominguez, M., Pérez-Bernal, M.F., Ruano-Casero, R.J., Barriga, C., Rives, V., Ferreira, R.A.S., Carlos, L.D., Rocha, J., 2011. Multiwavelength luminescence in lanthanide-doped hydroxylamine and mayenite. *Chem. Mater.* 23, 1993–2004.
- Gao, X.R., Lei, L.K., Kang, L.W., Wang, Y.Q., Luo, Y.W., Jiang, K.L., 2014. Synthesis, characterization and optical properties of a red organic-inorganic phosphor based on terephthalate intercalated Zn/Al/Eu layered double hydroxide. *J. Alloys Compd.* 585, 703–707.
- Gunawan, P., Xu, R., 2009. Lanthanide-doped layered double hydroxides intercalated with sensitizing anionic: efficient energy transfer between host and guest layers. *J. Phys. Chem. C* 113, 17206–17214.
- Hu, Z., Chen, G., 2014. Novel nanocomposite hydrogels consisting of layered double hydroxide with ultrahigh tensibility and hierarchical porous structure at low inorganic content. *Adv. Mater.* 26, 5950–5956.
- Jaubertie, C., Holgado, M.J., San Román, M.S., Rives, V., 2006. Molecular dynamics simulation of the energetics and structure of layered double hydroxides intercalated

- with carboxylic acids. *Chem. Mater.* 18, 3114–3121.
- Jayaram, M.K., Vallabhan, 1991. Cr<sup>3+</sup> AC thin film electroluminescent devices with rare earth doped ZnS. *Electrochim. Acta* 36, 1512–1515.
- Katelnikovas, A., Vitta, P., Pobedinskas, P., Tamulaitis, G., Zukauskas, A., Jørgensen, J.E., Kareiva, A., 2007. Photoluminescence in sol-gel-derived YAG:Ce phosphors. *J. Cryst. Growth* 304, 361–368.
- Katelnikovas, A., Jüstel, T., Uhlrich, D., Jørgensen, J.E., Sakirzanovas, S., Kareiva, A., 2008. Characterization of cerium-doped yttrium aluminum garnet nanopowders synthesized via sol-gel process. *Chem. Eng. Commun.* 195, 758–769.
- Katelnikovas, A., Barrika, T., Vitta, P., Jüstel, T., Winkler, H., Kareiva, A., Zukauskas, A., Tamulaitis, G., 2010. Warm-white light emitting diodes. *Opt. Mater.* 32, 1261–1265.
- Katelnikovas, A., Jurkevicius, J., Kazlauskas, K., Vitta, P., Jüstel, T., Kareiva, A., Zukauskas, A., Tamulaitis, G., 2011. Efficient cerium-based sol-gel derived phosphors in different garnet matrices for light-emitting diodes. *J. Alloys Compd.* 509, 6247–6251.
- Katelnikovas, A., Plewa, J., Sakirzanovas, S., Dutczak, D., Enseling, D., Baur, F., Winkler, H., Kareiva, A., Jüstel, T., 2012a. Synthesis and optical properties of green emitting garnet phosphors for phosphor-converted light emitting diode. *J. Mater. Chem.* 22, 22126–22134.
- Katelnikovas, A., Plewa, J., Dutczak, D., Möller, S., Enseling, D., Winkler, H., Kareiva, A., Jüstel, T., 2012b. Synthesis and optical properties of green emitting garnet phosphors for phosphor-converted light emitting diodes. *Opt. Mater.* 34, 1195–1201.
- Katelnikovas, A., Sakirzanovas, S., Dutczak, D., Plewa, J., Enseling, D., Winkler, H., Kareiva, A., Jüstel, T., 2013. Synthesis and optical properties of yellow emitting garnet phosphors for pLEDs. *J. Lumin.* 136, 17–25.
- Klemkaite, K., Prosycevas, I., Taraskevicius, R., Khinsky, A., Kareiva, A., 2011a. Synthesis and characterization of layered double hydroxides with different cations (Mg, Co, Ni, Al), decomposition and reforming of mixed metal oxides to layered structures. *Cent. Eur. J. Chem.* 9, 275–282.
- Klemkaite, K., Khinsky, A., Kareiva, A., 2011b. Reconstitution effect of Mg/Ni/Al layered double hydroxide. *Mater. Lett.* 65, 388–391.
- Klemkaite-Ramonauskė, K., Žilinskas, A., Taraskevicius, R., Khinsky, A., Kareiva, A., 2014. Preparation of Mg/Al layered double hydroxide (LDH) with structurally embedded molybdate ions and application as a catalyst for the synthesis of 2-aminantylidene(phenyl)amine Schiff base. *Polyhedron* 68, 340–345.
- Kämpfe, K., Borchert, H., Storz, J., Lobo, A., Adam, S., Müller, T., Hase, M., 2003. Nanoparticles with 70% photoluminescence quantum yield. *Angew. Chem. Int. Ed.* 42, 5513–5516.
- Kuwahara, Y., Tamagawa, S., Fujitani, T., Yamashita, H., 2016. Removal of phosphate from aqueous solution using layered double hydroxide prepared from waste iron-making slag. *Bull. Chem. Soc. Jpn.* 89, 472–480.
- Li, F.Y., Xia, Z.Q., Yang, S.P., Gao, S.Y., 2004. Synthesis of single-phase nanocrystalline garnet phosphor derived from gel-network coprecipitation. *J. Mater. Sci.* 39, 4711–4713.
- Li, H.J., Su, X.Y., Bai, C.H., Xu, Y.Q., Pei, Z.C., Sun, S.G., 2016. Graphene based sensor for environmental monitoring of NO<sub>2</sub>. *Sensors Actuators B Chem.* 225, 109–114.
- Liu, J., Chen, G., Yang, J., 2008. Preparation and characterization of poly(vinyl chloride)/layered double hydroxide nanocomposites with enhanced thermal stability. *Polymer* 49, 3923–3927.
- Liu, L.L., Xia, D., Liu, W.S., Tang, Y., 2013. Initial theoretical evaluation of pore structure for metal-organic frameworks. *Chinese J. Inorg. Chem.* 29, 1663–1667.
- Lu, P., Liang, S., Qiu, L., Gao, Y.S., Wang, Q., 2016. Layered double hydroxide/graphene oxide hybrid incorporated polysulfone substrate for thin-film nanocomposite forward osmosis membranes. *J. Membr. Sci.* 504, 196–205.
- Maqbool, M., 2006. Luminescence from thulium and samarium doped amorphous AlN thin films deposited by RF magnetron sputtering and the effect of thermal activation on luminescence. *Eur. Phys. J. Appl. Phys.* 34, 31–34.
- Maqbool, M., Ahmad, I., Richardson, H.H., Kordesch, M.E., 2007. Direct ultraviolet excitation of an amorphous AlN praseodymium phosphor by codoped Gd<sup>3+</sup> cathodoluminescence. *Appl. Phys. Lett.* 91 (193511), 1–3.
- Mascio, G., Mascolo, M.C., 2015. On the synthesis of layered double hydroxides (LDH) by reconstruction, method based on the “memory effect”. *Micro porous Mesoporous Mater.* 214, 246–248.
- Misevicius, M., Seit, O., Grigoraviciute-Purniene, I., Degutis, G., Bogdanoviciene, I., Kareiva, A., 2012. Synthesis, hydration and thermal stability of hydrates in strontium-aluminate cement. *Ceram. Int.* 38, 5915–5924.
- Miyata, S., 1983. Anion-exchange properties of thermal-stable compounds. *Clay Clay Miner.* 31, 305–314.
- Newman, S.P., Jones, W., 1998. Synthesis, characterization and applications of layered double hydroxides containing organic guests. *New J. Chem.* 22, 105–115.
- Newman, S.P., Jones, W., 2001. Layered double hydroxides as templates for the formation of supramolecular structures. In: Jones, W., Rao, C.N.R. (Eds.), *Supramolecular Organization and Materials Design*. Cambridge University Press, Cambridge, pp. 295–331.
- Okamoto, K., Yoshimi, T., Miura, S., 1988. TMOF complex centers in ZnS thin-film electroluminescent devices. *Appl. Phys. Lett.* 53, 678–680.
- Posati, T., Costantino, F., Latterini, L., Necochee, M., Palantoni, M., Tarpani, L., 2012. Hydroxalate-like materials as precursors of catalysts to produce hydrogen from methanol. *Inorg. Chem.* 51, 13229–13236.
- Richardson, I.G., 2012. The importance of proper crystal-chemical and geometrical reasoning demonstrated using layered single and double hydroxides. *Acta Crystallogr. B* 69, 150–162.
- Rives, V., 2001. *Layered Double Hydroxides: Present and Future*. Nova Science Publishers, New York.
- Salak, A.N., Tedim, J., Kuznetsova, A.I., Ribeiro, J.L., Vieira, L.G., Zheldukovich, M.L., Ferreira, M.G.S., 2012. Comparative x-ray diffraction and infrared spectroscopy study of Zn-Al layered double hydroxides: vanadate vs nitrate. *Chem. Phys.* 397, 102–108.
- Salak, A.N., Tedim, J., Kuznetsova, A.I., Vieira, L.G., Ribeiro, J.L., Zheldukovich, M.L., Ferreira, M.G.S., 2013. Thermal behavior of layered double hydroxide Zn-Al pyrovanadate: composition, structure transformations, recovering ability. *J. Phys. Chem. C* 117, 4152–4157.
- Salak, A.N., Ikenkov, A.D., Zheldukovich, M.L., Ferreira, M.G.S., 2014. Carbonate-free Zn-Al (1:1) layered double hydroxide film directly grown on zinc-aluminum alloy coating. *ECS Electrochem. Lett.* 3, C9–C11.
- Serdachynova, M., Salak, A.N., Barbosa, F.S., Vieira, D.E.L., Tedim, J., Zheldukovich, M.L., Ferreira, M.G.S., 2016. Interlayer intercalation and arrangement of 2-mercaptobenzothiazolate and 1,2,3-benzotriazole anions in layered double hydroxides: in situ x-ray diffraction study. *J. Solid State Chem.* 233, 158–165.
- Shannon, R.D., 1976. Revised effective ionic radii and systematic studies of interatomic distances in halides and chalcogenides. *Acta Crystallogr. A* 32, 751–767.
- Skaudzius, R., Jüstel, T., Kareiva, A., 2016. Study of Eu<sup>3+</sup> and Tm<sup>3+</sup> substitution effects in sol-gel fabricated calcium hydroxyapatite. *Mater. Chem. Phys.* 170, 229–238.
- Stanulis, A., Katelnikovas, A., Enseling, D., Dutczak, D., Sakirzanovas, S., Van Bael, M., Hanby, A., Kareiva, A., Jüstel, T., 2014. Luminescence properties of Sm<sup>3+</sup>-doped alkaline earth ortho-stannates. *Opt. Mater.* 36, 1146–1152.
- Tamboli, A.H., Jadhav, A.R., Chung, W.J., Kim, H., 2015. Catalyst for hydrogen production from sodium borohydride hydrolysis. *Energy* 93, 955–962.
- Vargas, D.R.M., Oviedo, M.J., Lisboa, F.D., Wypych, F., Hinata, G.A., 2013. Phosphor dysprosium-doped layered double hydroxides exchanged with different organic functional groups. *J. Nanomater.* 1–8, 730153.
- Vicente, P., Pérez-Bernal, M.E., Ruano-Canero, R.J., Ananias, D., Almeida Paz, F.A., Rocha, J., Rives, V., 2016. Luminescence properties of lanthanide-containing layered double hydroxides. *Micro porous Mesoporous Mater.* 228, 209–220.
- William, M.Y., Shiono, S., Yamamoto, H., 2006. *Fundamentals of Phosphors*. CRC Press, Inc. Ltd., Boca Raton FL, pp. 335.
- Wu, J., Ren, Z.Y., Du, S.C., Rong, L.J., Liu, B.W., Xi, W., Zhu, J.Q., Fu, H.G., 2016. Dehydrated layered double hydroxides: alcohol thermal synthesis and oxygen evolution activity. *Nano Res.* 9, 713–725.
- Xu, Z.P., Braterman, P.S., 2010. Synthesis, structure and morphology of organic layered double hydroxide (LDH) hybrids: comparison between aliphatic anions and their oxygenated analogs. *Appl. Clay Sci.* 48, 235–242.
- Yang, W., Kim, Y., Liu, P., Saito, M., Tsutsui, T., 2002. A study by in situ technique of the thermal evolution of the structure of a Mg-Al-CO<sub>3</sub> layered double hydroxide. *Chem. Eng. Sci.* 57, 2945–2953.
- Zablitis, A., Bukšė, S., Zukauskas, A., Vitta, P., Kareiva, A., 2014. Sol-gel synthesized far-red chromium-doped garnet phosphors for phosphor-conversion light-emitting diodes that meet the photomorphogenic needs of plants. *Appl. Opt.* 53, 907–914.
- Zhang, Z., Chen, G.M., Liu, J.G., 2014. Tuneable photoluminescence of europium-doped layered double hydroxides intercalated by coumarin-3-carboxylate. *RSC Adv.* 4, 7991–7997.
- Zhang, W.J., Li, Y.L., Fan, H.X., 2016. Lanthanide luminescence for biomedical analysis and imaging. *Opt. Mater.* 51, 78–83.
- Zhao, Y., Li, F., Zhang, R., Evans, D.G., Duan, X., 2002. Preparation of layered double-hydroxide nanomaterials with a uniform crystallite size using a new method involving separate nucleation and aging steps. *Chem. Mater.* 14, 4286–4291.



## RESEARCH ARTICLE

**Sol-gel Synthesis and Characterization of Non-Substituted and Europium-Substituted Layered Double Hydroxides Mg<sub>3</sub>/Al<sub>1-x</sub>Eu<sub>x</sub>**A. Smalenskaite<sup>1,\*</sup>, S. Şen<sup>2</sup>, A. N. Salak<sup>3</sup>, M. G. S. Ferreira<sup>3</sup>, R. Skaudzius<sup>1</sup>, A. Katelnikova<sup>4</sup> and A. Kareiva<sup>1</sup>

<sup>1</sup>Department of Inorganic Chemistry, Vilnius University, Naugarduko 24, LT-03225 Vilnius, Lithuania.; <sup>2</sup>Department of Chemistry, Faculty of Arts and Sciences, Dumlupınar University, 43820 Kütahya, Turkey; <sup>3</sup>Department of Materials and Ceramic Engineering/CICECO, University of Aveiro, 3810-193 Aveiro, Portugal and <sup>4</sup>Department of Analytical and Environmental Chemistry, Vilnius University, Naugarduko 24, LT-03225 Vilnius, Lithuania

## ARTICLE HISTORY

Received November 15, 2016

Revised January 04, 2017

Accepted January 26, 2017

DOI:

10.2174/1877944107666170201154647

**Abstract:** The Mg/Al layered double hydroxides (LDHs) were successfully synthesized by novel aqueous sol-gel method. A series of europium-substituted layered double hydroxides (Mg/Al/Eu LDHs) were also synthesized using the same sol-gel processing. The Eu<sup>3+</sup> substitution effects were investigated in the Mg<sub>3</sub>/Al<sub>1-x</sub>Eu<sub>x</sub> system by changing the amount of Eu<sup>3+</sup> in the crystal lattice from 0.05 to 10 mol%. The samples obtained were characterized by X-ray diffraction (XRD) analysis, Fourier Transform Infrared spectroscopy (FT-IR), thermogravimetric (TG) analysis, scanning electron microscopy (SEM) and fluorescence spectroscopy (FLS). The results revealed that europium enters into a hydroxalite structure containing Mg<sup>2+</sup> and Al<sup>3+</sup> cations in the brucite-like layers.

**Keywords:** Layered double hydroxides, Mg/Al/Eu, sol-gel processing, europium substitution effects, luminescent properties.

## 1. INTRODUCTION

Layered double hydroxides (LDHs) are compounds composed of positively charged brucite-like layers with an interlayer gallery containing charged compensating anions and water molecules. The metal cations occupy the centres of shared octahedral whose vertices contain hydroxide ions that connect to form infinite two-dimensional sheets [1-4]. With this structure the most know mineral is hydroxalite, [Mg<sub>0.75</sub>Al<sub>0.25</sub>(OH)<sub>2</sub>](CO<sub>3</sub>)<sub>0.125</sub>·0.5H<sub>2</sub>O. LDHs have a well-defined layered structure within nanometre scale (0.3-3 nm) of interlayer and contain important functional groups. After calcination at temperatures from 300 to 600 °C, LDHs were converted to mixed metal oxides (MMO), which have the ability to recover the original layered structure [5-7]. LDHs have unique intrinsic advantages: their layer sizes are highly tunable and their constituents can be conveniently controlled and varied. LDHs, unlike common clay minerals such as montmorillonite, cannot swell automatically in water, and their delamination is much more difficult due to their high surface charge density as well as the strong attractions between adjacent nanosheets [8]. The formation and exploitation of new types of layered double hydroxide (LDH)/polymer NC hydrogels with high performance has also been investigated [9].

One of the most important properties is the interlayer anion exchangeability, which endows LDHs the possibility of accommodating organic UV absorbers in the interlayer space [10]. Moreover, the LDHs have an HCl absorption capacity, and may be used as PVC thermal stabilizer [11].

In the positively charged brucite-like layers of LDHs, a fraction of the trivalent cations could be substituted by other same valence cations. Rare earth doped luminescent materials have drawn increasing attention as potential phosphor materials for use in optical devices [12-14].

Recently, considerable attention has been focused on incorporating rare earth ions into LDHs hosts to develop new functional materials, which resemble designed optical properties [15]. LDHs doped with Tb<sup>3+</sup> ions in the brucite-like layers were prepared by a simple one-step co-precipitation method [16, 17]. Nanosized LDHs doped with Eu<sup>3+</sup>, Yb<sup>3+</sup>, Tb<sup>3+</sup> and Nd<sup>3+</sup> were prepared through the microemulsion method [18]. The Eu<sup>3+</sup> and Nd<sup>3+</sup> were incorporated also into hydroxalite and mayenite [19]. The Zn/Al/Eu and Zn/Al/Dy LDHs were also reported as perspective and efficient luminescent materials [20-22]. Cerium-doped hydroxalite-like precursors were also recently synthesized by co-precipitation method [23].

LDHs can be prepared by a variety of synthesis methods. However, the most common preparation technique is co-precipitation method starting from soluble salts of the metals. Sol-gel synthesis route for mixed metal oxides and related

\*Address correspondence to this author at the Department of Inorganic Chemistry, Faculty of Chemistry, Vilnius University, P.O. Box: LT-03225, Vilnius, Lithuania; Tel/Fax +370 (5) 219 3111, +370 (5) 233 0987; E-mail: [surelija.smalenskaite@gmail.com](mailto:surelija.smalenskaite@gmail.com)

compounds have some benefits over other methods such as simplicity, synthesis at low temperatures, effectiveness, suitability for different systems and cost efficiency [24-27].

The main aim of this study was to investigate  $\text{Eu}^{3+}$  substitution effects in the  $\text{Mg}_3\text{Al}_x\text{Eu}_x$  systems (the  $\text{Eu}^{3+}$  concentration in the crystal lattice was changed from 0.05 to 10 mol%) fabricated for the first time to the best of our knowledge by sol-gel synthesis route. The luminescent properties of  $\text{Mg}_3\text{Al}_{1-x}\text{Eu}_x$  LDH samples were also investigated.

## 2. MATERIALS AND METHOD

Aluminium (III) nitrate nonahydrate ( $\text{Al}(\text{NO}_3)_3 \cdot 9\text{H}_2\text{O}$ ), 98.5% (Hempur); magnesium (II) nitrate hexahydrate ( $\text{Mg}(\text{NO}_3)_2 \cdot 6\text{H}_2\text{O}$ ), 99% (Hempur); europium (III) nitrate pentahydrate ( $\text{Eu}(\text{NO}_3)_3 \cdot 5\text{H}_2\text{O}$ ), 99.99% (Sigma-Aldrich); ethylene glycol ( $\text{C}_2\text{H}_6\text{O}_2$ ), 99.5% (Roth); citric acid ( $\text{C}_6\text{H}_8\text{O}_7$ ), 99.5% (Hempur).

X-ray diffraction patterns were recorded using MiniFlex II diffractometer (Rigaku) using a primary beam Cu K $\alpha$  radiation ( $\lambda=1.541838$  Å). The  $2\theta$  angle of the diffractometer was graduated from 8 to  $80^\circ$  in steps of  $0.02^\circ$ , with the measuring time of 0.4 s per step. FT-IR analysis of compounds was conducted using Perkin-Elmer FTIR spectrometer. All spectra were recorded at ambient temperature in the range of 4000-400  $\text{cm}^{-1}$ . Thermal analysis was carried out using a simultaneous thermal analyzer 6000 (Perkin-Elmer) in air atmosphere at scan rate of  $10^\circ\text{C}/\text{min}$  and the temperature range from  $30^\circ\text{C}$  up to  $900^\circ\text{C}$ . Excitation and emission spectra were recorded on an Edinburgh Instruments FLS 900 spectrometer. The morphology of particles was investigated using a scanning electron microscope (SEM) Hitachi SU-70.

## 3. EXPERIMENTAL:

The  $\text{Mg}_3\text{Al}_{1-x}\text{Eu}_x$  LDH samples were synthesised by the sol-gel method from the solution of metal nitrates  $\text{Mg}(\text{NO}_3)_2 \cdot 6\text{H}_2\text{O}$ ,  $\text{Al}(\text{NO}_3)_3 \cdot 9\text{H}_2\text{O}$  and  $\text{Eu}(\text{NO}_3)_3 \cdot 6\text{H}_2\text{O}$ , dissolved in 50 ml of distilled water. Secondly, 0.2 M citric acid was added and obtained solution was stirred for 1 h at  $80^\circ\text{C}$ . Next, 2 ml of ethylene glycol have been added to the resulted mixture with continued stirring at  $150^\circ\text{C}$  until the complete evaporation of solvent. The obtained gel was dried at  $105^\circ\text{C}$  for 24 h. The mixed metal oxides were obtained by heating the gels at  $650^\circ\text{C}$  for 4 h. The  $\text{Mg}_3\text{Al}_{1-x}\text{Eu}_x$  LDH specimens were obtained by reconstruction of MMO powders in water at  $50^\circ\text{C}$  for 6 h under stirring. For comparison, the Mg/Al hydroxalcite was also synthesized and analysed.

## 4. RESULTS AND DISCUSSIONS:

The synthesized Mg/Al and Mg/Al/Eu LDHs were characterized by XRD analysis (Figs. 1-3). Evidently, only amorphous Mg-Al-O gel has formed during the initial stage of sol-gel processing of LDHs (Fig. 1). After heat-treatment of Mg-Al-O precursor gel at  $650^\circ\text{C}$ , a high crystalline mixed-metal oxide (MMO) has formed. The obtained MMO powdered samples were treated in water at  $50^\circ\text{C}$  for 6 h under stirring. The XRD patterns of obtained specimens confirmed the formation of monophasic Mg/Al LDH during the "reconstruction" process in water. Three characteristic peaks of hydroxalcite at  $2\theta$  of about  $10^\circ$  (003),  $23^\circ$  (006) and  $35^\circ$  (009) were observed in sol-gel derived LDH samples. Moreover, two very important reflections for LDHs are also clear-

ly seen at about  $60.2^\circ$  (110) and  $61.5^\circ$  (113). Based on the XRD pattern, there are slight shifts of characteristic basal plane d (003) related to the existing of different anions in the interlayer regions. The carbonate acts as a balancing anion because of its high affinity in the hydroxide layer over nitrate anions. In the simplest case, anion exchange is achieved by stirring an aqueous solution of the LDH precursor with a large excess of the anion salt. LDHs containing carbonate anions within the host material are less susceptible to anion exchange reactions due to high selectivity for this anion.

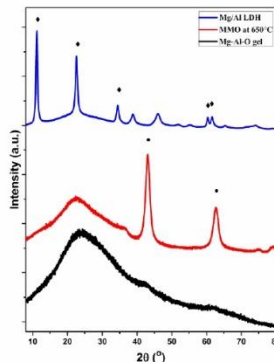


**Fig. (1).** XRD patterns of Mg-Al-O precursor gel, mixed-metal oxide obtained at  $650^\circ\text{C}$  and sol-gel derived Mg/Al LDH. The crystalline phases are marked: MgO - • and hydroxalcite - ♦.

All synthesized europium-substituted (1–10 mol%) Mg-Al-O gels also were amorphous powders to compare with Mg/Al LDH (Fig. 1). According to the XRD patterns presented in Fig. 2 the heat-treated Mg/Al/Eu gels resulted in high crystalline MMO samples. The mixed-metal oxides transformed fully to LDH structures independent on the Eu substitution level (see Fig. 3). The observed shift of the (110) reflections displacement signal toward lower values of  $2\theta$  containing different concentration of  $\text{Eu}^{3+}$  can be an evidence of isomorphic incorporation of lanthanide ion in LDH. The calculated d values for (110) peak (for 1 mol%  $\text{Eu}^{3+}$  1.5288 Å; 5 mol%  $\text{Eu}^{3+}$  1.5302 Å; 7.5 mol%  $\text{Eu}^{3+}$  1.5330 Å and 10 mol%  $\text{Eu}^{3+}$  1.5359 Å), compared with non-doped Mg/Al  $d(110) = 1.5274$  Å monotonically increased by increasing the  $\text{Eu}^{3+}$  concentration. The monophasic Mg/Al/Eu LDHs were obtained with amount of Eu less than 5 mol%. With increasing concentration of europium till 7.5 mol% the negligible amount of side  $\text{Eu}(\text{OH})_3$  phase has formed. The formation of  $\text{Eu}(\text{OH})_3$  is mainly due to the larger ionic radius of  $\text{Eu}^{3+}$  ions (1.08 Å) in comparison of ionic radius of  $\text{Al}^{3+}$  ions (0.53 Å). The  $\text{Eu}^{3+}$  ions taking up the octahedral positions of  $\text{Al}^{3+}$  ions led to the deformation of crystal lattice, and the excess  $\text{Eu}^{3+}$  ions in high basic condition crystallized as  $\text{Eu}(\text{OH})_3$ .

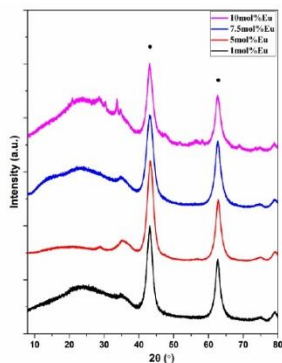


Fig. (2). XRD patterns of Mg/Al/Eu 1–10 mol% gels calcined at 650 °C. The crystalline phase is marked: MgO - \*.

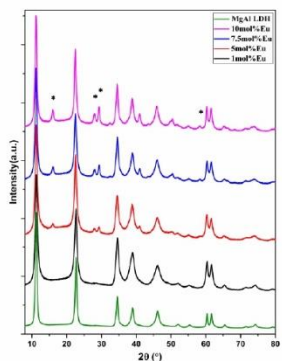


Fig. (3). XRD patterns of synthesized by sol-gel method Mg/Al/Eu 1 – 10 mol% LDHs. The  $\text{Eu}(\text{OH})_3$  phase is marked: \*.

Thus, these results confirmed once again that highly crystalline LDHs could be synthesized during hydroxylation sol-gel derived crystalline MMO samples in aqueous media. At high temperature of calcination, crystalline mixed oxide and partial changes result in the local structure of the  $M_{II}$  cations. A partial regeneration of the layered phase takes place which is characterized by different composition and morphology.

The XRD patterns of the synthesized LDHs contain very sharp diffraction lines attributable only to LDH crystalline phase at low concentration of europium. Interestingly, the formation of sol-gel based LDHs depends on the concentration of europium in the samples.

FT-IR spectra of Mg/Al and Mg/Al/Eu LDH samples in the region of 4000–500  $\text{cm}^{-1}$  are shown in Fig. 4. The spectra recorded for all samples are very similar to each other without any important differences. The absorption bands observed at around 3500–3000  $\text{cm}^{-1}$  correspond to the stretching vibrations of hydroxyl (-OH) groups from the hydroxyl layers and from intercalated and externally adsorbed water molecules [28]. The broad band identified at 2974  $\text{cm}^{-1}$  is assigned to the stretching mode of hydroxyl groups hydrogen-bonded to interlayer carbonate anions. The presence of adsorbed molecular water was confirmed by the medium intensity band at 1629  $\text{cm}^{-1}$ . The strong absorption band visible at 1353  $\text{cm}^{-1}$  is attributed to the asymmetric vibrations modes of  $\text{CO}_3^{2-}$ . The absorption bands observed at 613  $\text{cm}^{-1}$  can be ascribed to the metal-oxygen  $M^{2+}\text{-O}$  and  $M^{3+}\text{-O}$  stretching mode.

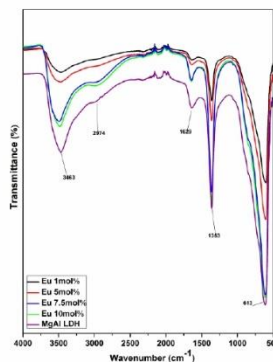


Fig. (4). FT-IR spectra of Mg/Al and Mg/Al/Eu 1 – 10 mol% LDHs.

The TG-DSC curves of synthesized Mg/Al and Mg/Al/Eu 10mol% LDHs are shown in Figs. 5 and 6, respectively. As seen, the thermal behaviour of synthesized LDH is not dependent on the europium substitution in the structure. The initial mass loss about ~15% was observed in the temperature range of 30–200 °C for the Mg/Al and Mg/Al/Eu LDHs prepared by sol-gel method. These changes in mass are due to the collapse of interlayer and evolution of adsorbed water. The main decomposition of LDH samples occurs via one step in the temperature range of 200–600 °C (the mass loss ~45–48%). The second mass loss step is due to the dihydroxylation and decomposition of the impurities of interlayer ionic carbonate. The observed thermal effects in DSC

curves support the results obtained from TG measurements. Above 600 °C the brucite-type structure collapses and a solid solution of mixed spinel ( $MgAl_2O_4$ ) and  $MgO$ , or  $Al_2O_3$  and  $MgO$  is formed.

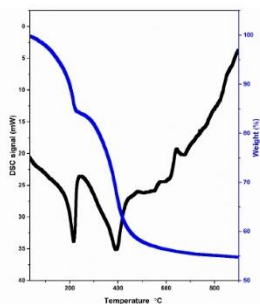


Fig. (5). TG-DSC curves of the Mg/Al LDH.

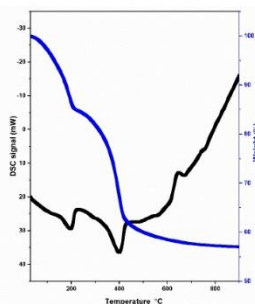


Fig. (6). TG-DSC curves of the Mg/Al/Eu 10 mol% LDH.

The microstructure for the synthesized LDH samples was determined from the SEM micrographs. The SEM micrographs of calcined Mg/Al precursor and sol-gel derived LDH sample are shown in Fig. 7. The mixed metal oxide obtained by calcination of Mg-Al-O gel at 650 °C is composed of the network of spherical nanoparticles varying in size from approximately 2 to 5  $\mu m$ . A layered double structure was recovered after reconstruction procedure in water, showing the formation of plate-like particles with hexagonal shape (Fig. 7b). The surface morphology of  $Eu^{3+}$ -substituted LDH samples is very similar for all specimens independent of the substitutional level. Fig. 8 shows the representative SEM micrographs of sol-gel synthesized Mg/Al/Eu 1mol% and Mg/Al/Eu 10mol% samples. As seen, small fibrous plate-like

particles with hexagonal structure are aggregated as in the case of non-substituted LDH sample. So, all sol-gel derived Mg/Al/Eu LDHs consist of the larger hexagonally shaped particles varying in size from approximately 250 to 500 nm. The surface morphological features of sample with highest europium content are more pronounced consisting of hexagonally shaped nanostructures in LDHs. Finally, the complete regeneration LDHs samples from MMO in aqueous media has been observed.

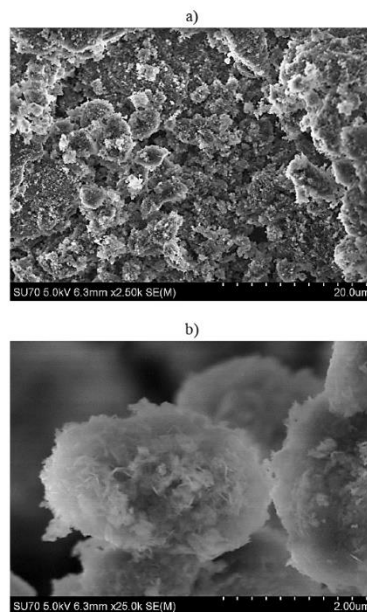


Fig. (7). SEM micrographs of MMO (a) and sol-gel synthesized Mg/Al LDH (b).

The emission spectra obtained at room temperature of all the Mg/Al/Eu LDH samples under excitation at 320 nm are presented in Fig. 9. As seen, all samples share similar emission profiles. The emission spectra of Mg/Al/Eu LDHs shows three main emissions in the wavelength range of 500–740 nm. In all spectra, the emission bands characteristic for  ${}^3D_0-{}^3F_1$  ( $J=1, 2, 3, 4$ ) transitions of  $Eu^{3+}$  ions were observed. The emission peaks are referred to the typical three  ${}^3D_0-{}^3F_1$  (591 nm)  ${}^3D_0-{}^3F_2$  (615 nm) and  ${}^3D_0-{}^3F_4$  (703) transitions of  $Eu^{3+}$  ion. The emission due to  ${}^3D_0-{}^3F_2$  transition is the strongest, indicating that  $Eu^{3+}$  ions occupy a low-symmetry

site.  $^5D_0 \rightarrow ^7F_2$  transition called as a hypersensitive transition. This can be caused by the addition of another molecule (for example, a competitive ligand) by a variation of the ionic strength of the solution (addition of a salt), by a variation of the polarity of the solvent (addition of another solvent), or by a variation of the pH value of the solution (addition of an acid or a base) when working in aqueous solutions. The presence of the low-symmetry structure containing the  $\text{Eu}^{3+}$  can only be observed in the nanocrystal line products, the results allow to exclude the adsorption of  $\text{Eu}^{3+}$  on the surface of LDHs [29]. When  $\text{Eu}^{3+}$  ions occupy the sites with inversion symmetry, the  $^5D_0 \rightarrow ^7F_1$  transition, typical magnetic dipole transition, should be relatively dominant; while, if there is no inversion symmetry at the sites of  $\text{Eu}^{3+}$  ions,  $^5D_0 \rightarrow ^7F_2$  transition should be relatively dominant [30]. It is clear that the photoluminescence intensity in the Mg/Al/Eu LDH phase increases with increasing the  $\text{Eu}^{3+}$  concentration, and reaches the maximum when the concentration of  $\text{Eu}^{3+}$  is 7.5%. With further increasing amount of europium the intensity of emission decreases due to the concentration quenching. As the concentration of  $\text{Eu}^{3+}$  increases, the distances between  $\text{Eu}^{3+}$  ions in the layers will be shortened, which dramatically increases the interaction of ions and causes serious concentration quenching. This fact suggested that  $\text{Eu}^{3+}$  ions replaced  $\text{Al}^{3+}$  in the host lattice.

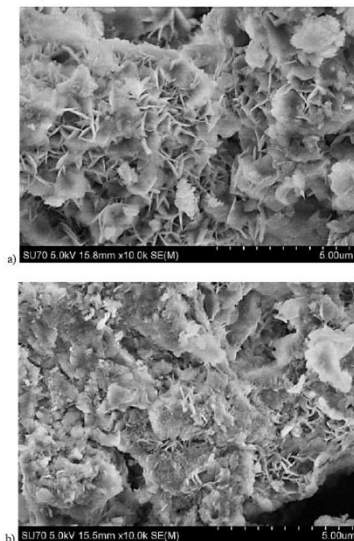


Fig. (8). SEM micrographs of Mg/Al/Eu 1mol% (a) and Mg/Al/Eu 10mol% (b) LDHs.

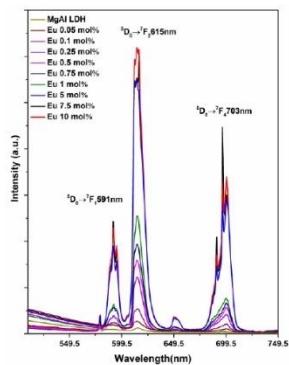


Fig. (9). Photoluminescence emission spectra of Mg/Al/Eu<sup>3+</sup> LDHs ( $\lambda_{exc} = 320$  nm).

## CONCLUSION

The Mg/Al layered double hydroxides (LDHs) were successfully synthesized by novel aqueous sol-gel method. In the sol-gel processing route, the LDHs were obtained after the decomposition of Mg-Al-O precursor gels and following "reconstruction" of intermediate crystalline MMO samples in aqueous media. The same synthesis parameters were successfully applied for the synthesis of europium-substituted Mg/Al/Eu<sup>3+</sup> 0.05–10 mol% LDHs. Interestingly, the formation of sol-gel based Mg/Al/Eu<sup>3+</sup> LDHs depends slightly on the concentration of europium used in the samples. With increasing the concentration of europium till 7.5 mol% the negligible amount of side Eu(OH)<sub>3</sub> phase has formed. The typical LDH microstructure was determined from the SEM micrographs. The sol-gel synthesized LDH samples consisted of hexagonally shaped particles varying in size from approximately 250 to 500 nm. The luminescence of Mg/Al/Eu<sup>3+</sup> LDHs was also investigated in this study. The emission peaks are referred to the typical three  $^5D_0 \rightarrow ^7F_1$  (591 nm) and  $^5D_0 \rightarrow ^7F_2$  (615 nm)  $^5D_0 \rightarrow ^7F_4$  (703 nm) transitions of  $\text{Eu}^{3+}$  ion. It was also suggested from these results, that  $\text{Eu}^{3+}$  replaced  $\text{Al}^{3+}$  ions in the host lattice.

## CONFLICT OF INTEREST

The authors confirm that this article content has no conflict of interest.

## ACKNOWLEDGEMENTS

The work has been performed as part of the TUMOCs project. This project has received funding from the European Union's Horizon 2020 research and innovation programme under the Marie Skłodowska-Curie grant agreement No 645660. The financial support of P2020 COMPETE and FCT-Portugal through project POCI-01-0145-FEDER-

016686 - PTDC/CTM-NAN/2418/2014 (NANOCONCOR) is also acknowledged.

## REFERENCES

- [1] Klenkate, K., Prosycevas, I., Taraskevicius, R., Khinsky, A.; Synthesis and characterization of layered double hydroxides with different cations (Mg, Co, Ni, Al), decomposition and reformation of mixed metal oxides to layered structures Kareiva A. *Centr Eur. J. Chem.*, **2011**, *9*, 275-282.
- [2] Bi, X.; Zhang, H.; Dou, L. Layered Double Hydroxide-Based Nanocarriers for Drug Delivery. *Pharmaceutics*, **2014**, *6*, 298-332.
- [3] Wu, J.; Ren, Z.Y.; Du, S.C.; Kong, L.J.; Liu, B.W.; Xi, W.; Zhu, J.Q.; Fu, H.G. Layered Double Hydroxide-Based Nanocarriers for Drug Delivery. *Pharmaceutics Nano Res.*, **2016**, *9*, 713-725.
- [4] Rives, V. *Layered Double Hydroxides: Present and Future*. Nova Science Publishers, New York, **2001**.
- [5] Klenkate, K.; Khinsky, A.; Kareiva, A. Reconstitution effect of Mg/Ni/Al layered double hydroxide. *Mater Lett.*, **2011**, *65*, 388-391.
- [6] Cosmo, D.; Esquinas, C.; Jimenez-Sanchidrian, C.; Ruiz, J.R. Use of Raman spectroscopy to assess the efficiency of Mg/Al mixed oxides in removing cyanide from aqueous solutions. *Appl. Surf. Sci.*, **2016**, *3644*, 28-433.
- [7] Ivanov, M.; Klenkate, K.; Khinsky, A.; Kareiva, A.; Banyo, J. Dielectric and Conductive Properties of Hydrocalcite. *Ferroelectrics*, **2011**, *417*, 136-142.
- [8] Hu, Z.; Chen, G. Aqueous dispersions of layered double hydroxide/polyacrylamide nanocomposites: preparation and rheology. *J. Mater. Chem. A*, **2014**, *2*, 13593.
- [9] Hu, Z.; Chen, G. Novel nanocomposite hydrogels consisting of layered double hydroxide with ultrahigh tensibility and hierarchical porous structure at low inorganic content. *Adv. Mater.*, **2014**, *26*, 5950.
- [10] Cao, T.; Xu, K.; Chen, G.; Guo, C. Poly (ethylene terephthalate) nanocomposites with a strong UV-shielding function using UV-absorber intercalated layered double hydroxides. *RSC Advances*, **2013**, *3*, 6282.
- [11] Liu, J.; Chen, G.; Yang, J. Preparation and characterization of poly (vinyl chloride)/layered double hydroxide nanocomposites with enhanced thermal stability. *Polymer*, **2008**, *49*, 3923.
- [12] Stambulic, A.; Katalnikovas, A.; Enseling, D.; Duteznik, D.; Sakirzanovas, S.; Van Bael, M.; Hardy, A.; Kareiva, A.; Jüstel, T. Luminescence properties of Sm<sup>3+</sup>-doped alkaline earth ortho-stannates. *Opt. Mater.*, **2014**, *36*, 1146-1152.
- [13] Skaidzins, R.; Jüstel, T.; Kareiva, A. Study of Eu<sup>3+</sup> and Tm<sup>3+</sup> substitution effects in sol-gel fabricated calcium hydroxyapatite. *Mater Chem. Phys.*, **2016**, *170*, 229-238.
- [14] Binemans, K. Lanthanide-based luminescent hybrid materials. *Chem. Rev.*, **2009**, *109*(9), 4283-4374.
- [15] Guasuvan, P.; Xu, R. Lanthanide-doped layered double hydroxides intercalated with sensitizing anions: efficient energy transfer between host and guest layers. *J. Phys. Chem. C*, **2009**, *113*, 17206-17214.
- [16] Vicente, P.; Perez-Bernal, M.E.; Ruano-Casero, R.J.; Ananias, D.; Paz, P.A.A.; Rocha, J.; Rivas, V. Luminescence properties of lanthanide-containing layered double hydroxides. *Micropor. Mesopor. Mater.*, **2016**, *226*, 209-220.
- [17] Posati, T.; Costantino, F.; Lattenni, L.; Nocchetti, M.; Paolantonio, M.; Tarpani, L. New insights on the incorporation of lanthanide ions into nanosized layered double hydroxides. *Inorg. Chem.*, **2012**, *51*, 13229-13236.
- [18] Dominguez, M.; Perez-Bernal, M.E.; Ruano-Casero, R.; Barriga, C.; Rives, V.; Ferreira, R.A.S.; Carlos, L.D.; Rocha, J. Multiwavelength luminescence in lanthanide-doped hydrocalumite and mayenite. *Chem. Mater.*, **2011**, *23*, 1993-2004.
- [19] Zhang, Z.; Chen, G.M.; Liu, J.G. Tunable photoluminescence of europium-doped layered double hydroxides intercalated by coumarin-3-carboxylate. *RSC Adv.*, **2014**, *4*, 7991-7997.
- [20] Gao, X.R.; Lei, L.X.; Kang, L.W.; Wang, Y.Q.; Lian, Y.W.; Jiang, K.L. Synthesis, characterization and optical properties of a red organic-inorganic phosphor based on terephthalate intercalated Zn/Al/Eu layered double hydroxide. *J. All Compd.*, **2014**, *585*, 703-707.
- [21] Vargas, D.R.M.; Oviedo, M.J.; Lisboa, F.D.; Wypych, F.; Hirata, G.A.; Antzaga, G.G.C. Phosphor dysprosium-doped layered double hydroxides exchanged with different organic functional groups. *J. Nanomater.*, **2013**, Art No. 730153.
- [22] Tanboli, A.H.; Jadhav, A.R.; Chung, W.J.; Kim, H. Catalyst for hydrogen production from sodium borohydride hydrolysis. *Energy*, **2015**, *93*, 955-962.
- [23] Brinker, C.J.; Sherer, G.W. *The Physics and Chemistry of Sol-Gel Processing*. Academic Press, San Diego, **1990**.
- [24] Brinker, C.J.; Sherer, G.W. *The Physics and Chemistry of Sol-Gel Processing*. Academic Press, San Diego, **1990**.
- [25] Kareiva, A. Aqueous sol-gel synthesis methods for the preparation of gemet crystal structure compounds. *Mater. Sci. (Medžiagotyra)*, **2011**, *17*, 428-437.
- [26] Li, T.; He, H.F.; Zhang, T.; Zhao, B.; Chen, Z.Q.; Dai, H.Y.; Xue, R.Z.; Chen, Z.P. Effect of synthesizing temperatures on the microstructure and electrical property of CaCu<sub>2</sub>Ti<sub>2</sub>O<sub>7</sub> ceramics prepared by sol-gel process. *J. All Compd.*, **2016**, *684*, 315-321.
- [27] Skrudene, M.; Misericic, M.; Sakalanskaite, M.; Katalnikovas, A.; Skaidzins, R. Doping effect of Tb<sup>3+</sup> ions on luminescence properties of Y<sub>3</sub>Al<sub>5</sub>O<sub>12</sub>:Cr<sup>3+</sup> phosphor. *J. Lumin.*, **2016**, *179*, 355-360.
- [28] Klopogge, J.T.; Frost, R.L. Infrared and Raman spectroscopic studies of layered double hydroxides (LDHs). *Nova Sci. Pub. Inc. New York*, **2001**, 139-192.
- [29] Posati, T.; Bellezza, F.; Cipiciani, A.; Costantino, F.; Nocchetti, M.; Tarpani, L.; Lattenni, L. Synthesis and characterization of luminescent nanoclays. *Cryst. Growth Des.*, **2010**, *10*, 2847-2850.
- [30] Gago, S.; Pillingier, M.; Ferreira, R.A.S.; Carlos, L.D.; Santos, T.M.; Goncalves, I.S. Immobilization of lanthanide ions in a pillared layered double hydroxide. PhD thesis, *Chem. Mater.*, **2005**, 5803-5809.

A. Smalenskaite, A.N. Salak, A. Kareiva, Induced neodymium luminescence in sol-gel derived layered double hydroxides, *Mendeleev Communications*, 28 (2018) 493-494. <https://doi.org/10.1016/j.mencom.2018.09.013>

## MOKSLINIŲ PUBLIKACIJŲ NE DISERTACIJOS TEMA SĄRAŠAS

Straipsniai recenzuojamuose žurnaluose:

1. D.E.L. Vieira, D. Sokol, A. Smalenskaite, A. Kareiva, M.G.S. Ferreira, J.M. Vieira, A.N. Salak, Cast iron corrosion protection with chemically modified Mg/Al layered double hydroxides synthesized using a novel approach, *Surface & Coatings Technology*, 375 (2019) 158–163.
2. B. Buckus, G. Brimas, A. Stašinskas, A. Smalenskaitė, S. Tautkus, A. Beganskienė, A. Kareiva, Analytical characterization of adipose tissue structure and composition: A novel approach towards diagnosis of metabolic disturbances in human body. *Chemija*, 26 (2015) 98-106.

### Pranešimų mokslinėse konferencijose tezės:

1. D. Sokol, A. Smalenskaitė, A. Kareiva, V.V. Rubanik, A.D. Shilin, V.V. Rubanik, D.E.L. Vieira, A.N. Salak, M.G.S. Ferreira, Ultrasound-assisted formation of multifunctional layered double hydroxides, *Ultrasonics 2016 : 2nd international conference on ultrasonic- based applications: from analysis to synthesis*, 6-8th June 2016, Caparica, Portugal.
2. B. Buckus, G. Brimas, Z. Juodeikis, A. Smalenskaitė, A. Beganskiene, A. Kareiva, Evaluation of adipose tissue composition by  $^1\text{H}$  NMR and its relationship to ultrasonoscopic measurements in obese patients. *8<sup>th</sup> Congress of the Baltic Association of Surgeons. Tallinn, Estonia, September 10-12, (2015)*.
3. B. Buckus, G. Brimas, A. Smalenskaitė, A. Beganskiene, A. Kareiva, Evaluation of adipose tissue composition by  $^1\text{H}$  NMR and its relationship to ultrasonoscopic measurements in obese patients. *20<sup>th</sup> World Congress "IFSO15". Vienna, Austria, August 26-29, (2015)*.
4. A. Smalenskaite, B. Buckus, S. Tautkus, A. Beganskiene, G. Brimas, A. Kareiva, Determination of fatty acid composition of adipose tissue by  $^1\text{H}$  NMR spectroscopy. *International Conference of Lithuanian Chemical Society „Chemistry and Chemical Technology 2015“ Vilnius, Lithuania, January 23, (2015)*.
5. A. Smalenskaite, B. Buckus, S. Tautkus, A. Beganskiene, G. Brimas, A. Kareiva, Analytical characterization of adipose structure and composition: A novel approach towards diagnostics and therapeutics. *19<sup>th</sup> International Scientific Conference "EcoBalt 2014". Riga, Latvija*.

## GYVENIMO APRAŠYMAS

### CURRICULUM VITAE

1. Vardas: Aurelija
2. Pavardė: Smalenskaitė
3. Gimimo data: 1990 - 05 - 04
4. Pilietybė: Lietuvos Respublikos
5. Adresas namų: M. Mažvydo 6-45, LT-06287 Vilnius
6. Telefonai: +370 62360986
7. El. paštas: aurelija.smalenskaite@gmail.com

#### 8. Išsilavinimas

Institucija:	Baigimo metai	Specialybė
Lietuvos Edukologijos universitetas	2013	Chemiko-mokytojo
Vilniaus Universitetas	2015	Chemiko magistro laipsnis

#### 9. Darbo patirtis

Data (nuo–iki)	Institucija	Pareigos
2010 – 2013 m.	Lietuvos Edukologijos universitetas, Chemijos katedra	Vyresnioji specialistė
2014 – 2019/08/31	Vilniaus universitetas, bendrosios ir Neorganinės Chemijos laboratorija	Vyresnioji specialistė
2015 – 2019/08/31	Vilniaus universitetas, Chemijos ir Geomokslų fakultetas Chemijos institutas, Neorganinės chemijos katedra	Jaunesnioji mokslo darbuotoja
2019/02/01- 2019/08/31	Vilniaus universitetas, Chemijos ir Geomokslų fakultetas Chemijos institutas, neorganinės chemijos katedra	Jaunesnioji asistentė



**10. Kita patirtis** (*Dalyvavimas organizacijose, komitetuose, ekspertinė veikla, apdovanojimais*)

<b>Data</b>	<b>Programa, projektai</b>
2016-2018 m.	Mokslinis projektas LMT, SEN-02/2016
2015-2018 m.	ES programa HORIZON 2020 MSCA-RISE-2014: Marie Skłodowska-Curie Research and Innovation StaffExchange (RISE) project „TUMOCS: TUneable Multiferroics based on oxygen Octahedral Structures” , Aveiro, Portugalija.
2019 m.	LMT projektas "Naujos kietakūnės ir nano kompozitinės medžiagos-kelias į geresnes multiferroines savybes", Lietuva.

**11. Kita svarbi informacija** (*Atskleidžianti turimas kompetencijas, kvalifikacijos kėlimas*).

<b>Data</b>	<b>Įstaiga</b>
<b>Kvalifikacijos kėlimas (mokslinės stažuotės):</b>	
2016 m. (1 mėn.)	Mokslinė stažuotė Aveiro universitete, Portugalija, TUMOCS projekto kvietimu.
2017 m. (1 mėn.)	Mokslinė stažuotė Aveiro universitete, Portugalija, TUMOCS projekto kvietimu.
2017 m. (4 mėn.)	Kuratorė - Erasmus programos, magistro studijų studentės.
2017-2019 m.	Vadovė, Neorganinės katedros mokslinių darbų laboratorijos.
2018 m. (2 sav.)	Mokymai Tartu, Estija, „Neutron Scattering“ organizatorių kvietimu.
2017-2018 m.	Vadovė, Neorganinės katedros bakalauro studijų studento.
2018-2019 m.	Kuratorė, Neorganinės katedros doktorantūros studijų užsienio studento.

2018-2019 m.	Asistentė, Bendrosios ir neorganinės chemijos laboratorijos respublikinių mokyklų mokinių laboratorinių darbų praktikos.
2018-2019 m.	Asistentė, Bendrosios ir neorganinės chemijos laboratorijos I kurso bakalauro studijų studentų laboratorinių darbų atlikime.
2018 m. (5 d.)	Ukraine and Lithuania R&D projekto mokslinių darbų aptarimas, Lvovo Nacionalinis politechnikos universitetas, Ukraina.

## NOTES

Vilniaus universiteto leidykla  
Saulėtekio al. 9, LT-10222 Vilnius  
El. p. [info@leidykla.vu.lt](mailto:info@leidykla.vu.lt),  
[www.leidykla.vu.lt](http://www.leidykla.vu.lt)  
Tiražas 15 egz.